(2)

Western New England College
School of Engineering

Springfield, Massachussetts

Drag Reduction and Wake Minimization on Marine Vehicles

By:
Craig A. Hunter
Pasquale Delore
Walter M. Presz, Jr.

Final Report
Office of Naval Research
Grant N00014-89-J-1883
July 1991

Abstract

Fluid dynamic research at Western New England College and the United Technologies Research Center has shown that novel, three dimensional contouring can be used to generate streamwise vorticity. Such streamwise vorticity enhances two stream mixing and can reduce separation regions on bluff bodies. This program investigated the possibility of using similar three dimensional contouring to passively control flow separation, wake mixing, and tip vortices on marine vehicles.

Experimentally, sub scale screening tests of three dimensionally contoured airfoils were conducted in an existing wind tunnel at Western New England College. Seven airfoil models were designed, fabricated, and tested. The seven contours included a baseline airfoil, two leading edge groove contours. a midspan groove contour, a triangular trailing edge contour, and two lobed trailing edge contours. Traverse data and lift/drag balance data were taken with each airfoil.

Test results indicate the following: leading edge grooves show the most promise for airfoil lift and drag improvements, triangular trailing edge contours for wake mixing enhancements, and lobed trailing edge contours for tip vortex dispersion. These three airfoil contours were recommended for more detailed, higher Reynolds Number testing at the United Technologies Research Center.

Acknowledgements

We would like to thank David Sheppard and Craig Addis, who, as students at Western New England College, contributed significantly to the work presented in this report. We would also like to thank Dick DeCelle and Bill Fitzgerald for their support efforts in the Mechanical Engineering Laboratory.

Drag Reduction and Wake Minimization on Marine Vehicles

Table of Contents

List of Figures

Nomenclature

Symbols

α	Angle of Attack
A_P	Planform Area
AR	Aspect Ratio
b	Wake Width
C_D	Coefficient of Drag
C_L	Coefficient of Lift
D	Drag Force
H_{VE}	Hunter's Number for Vortex Energy
KE	Kinetic Energy
L	Lift Force
LE	Leading Edge
p	Fluid Density
r	radius
TE	Trailing Edge
V	Velocity
X	Distance from Wing Trailing Edge

Subscripts

c	At Vortex Core
eff	Effective
i	Induced
max	Maximum
min	Minimum
0	$\alpha = 0$
v	At Vortex Outer Radius
1	Control Volume Entrance
2	Control Volume Exit

I. Introduction

Control surface wing sections are used on submarines to provide stability and control. Figure 1 shows control surfaces on a submarine and the wakes they produce. These wakes can cause noise and performance problems when coming in contact with a spinning propeller.

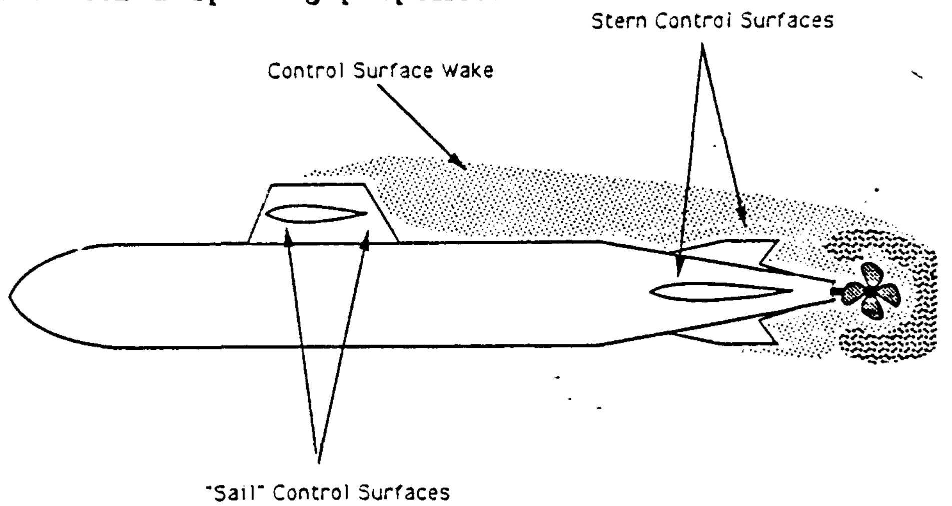

FIGURE 1: Submarine Control Wakes

The shape of submarine wing sections is governed by required control forces and structural reliability. Therefore, the wing sections are symmetrical and tend to be thick. Studies have been conducted on submarine control surfaces in a previous research program. Reference 1 details these studies, and presents typical submarine wing section geometries.

Thick airfoils result in large downstream wake regions. A wake is a region of momentum and velocity deficit in the flowfield caused by shear forces near the airfoil surface.

The size and extent of the velocity deficit behind an airfoil is directly related to the thickness of the airfoil boundary layer. Since thicker airfoils cause more severe adverse pressure gradients, these airfoils have thicker boundary layers and larger wakes. Airfoil wakes convect downstream with the flowfield and can pass through the propulsor. Large wakes will result in detrimental interference on propulsor performance and noise.

Thick airfoils can also have trailing edge separation at small angles of attack. The separation is a result of large adverse pressure gradients occurring on the airfoil suction surface. Figure 2 presents pressure distributions on the suction surface of an airfoil, with and without boundary layer separation.

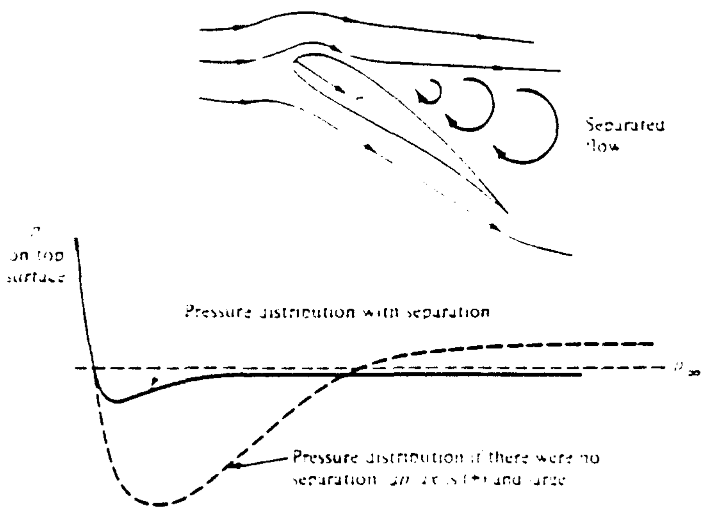

FIGURE 2:

Airfoil Pressure Distributions (REFERENCE 9)

Since the lift force on the wing is due to the pressure difference between the upper and lower surfaces of the wing, there is a loss of lift with separation. In addition there is a pressure force directed in the drag direction. So, flow separation on the control surface of a marine vehicle results in a loss of vehicle maneuverability, an increase in drag, and larger wakes.

Detrimental propulsor interaction can also be caused by wingtip vortices. A wing tip vortex is the result of the pressure difference between the upper and lower surfaces of a wing at an angle of attack. At the wingtip, high pressure fluid under the wing "leaks" onto the low pressure fluid above the wing, causing the formation of a vortex. This vortex trails downstream of the wing tip, as shown in Figure 3. Such vortices can have large non axial center velocities, resulting in detrimental effects on propulsor noise and performance.

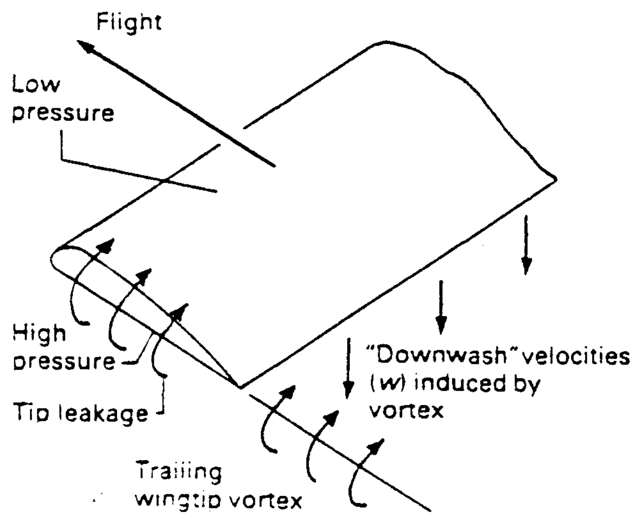

FIGURE 3: Fluid Flow Near a Wingtip (REFERENCE 9)

Thus, submarine control surfaces can cause wakes or large flow nonuniformities approaching the propulsor. The wakes are a result of surface shear forces, boundary layer separation, and/or wing tip vortices. This program investigates novel, three dimensional contouring to enhance wake mixing downstream of a wing section.

II. Background and Related Experience

Mixing of non-uniformities within a fluid stream is one of the most critical technologies in fluid dynamics. Mixing determines the length of combustors, the effectiveness of heat exchangers, and the efficiency of ejectors. Recent programs at Western New England College and the United Technologies Research Center have demonstrated that the generation and control of streamwise vorticity can greatly enhance flow mixing.

Figure 4 shows a convoluted trailing edge mixer lobe. When properly designed, these lobes generate three dimensional pressure gradients, resulting in low loss mixing vortices at the lobe exit plane. As shown in Figure 4, flow over the top of the lobes is directed down into lobe valleys, while flow under the lobes is directed upward into lobe hills.

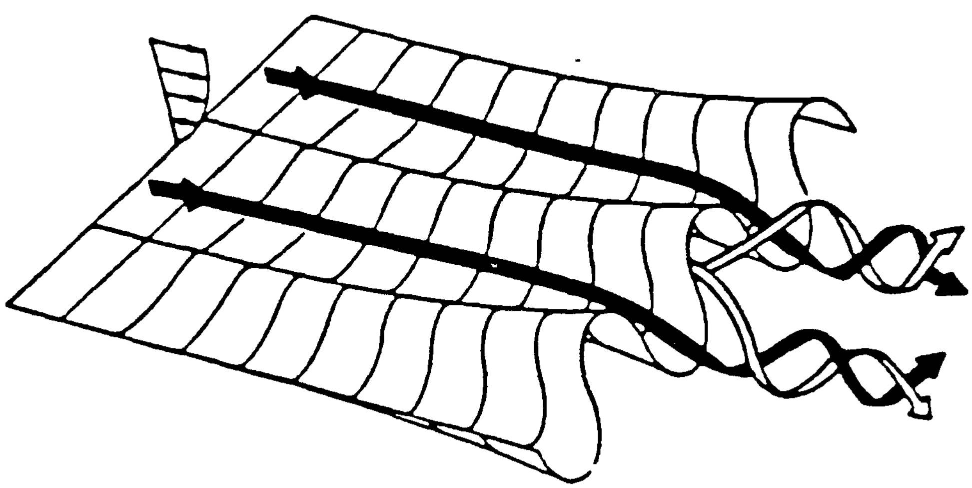

FIGURE 4: Mixer Lobes

(REFERENCE 3)

These pressure driven secondary flows result in large scale, streamwise vorticity downstream of the lobe exit. Figure 5 shows the entire wake flow structure of a convoluted trailing edge mixer. The mixing lobe causes flow to roll up quickly, creating very rapid mixing.

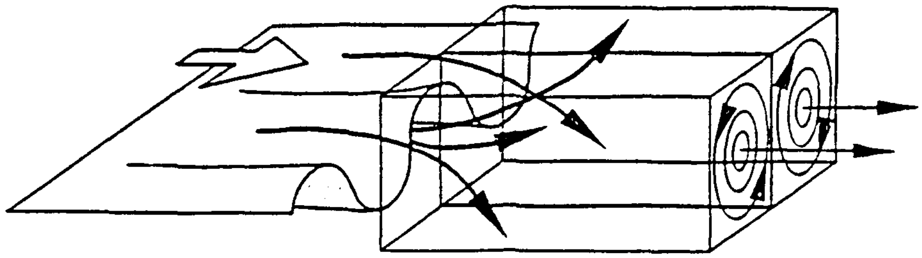

FIGURE 5: Convoluted TE Wakes

(REFERENCE 3)

A series of tests (Reference 3) were run in a water tunnel at Western New England College in an effort to obtain design guidelines for generating streamwise vorticity using mixer lobes. Three dimensional lobe contours were designed, fabricated, and setup for flow visualization testing. Dye was injected over the top and bottom surfaces of the mixer lobes at a variety of flow velocities.

The large scale, streamwise vorticies set up by the lobes were found to be independent of Reynolds Number. Figure 6 presents a laminar flow, low Reynolds Number test result. This side view of the flowfield downstream of the lobes shows large scale stirring vortices, resulting in thorough mixing of top and bottom dye streams. In addition,

FLUID DYNAMIC TESTING FACILITIES

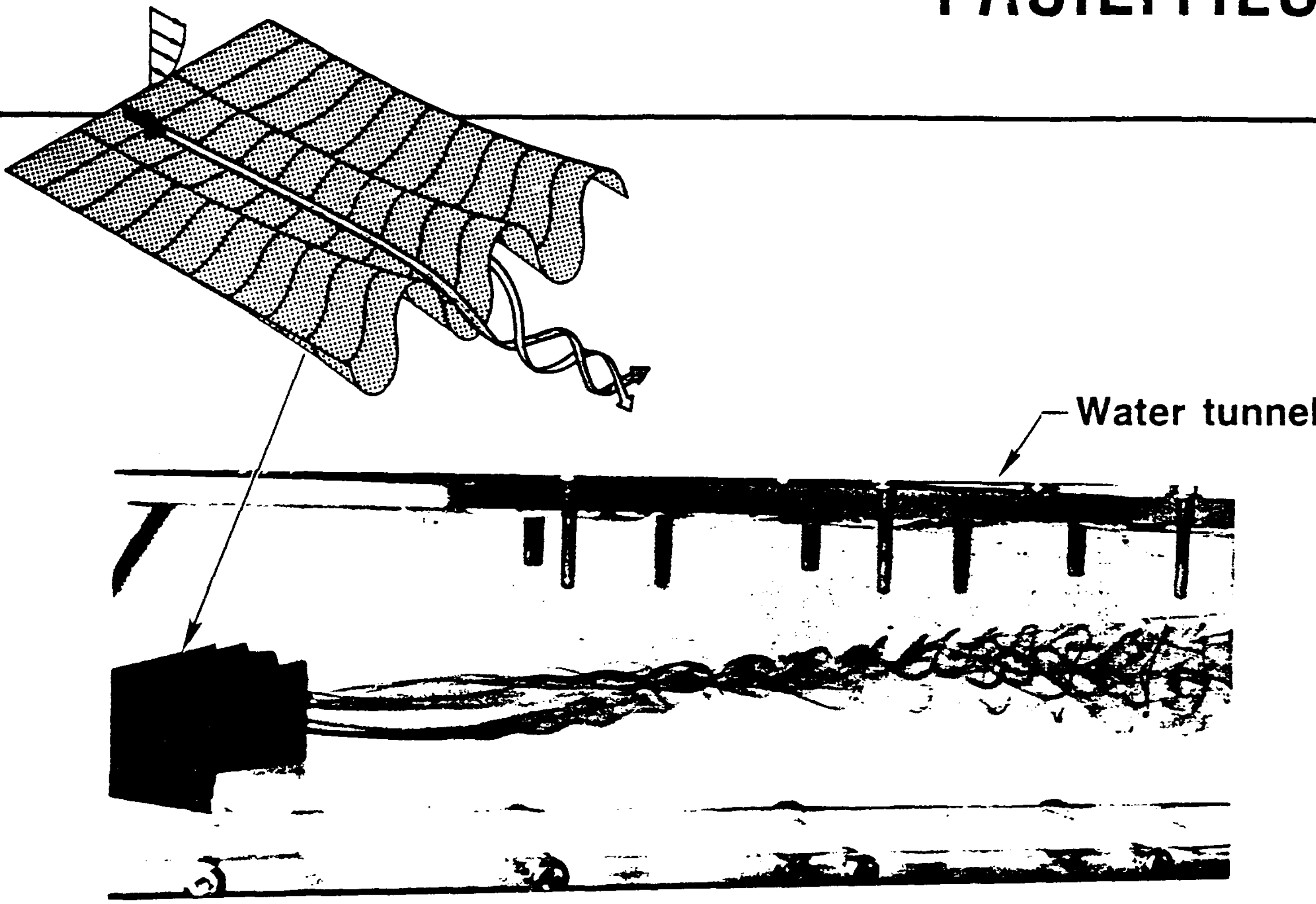

FIGURE 6: Mixer Lobe Testing

Western New England College

three distinct regions are visible; an initial roll up region, a necking vortex intensification region, and a downstream vortex decay region. These results are typical of all the streamwise vortex patterns obtained.

Additional tests (Reference 4) have also shown that properly contoured lobe shapes delay or eliminate boundary layer separation in the lobe section itself. Lobe angles of twenty five degrees and higher were tested without separation. Lobe contouring provides three dimensional relief for a low energy boundary layer approaching a severe adverse pressure gradient. In addition, the pressure gradients set up in the lobes generate secondary flows which efficiently mix boundary layer flow with higher energy free stream flow.

Tests were conducted at Western New England College to investigate the potential of improving the lift/drag characteristics of airfoils using similar lobed trailing edge contours. Figure 7 shows the lobed trailing edge airfoil, configured from a NACA 21% thick symmetrical airfoil section. Both the convoluted trailing edge airfoil and a conventional airfoil were wind tunnel tested over a range of angles of attack. Figure 8 presents the measured coefficients of lift as a function of angle of attack for both airfoils. The convoluted trailing edge significantly improves the performance of the airfoil by delaying trailing edge separation. This shows up as an increase in lift on the airfoil.

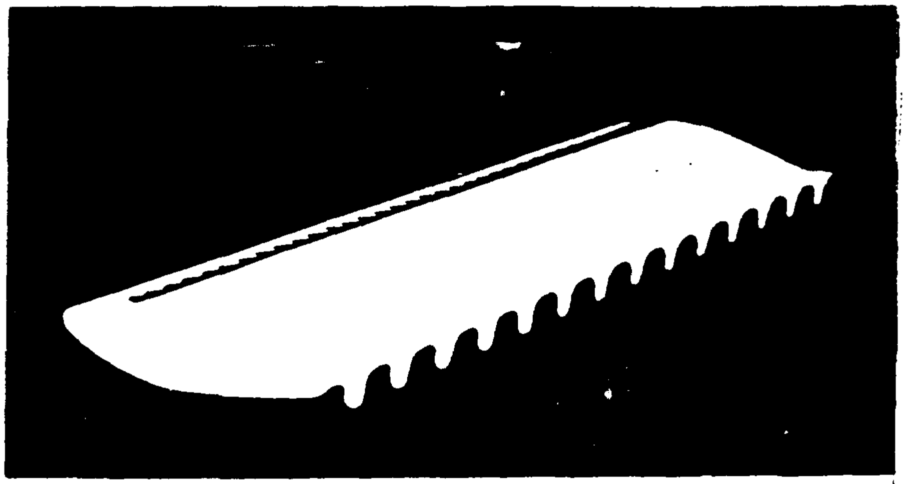

FIGURE 7: Convoluted TE Airfoil

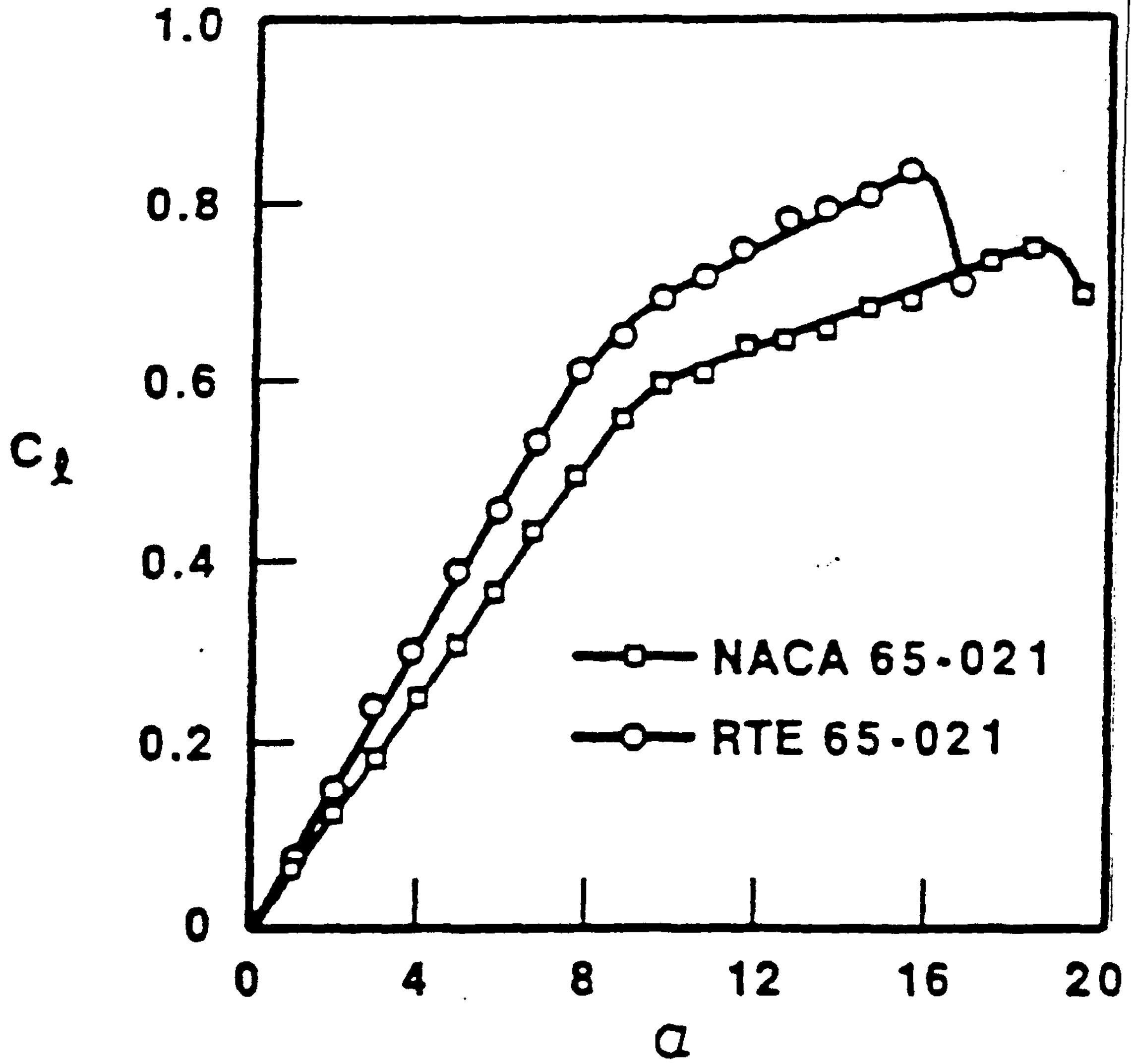

FIGURE 8: Baseline and RTE Performance

III. Technical Approach

Research work at Western New England College and the United Technologies Research Center has shown that three dimensional lobed and grooved contouring can be used to generate streamwise vorticity. Such contouring has been very successful in improving the performance of ejectors, airfoils, and jet engines by delaying separation or improving mixing. The purpose of this research program was to investigate the potential of using similar contouring to rapidly mix out the wakes downstream of control surfaces on marine vehicles.

Screening tests of several three dimensional airfoil contours were conducted at model scale in an existing wind tunnel at Western New England College. Contours showing the most promise for improving the wake characteristics of control surfaces on marine vehicles were recommended to United Technologies Research Center for higher Reynolds Number, more detailed testing.

IV. Analytical Effort

A literature search into the areas of lift, drag, and wing tip vortices was conducted. A review of two dimensional wake decay theory was performed, and ideal predictions for wake decay were generated. Control volume analyses were conducted to obtain expressions for drag coefficients from wake decay deficits. Finally, dimensional analysis procedures were used to generate parameters indicating the strength of wingtip vortices. These ideal relationships were used to compare and verify test results.

The lift on an airfoil is due to the circulation induced around it as it moves through a fluid. The flow coming off the trailing edge of the wing cannot follow the wing to the very tip, and seperates. This seperation near the trailing edge forms a starting vortex.

Kelvin's Theorem states that the circulation of a closed fluid curve remains constant (Reference 11). Therefore, an equal and opposite circulation must form around the wing to counteract the starting vortex. Figure 9 shows the start of circulation around an airfoil while Figure 10 shows its effect.

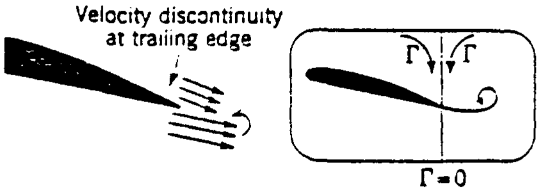

FIGURE 9: Starting Vortex

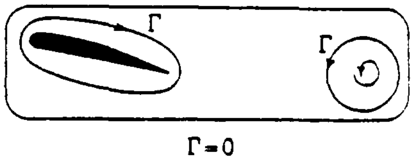

FIGURE 10: Vortex Effect

(REFERENCE 11)

The circulation around the wing adds to the velocity on top of the wing and subtracts from the velocity on the bottom of the wing. According to Bernoulli's Equation, the higher velocity fluid on top of the wing has a lower pressure than the fluid under the wing. The pressure difference between the two surfaces of a wing produces a lift force on the wing.

The total drag on an airfoil is composed of three different types of drag. The first of these is due to the viscous shear effects on the surface of the airfoil and is called skin friction drag. The second type of drag on an airfoil is due to the shape and frontal area of the airfoil. These first two types of drag are independent of lift forces acting on the wing. The combination of these two types of drag is known as profile drag, D_o (Reference 15).

The third type of drag on a wing is a result of the lift force on the wing and is called induced drag or drag due to lift. This drag comes about because of the induced angle of attack on the wing. The geometric angle of attack, α, is the angle between the chord line of the wing and the freestream velocity. But, the flow near the wing (i.e.; the local flow), tends to get deflected downward by an angle, α_i. This induced angle of attack is the angle between the local flow direction and the freestream direction as shown in Figure 11. The effective angle that the airfoil sees is given by;

$$\alpha_{EFF} = \alpha - \alpha_i, \qquad [1]$$

and a resultant force perpendicular to the local flow is produced.

Figure 11 shows that the component in the vertical direction is the lift force while the component in the horizontal direction is the induced drag, D_i.

(REFERENCE 11)

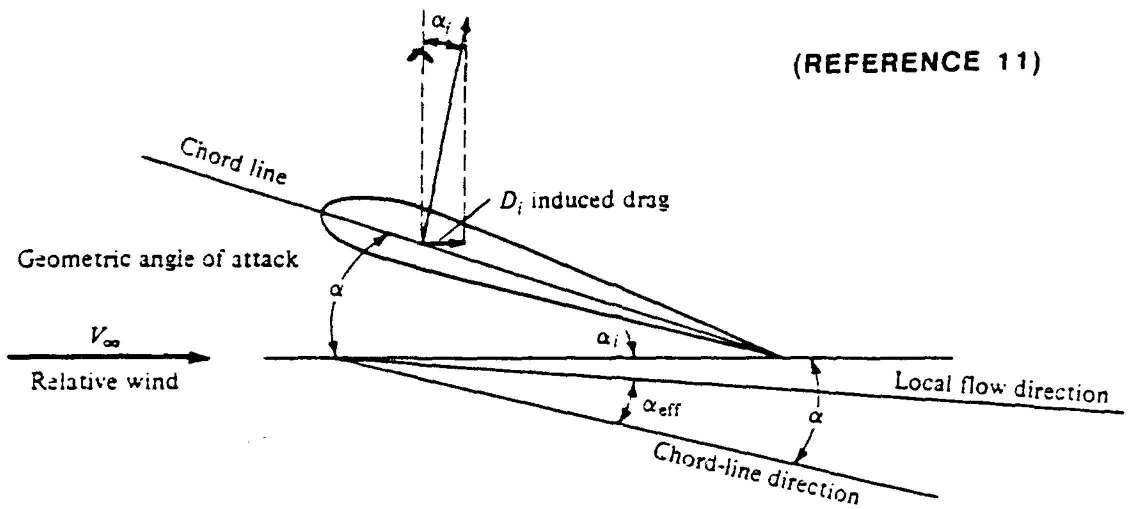

FIGURE 11: Induced Drag

The total drag on an airfoil is the combination of profile and induced drag:

$$D = D_o + D_i. \qquad [2]$$

In order to compare the drag and lift of different wings with the same aspect ratio, it is convenient to define two non-dimensional parameters, C_L and C_D (Reference 2):

$$C_L = (\text{Lift Force})/\tfrac{1}{2}\rho V^2 A_P \qquad [3]$$

$$C_D = (\text{Drag Force})/\tfrac{1}{2}\rho V^2 A_P. \qquad [4]$$

Having defined the coefficients of lift and drag for a finite wing, the equations for ideal lift and drag coefficients can now be defined (Reference 7):

$$C_L = 2\pi\alpha/(1+2/AR) \qquad [5]$$

$$C_D = C_{DO} + (C_L)^2/\pi AR. \qquad [6]$$

The ideal equations were used to verify experimental data relationships. Note that the slope of the ideal C_L curve is steeper than actual C_L curves because the wing sees an angle of attack less than the geometric angle. Appendix A contains a simplified derivation of the ideal equations.

Another analytical comparison deals with two dimensional wake decay. The wake decay relationship for flow behind a two dimensional body states that the wake width is proportional to the square root of the distance behind the trailing edge of the object (Reference 14):

$$b \propto X^{1/2}. \qquad [7]$$

Also, the center line velocity of the wake is proportional to the inverse square root of the distance behind the trailing edge of the object:

$$V_{min} \propto 1/X^{1/2}. \qquad [8]$$

These two relationships were used to confirm that the velocity profile data at the mid span of the wings tested was two dimensional.

After verifying that the flow over the wings were two dimensional, a control volume analysis of a wing in the test section of the wind tunnel was performed. The result produced the following expression for the profile drag coefficient of a wing:

$$C_{DO} = (2/t)\cdot(V_2/V_1)\cdot(1-V_2/V_1)\cdot dy. \qquad [9]$$

Appendix B contains the detailed derivation of the expression.

This equation was used to confirm the drag coefficient data obtained from the mechanical balance using wake decay profiles.

Finally, a dimensional analysis was performed in an effort to estimate the energy in wing tip vortices and provide a standard for comparing different wing configurations on the basis of vortex size and strength. The following equations were obtained from dimensional analysis, and approximate the kinetic energy at the vortex outer radius and the vortex core, respectively:

$$KE_v \approx \rho(V_v)^2(r_v)^3 \qquad [10]$$

$$KE_c \approx \rho(V_c)^2(r_c)^3. \qquad [11]$$

A third expression was derived to approximate the intensity of a vortex and is defined as Hunter's number. It is the ratio of the kinetic energies in the vortex:

$$H_{vn} = KE_c/KE_v. \qquad [12]$$

The entire dimensional analysis can be found in Appendix C.

V. Experimental Effort

This research project deals primarily with the experimental study of novel wing design concepts in an effort to increase stability, delay separation, and reduce wakes. Scale model tests were conducted in a small wind tunnel to obtain wake decay profiles, velocity traverses, and lift and drag polars. Test results were verified by using analytical wake decay data, control volume theory, and by comparison to ideal C_L and C_D curves.

V.1. Scale Models

The scale models tested in this project were constructed of wood and aluminum. Figures 12 through 18 show drawings of the baseline, longitudinal groove, leading edge groove, venturi leading edge groove, wide rippled trailing edge (WRTE), symmetric rippled trailing edge (SRTE), and triangular trailing edge (TTE) wings, respectively. Each wing has a span of 4.5 inches, a chord length of 3.0 inches, and conforms to the shape of a NACA 0023 wing from the point of maximum thickness to the trailing edge. From the point of maximum thickness to the leading edge, the wings have a 3 by 2 elliptical nose, with the minor axis of the ellipse perpendicular to the chord. This baseline airfoil shape was the same configuration tested in Reference 1.

Figures 19 through 25 show photos of the wings tested. Several wings are shown with a leading edge foil boundary

FIGURE 12: Baseline Wing

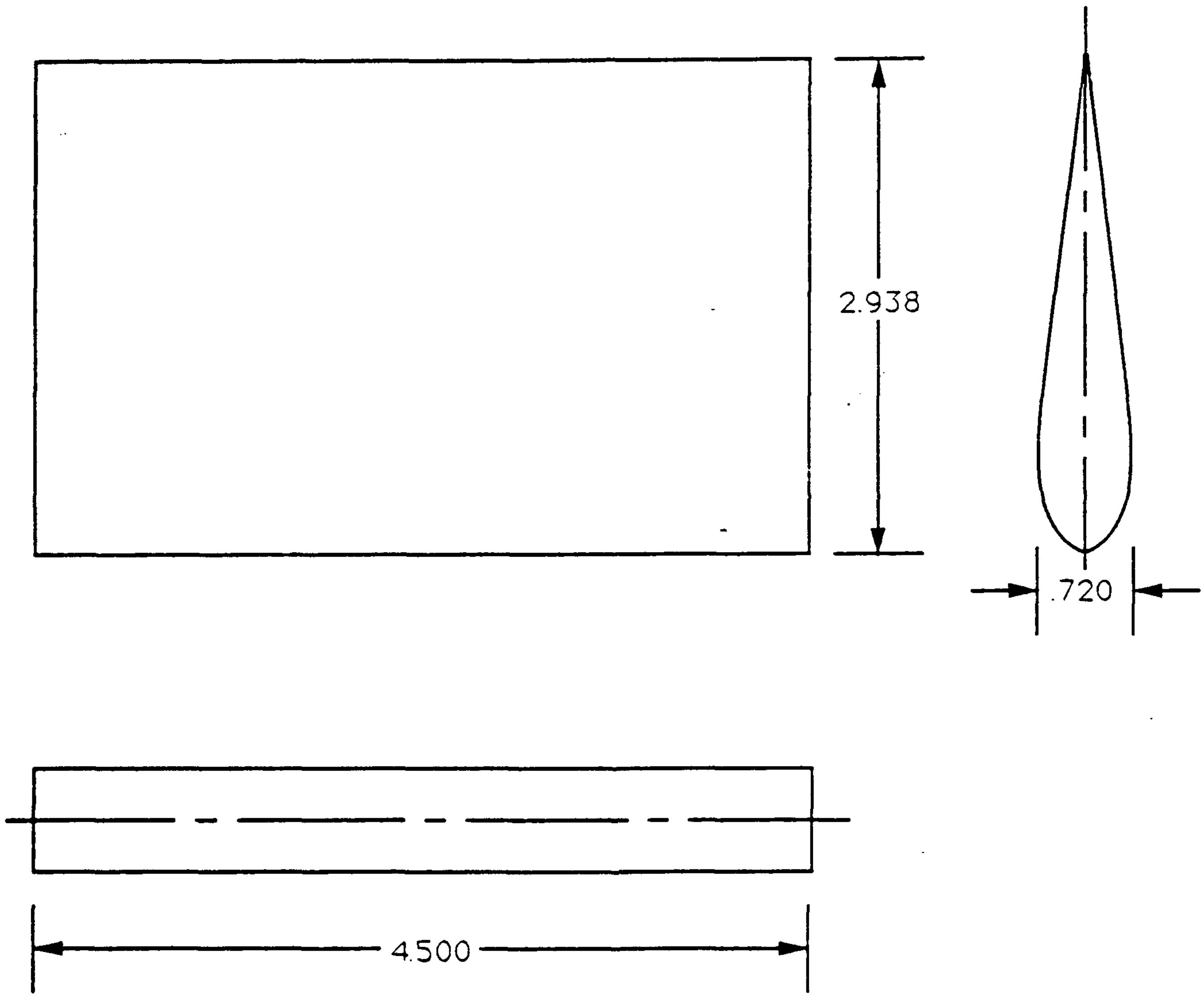

NOTE: ALL DIMENSIONS IN INCHES

FIGURE 13: Venturi LE Wing

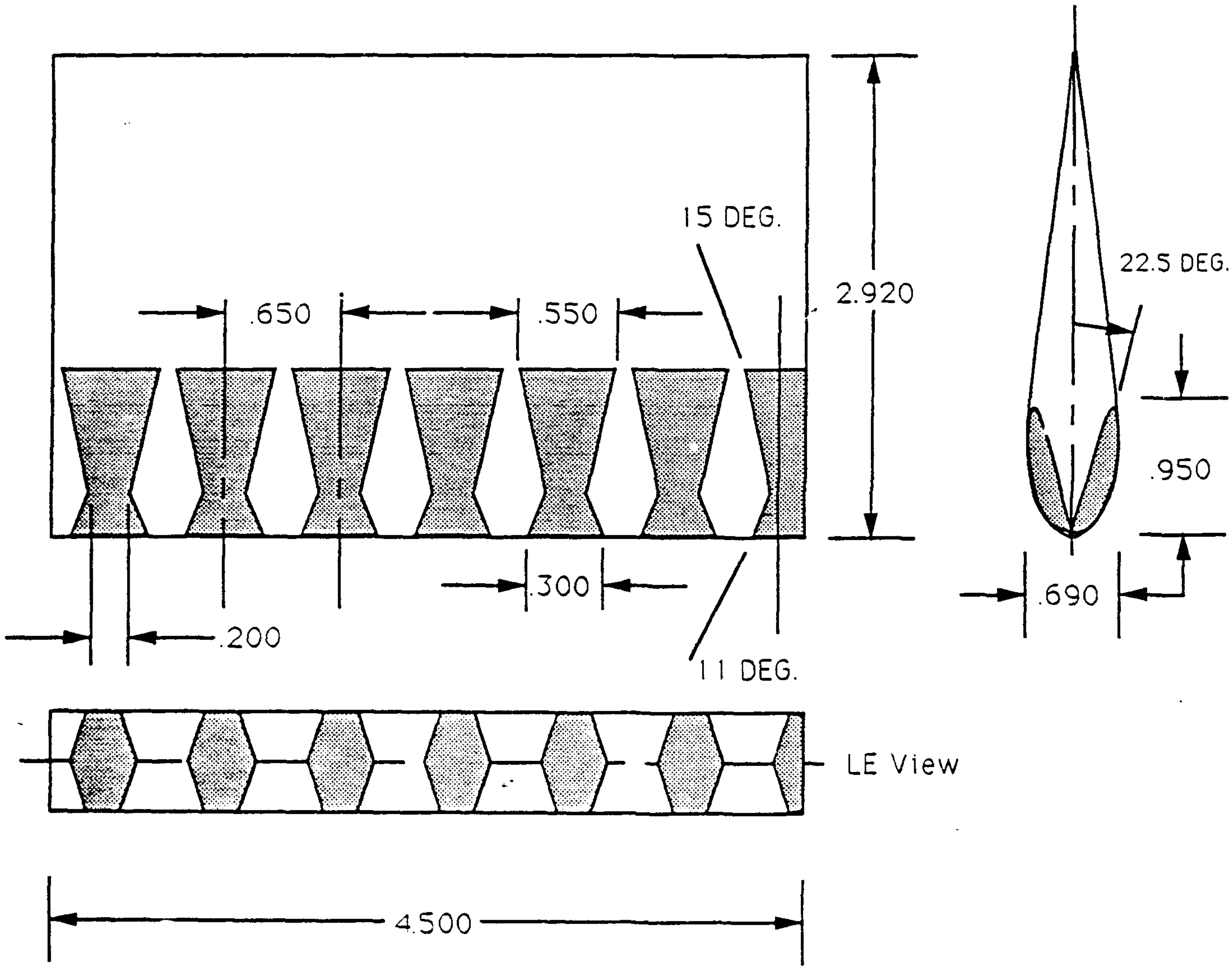

NOTE. ALL DIMENSIONS IN INCHES

FIGURE 14: LE Groove Wing

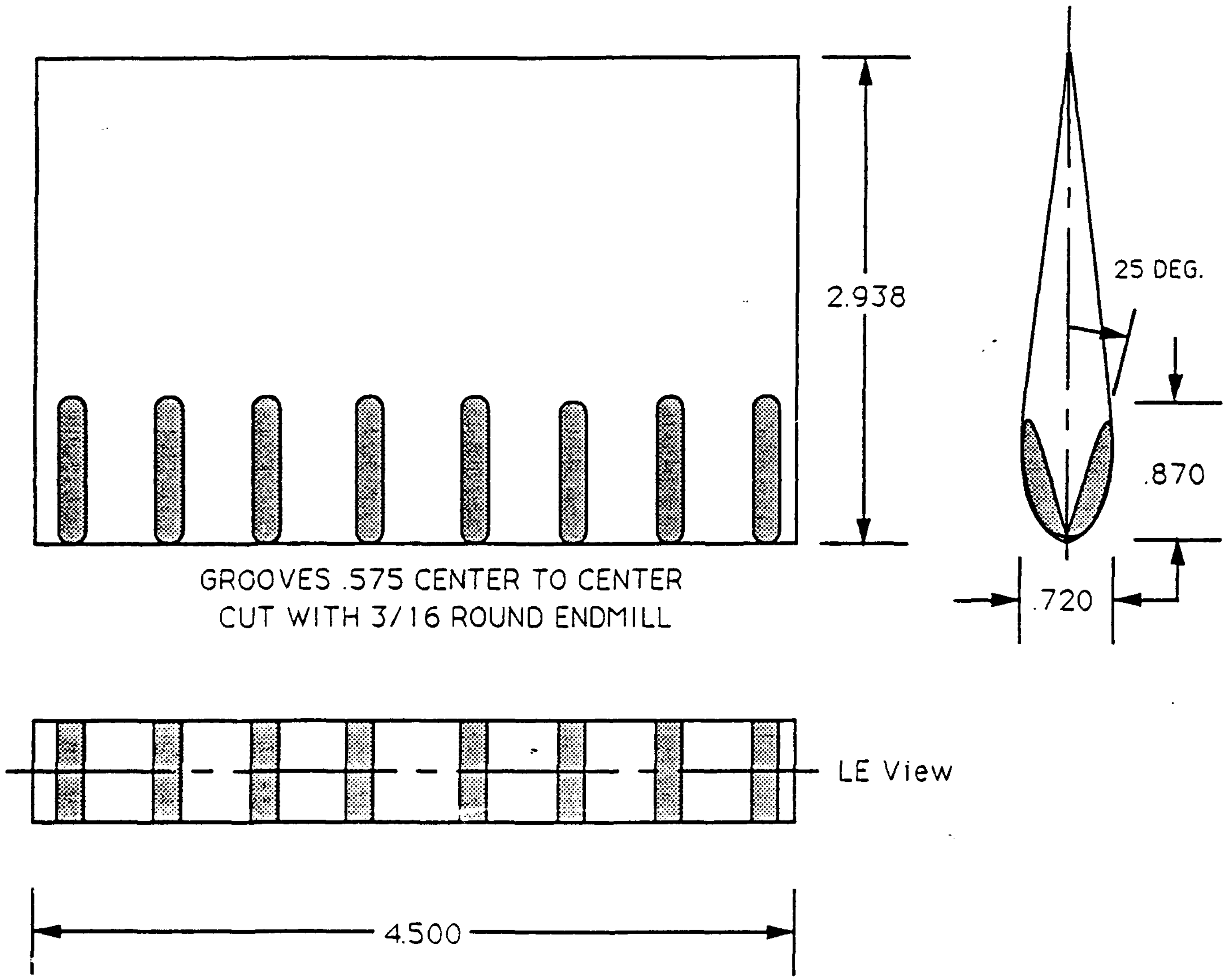

NOTE: ALL DIMENSIONS IN INCHES

FIGURE 15: Longitudinal Groove Wing

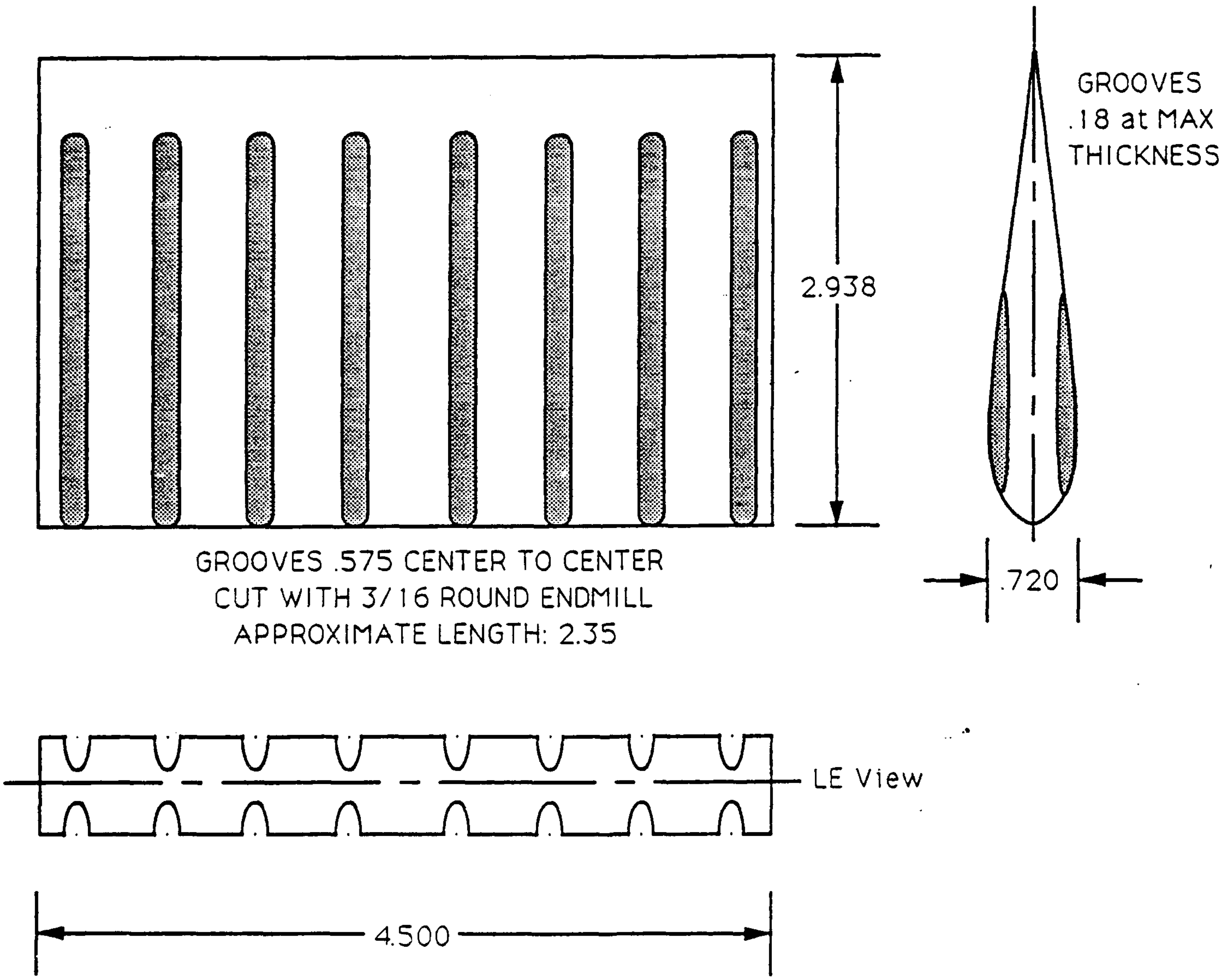

NOTE: ALL DIMENSIONS IN INCHES

FIGURE 16: Triangular TE Wing

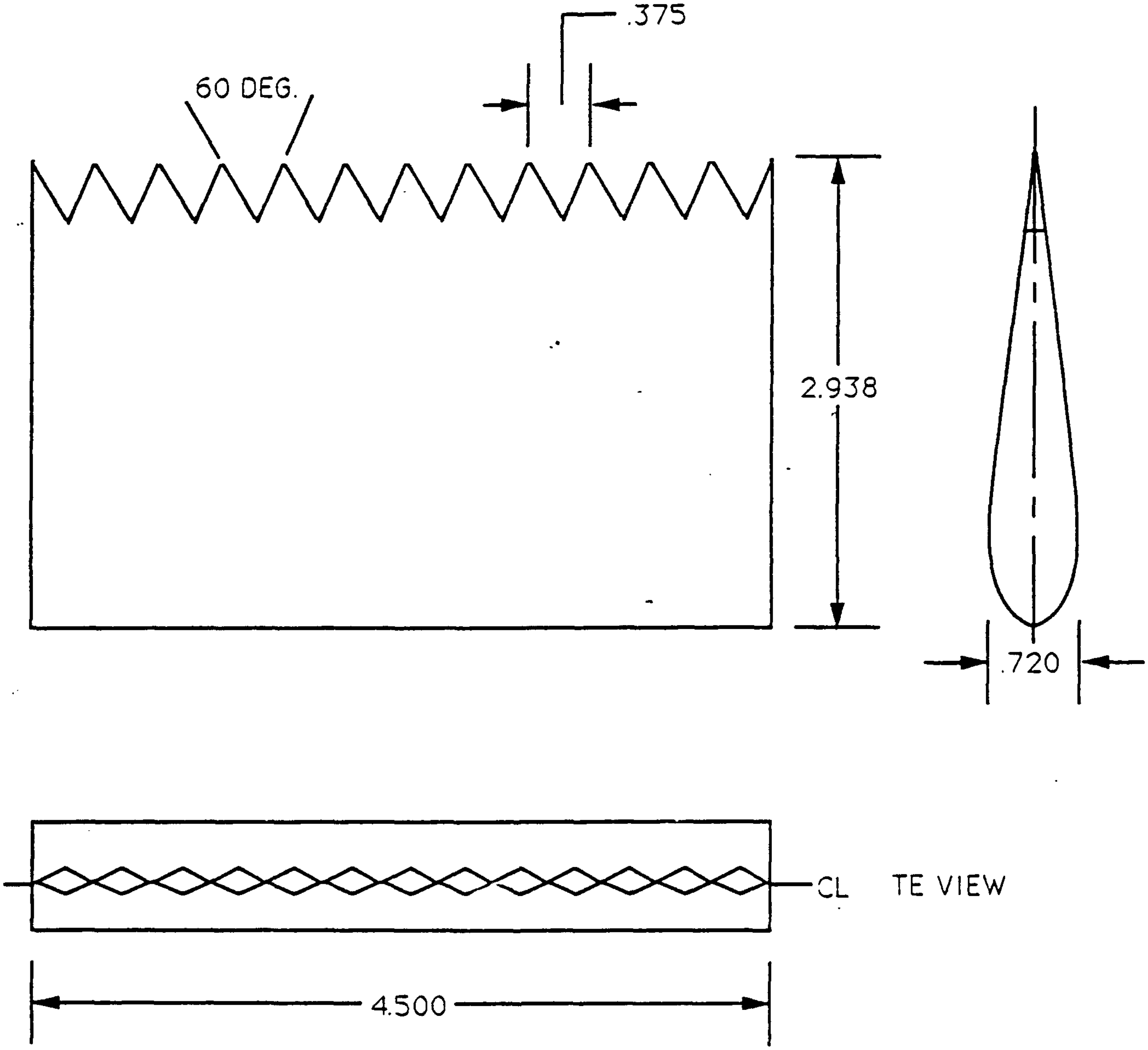

NOTE: ALL DIMENSIONS IN INCHES

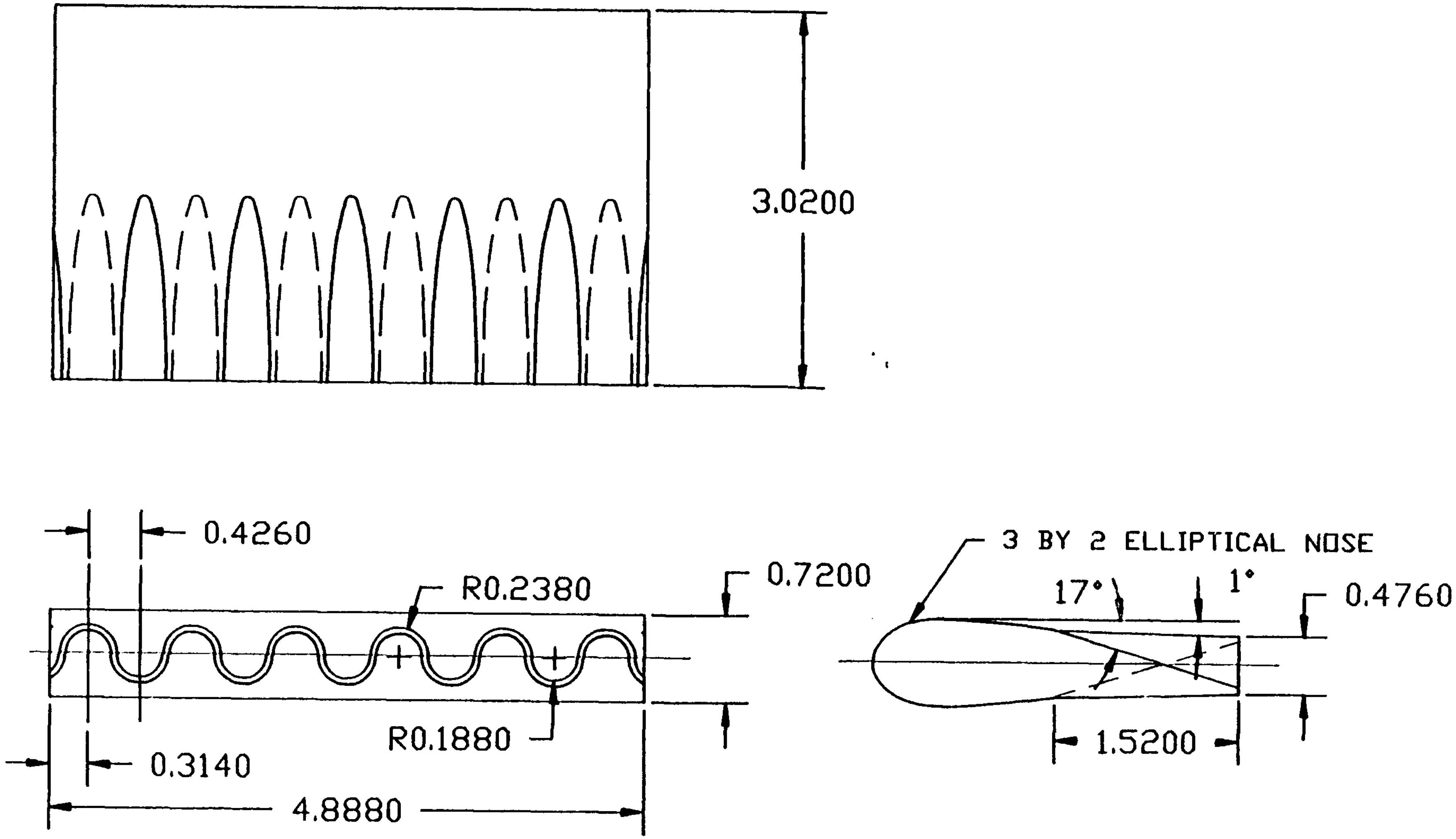

FIGURE 17: SRTE Wing

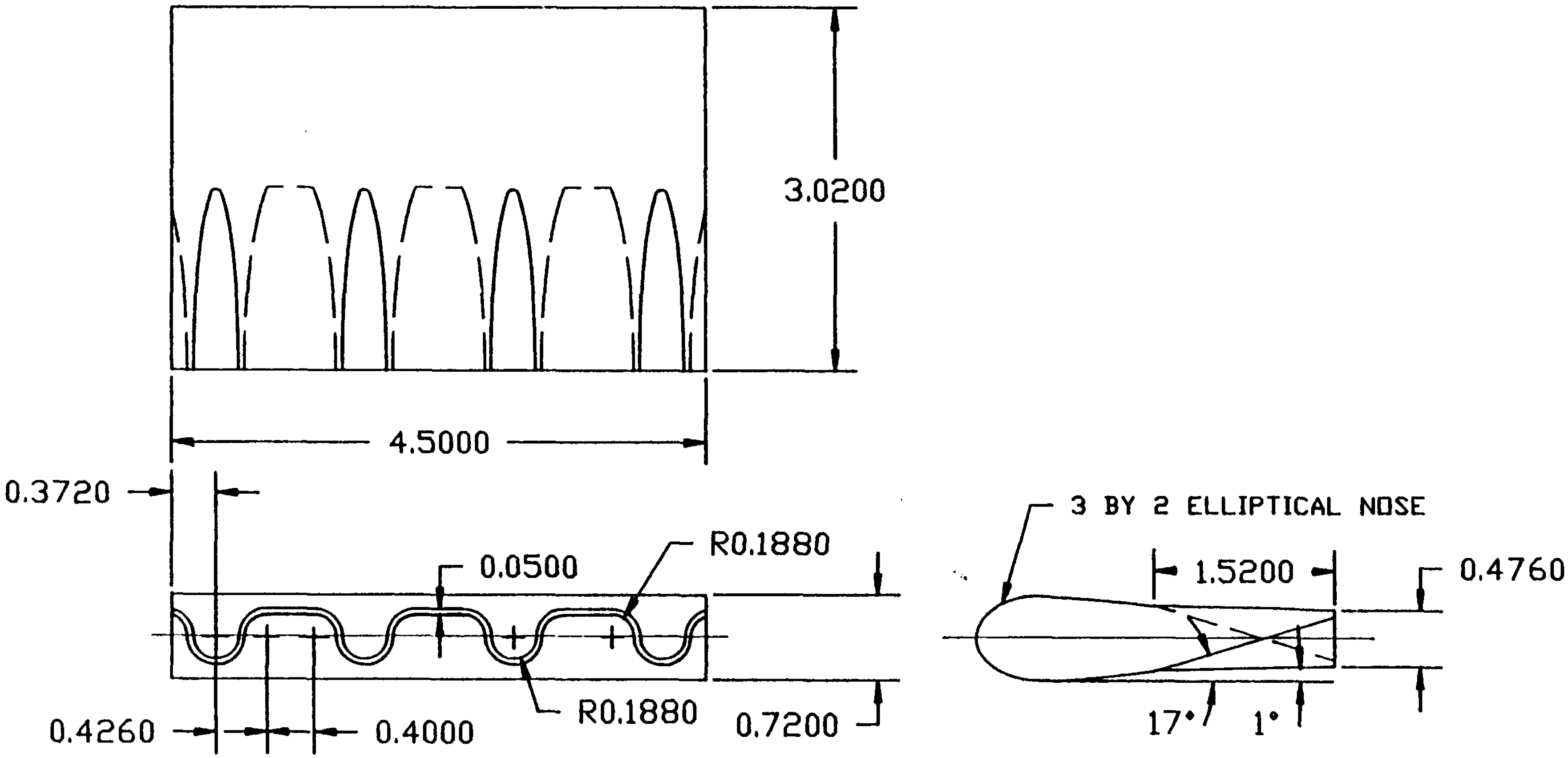

FIGURE 18: WRTE Wing

FIGURE 19: Baseline Wing

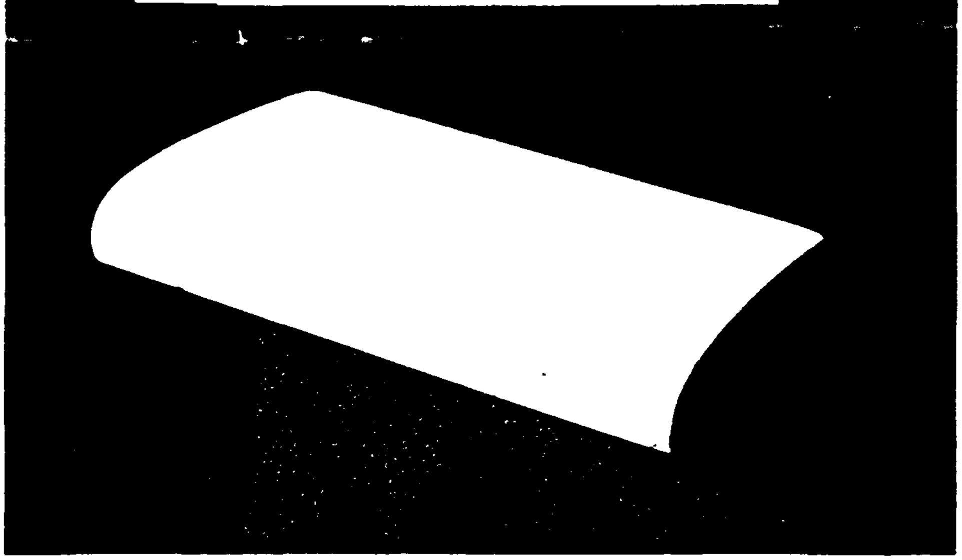

FIGURE 20: Venturi LE Wing

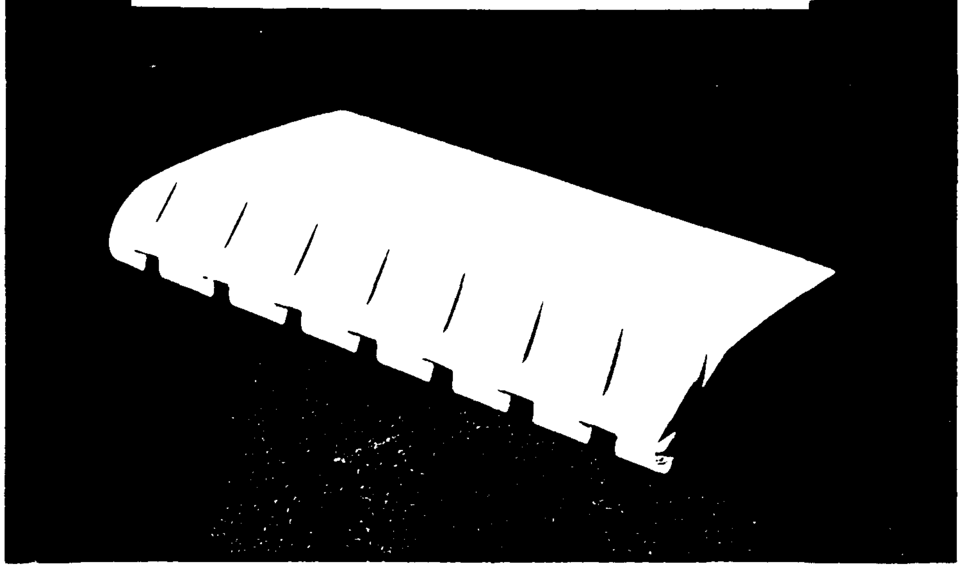

FIGURE 21: LE Groove Wing

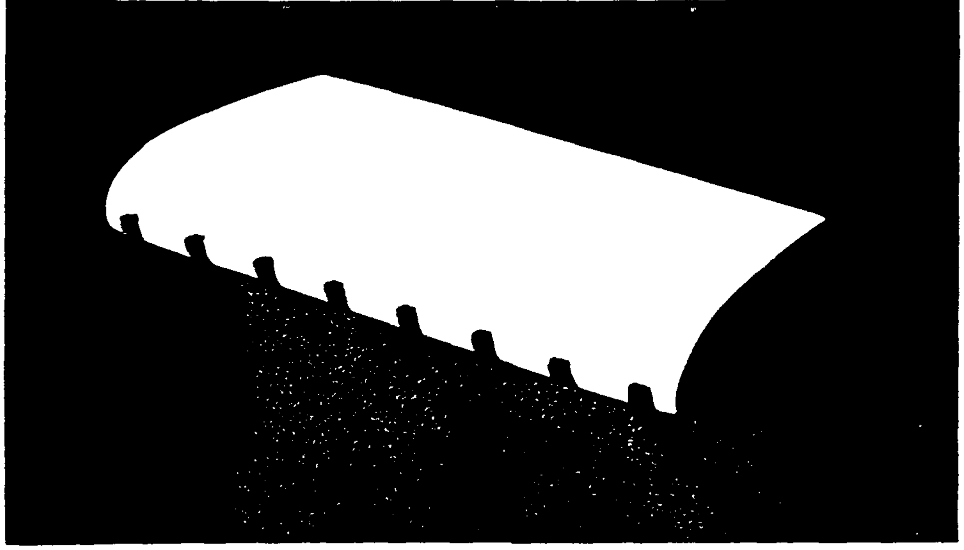

FIGURE 22: Long. Groove Wing

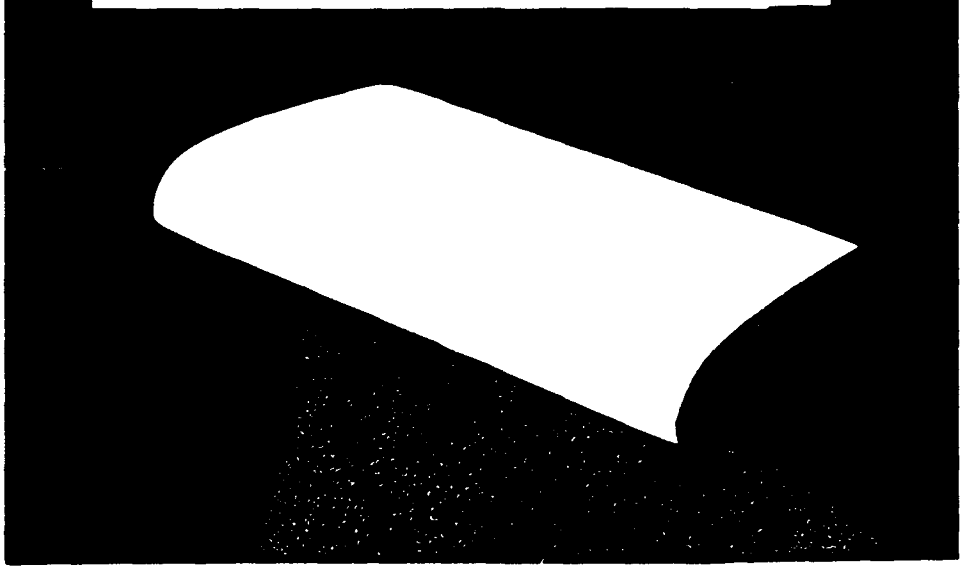

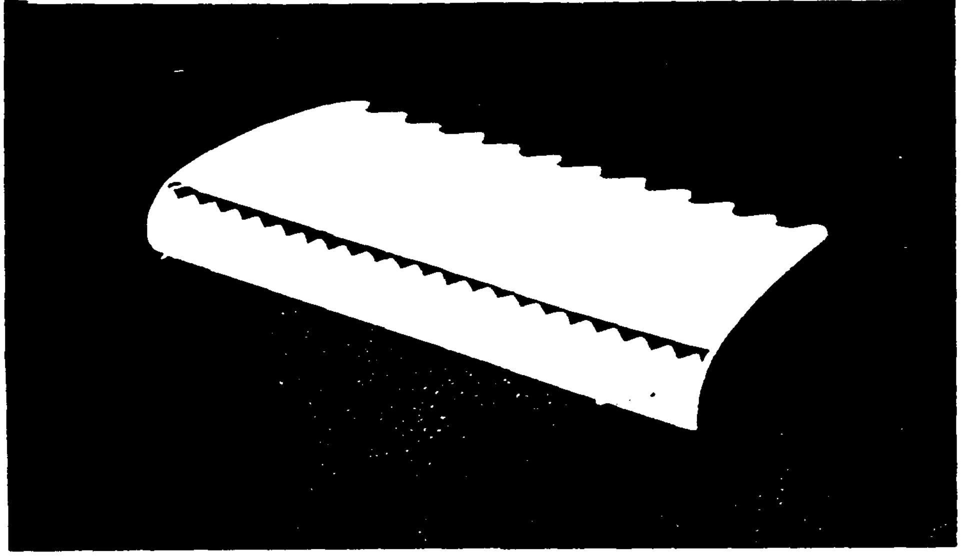

FIGURE 23: Triangular TE Wing (LE Trip)

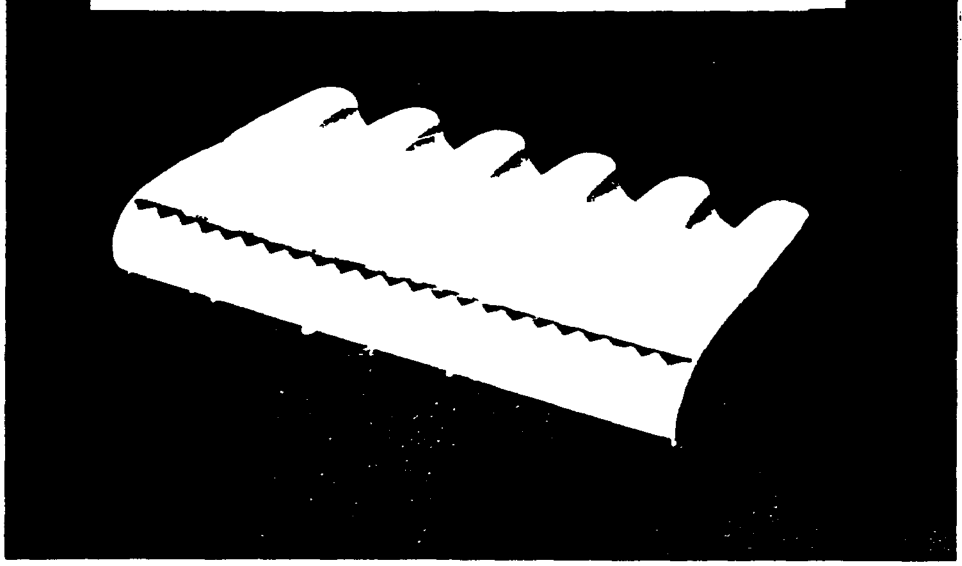

FIGURE 24: SRTE Wing (LE Trip)

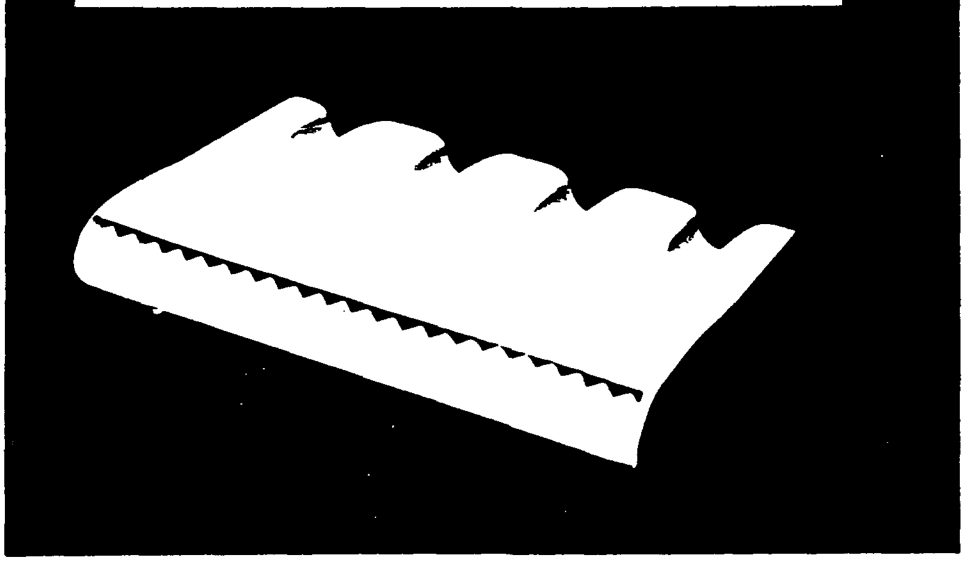

FIGURE 25: WRTE Wing (LE Trip)

layer trip. This trip was used on the baseline, WRTE, SRTE, and TTE wings to investigate turbulent flow effects on wing performance.

V.2. Test Facility

Wing models were tested in the small open circuit wind tunnel located in the mechanical engineering laboratory at Western New England College. The tunnel is shown in Figures 26 and 27. The tunnel has two 12 inch diameter test sections, one 18 inches long and the other 26 inches long. The 26 inch test section was used for velocity profile and traverse measurements, and the 18 inch test section was used with the mechanical lift/drag balance.

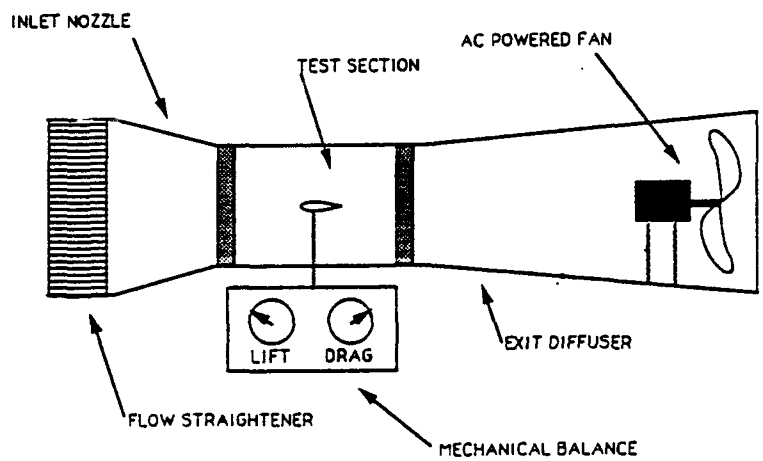

FIGURE 26: Wind Tunnel Schematic

The average test section velocity of this wind tunnel was 72 ft/s, with a maximum center velocity of 80 ft/s. The wind tunnel had a test section Reynolds Number of 4.5×10^6. Wing model Reynolds Numbers were 1.1×10^6.

Figure 28 shows a wing model mounted in the wind tunnel for lift and drag testing. The model support rod was capable of a full ±90° range of attack angles relative to vertical. Lift and drag balances had a measurement range of 0 to 1 lb.

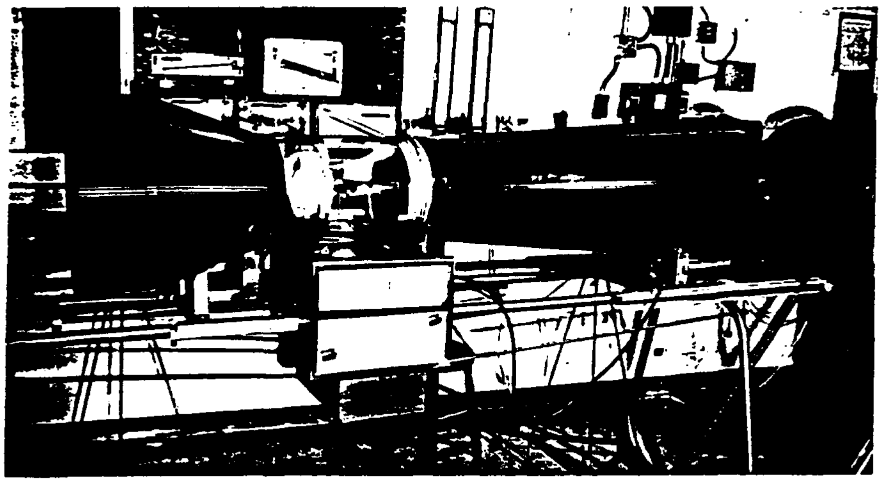

FIGURE 27: Small Wind Tunnel

V.3. Lift/Drag Testing

The mechanical lift/drag balance on the small wind tunnel was calibrated using standard balance weight components. Calibration data and information can be found in Appendix F. Following the calibration, each wing was tested in the wind tunnel as shown in Figure 28.

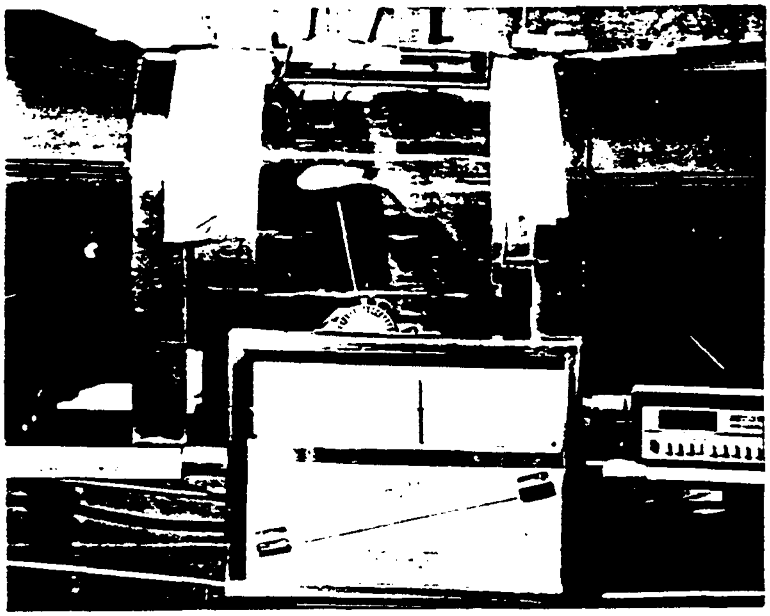

FIGURE 28:

Lift/Drag Testing

The drag polar for the baseline wing is shown in Figure 29. It can be seen that this wing stalls at a 14° angle of attack, with a maximum lift coefficient of 0.56 and a profile drag coefficient of 0.044. At stall, there was a 59% loss of lift and a corresponding 92% increase in drag.

Figure 30 shows the baseline wing polar again, the ideal polar curve, and the polar from the baseline wing with a foil boundary layer trip. This trip was used to better simulate the wing control surface on a submarine. The wind tunnel model Reynolds Number is much lower than the actual Reynolds Number on a submarine, so this trip was necessary to assure turbulent flow at the model scale. An explanation of the tripping device used can be found in Reference 16, on pages 30 to 33. The trip is 0.125 inches wide and has a serrated edge with 0.125 inch triangular teeth. The trip is located 0.10 inches from the leading edge of the wing along the chord.

BASELINE WING

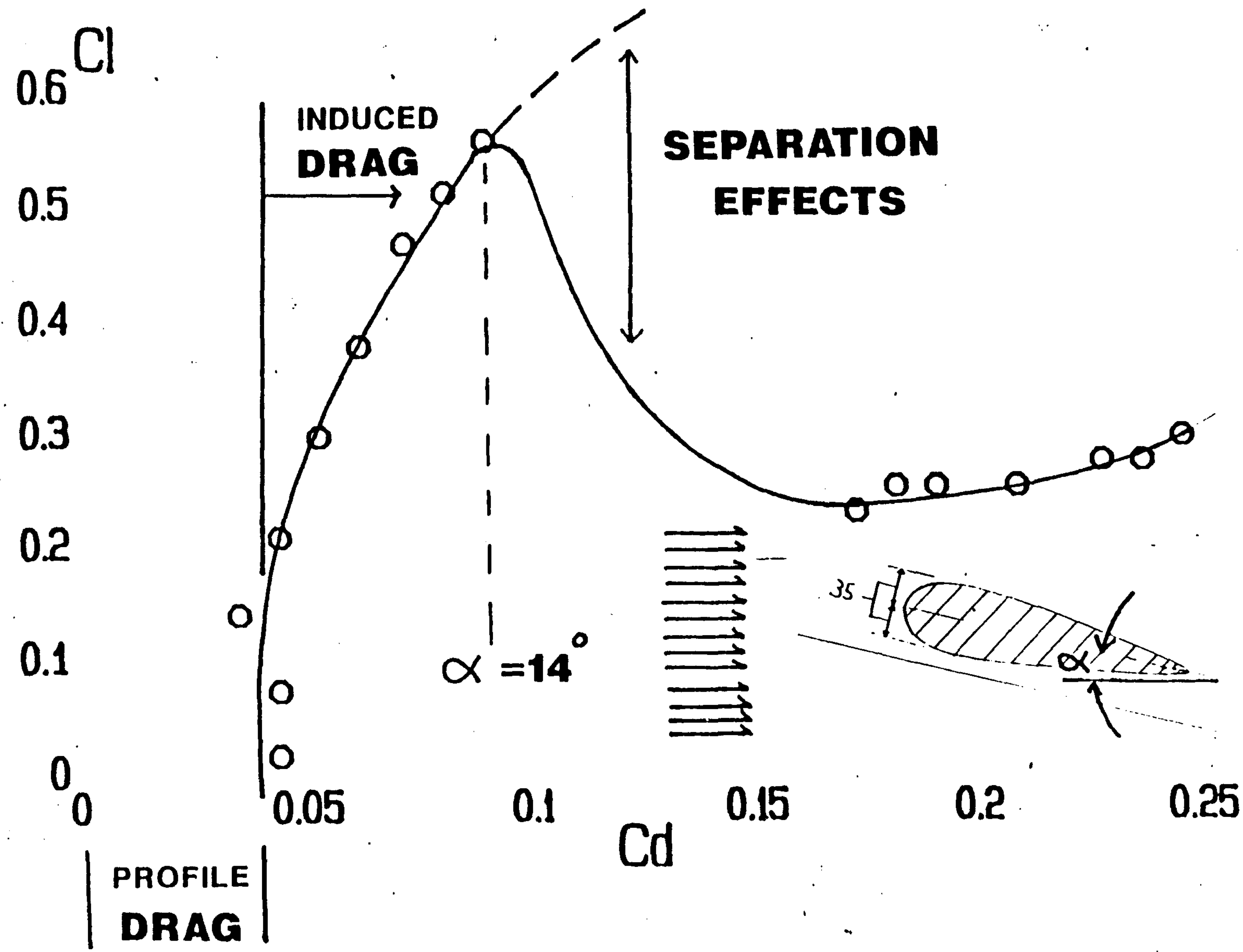

FIGURE 29:

TRIP EFFECTS ON LIFT/DRAG

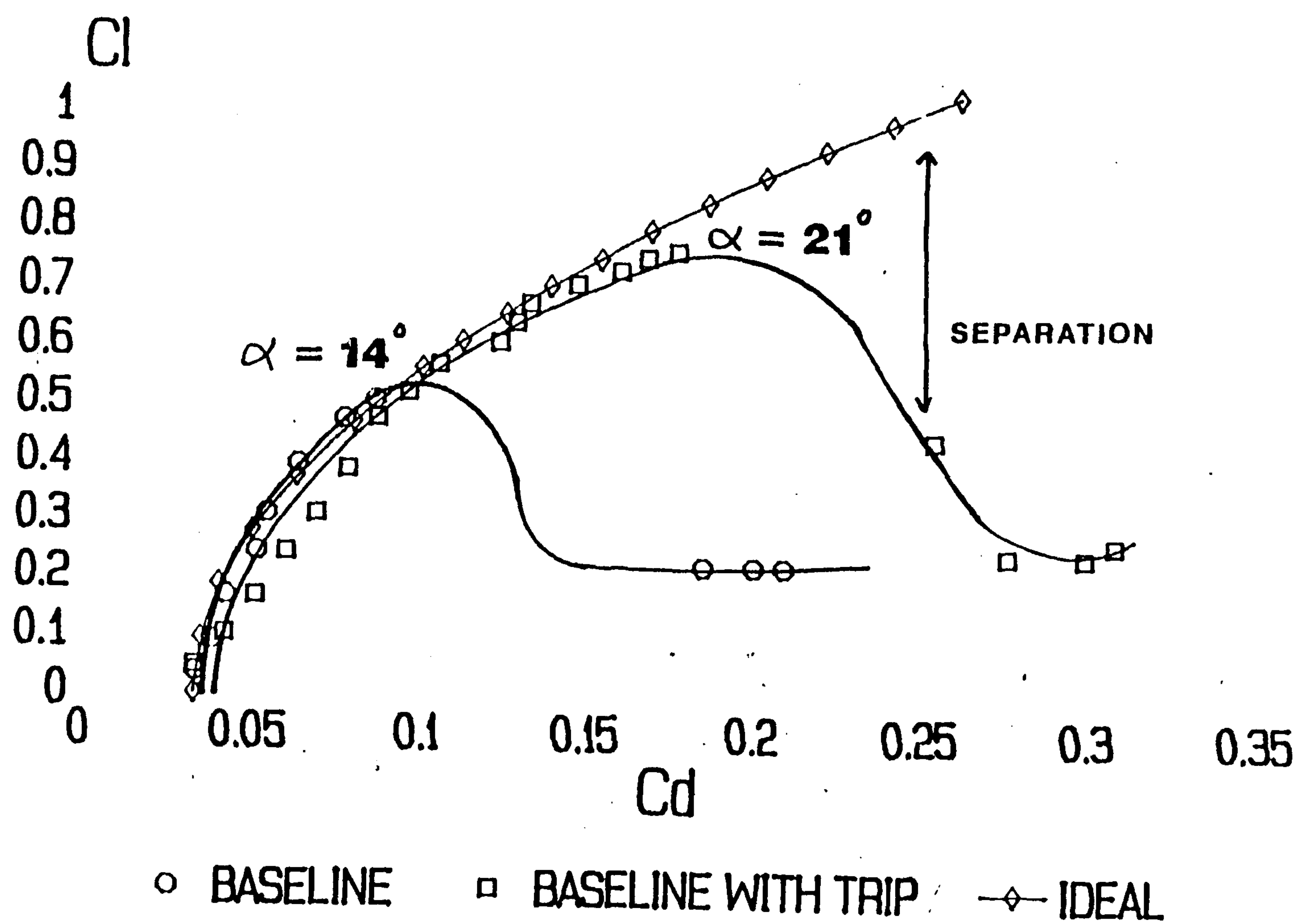

FIGURE 30:

Figure 30 shows that the tripped baseline wing stalls at a 21° angle of attack. In addition, its maximum lift coefficient was 37% higher than that of the baseline wing. There was also an improvement in profile drag due to the trip, which reduced profile drag by 23% to 0.034. However, there was still a large 68% loss of lift and a 44% increase in drag at the stall point.

In Figure 31, the leading edge groove wing drag polar shows a dramatic improvement in airfoil characteristics. The maximum lift coefficient of this wing was 0.65, a 17% increase over the baseline wing. In addition, the profile drag coefficient was reduced 60% to 0.017, and the stall angle increased 3° beyond the untripped baseline wing, to 17°. These improvements are due to the fact that leading edge grooves energize the fluid within the boundary layer of the flow around the wing. This leads to a delay in separation and a reduction in the profile and induced drag.

Also shown in Figure 31 is the drag polar for the longitudinal groove wing. The profile drag for this wing is 3% higher than that of the baseline wing, due to the fact that surface area, and thus skin friction, was increased by the addition of grooves. It is interesting to note that neither a maximum lift or a stall angle was found for this wing, though lift leveled of to a C_L=0.417 past 18°. A look at the curve for this wing shows that the longitudinal groove pattern provided stability over a wide range of angles of attack.

Figure 32 shows the drag polar of the venturi leading

DRAG POLARS

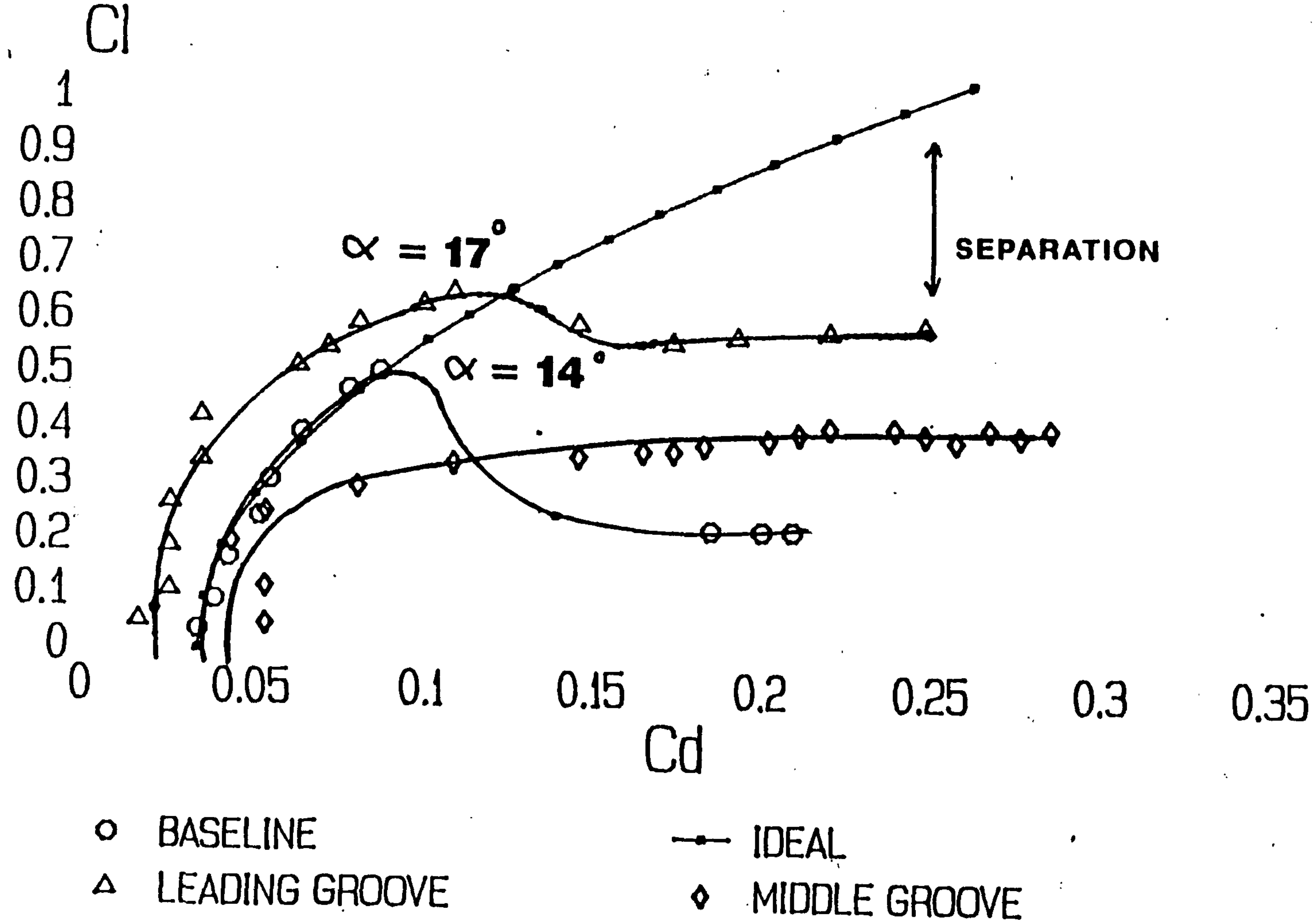

LEADING EDGE GROOVES SHOW A DRAG BENEFIT

FIGURE 31:

VENTURI GROOVE DECREASES STALL EFFECT

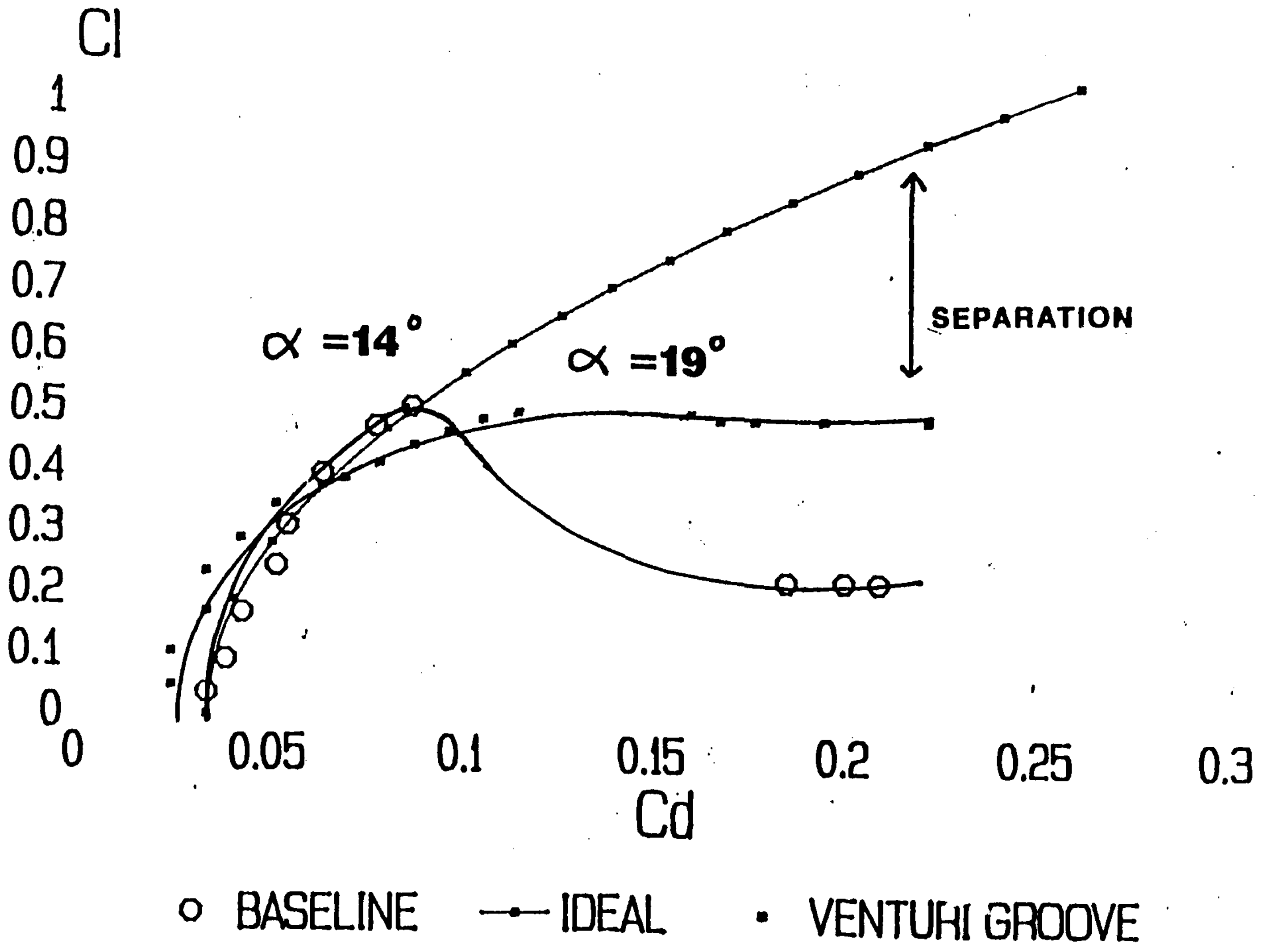

FIGURE 32:

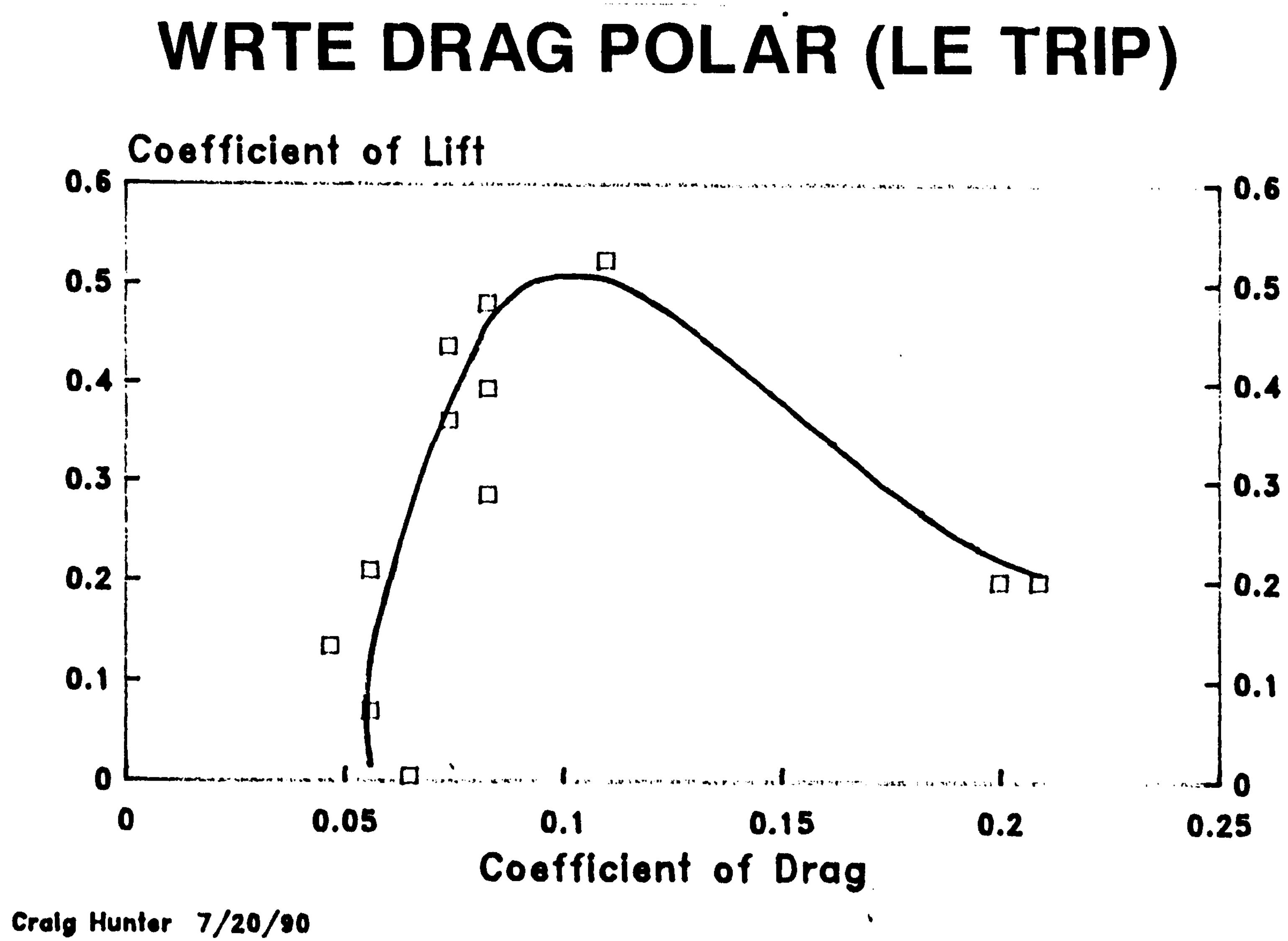
WRTE DRAG POLAR (LE TRIP)
Coefficient of Lift
0.6
0.5
0.4
0.3
0.2
0.1
0
0
0.05
0.1
0.15
0.2
0.25
Coefficient of Drag
Craig Hunter 7/20/90

FIGURE 33:

edge wing. Like other leading edge grooves, the venturi grooves energize the fluid within the boundary layer, delaying separation and lowering profile drag. This particular wing did not stall until a 19° angle of attack, 5° higher than baseline. In addition, its profile drag was 0.025, 43% less than baseline. Unfortunately, this wing suffered a 10% loss in maximum lift when compared to the baseline.

Wings with trailing edge modifications, while superior in reducing wakes, did not produce any improvements in lift, drag, or stall. Figure 33 shows the drag polars for the tripped WRTE wing. This wing was the closest in performance to the baseline wing. The WRTE trip wing stalled at 14°, had a maximum C_L=0.51, and a profile C_D=0.055. The WRTE trip wing had a 25% higher profile drag coefficient, and a 1% decrease in lift compared to the baseline. Other trailing edge modified wings showed a similar lack of improvement.

It is important to note that all wings had parabolic curves that followed the same pattern as the ideal curve up to the stall point. Additional drag polars can be found in Appendix G along with lift and drag plots. A summary of major facts for lift and drag data is shown in Table 1.

In summary, the balance lift/drag data indicated that the baseline wing model stalled early due to laminar flow. This laminar flow was a result of the low Reynolds Number, sub scale testing. Boundary layer trips eliminated this laminar separation problem, and provided a better simulation

Table 1: Summary of Lift/Drag Data

Wing	Stall Angle, deg.	Maximum Lift (Cl)	Profile Drag (Cd)
Baseline	14.0	0.560	0.044
Baseline Trip	21.0	0.760	0.034
Long. Groove	Never Reached	0.410	0.045
LE Groove	17.0	0.650	0.017
Venturi LE	19.0	0.500	0.025
Triangular TE	12.0	0.450	0.053
Tri. TE Trip	13.6	0.460	0.070
WRTE	13.0	0.480	0.030
WRTE Trip	14.0	0.510	0.055
SRTE	11.0	0.410	0.025
SRTE Trip	12.0	0.380	0.075

of the actual submarine control surface flowfield. None of the wing modifications increased the stall angle beyond that of the tripped baseline wing. Both leading edge grooves and midspan grooves decreased the loss in lift occurring with stall, but these modifications both resulted in earlier stall angles. The leading edge grooved contour did show a significant decrease in drag over the entire range of parameters tested when compared to the baseline airfoil.

V.4. Mid Span Wake Measurements

A 1/16 inch O.D. pitot-static pressure probe was used to obtain the velocity profile data behind the wings. The probe was mounted in a probe stand which could be moved in position downstream of the wing. Output from the probe fed into two large block manometers. Velocity profiles were taken in the midspan plane at four different axial locations behind each wing. Figure 34 shows a sketch of the test setup.

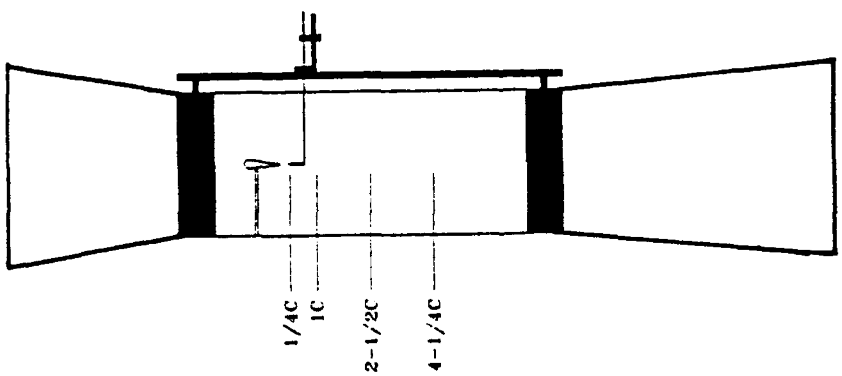

FIGURE 34: Mid Span Traverse Setup

Velocity Profiles of the baseline wing are shown in

VELOCITY PROFILES BEHIND WING
BASELINE WING

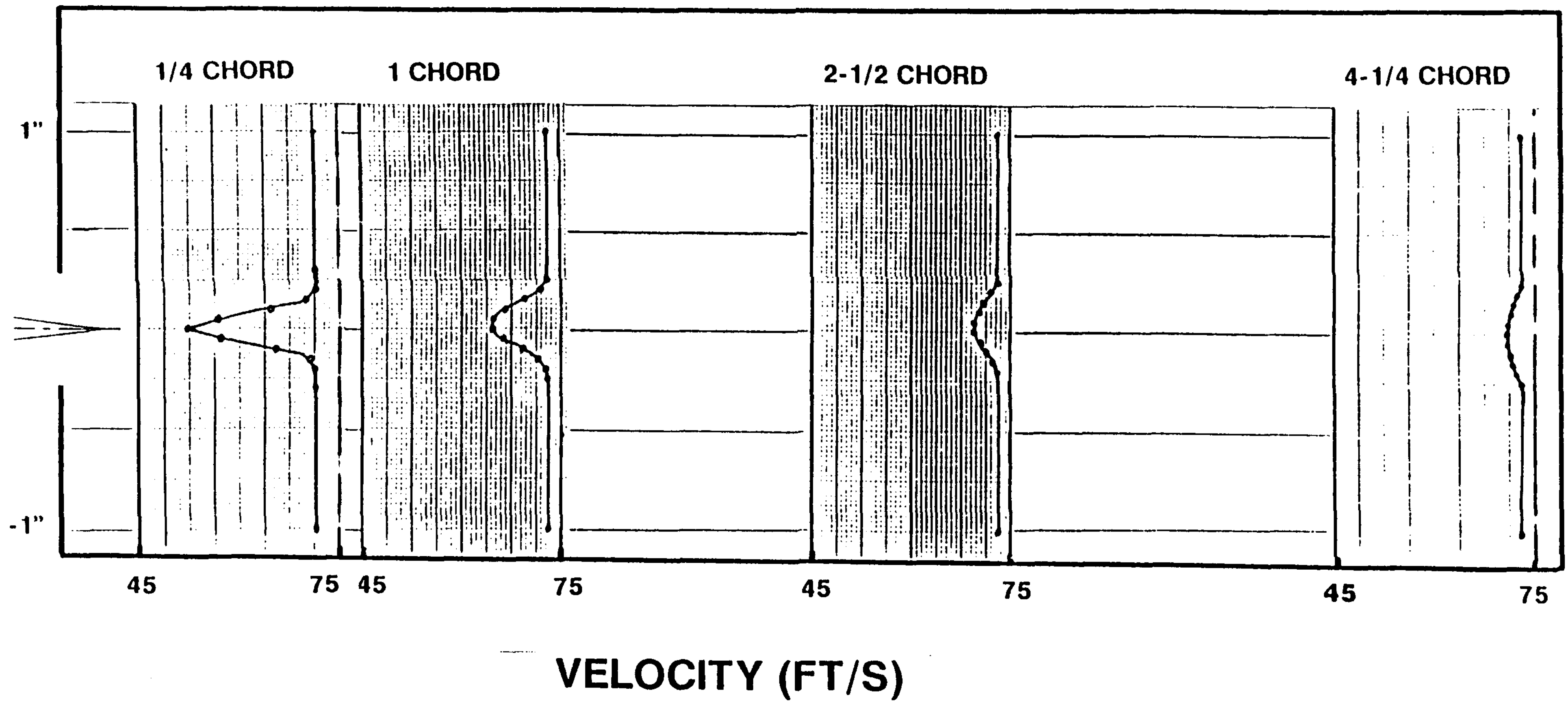

FIGURE 35:

VELOCITY PROFILES BEHIND WING
TRIANGULAR TRAILING EDGE WING

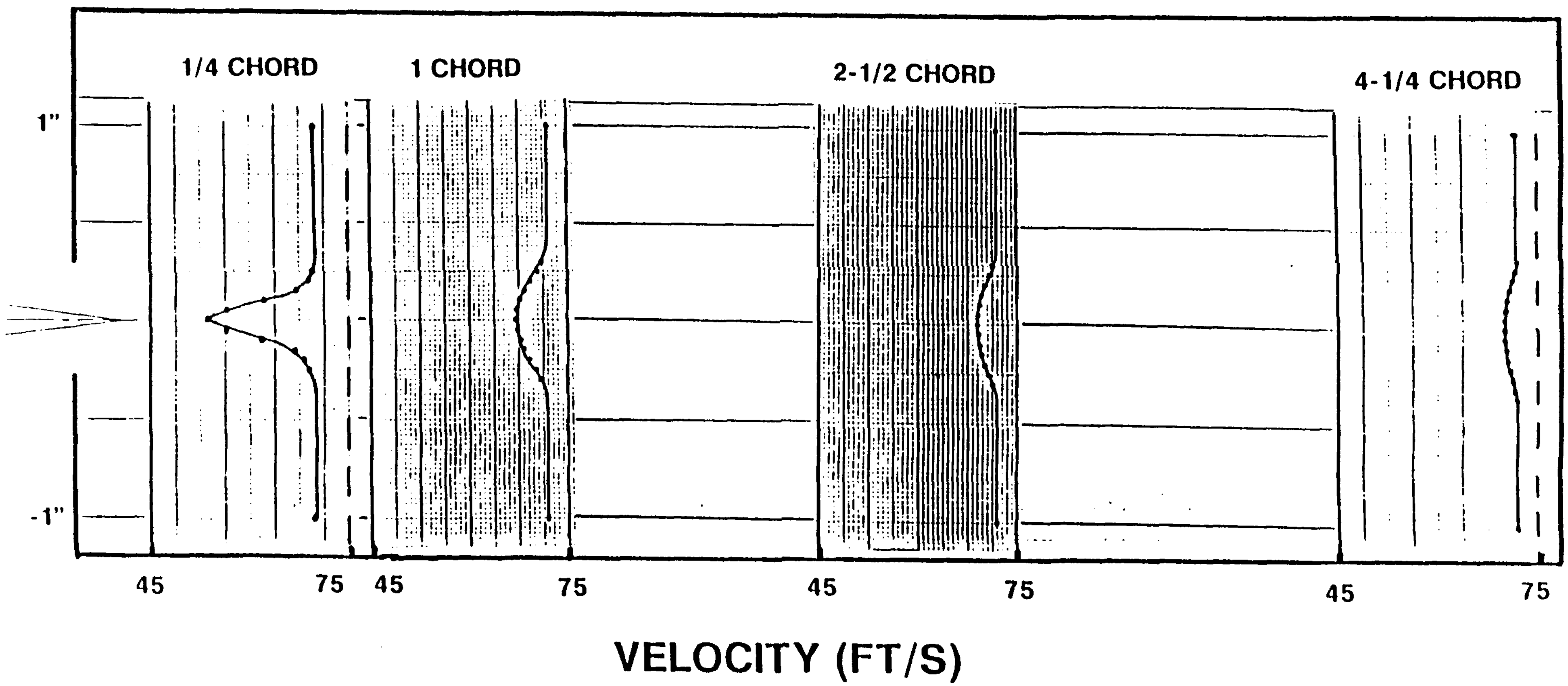

FIGURE 36:

Figure 35. As the wake travels down the flow field, two things happen. First, the width of the wake increases. For example, the the wake width at 1/4 chord downstream of the wing's trailing edge is 0.3 inches but increases to 1.1 inches at a location 4-1/4 chords downstream. The second observation from Figure 35 is that the wake intensity is decreasing as the wake travels down the flow field. At the 1/4 chord position, the center line velocity is 52.5 ft/s. At the 4-1/4 chord position, the center line velocity increased to 71 ft/s, indicating a decrease in wake intensity.

The best wake decay improvement was obtained from the triangular trailing edge wing, as shown in Figure 36. At each position behind the wing, the wake width is wider and the wake intensity less than that of the baseline wing. For example, at the 1 chord location downstream, the baseline wing has a center line velocity of 64.8 ft/s. The TTE wing center line velocity is 3% greater, at 66.9 ft/s. In addition, the baseline wake width at the 1 chord position is 0.55 inches while the TTE wake is 82% wider, 1 inch, at the same location. This indicates that the wake is dissapating sooner for the TTE wing.

Wings with leading edge modifications had wake decay patterns similar to that of the venturi leading edge wing, shown in Figure 37. The wake dispersion width of this wing was greater than that of the baseline wing, but its wake velocities were lower. At the 4-1/4 chord position, the venturi leading edge wing had a wake almost twice as wide as

VELOCITY PROFILES BEHIND WING
VENTURI LEADING EDGE WING

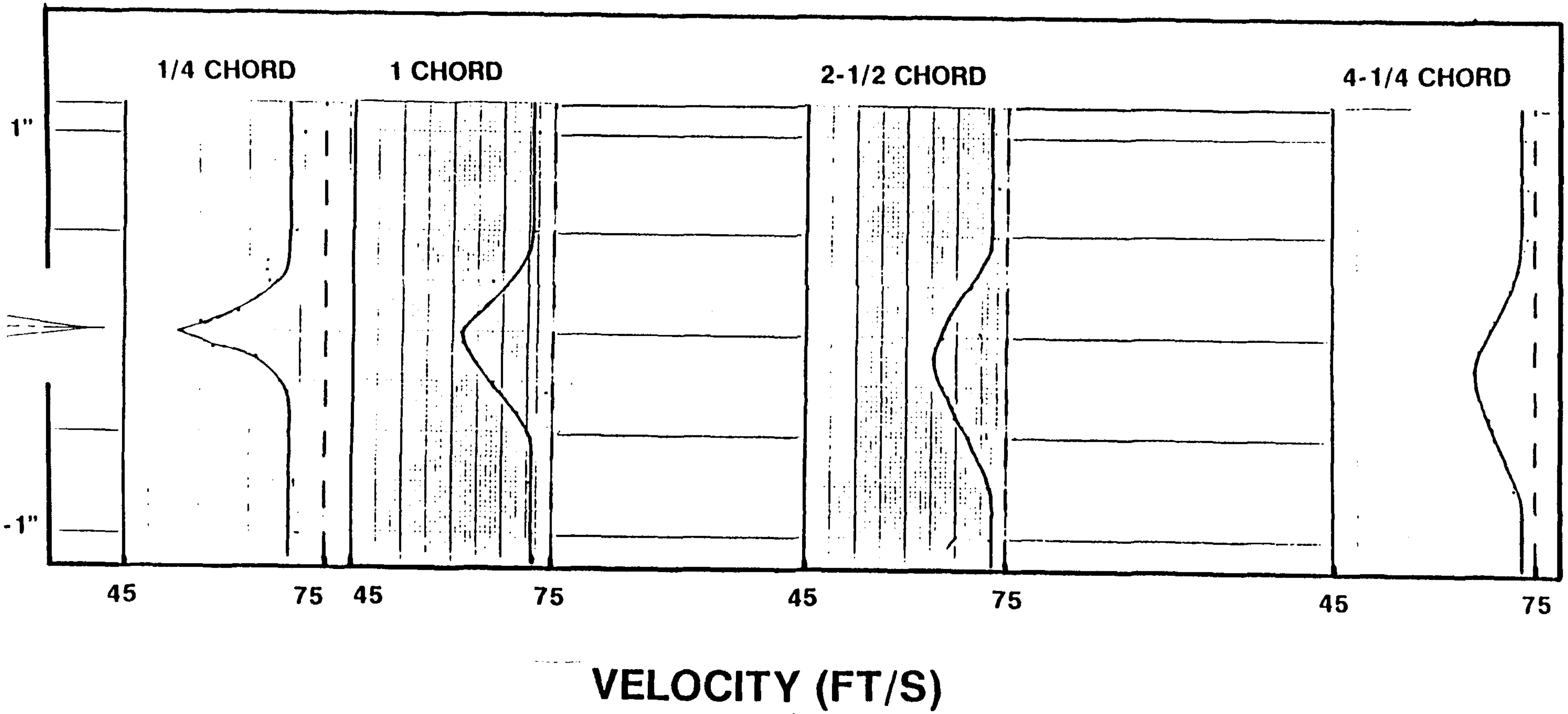

FIGURE 37:

VELOCITY PROFILES BEHIND WING
WIDE RIPPLED TRAILING EDGE WING

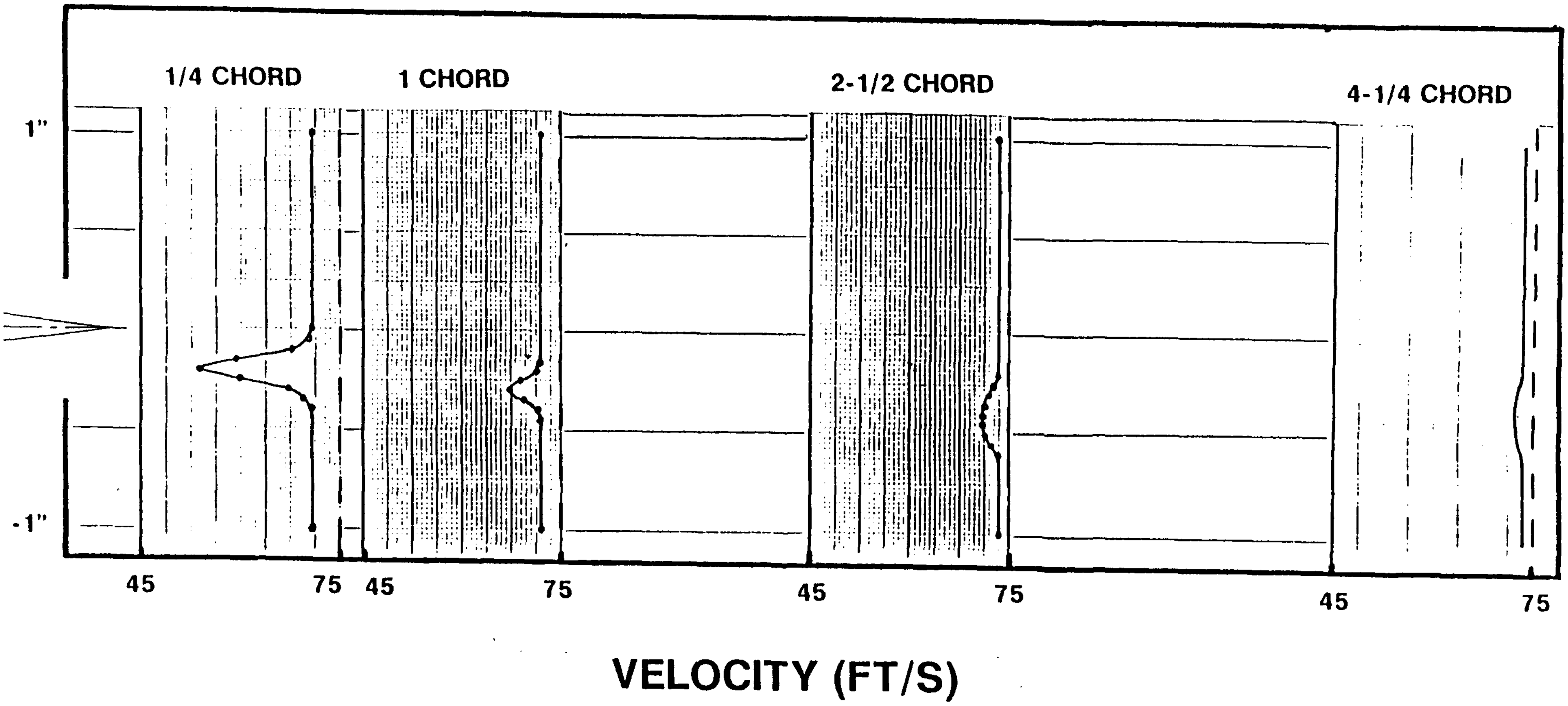

FIGURE 38:

the baseline wing, but its minimum velocity was 6 ft/s lower than the baseline.

Rippled trailing edge wings had wake center span decay patterns like those of the wide rippled trailing edge wing, shown in Figure 38. On these wings, the wake velocities were higher than the baseline, but wake widths were lower. For example, at the 4-1/4 chord position, the WRTE wing had a minimum velocity 3 ft/s higher than the baseline, but its wake width was 20% smaller.

These results caused considerable concern. It was also noticed that the centerspan wake deficit convected downward with axial distance downstream of the wing trailing edge. These two results indicated the possibility that the wake was moving due to secondary flows, or streamwise vorticity, generated by the lobe contours. For this reason, a decision was made to conduct complete planar traverses at several axial locations downstream of the airfoil trailing edge. Results of these traverses are presented in the next section.

All wake decay data was compared to two dimensional relationships developed in the analytical section. Figure 39 presents wake width plotted against the square root of the distance from the trailing edge of the wing for all configurations tested. All data is seen to generate straight lines consistent with theory.

The venturi leading edge airfoil showed a displacement effect from the origin, indicating a large loss phenomena. This result is consistent with the large drags measured for this wing. The triangular trailing edge airfoil is seen to

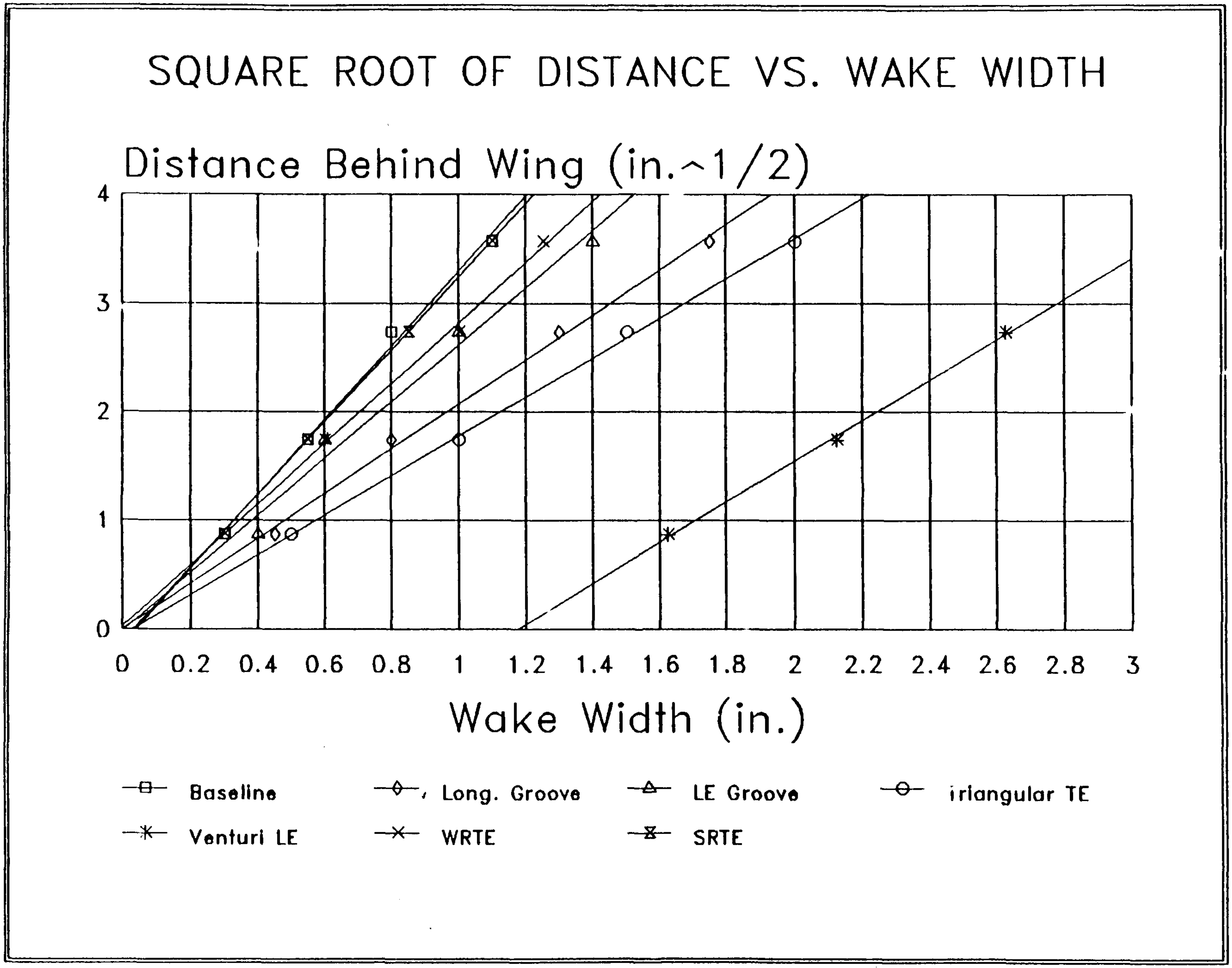
SQUARE ROOT OF DISTANCE VS. WAKE WIDTH
Distance Behind Wing (in.^1/2)
0
1
2
3
4
0
0.2
0.4
0.6
0.8
1
1.2
1.4
1.6
1.8
2
2.2
2.4
2.6
2.8
3
Wake Width (in.)
Baseline
Long. Groove
LE Groove
iriangular TE
Venturi LE
WRTE
SRTE

FIGURE 39:

provide the most rapid mixing of the midspan wake.

Wake decay results for the other wings tested can be found in Appendix D.

V.5. Wake Traverse Plane Measurements

Downstream traverse tests were performed using an automated data acquisition system, diagrammed in Figure 40. A pitot-static probe measured pressures over a 2 inch by four inch grid area downstream of the wing. The traverse plane and wing location is shown in Figure 41. All traverse tests were performed with wings at a ten degree angle of attack, and planes were located 1/4 chord, 1 chord, and 1-1/2 chords downstream of the wings trailing edge. See Figure 42 for an illustration of the traverse test setup on the small wind tunnel.

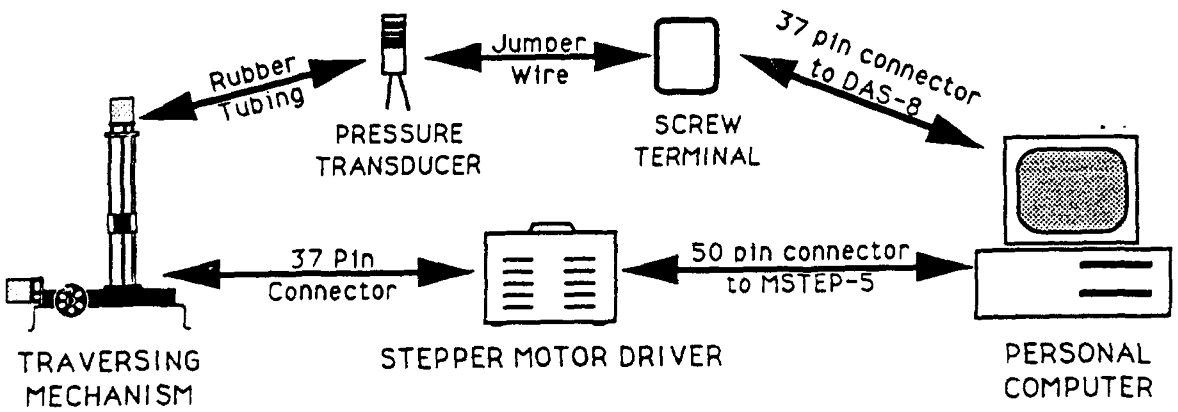

FIGURE 40: Data Acquisition System

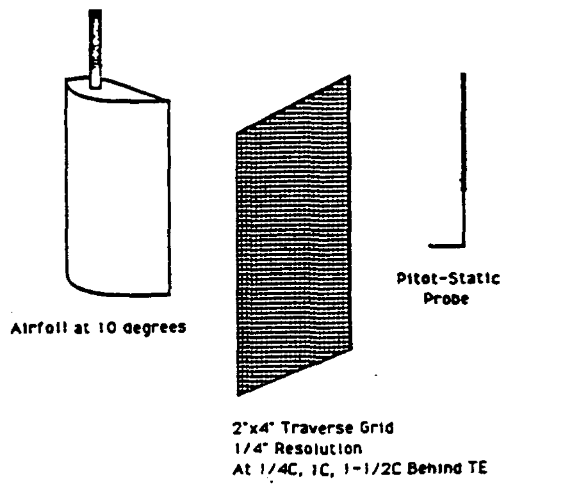

FIGURE 41: Traverse Plane

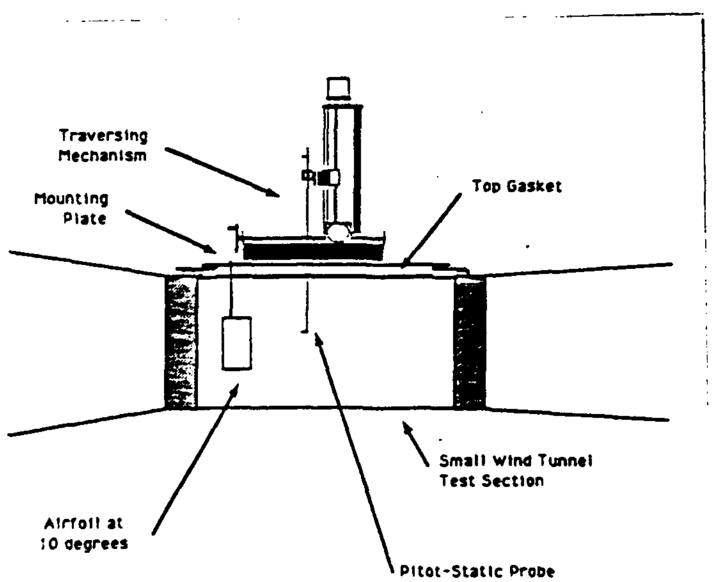

FIGURE 42: Traverse Setup

The pressure probe was located by a stepper motor driven traversing mechanism, shown in Figures 43 and 44. The pressure reading recorded by the probe was sent to a differential pressure transducer and passed electrically to an analog to digital converter board on a personal computer. Calculations were made to convert the pressure reading to a velocity. The computer then prompted the traversing mechanism to move the probe to its next location.

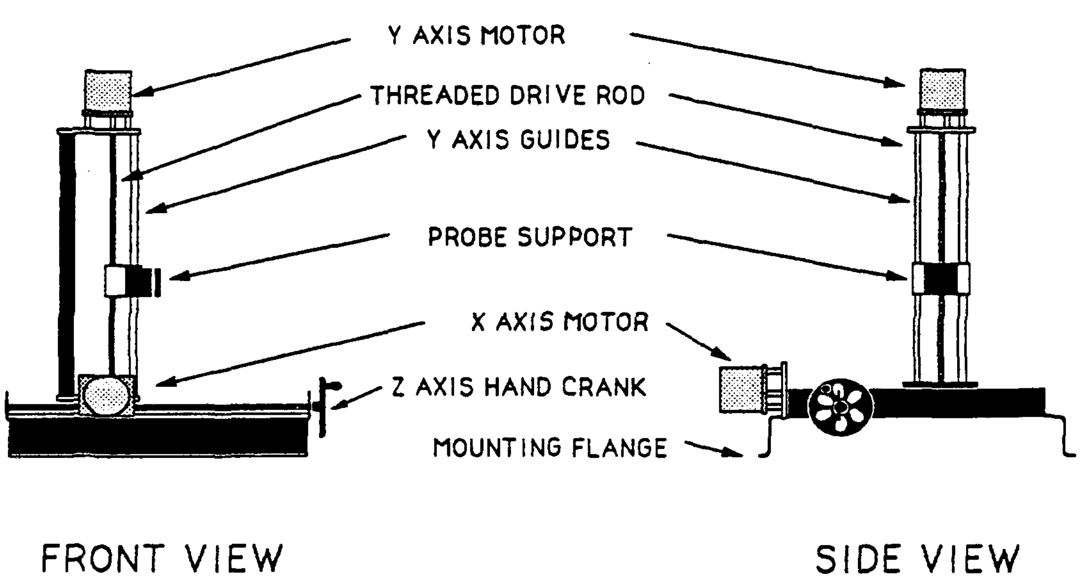

FIGURE 43: Traverse Mechanism

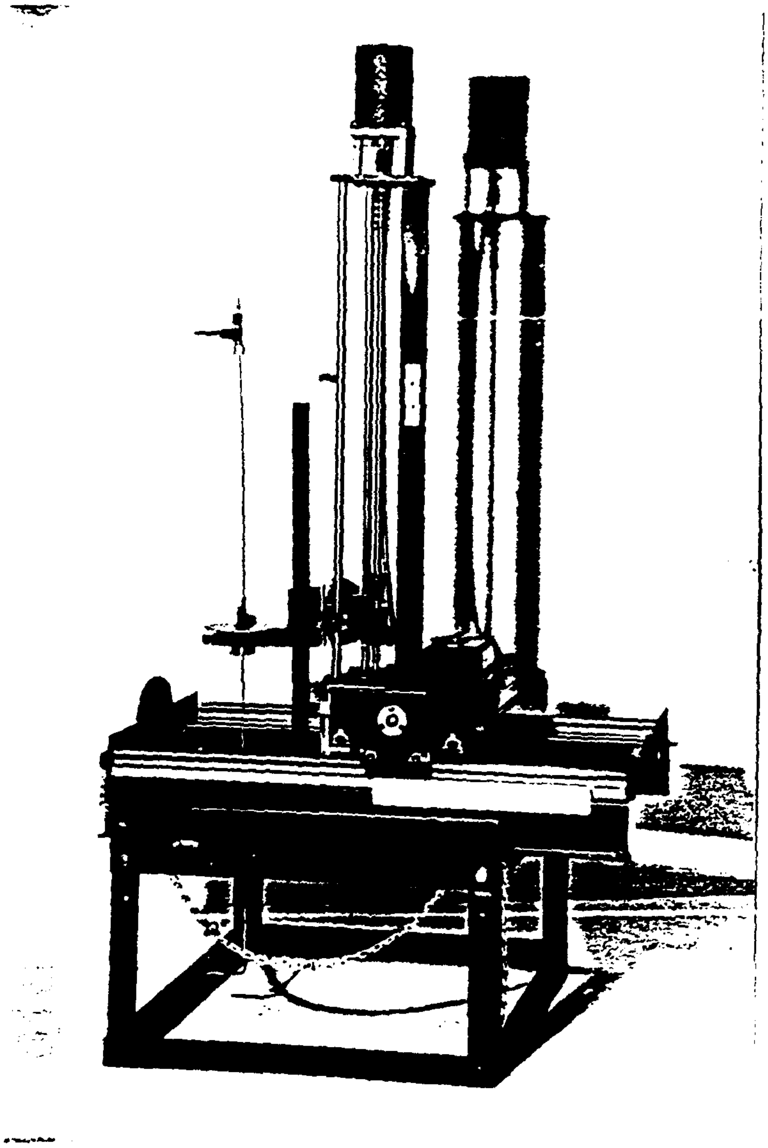

FIGURE 44: Traversing Mechanism

Figures 45 through 47 show the non-dimensionalized velocity contours obtained in the baseline wing traverse test. The 1/4 chord plot shown in Figure 46 shows a large wake deficit region and an intense wing tip vortex, both composed of low velocity fluid. 1 chord and 1-1/2 chord plots in Figures 47 and 48 show that the wake decayed to higher velocities, but the wing tip vortices were still quite intense. It is important to note that baseline test results show strong agreement with results obtained in Reference 1.

Adding a leading edge trip to the baseline wing widened the wake region at all downstream locations, yet wake velocities remained essentially the same as the untripped wing. Wingtip vortices also remained unaffected. Comparison plots for the tripped baseline wing are shown in Figures 48 through 50.

Velocity contours for the triangular trailing edge wing are shown in Figures 51 through 53. This was the best wake reducing wing tested with TE modifications. is immediately evident that the wake and tip vortex deficits are spread out and less intense at the 1/4 chord location when compared to the baseline wing. When comparing 1 chord and 1-1/2 chord plots of the baseline and TTE wings, it can be seen that the wakes of the TTE wing decayed much faster and decayed to higher velocities. In fact, by 1-1/2 chords downstream, the wake deficits and tip vortices of the TTE wing are almost completely mixed out.

Rippled trailing edge wings also had mixed out wakes, shown by the WRTE wing contour plots in Figures 54 through

Baseline Wing L=1/4C

Wake Patterns

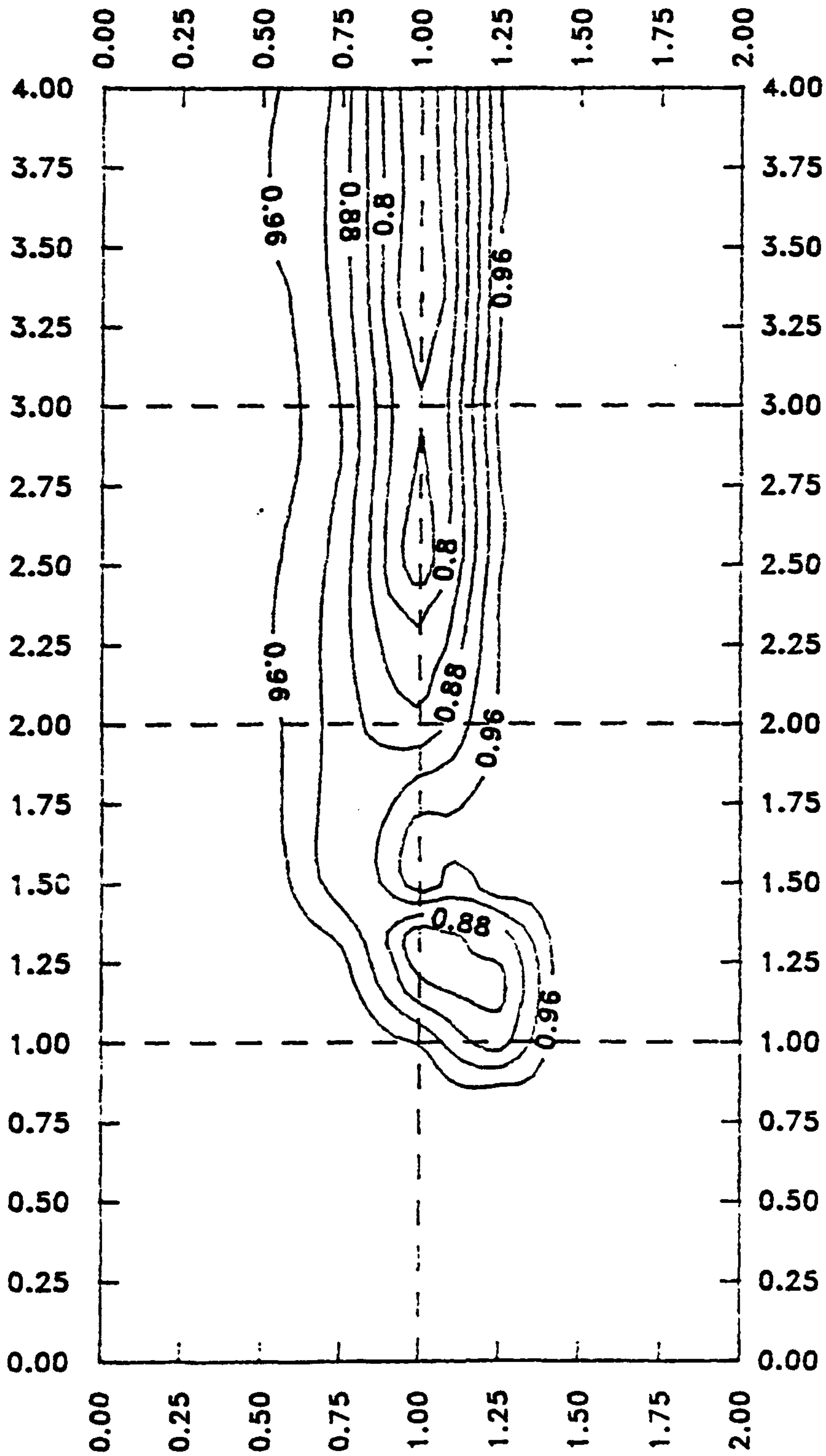

TRAVERSE PLANE SCALED IN INCHES
WINGTIP AT 1,1
VELOCITIES NON-DIMENSIONALIZED BY $u_{INFINITY}$

FIGURE 45:

Baseline Wing L=1C

Wake Patterns

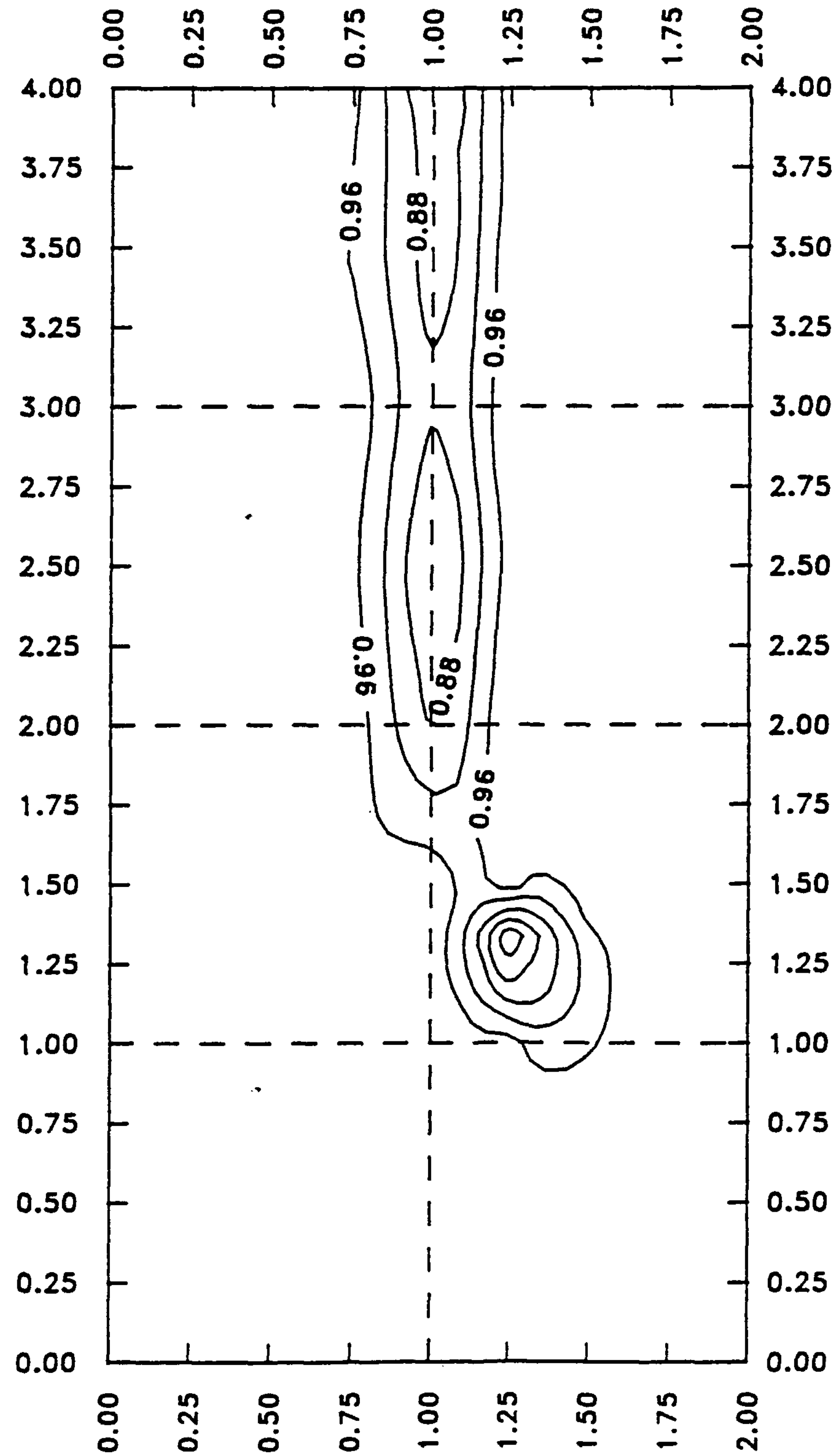

TRAVERSE PLANE SCALED IN INCHES
WINGTIP AT 1,1
VELOCITIES NON-DIMENSIONALIZED BY $u_{INFINITY}$

FIGURE 46:

Baseline Wing L=1.5C

Wake Patterns

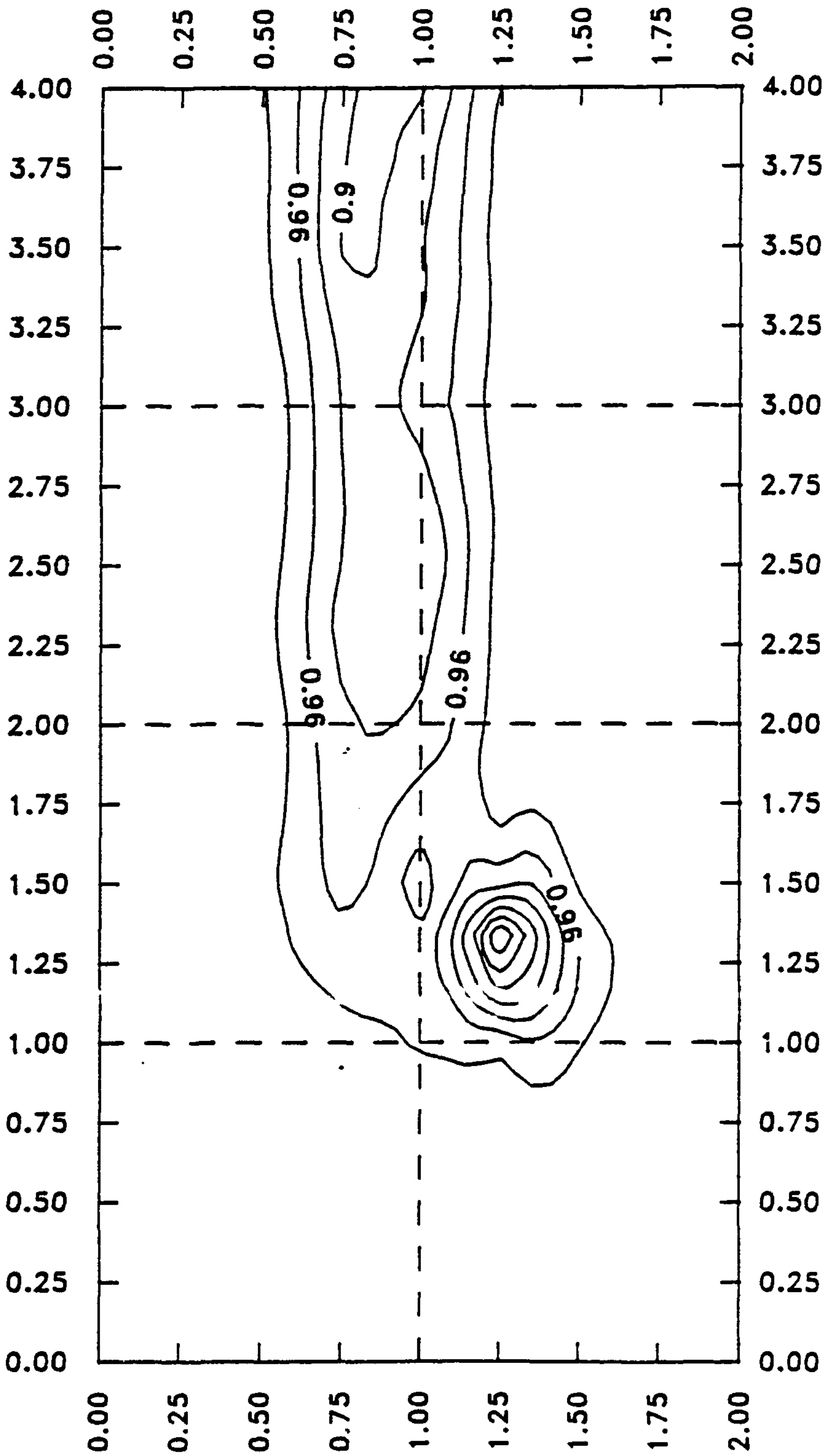

TRAVERSE PLANE SCALED IN INCHES
WINGTIP AT 1,1
VELOCITIES NON-DIMENSIONALIZED BY $u_{INFINITY}$

FIGURE 47:

Baseline Trip Wing L=1/4C

Wake Patterns

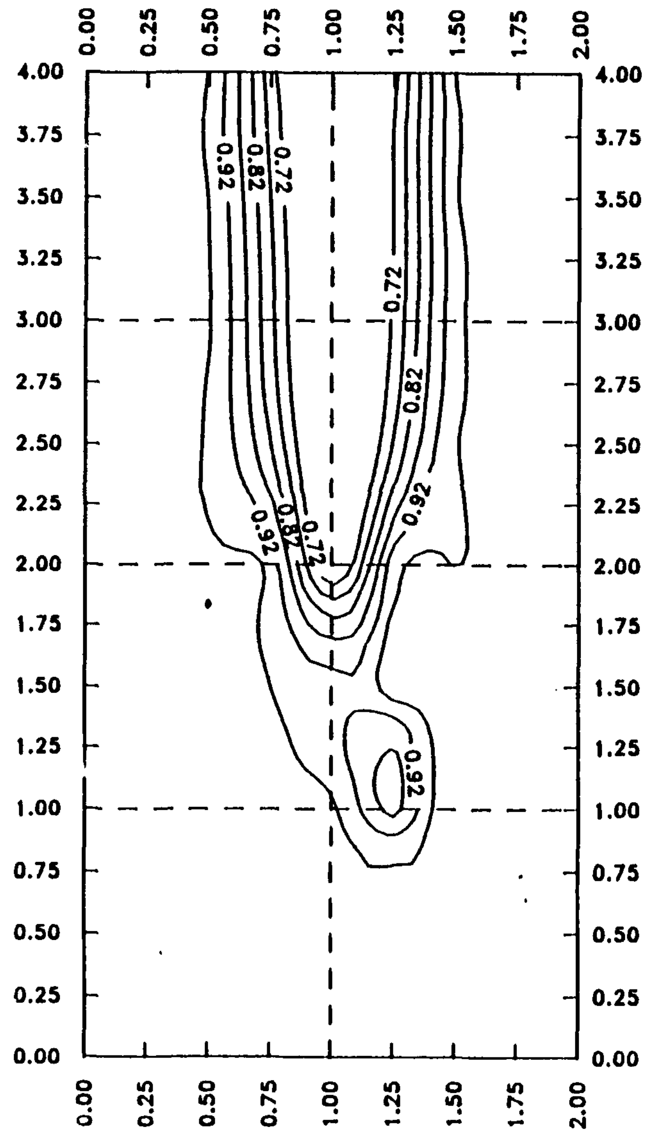

TRAVERSE PLANE SCALED IN INCHES
WINGTIP AT 1,1
VELOCITIES NON-DIMENSIONALIZED BY $u_{INFINITY}$

Baseline Wing L=1/4C

Wake Patterns

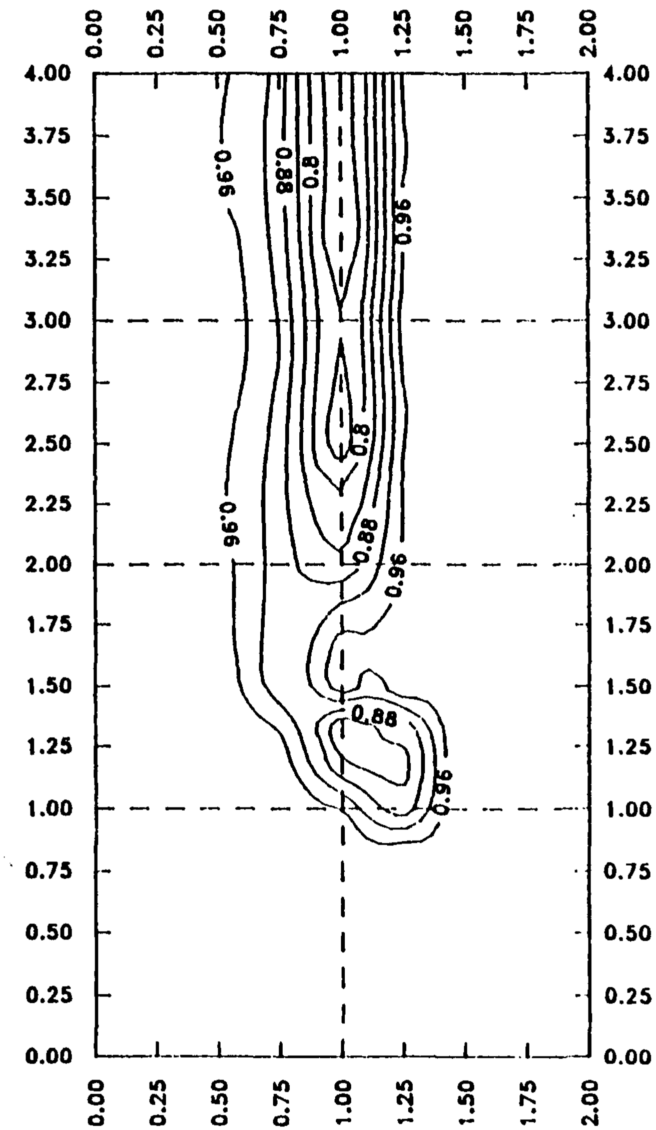

TRAVERSE PLANE SCALED IN INCHES
WINGTIP AT 1,1
VELOCITIES NON-DIMENSIONALIZED BY $u_{INFINITY}$

FIGURE 48:

Baseline Trip Wing L=1C

Wake Patterns

Baseline Wing L=1C

Wake Patterns

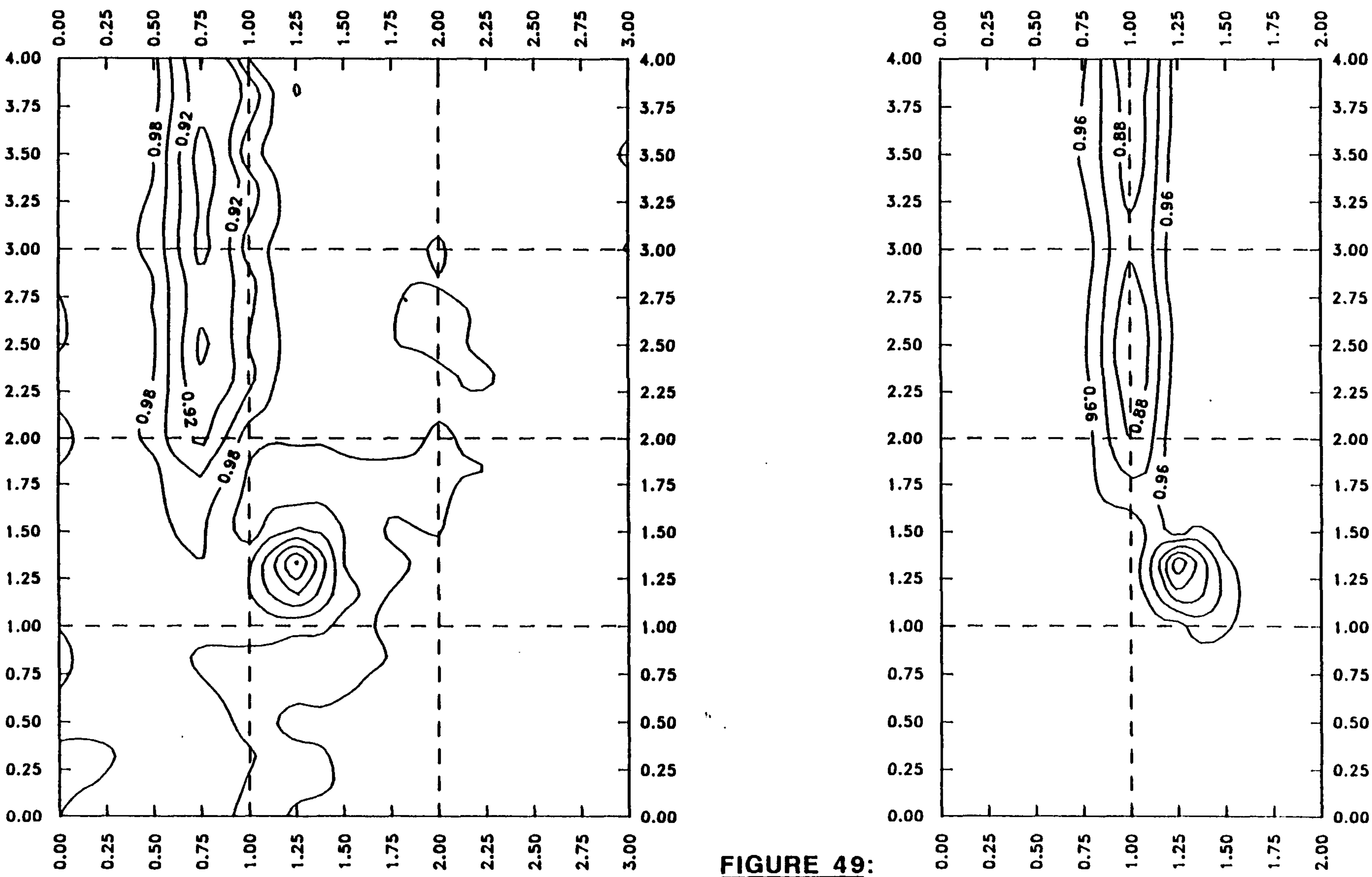

FIGURE 49:

TRAVERSE PLANE SCALED IN INCHES
WINGTIP AT (1,1)
VELOCITIES NON-DIMENSIONALIZED BY $u_{INFINITY}$

TRAVERSE PLANE SCALED IN INCHES
WINGTIP AT 1,1
VELOCITIES NON-DIMENSIONALIZED BY $u_{INFINITY}$

Baseline Trip Wing L=1.5C

Wake Patterns

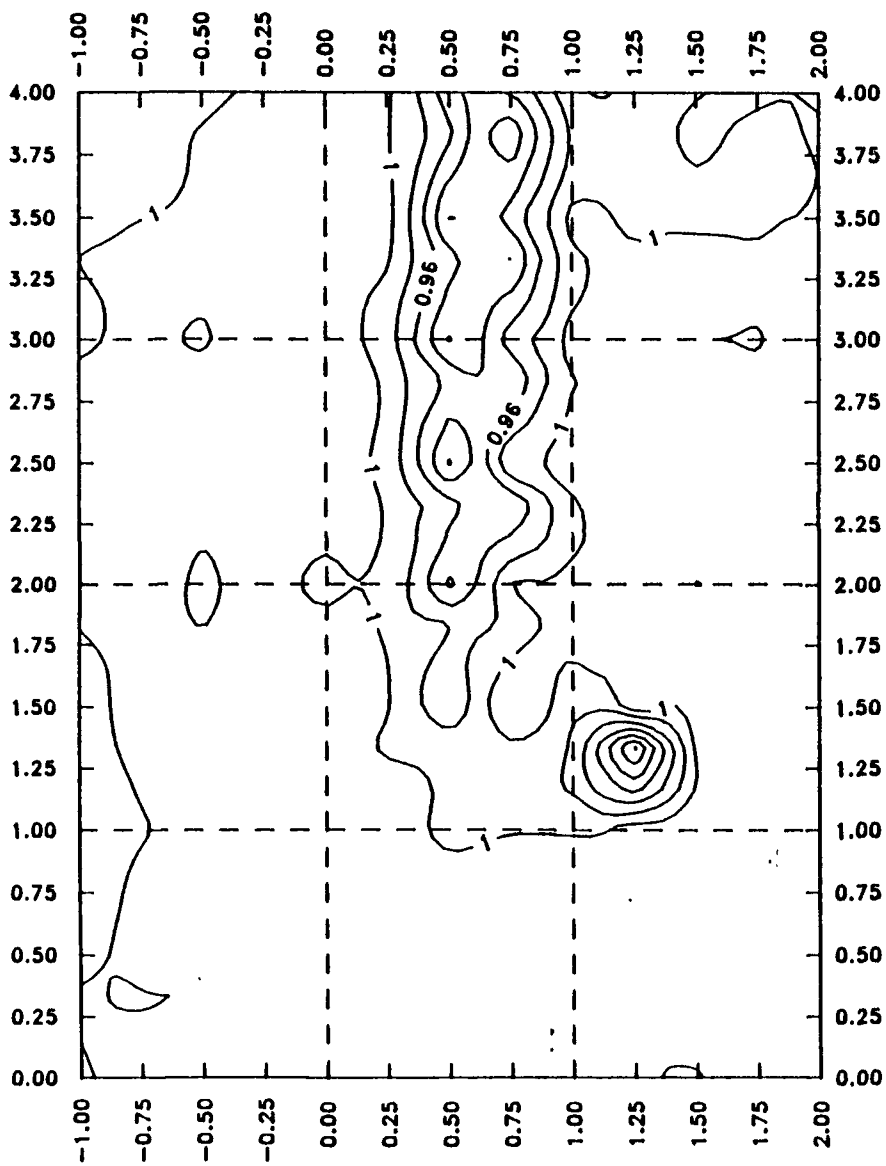

TRAVERSE PLANE SCALED IN INCHES
WINGTIP AT 1,1
VELOCITIES NON-DIMENSIONALIZED BY $u_{INFINITY}$

FIGURE 50:

Baseline Wing L=1.5C

Wake Patterns

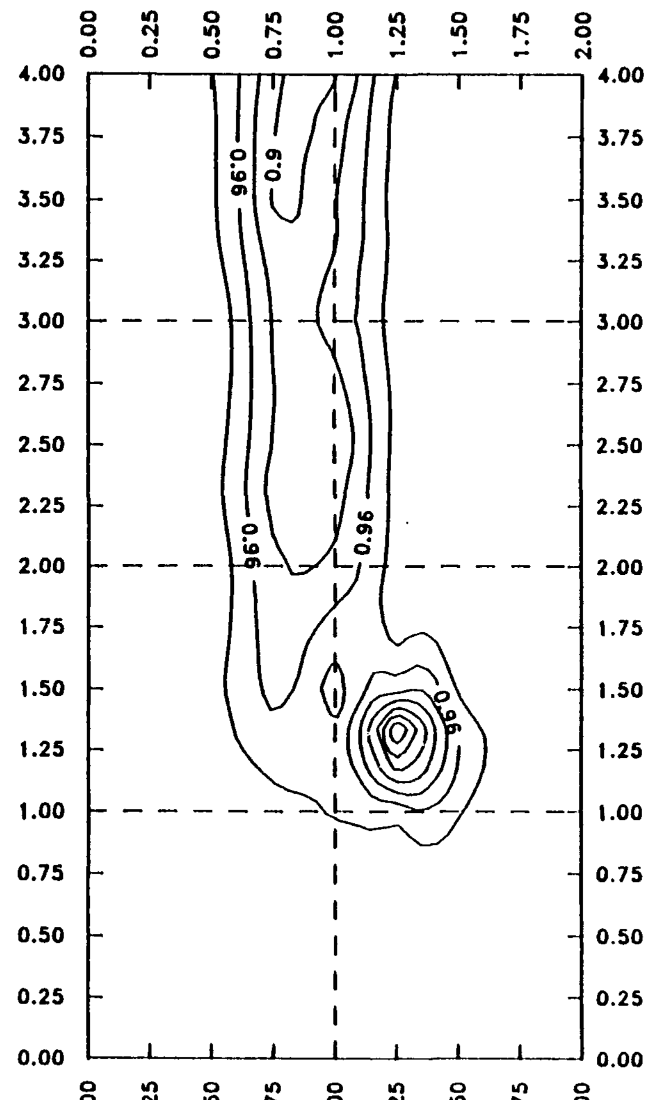

TRAVERSE PLANE SCALED IN INCHES
WINGTIP AT 1,1
VELOCITIES NON-DIMENSIONALIZED BY $u_{INFINITY}$

Triangular TE Wing L=1/4C

Wake Patterns

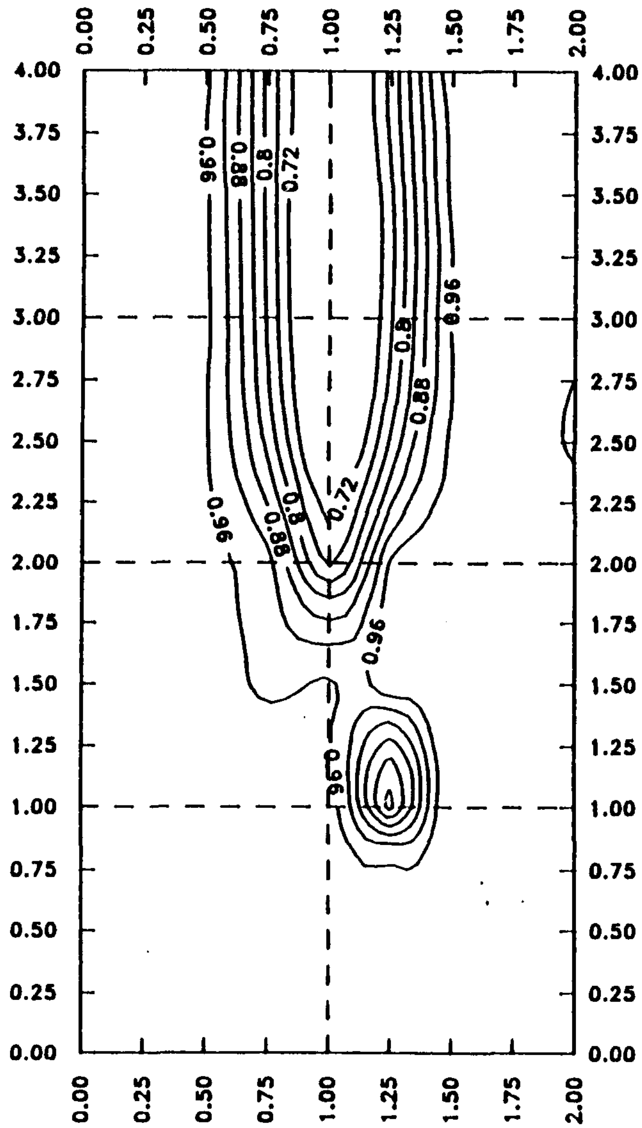

TRAVERSE PLANE SCALED IN INCHES
WINGTIP AT 1,1
VELOCITIES NON-DIMENSIONALIZED BY $u_{INFINITY}$

Baseline Wing L=1/4C

Wake Patterns

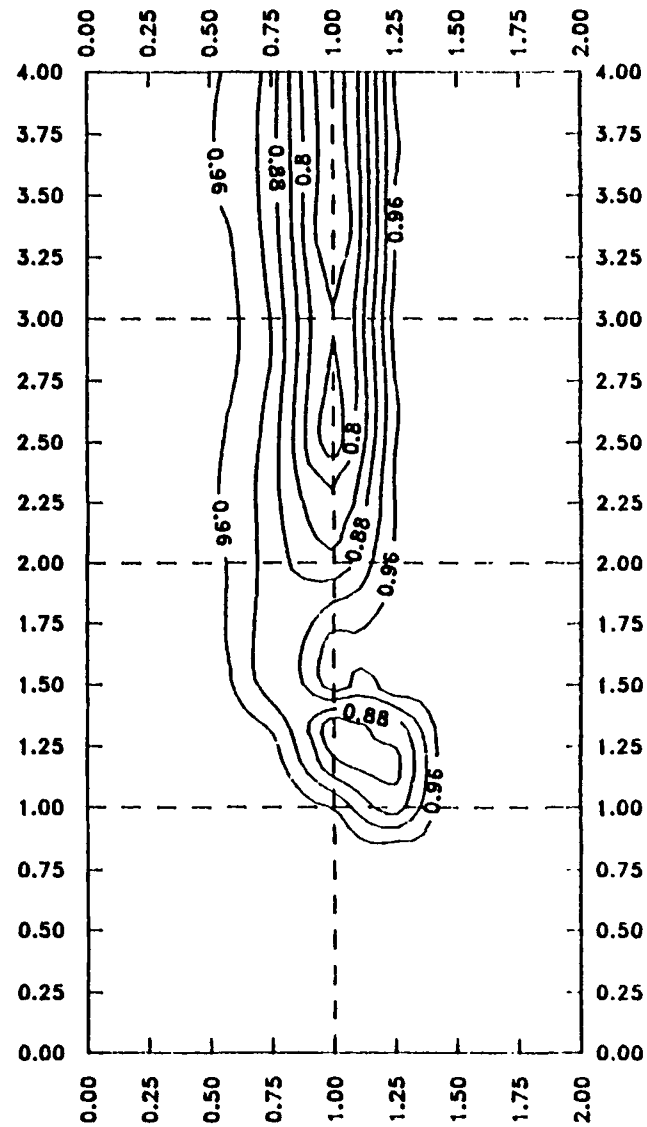

TRAVERSE PLANE SCALED IN INCHES
WINGTIP AT 1,1
VELOCITIES NON-DIMENSIONALIZED BY $u_{INFINITY}$

FIGURE 51:

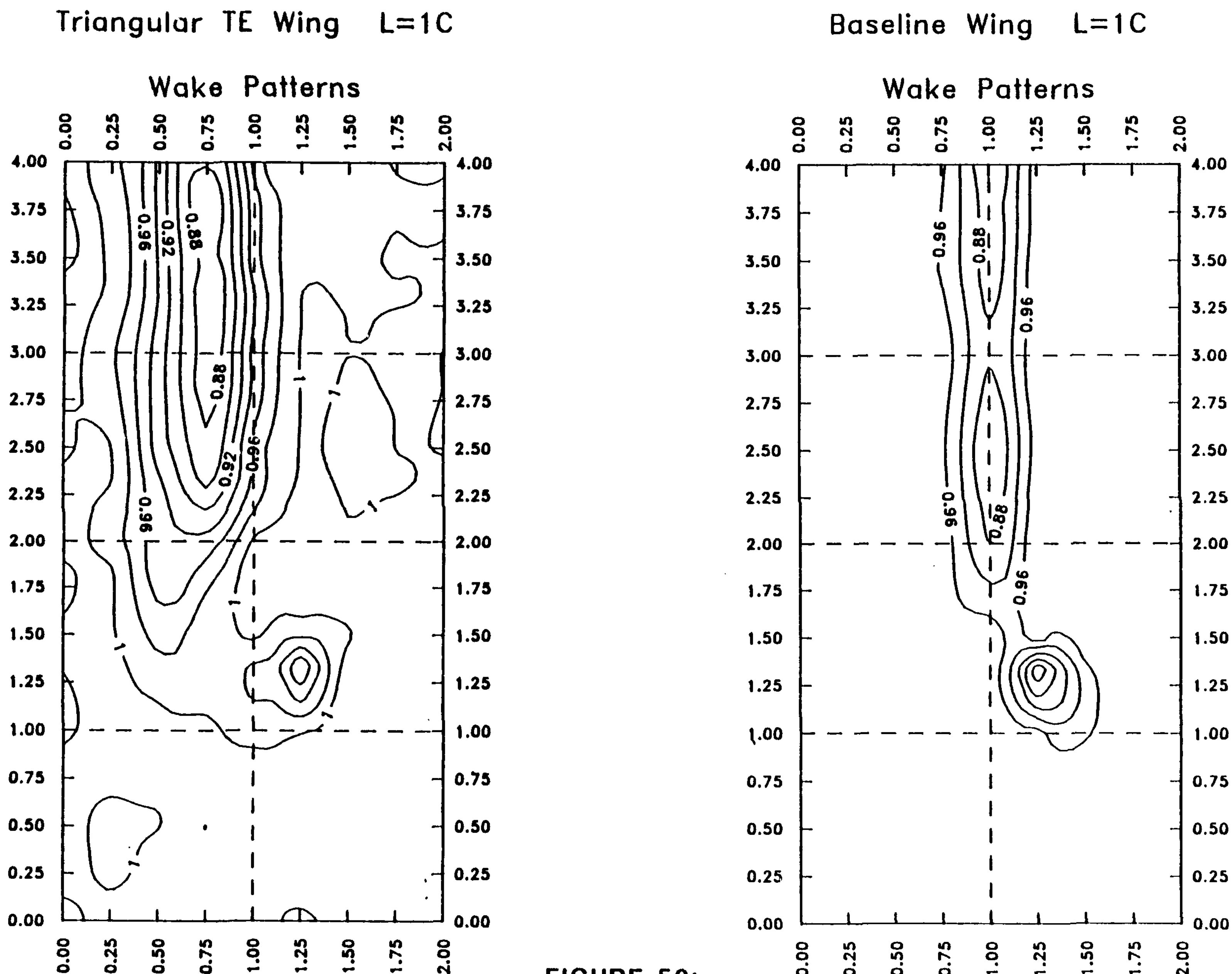

TRAVERSE PLANE SCALED IN INCHES
WINGTIP AT 1,1
VELOCITIES NON-DIMENSIONALIZED BY $u_{INFINITY}$

FIGURE 52:

TRAVERSE PLANE SCALED IN INCHES
WINGTIP AT 1,1
VELOCITIES NON-DIMENSIONALIZED BY $u_{INFINITY}$

Triangular TE Wing   L=1.5C

Wake Patterns

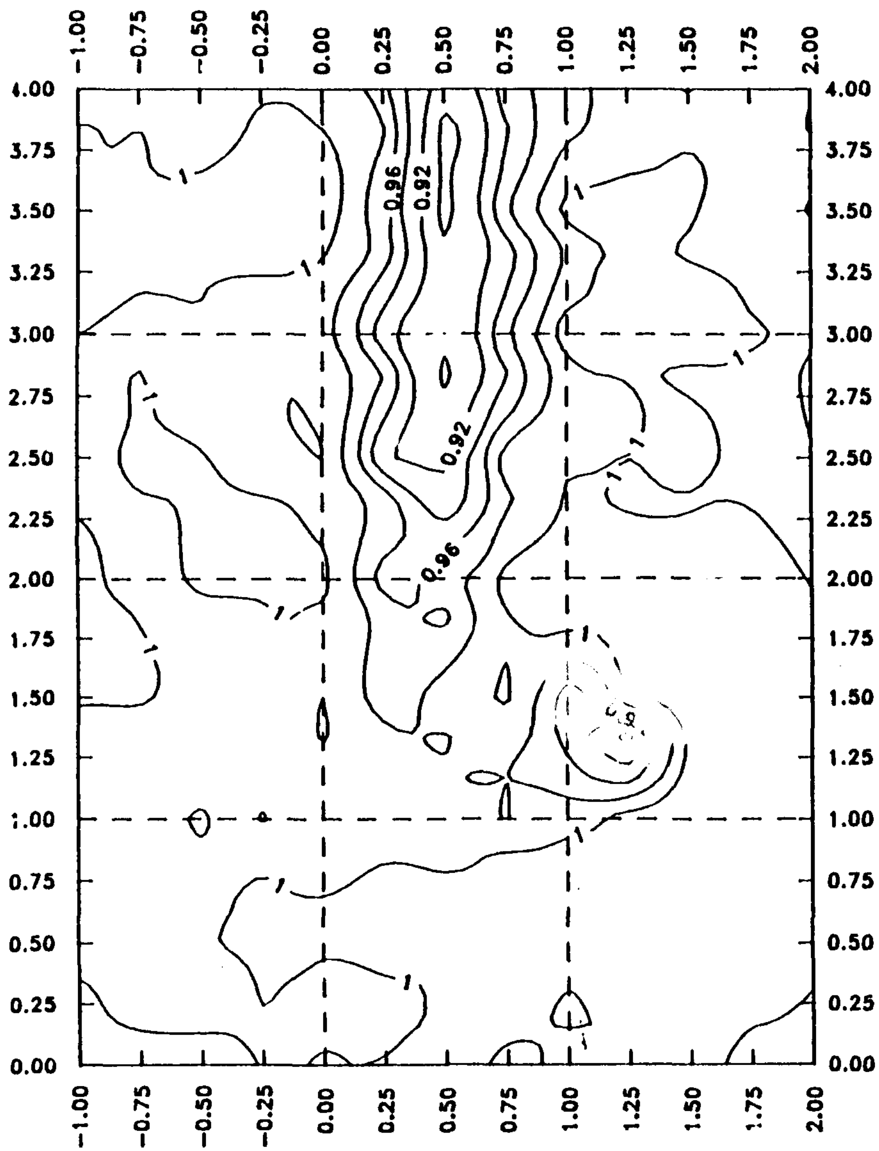

TRAVERSE PLANE SCALED IN INCHES
WINGTIP AT 1,1
VELOCITIES NON-DIMENSIONALIZED BY $u_{INFINITY}$

Baseline Wing   L=1.5C

Wake Patterns

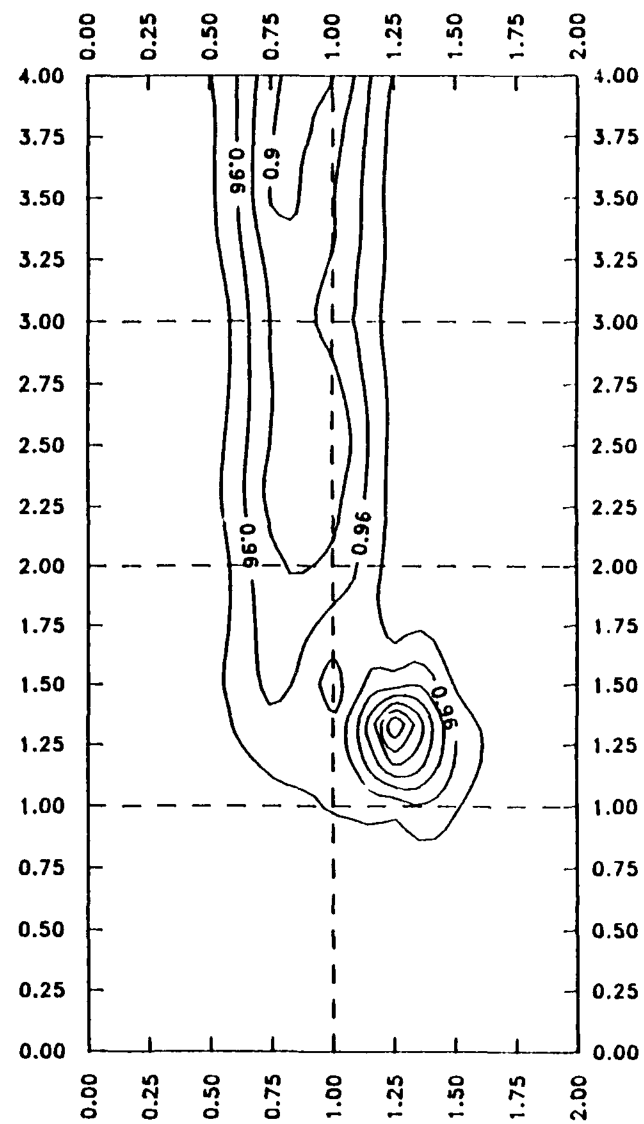

TRAVERSE PLANE SCALED IN INCHES
WINGTIP AT 1,1
VELOCITIES NON-DIMENSIONALIZED BY $u_{INFINITY}$

FIGURE 53:

56. It is evident that the lobed trailing edge caused streamwise vorticity downstream of the wing trailing edge. The result is mixed wake regions of freestream velocity and less severe velocity deficits and wingtip vortices compared to the baseline wing.

WRTE plots show that midspan wake decay traverses could be misleading. For example, a traverse taken across the wing trailing edge at a position of 1.75 on the vertical scale in Figure 56 would show no wake at all for this wing! This emphasizes the importance of a complete, two dimensional traverse test for wings with trailing edge convolutions.

In contrast to wings with trailing edge modifications, all wings with leading edge modifications showed little or no improvement in wake reduction over the baseline wing. This is exemplified by contour plots of the Venturi leading edge wing, shown in Figures 57 through 59. Contour plots for other wings tested can be found in Appendix E.

V.6. Wake and Balance Drag Comparisons

A comparison was made between the coefficient of profile drag obtained from the mechanical balance and that which was derived from control volume theory. To obtain the analytical C_{Do}, the velocity profile at the control volume exit was needed. Profiles for all untripped wings were completed; therefore, the profile drag for three axial locations behind each wing was calculated. In each case, the 1/4 chord profile was not used since the width of the wake at this point was small and only 7 to 10 data points were available.

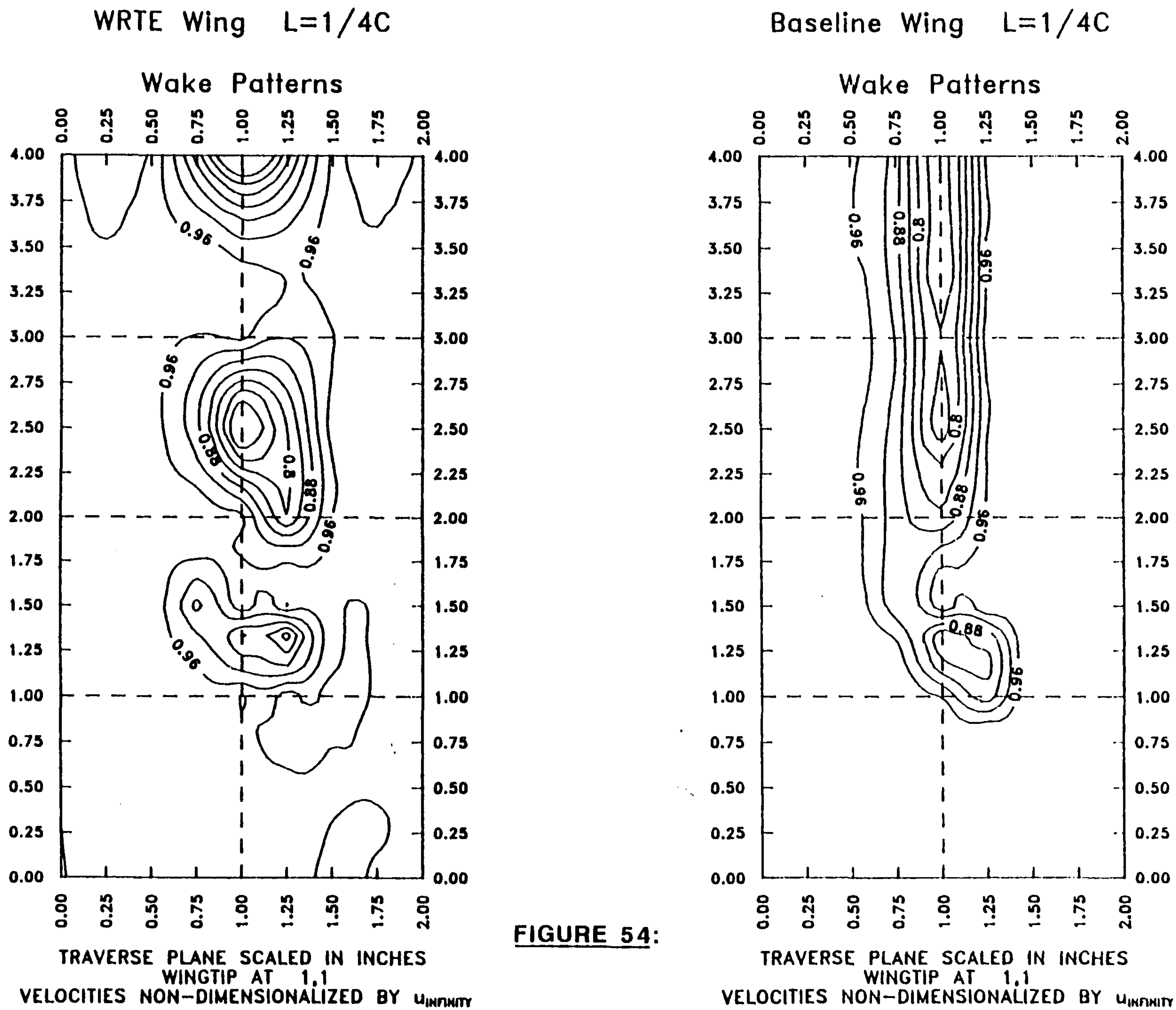
WRTE Wing L=1/4C
Wake Patterns
0.96
0.88
0.8
TRAVERSE PLANE SCALED IN INCHES
WINGTIP AT 1,1
VELOCITIES NON-DIMENSIONALIZED BY $u_{INFINITY}$
Baseline Wing L=1/4C
Wake Patterns
0.96
0.88
0.8
TRAVERSE PLANE SCALED IN INCHES
WINGTIP AT 1,1
VELOCITIES NON-DIMENSIONALIZED BY $u_{INFINITY}$

FIGURE 54:

WRTE Wing L=1C

Wake Patterns

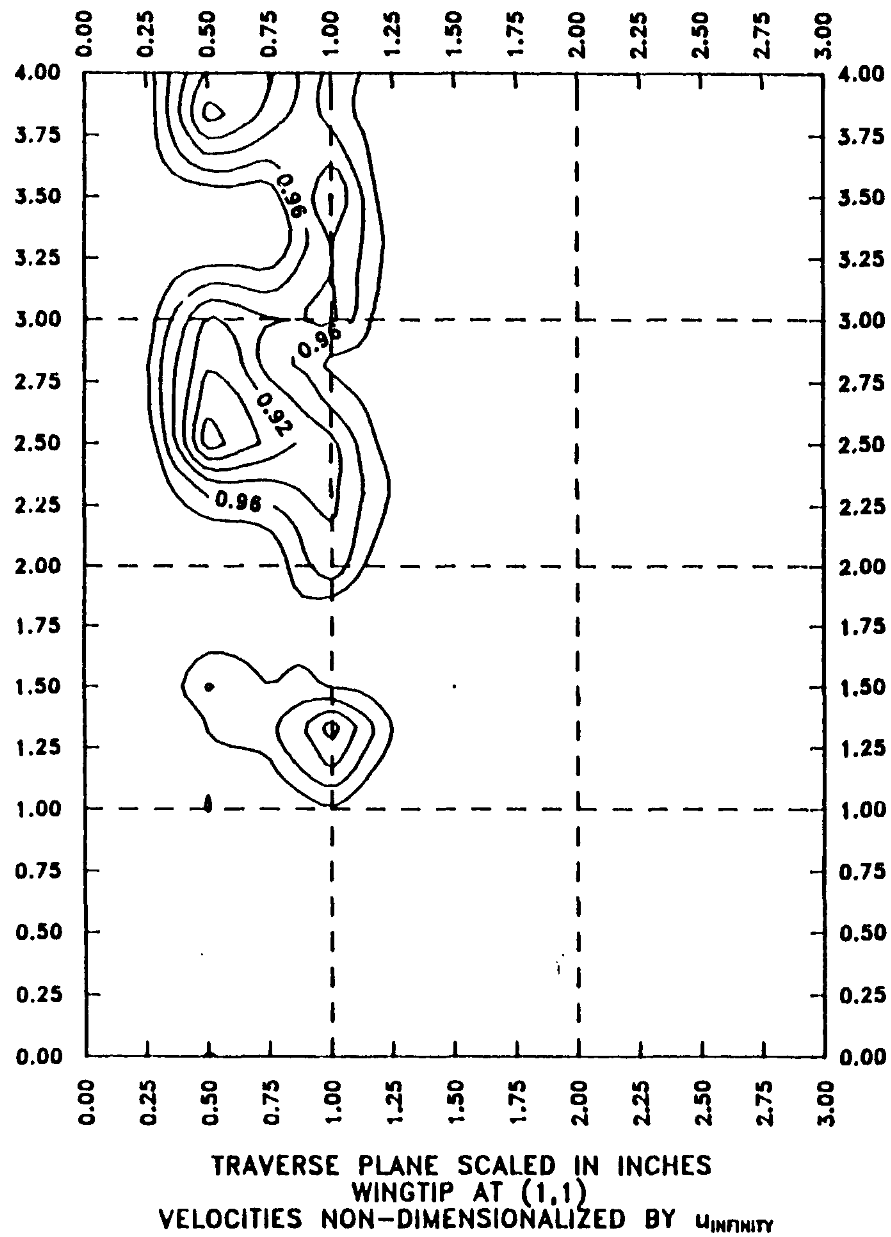

Baseline Wing L=1C

Wake Patterns

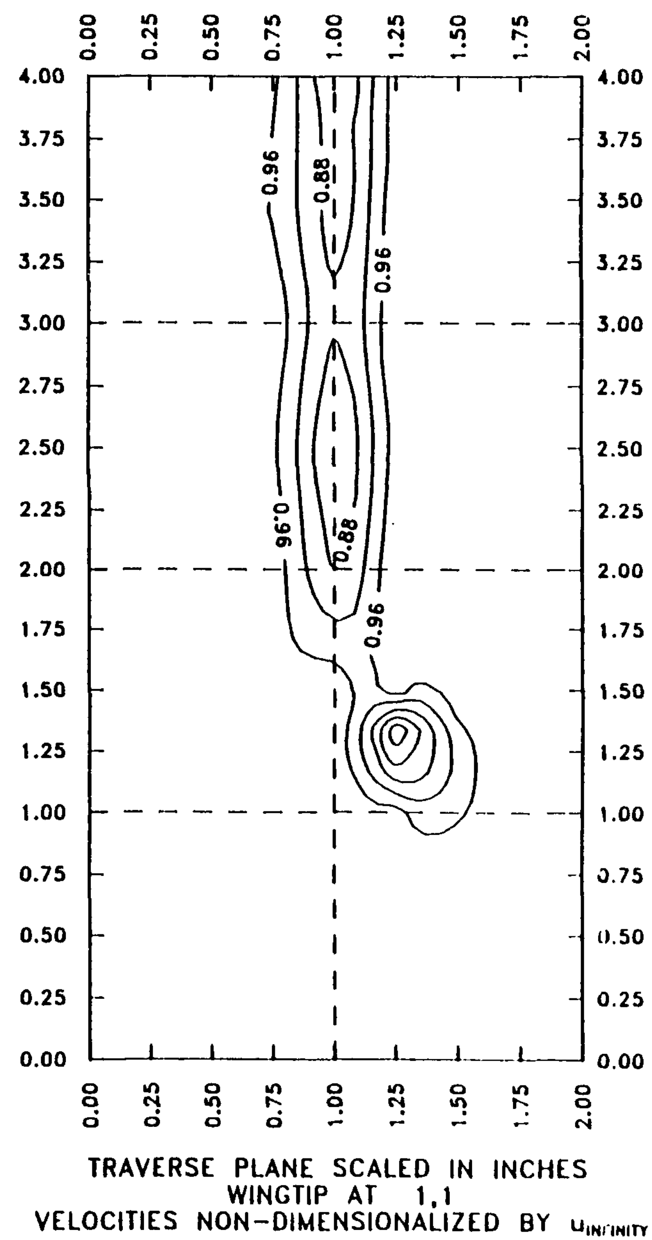

FIGURE 55:

WRTE Wing L=1.5C

Wake Patterns

Baseline Wing L=1.5C

Wake Patterns

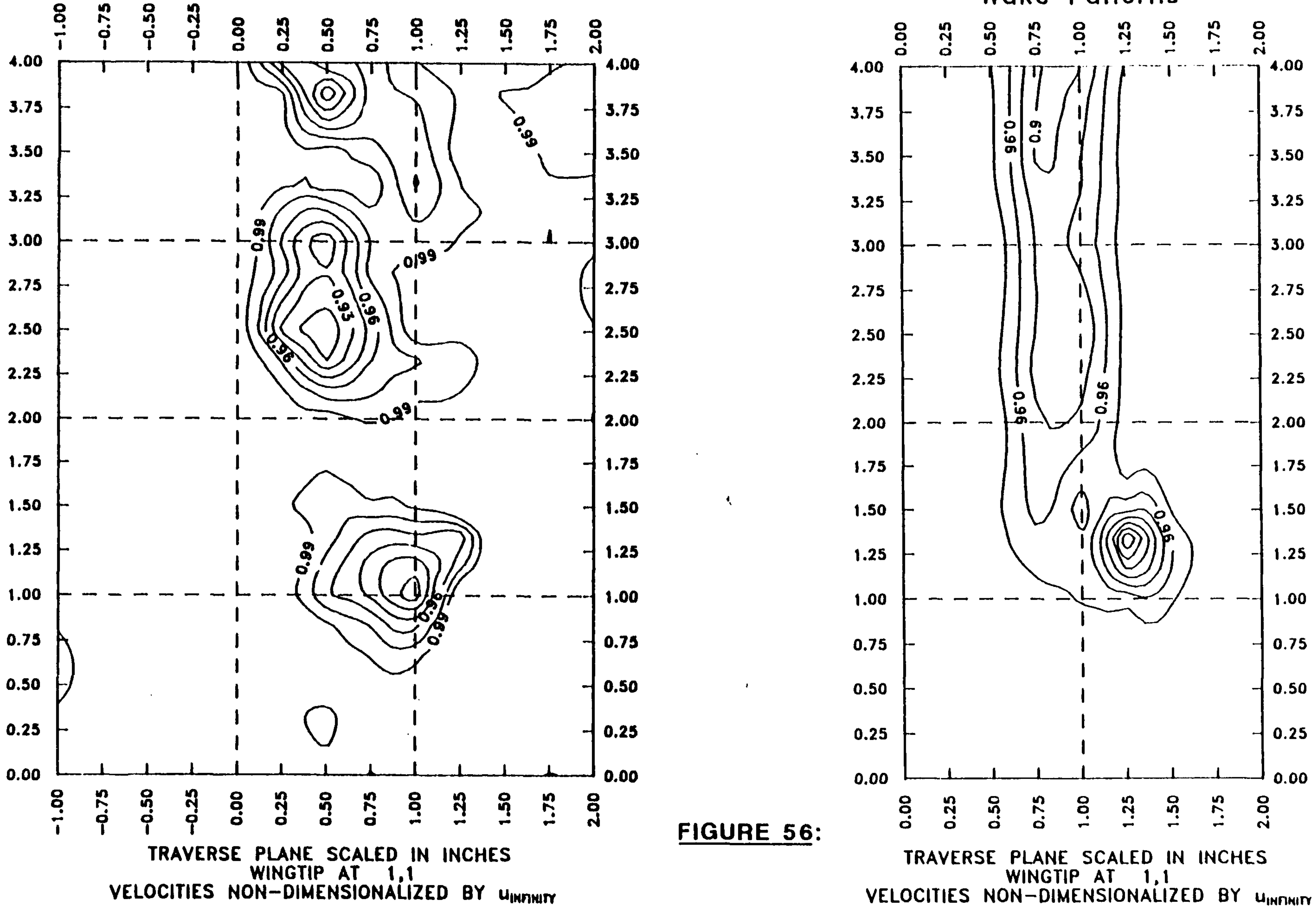

FIGURE 56:

Venturi LE Wing L=1/4C

Wake Patterns

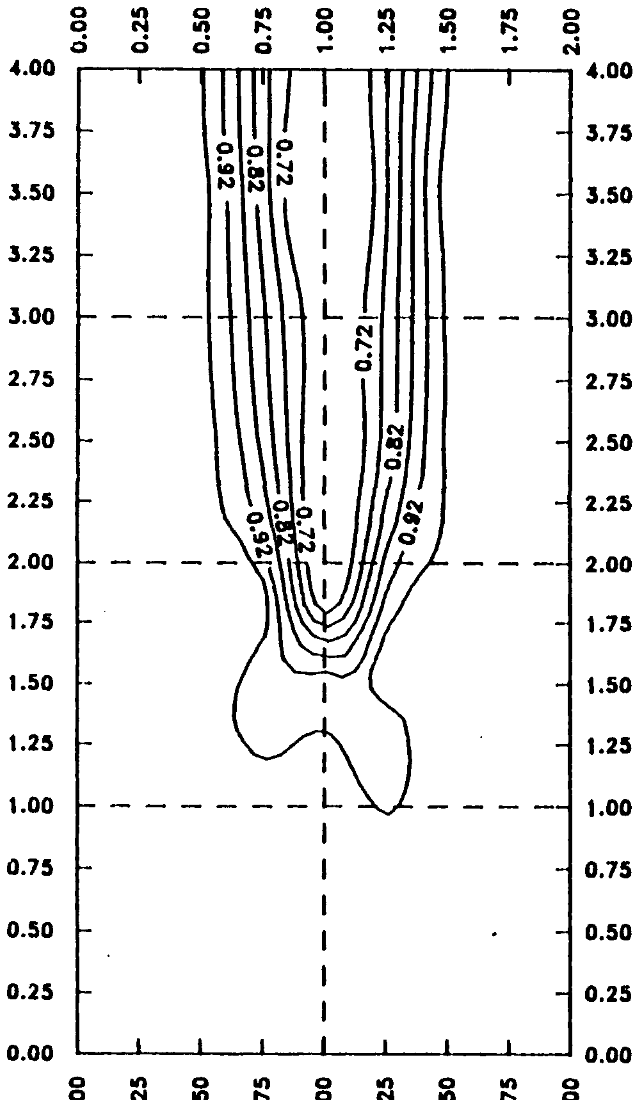

TRAVERSE PLANE SCALED IN INCHES
WINGTIP AT 1,1
VELOCITIES NON-DIMENSIONALIZED BY $u_{INFINITY}$

Baseline Wing L=1/4C

Wake Patterns

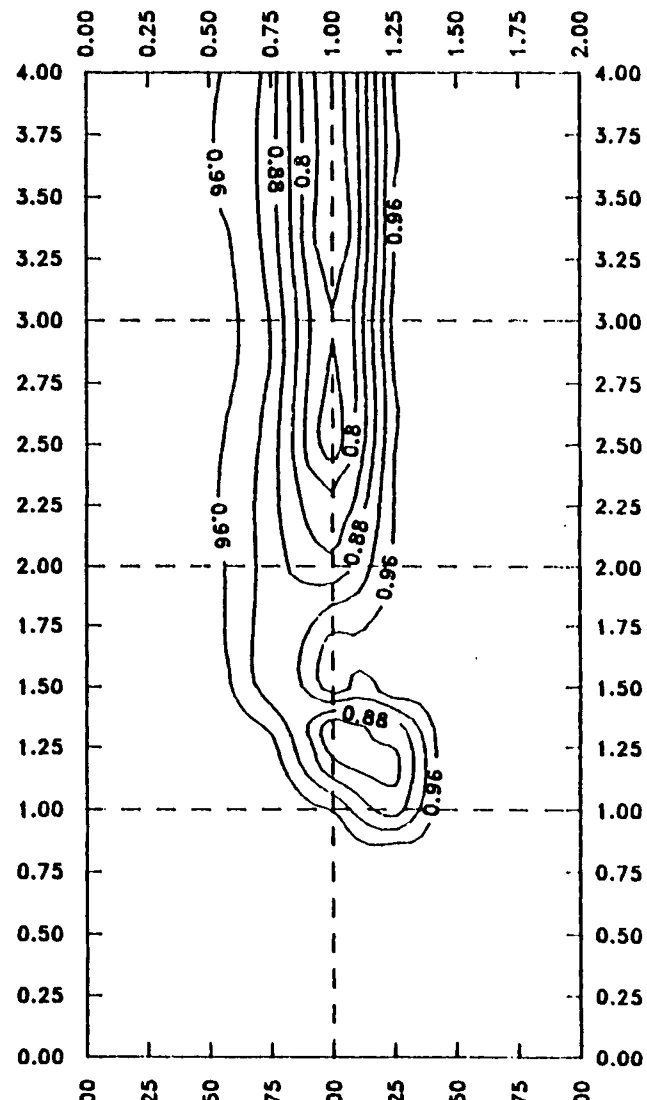

TRAVERSE PLANE SCALED IN INCHES
WINGTIP AT 1,1
VELOCITIES NON-DIMENSIONALIZED BY $u_{INFINITY}$

FIGURE 57:

Venturi LE Wing L=1C

Wake Patterns

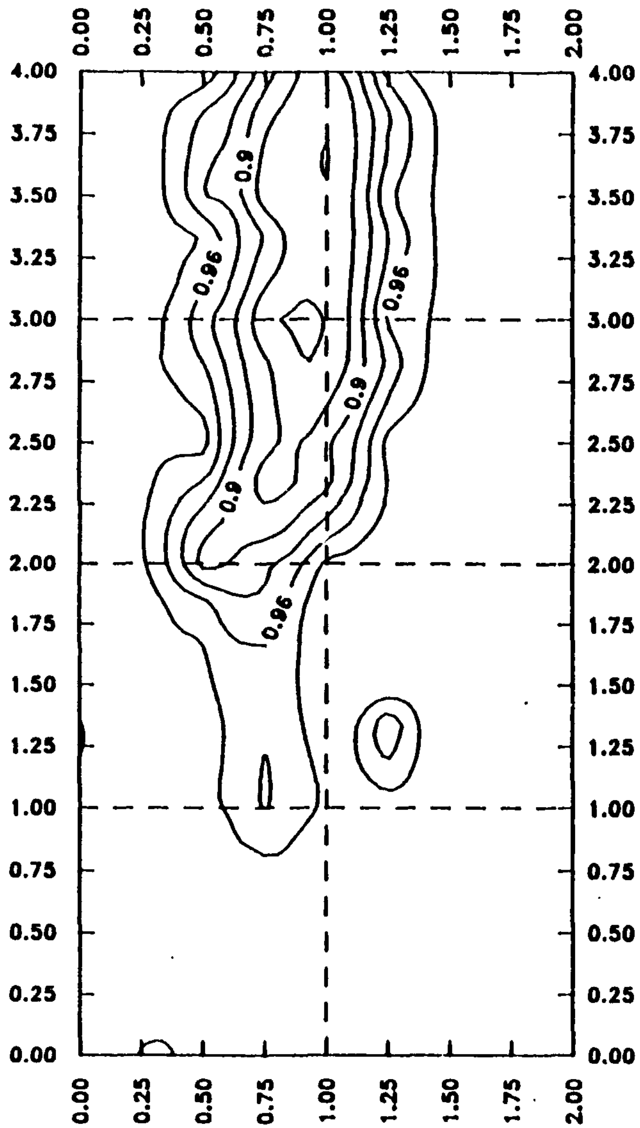

TRAVERSE PLANE SCALED IN INCHES
WINGTIP AT 1,1
VELOCITIES NON-DIMENSIONALIZED BY $u_{INFINITY}$

Baseline Wing L=1C

Wake Patterns

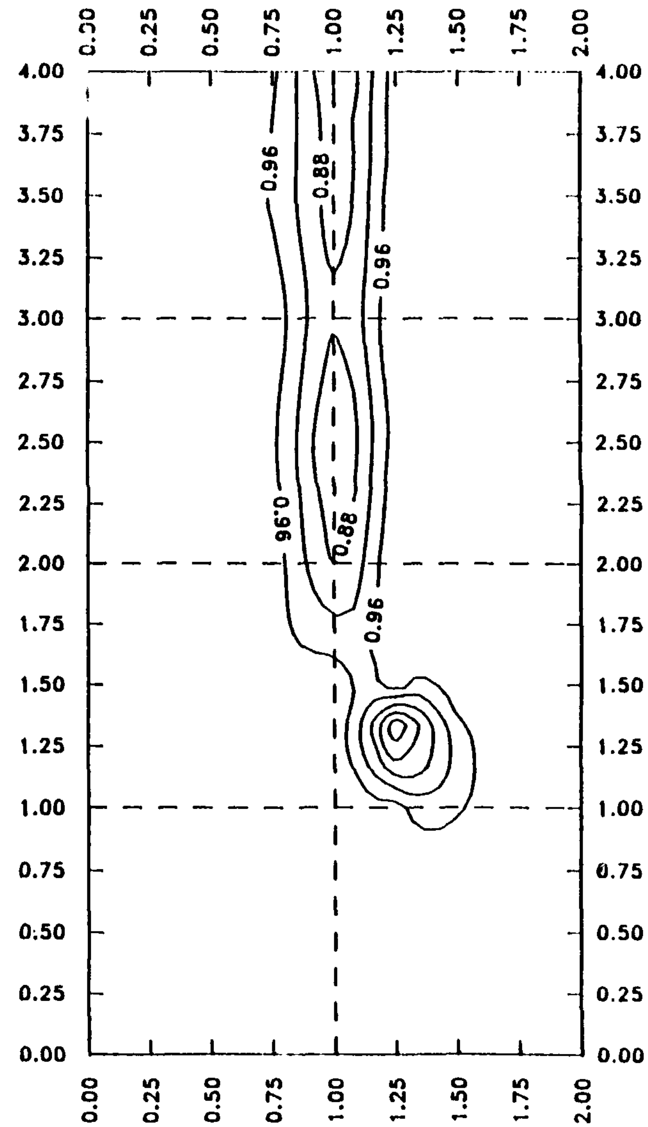

TRAVERSE PLANE SCALED IN INCHES
WINGTIP AT 1,1
VELOCITIES NON-DIMENSIONALIZED BY $u_{INFINITY}$

FIGURE 58:

Venturi LE Wing L=1.5C

Wake Patterns

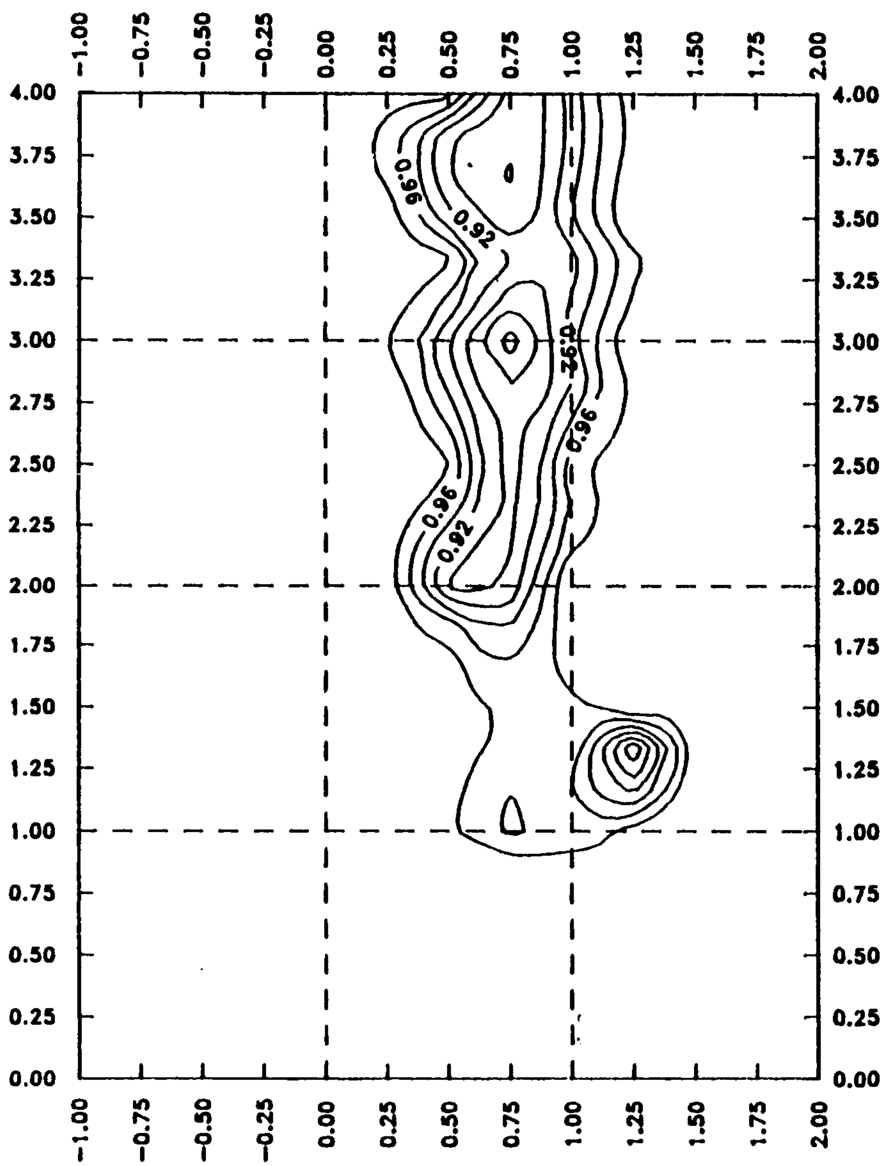

TRAVERSE PLANE SCALED IN INCHES
WINGTIP AT 1,1
VELOCITIES NON-DIMENSIONALIZED BY $u_{INFINITY}$

Baseline Wing L=1.5C

Wake Patterns

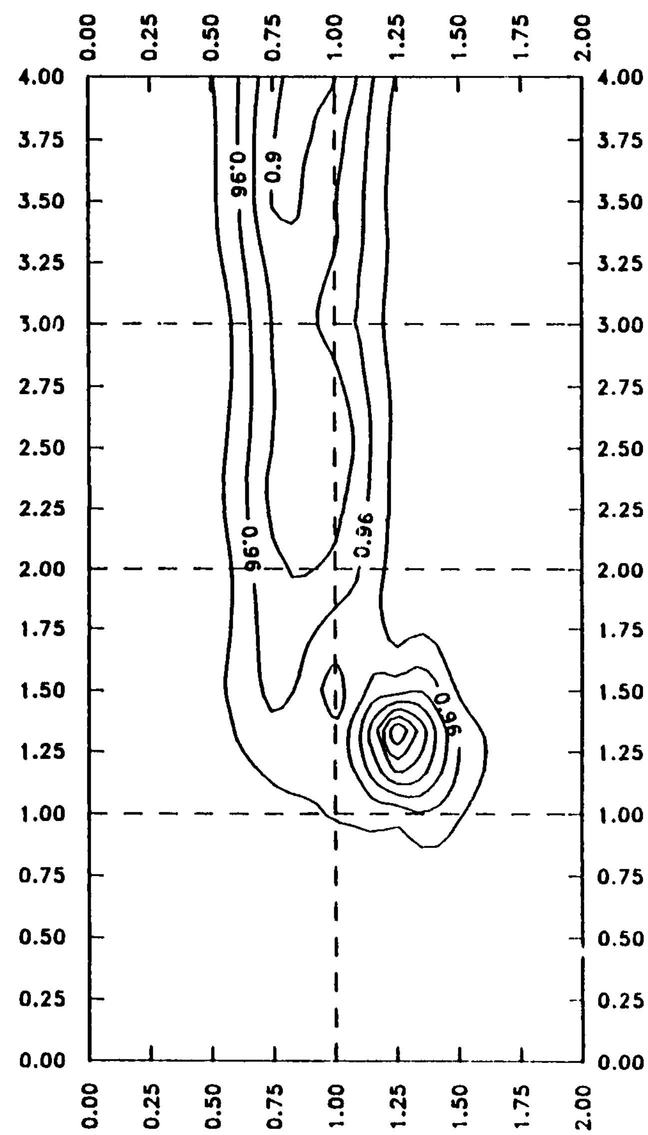

TRAVERSE PLANE SCALED IN INCHES
WINGTIP AT 1,1
VELOCITIES NON-DIMENSIONALIZED BY $u_{INFINITY}$

FIGURE 59:

A rough numerical integration was performed on the profile data using a Lotus spreadsheet. Results are summarized in Tables 2 through 7. There is strong aggreement between the control volume analysis for the profile drag and the mechanical balance. The largest difference found was only 5.9% for the leading edge groove wing and the WRTE wing. In some cases, even for those same wings at different axial locations, the values matched closely. The data used for the integration can be found in Appendix F.

Table 2: Baseline Wing Profile Drag Comparison

Wake Location	Control Volume Cd	Mechanical Balance Cd	Difference
1 Chord	0.045	0.044	2.3%
2.5 Chords	0.044	0.044	0%
4.25 Chords	0.045	0.044	2.3%

Table 3: Leading Edge Groove Wing Profile Drag Comparison

Wake Location	Control Volume Cd	Mechanical Balance Cd	Difference
1 Chord	0.018	0.017	5.9%
2.5 Chords	0.017	0.017	0%
4.25 Chords	0.016	0.017	5.9%

Table 4: Wide Rippled TE Wing Profile Drag Comparison

Wake Location	Control Volume Cd	Mechanical Balance Cd	Difference
1 Chord	0.035	0.034	2.9%
2.5 Chords	0.034	0.034	0%
4.25 Chords	0.036	0.034	5.9%

Table 5: Symmetric Rippled TE Wing Profile Drag Comparison

Wake Location	Control Volume Cd	Mechanical Balance Cd	Difference
1 Chord	0.026	0.025	4%
2.5 Chords	0.026	0.025	4%
4.25 Chords	0.026	0.025	4%

Table 6: Longitudinal Wing Profile Drag Comparison

Wake Location	Control Volume Cd	Mechanical Balance Cd	Difference
1 Chord	0.046	0.045	2.2%
2.5 Chords	0.046	0.045	2.2%
4.25 Chords	0.045	0.045	0%

Table 7: Triangular TE Wing Profile Drag Comparison

Wake Location	Control Volume Cd	Mechanical Balance Cd	Difference
1 Chord	0.055	0.053	3.8%
2.5 Chords	0.054	0.053	1.9%
4.25 Chords	0.053	0.053	0%

Table 8: Venturi LE Wing Profile Drag Comparison

Wake Location	Control Volume Cd	Mechanical Balance Cd	Difference
1 Chord	0.025	0.025	0%
2.5 Chords	0.025	0.025	0%
4.25 Chords	0.024	0.025	4%

VI. Conclusions

Three dimensional surface contouring of airfoils can improve the performance of submarine control surfaces. Leading edge grooves were found to decrease airfoil drag at angle of attack and also to decrease loss of lift at stall. This effect is a result of the grooves energizing the airfoil boundary layer.

Triangular trailing edge airfoils were found to rapidly mix out wake deficits. The increased wake mixing is believed due to shear layer instabilities and vortices set up by the triangular surface. Lobed trailing edge airfoils were found to both mix out the airfoil wake and to decrease wing tip vortex strength. The lobed surfaces generate large scale axial vorticity which breaks up the wake and interacts with the tip vortex.

All results were obtained from scale model testing at a low Reynolds Number. Boundary layer trips were needed to help simulate actual turbulent boundary layer flowfields.

VII. Recommendations

Test results indicate that leading edge grooves show the most promise for airfoil lift/drag improvements, triangular trailing edge airfoils for wake mixing enhancements, and lobed trailing edge contours for wake and tip vortex dispersion. It is recommended that these three dimensional airfoil shapes be tested in more detail and at higher Reynolds Numbers at the United Technologies Research Center to determine if the benefits achieved remain at Reynolds Numbers associated with submarine applications.

Several airfoil trailing edge contours combining lobes and non constant axial trailing edge locations should be built and tested. Figure 60 presents typical shapes using scalloping, scarfing, and serrations. Such contours can enhance mixing through interactions caused by streamwise and normal vorticity generation.

FIGURE 60: Proposed Contours

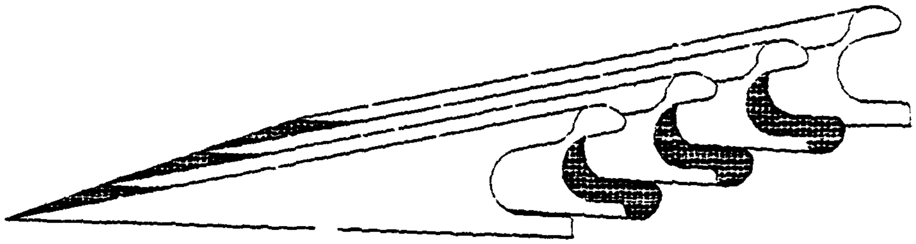

SCALLOPING

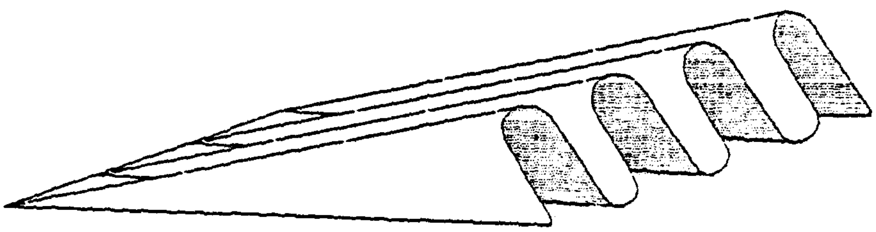

SCARFING

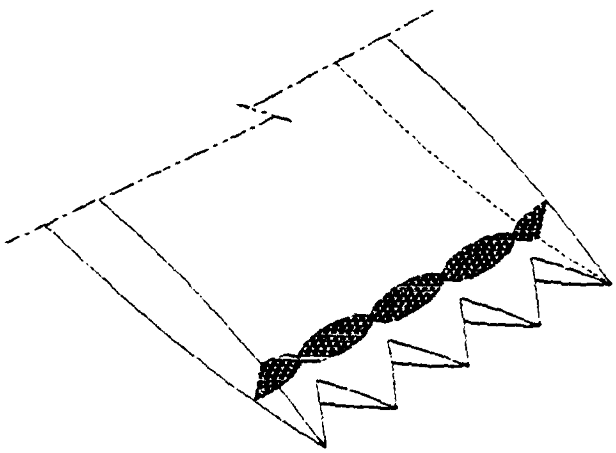

SERRATIONS

List of References

[1] Devenport, W.J. and others. An Experimental Study of Devices for Controlling the Flow Past a Wing-Body Junction. VPI Report AERO-162, 1989.

[2] Avallone, Eugene. Mark's Standard Handbook for Mechanical Engineers. Ninth Edition. McGraw-Hill Book Co., 1987.

[3] Presz, W. and others. Flow Structure in a Periodic Axial Vortex Array. Paper 87-0610, AIAA 25th Aerospace Science Meeting. January 1987.

[4] Presz, W. and others. Trailing Edge Separation/Stall Alleviation. Journal of Propulsion and Power, Vol. 25, 1987.

[5] Preston, Antony. Warships of the World. Jane's Publishing, 1980.

[6] Dwinnel, James H. Principles of Aerodynamics. McGraww-Hill, 1949.

[7] Blevins, Robert D. Applied Fluid Dynamics Handbook. Van Nostrand Reinhold, 1984.

[8] Carrol, Robert. The Aerodynamics of Powered Flight. Bell Aircraft/John Wiley & Sons, 1960.

[9] Fox-McDonald. Fluid Mechanics. Third Edition. John Wiley & Sons, 1985.

[10] Preston, Antony. Navies of World War 2. Benson Books, 1984.

[11] Daugherty, R., and others. Fluid Mechanics with Engineering Applications. Eighth Edition. McGraww-Hill, 1985.

[12] Airle, N., and others. Modern Fluid Dynamics: Vol. 1: Incompressible Flow. Van Nostrand, 1968.

[13] Anderson, John D. Introduction to Flight. McGraw-Hill, 1978.

[14] Schlichting, Hermann. Boundary Layer Theory. Seventh Edition. McGraw-Hill, 1979.

[15] Layton, Donald. Aircraft Performance. Matrix Publishing, 1988.

[16] Crotau, Paul F. Rippled Trailing Edge Airfoil. ME Report, Western New England College.

[17] Delore, Pasquale. Improving the Stability of Submarine Control Surfaces. ME Report, Western New England College, 1990.

[18] Dwinnel, James H. Principles of Aerodynamics. McGraw-Hill, 1949.

[19] Goldstein, S., ed. Modern Developments in Fluid Dynamics. Dover Publishing, 1965.

[20] Abbott, Ira H. Theory of Wing Sections. Dover Publishing, 1959.

[21] Anderson, John D. Fundamentals of Aerodynamics. McGraww-Hill, 1984.

Appendices

Appendix A

Ideal C_L and C_D Derivations

Coefficients of Lift and Drag, Ideal

$$C_L = 2\pi(\alpha - \alpha_i) \quad \text{(Ref. 1)}$$

α = Actual Angle of Attack

α_i = Induced Angle of Attack

AR = Aspect Ratio $= \dfrac{\text{Span}}{\text{Chord}}$

$$\alpha_i = \frac{C_L}{\pi AR} \quad \text{(Ref. 13)}$$

For Wings with an Elliptical Lift Distribution

$$C_L = 2\pi\left(\alpha - \frac{C_L}{\pi AR}\right)$$

$$C_L = \left(2\pi\alpha - \frac{2\cancel{\pi} C_L}{\cancel{\pi} AR}\right)$$

$$C_L = 2\pi\alpha - \frac{2C_L}{AR}$$

$$C_L + \frac{2C_L}{AR} = 2\pi\alpha$$

$$C_L\left(1 + \frac{2}{AR}\right) = 2\pi\alpha$$

Equation Used for Ideal C_L

$$\boxed{C_L = \frac{2\pi\alpha}{\left(1 + \frac{2}{AR}\right)}}$$

(Ref. 13) $\text{Drag}_{\text{induced}} = L\alpha_i$ for small angle α_i ← Induced Angle of Attack

(Ref. 13) $\alpha_i = \dfrac{C_L}{\pi AR}$ For Wings having AN Elliptical Lift Distribution

$$\text{Drag Force}_{\text{induced}} = \text{Lift Force}\left(\frac{C_L}{\pi AR}\right)$$

$$C_{D_i} = \frac{\text{Drag Force}_{\text{ind.}}}{\frac{1}{2}\rho V^2 A_p}$$

A_p = Planform Area = (Span)(Chord)

$$C_L = \frac{\text{Lift Force}}{\frac{1}{2}\rho V^2 A_p}$$

$$\text{Drag Force}_{\text{ind.}} = C_{D_i}\tfrac{1}{2}\rho V^2 A_p$$

$$\text{Lift Force} = C_L\tfrac{1}{2}\rho V^2 A_p$$

$$C_{D_i}\cancel{\tfrac{1}{2}}\cancel{\rho}\cancel{V^2}\cancel{A_p} = C_L\tfrac{1}{2}\rho V^2 A_p\left(\frac{C_L}{\pi AR}\right)$$

$$C_{D_i} = C_L\left(\frac{C_L}{\pi AR}\right)$$

$$\boxed{C_{D_i} = \frac{C_L^2}{\pi AR}}$$

Equation Used for Ideal C_{D_i}

Appendix B

Control Volume Analysis

Derivation of Cd from Control Volume Analysis

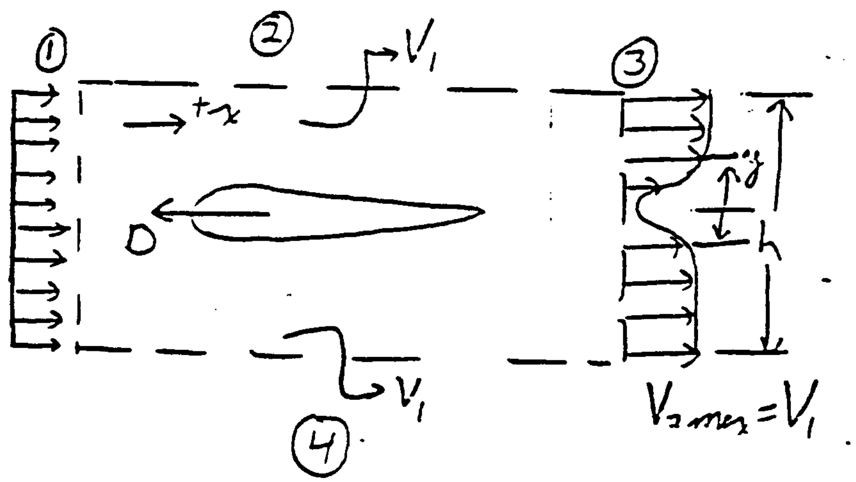

Conservation of Mass

ρ = constant, Steady State

$V_{2max} = V_1$

$A_2 = A_1 = A$

$\rho_2 = \rho_1$

$$\iint_{CS} \rho \vec{V} \cdot dA = 0$$

$$\dot{m}_{out} - \dot{m}_{in} = 0$$

$$\dot{m}_2 + \dot{m}_3 + \dot{m}_4 - \dot{m}_1 = 0$$

$$\dot{m}_2 + \dot{m}_4 = \dot{m}_1 - \dot{m}_3$$

$$\dot{m}_2 + \dot{m}_4 = \int \rho V_1 dA - \int \rho V_2 dA$$

$$\dot{m}_2 + \dot{m}_4 = \int \rho (V_1 - V_2) dA$$

Conservation of Momentum

ρ is constant
Steady State $P_2 = P_1$

$$\sum \vec{F}_x = \oiint_{out} \rho \vec{V} d\vec{A}\, V_{x\,out} - \oiint_{in} \rho \vec{V} \cdot d\vec{A}\, V_{x\,in}$$

$$-D = \rho \int V_2^2 dA + \dot{m}_2 V_1 + \dot{m}_4 V_1 - \rho V_1^2 A$$

$$-D = \int \rho V_2^2 dA - \rho V_1^2 A + (\dot{m}_2 + \dot{m}_4) V_1$$

$$-D = \int \rho V_2^2 dA - \rho V_1^2 A + \left(\int \rho (V_1 - V_2) dA \right) V_1$$

from Conservation of mass

$$-D = \int \rho V_2^2 dA - \rho V_1^2 A + \int \rho (V_1^2 - V_1 V_2) dA$$

$$D = \rho V_1^2 A - \int \rho V_2^2 dA - \int \rho (V_1^2 - V_1 V_2) dA$$

$$D = \int \rho V_1^2 dA - \int \rho V_2^2 dA - \int \rho (V_1^2 - V_1 V_2) dA$$

$$D = \int \rho \left(\cancel{V_1^2} - V_2^2 - \cancel{V_1^2} + V_1 V_2 \right) dA$$

$$D = \int \rho \left(V_1 V_2 - V_2^2 \right) dA$$

$A = h(\text{Span})$

$dA = dy(\text{Span})$

$A_a = t(\text{Span})$

t = maximum wing thickness

h = height of Control Volume

Control Values Continued

$$\text{Coefficient of Drag} \equiv \frac{\text{Drag Force}}{\frac{1}{2}\rho V_1^2 A_a}$$

$$C_d = \frac{\rho \int (V_1 V_2 - V_2^2)\, dA}{\frac{1}{2}\rho V_1^2 A_a}$$

$$C_d = \frac{\int V_1 V_2 - V_2^2 \left(dy\, \cancel{\text{Span}}\right)}{\frac{1}{2} V_1^2\, t \left(\cancel{\text{Span}}\right)}$$

$$\boxed{C_d = \int \frac{2}{t}\left(\frac{V_2}{V_1}\right)\left(1 - \frac{V_2}{V_1}\right) dy}$$

V_2 = Velocity at point y

$V_1 = V_{2\,max}$ = Freestream Velocity

t = maximum wing thickness

Appendix C

Dimensional Analysis

The Analysis of Wing Tip Vortices: A Non-Dimensional Approach

Craig Hunter
Western New England College
School of Engineering

August 6, 1990

Introduction

A wing tip vortex is the result of the pressure difference between the upper and lower surfaces of a wing. At the wing edge, high pressure fluid under the wing "leaks" onto the low pressure fluid on top of the wing, causing the formation of a vortex. This vortex trails downstream of the wing tip. See Figure 1, below.

FIGURE 1 Detail of flow near the tip of a finite wing.

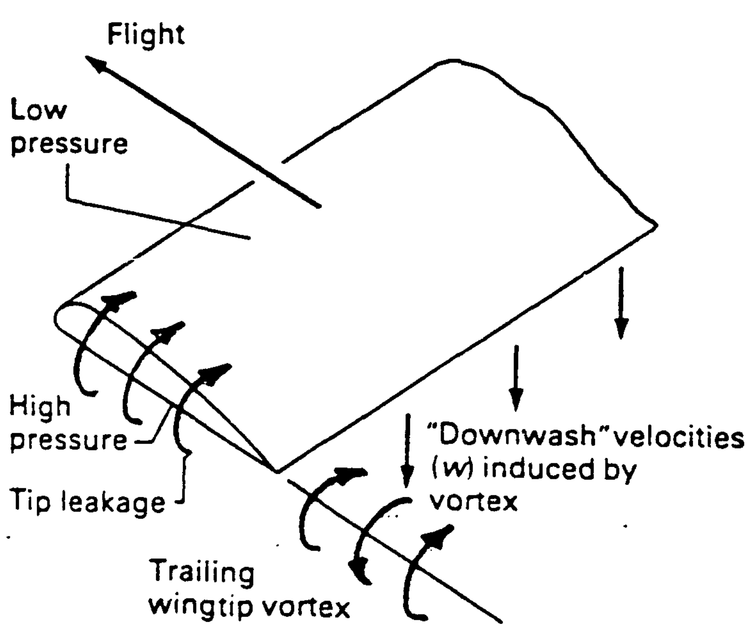

An undesirable effect of wing tip vortices is induced downwash behind the wing. Downwash reduces the effective angle of attack of the wing with two results. The first is an increase in drag, the second a decrease in lift.

In addition to lift and drag losses generated by wing tip vortices, there is an accompanying increase in wake activity. Downwash and tip vortices show up as regions of low velocity in downstream wakes. These regions are the primary cause of wake turbulence.

A method of classifying wing tip vortices was needed to supplement information taken from wake measurements and lift and drag testing. A literature search was performed in an effort to find vortex theory and applications. However, no useful information was found. This temporary roadblock led to the use of dimensional analysis in an effort to establish a means of estimating the energy in wing tip vortices, and provide a standard for comparing different wing configurations on the basis of vortex size and strength.

What follows is the dimensional analysis performed and the development of that analysis.

Dimensional Analysis

Relevant Parameters:

Kinetic Energy (kE)
Fluid Density (ρ)
Vortex Core Radius (r_c)
Vortex Outer Radius (r_v)
Outer Radius Velocity (V_v)
Core Radius Velocity (V_c)

number of parameters = $n = 6$

kE	ρ	r_c	r_v	V_v	V_c
$\frac{m\ell^2}{t^2}$	$\frac{m}{\ell^3}$	ℓ	ℓ	$\frac{\ell}{t}$	$\frac{\ell}{t}$

number of key parameters = $m = 3$

$n - m = 3 \Rightarrow 3$ dimensionless parameters

$r = m = 3 \Rightarrow \{\rho, V_v, r_v\}$

$G(\pi_1, \pi_2, \pi_3) = 0$

$$\pi_1 = \rho^a V_v^b r_v^c r_c$$

$$\pi_2 = \rho^d V_v^e r_v^f V_c$$

$$\pi_3 = \rho^g V_v^h r_v^i \, kE$$

<u>π_1</u>

$$\left(\frac{m}{\ell^3}\right)^a \left(\frac{\ell}{t}\right)^b (\ell)^c (\ell) = m^0 \ell^0 t^0$$

$a = 0$
$b = 0$
$c = -1$

$$\boxed{\pi_1 = \frac{r_c}{r_v}}$$

<u>π_2</u>

$$\left(\frac{m}{\ell^3}\right)^d \left(\frac{\ell}{t}\right)^e (\ell)^f \left(\frac{\ell}{t}\right) = m^0 \ell^0 t^0$$

$d = 0$
$f = 0$
$e = -1$

$$\boxed{\pi_2 = \frac{V_c}{V_v}}$$

$\underline{\pi_3}$ $\left(\frac{m}{\ell^3}\right)^g \left(\frac{\ell}{t}\right)^h (\ell)^i \left(m\frac{\ell^2}{t^2}\right) = m^0 \ell^0 t^0$

$g = -1$
$h = -2$
$i = -3$

$$\boxed{\pi_3 = \frac{KE}{\rho V_v^2 r_v^3}}$$

$$G\left(\frac{r_c}{r_v}, \frac{V_c}{V_v}, \frac{KE}{\rho V_v^2 r_v^3}\right) = 0$$

$$\boxed{KE = \rho V_v^2 r_v^3 \cdot G\left(\frac{r_c}{r_v}, \frac{V_c}{V_v}\right)}$$

Development

$$\pi_1 = \frac{r_c}{r_v} = \text{Radial Aspect Ratio (RAR)}$$

$$\pi_2 = \frac{V_c}{V_v} = \text{Radial Velocity Ratio (RVR)}$$

$$\text{Vorticity} = \omega = \frac{V_c}{r_c} = \frac{V_v}{r_v}$$ Assuming constant vorticity.

$$\boxed{V_c r_v = V_v r_c}$$

$$\frac{V_c}{V_v} = \frac{r_c}{r_v} \Rightarrow \text{RAR} = \text{RVR}$$

From experimental measurements,

V_c, V_v, and r_v are known.

$\Rightarrow$ r_c can be determined.

$$\boxed{r_c = \frac{V_c r_v}{V_v}}$$ Equation 1

$$\pi_3 = \frac{kE}{e V_v^2 r_v^3}$$

$$kE \sim e V_v^2 r_v^3$$

$$\boxed{(kE)_v \sim e V_v^2 r_v^3}$$ $\Rightarrow$ kE at outer radius EQ 2

$$\boxed{(kE)_c \sim e V_c^2 r_c^3}$$ $\Rightarrow$ kE at vortex core EQ 3

$$\frac{kE_v}{kE_c} = \frac{\cancel{e} V_v^2 r_v^3}{\cancel{e} V_c^2 r_c^3}$$

$$\frac{kE_v}{kE_c} = \frac{1}{(RVR)^2 (RAR)^3}$$

$$kE_c = kE_v (RVR^2 \cdot RAR^3)$$

since $RVR = RAR$

$$kE_c = kE_v (RVR)^5 = kE_v (RAR)^5$$

$$\boxed{\frac{kE_c}{kE_v} = RAR^5 = RVR^5 = H_{VE}}$$

Hunter's Number for Vortex Energy

Equation 4

Discussion

The analysis completed above nets several useful relations. First, the vortex core radius can be determined using Equation 1. To accomplish this, the vortex outer radius, outer velocity, and core velocity must be known. This information is available from wake measurements. It is important to note that Equation 1 is only valid when assuming constant vorticity.

Equations 2 and 3 give approximations of the kinetic energy in a vortex. Equation 2 approximates the KE at the outer radius of the vortex, and Equation 3 gives the KE at the vortex core. Again, wake measurements are needed to use Equations 2 and 3. While these equations allow an approximation of vortex energy, they are by no means comparable to other methods of calculating vortex energy. However, as a stand alone method of comparing vortex energy in different wing configurations, the expression used in Equations 2 and 3 is certainly valid.

Finally, the ratio of the kinetic energy at the vortex core to the kinetic energy at the outer radius of the vortex can be determined with Equation 4. This ratio has aptly been named "Hunter's Number", and is a quantity between 0 and 1. Though not directly useful in determining vortex strength, Hunter's Number can be an indication of the change of energy within a vortex, thus describing the vortex intensity. A vortex with a Hunter's Number of 1 would not be very intense. On the other hand, a vortex with a Hunter's Number of .5 would be very intense, having a 50% change in KE from outer radius to core. A useful feature of Hunter's number is its derivation, which demonstrates the capabilities of dimensional analysis.

All equations have been applied to actual measured tip vortices. Applications can be found in the Appendix.

Conclusion

In an effort to reduce the wake of submarine control surfaces while improving lift and drag characteristics, a method of describing the profile and strength of wing tip vortices was developed. Through the use of dimensional analysis, an approximation for vortex energy was produced. In addition, several useful ratios were established that give a vortex profile.

Applications:

Example 1 Tri TE Wing

$\alpha = 10°$

Probe at 1.5 Chord

$\rho = .002272 \frac{slug}{ft^3}$

$r_v = .1625''$

$V_v = 72.6 ft/s$

$V_c = 68 ft/s$

① $$r_c = \frac{V_c r_v}{V_v} = \frac{(68 ft/s)(.1625'')}{(72.6 ft/s)}$$

$$r_c = .1522''$$

② $$KE_v \sim \rho V_v^2 r_v^3 = (.002272 \tfrac{sl}{ft^3})(72.6 ft/s)^2(\tfrac{.1625}{12} ft)^3$$

③ $$KE_c \sim \rho V_c^2 r_c^3 = (.002272 \tfrac{sl}{ft^3})(68 ft/s)^2(\tfrac{.1522}{12} ft)^3$$

$$KE_v \sim 2.974(10^{-5}) \ ft \cdot lb$$

$$KE_c \sim 2.1435(10^{-5}) \ ft \cdot lb$$

④ $$H_{VE} = \frac{KE_c}{KE_v} = \frac{2.1435}{2.9740} = .72075$$

Also applied to Triangular TE Wing at 1C and 1.5C.

Summary

ΔTE Wing Results	¼ C	1 C	1.5 C
r_c	.3875"	.1436	.1522"
r_v	.425"	.155	.1625"
KE_c	$2.9407(10^{-4})$ ft·lb	$1.749(10^{-5})$ ft·lb	$2.135(10^{-5})$ ft·lb
KE_v	$4.6671(10^{-4})$ ft·lb	$2.563(10^{-5})$ ft·lb	$2.974(10^{-5})$ ft·lb
H_{VE}	.630	.682	721

Appendix D

Wake Decay Profiles

VELOCITY PROFILES BEHIND WING
SYMMETRIC RIPPLED TRAILING EDGE WING

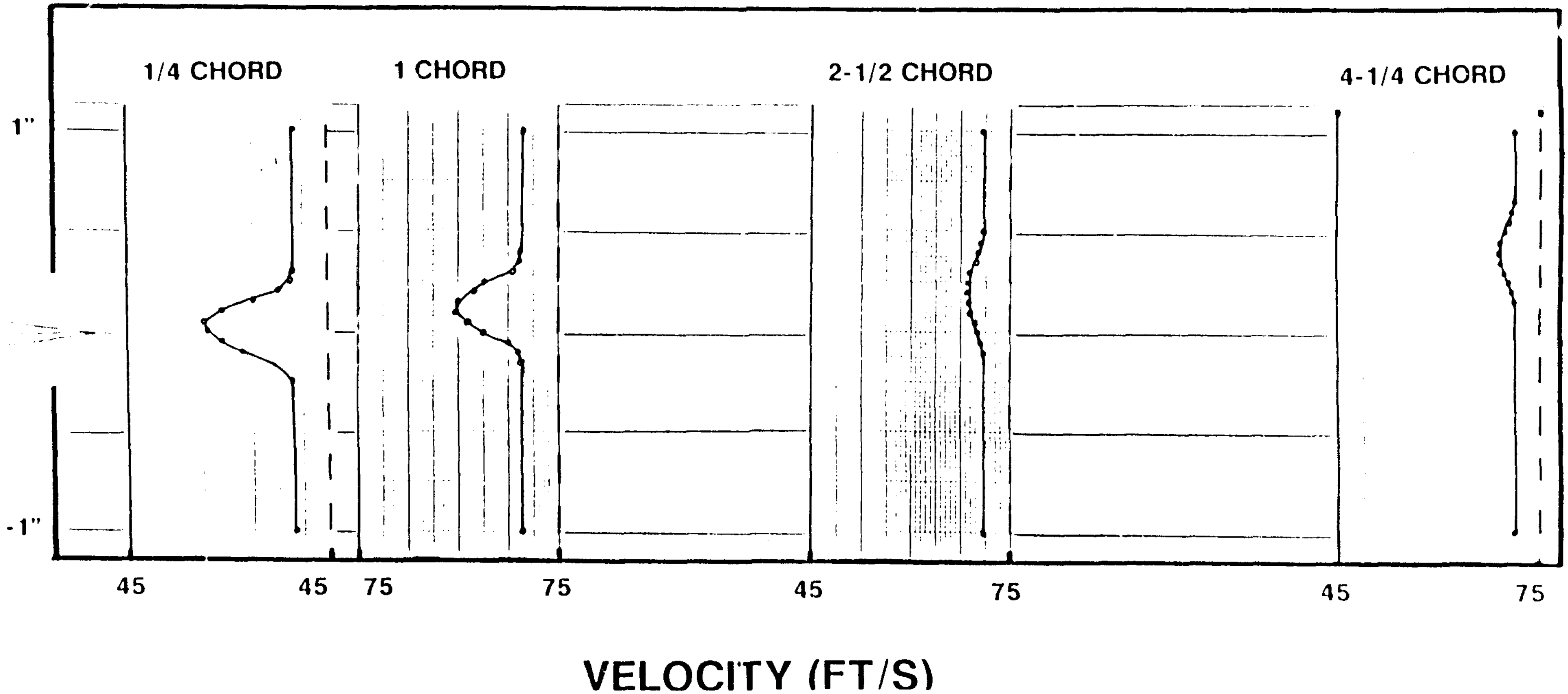

VELOCITY PROFILES BEHIND WING
MIDDLE GROOVE WING

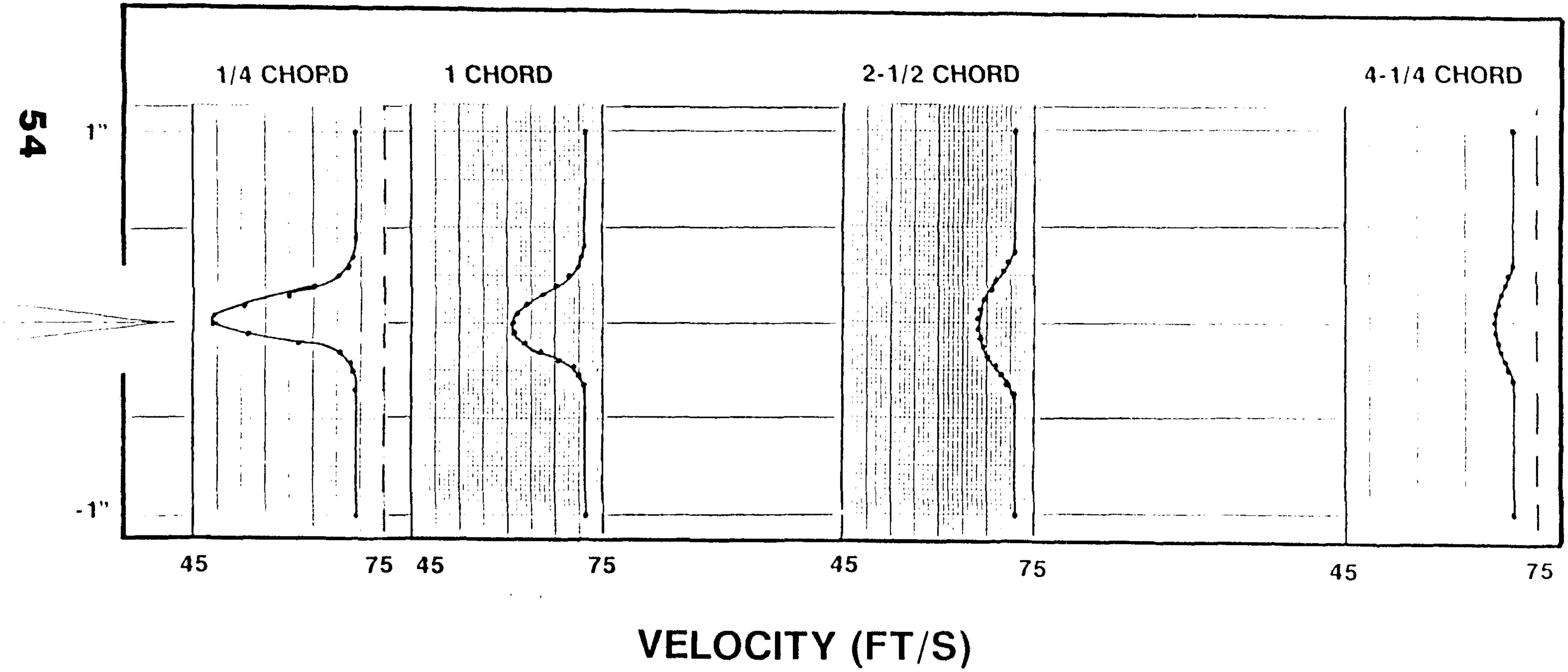

VELOCITY PROFILES BEHIND WING
LEADING EDGE GROOVE WING

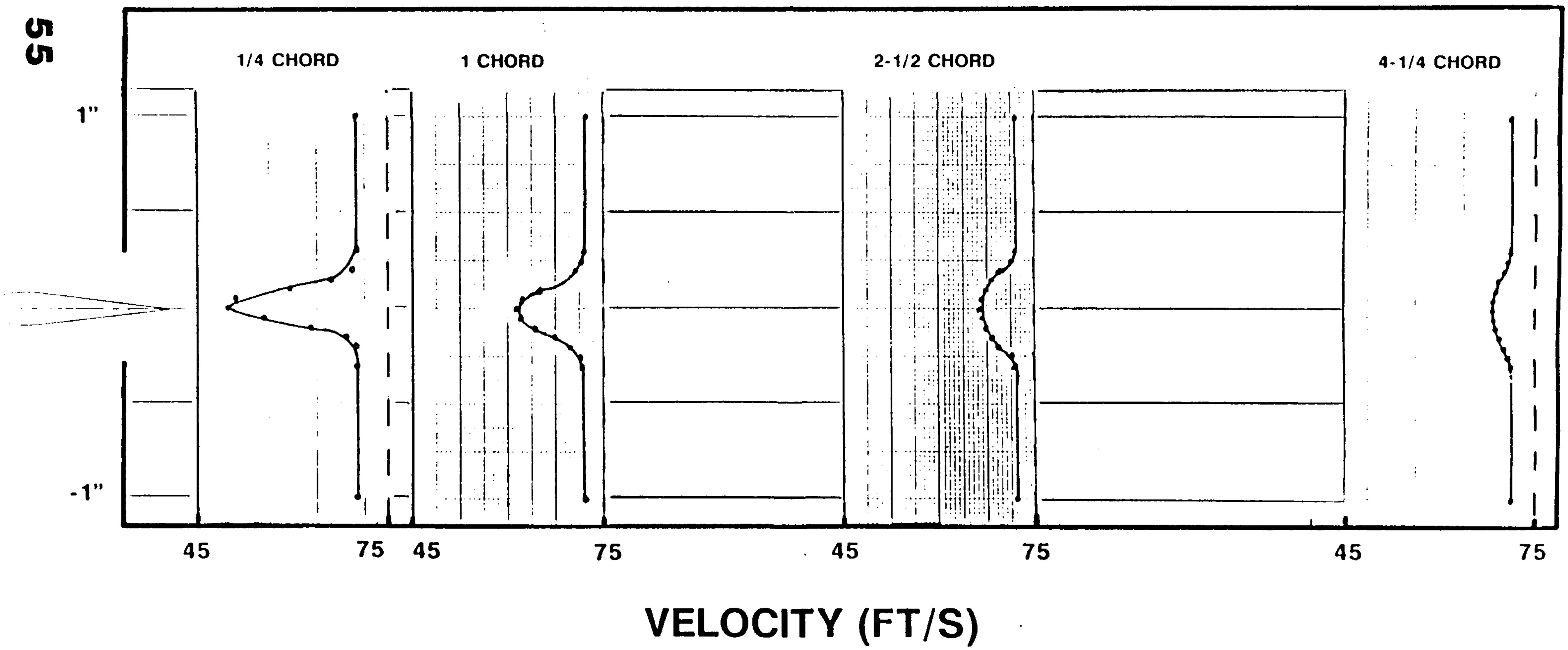

Appendix E

Velocity Contours

Venturi LE Wing L=1/4C

Wake Patterns

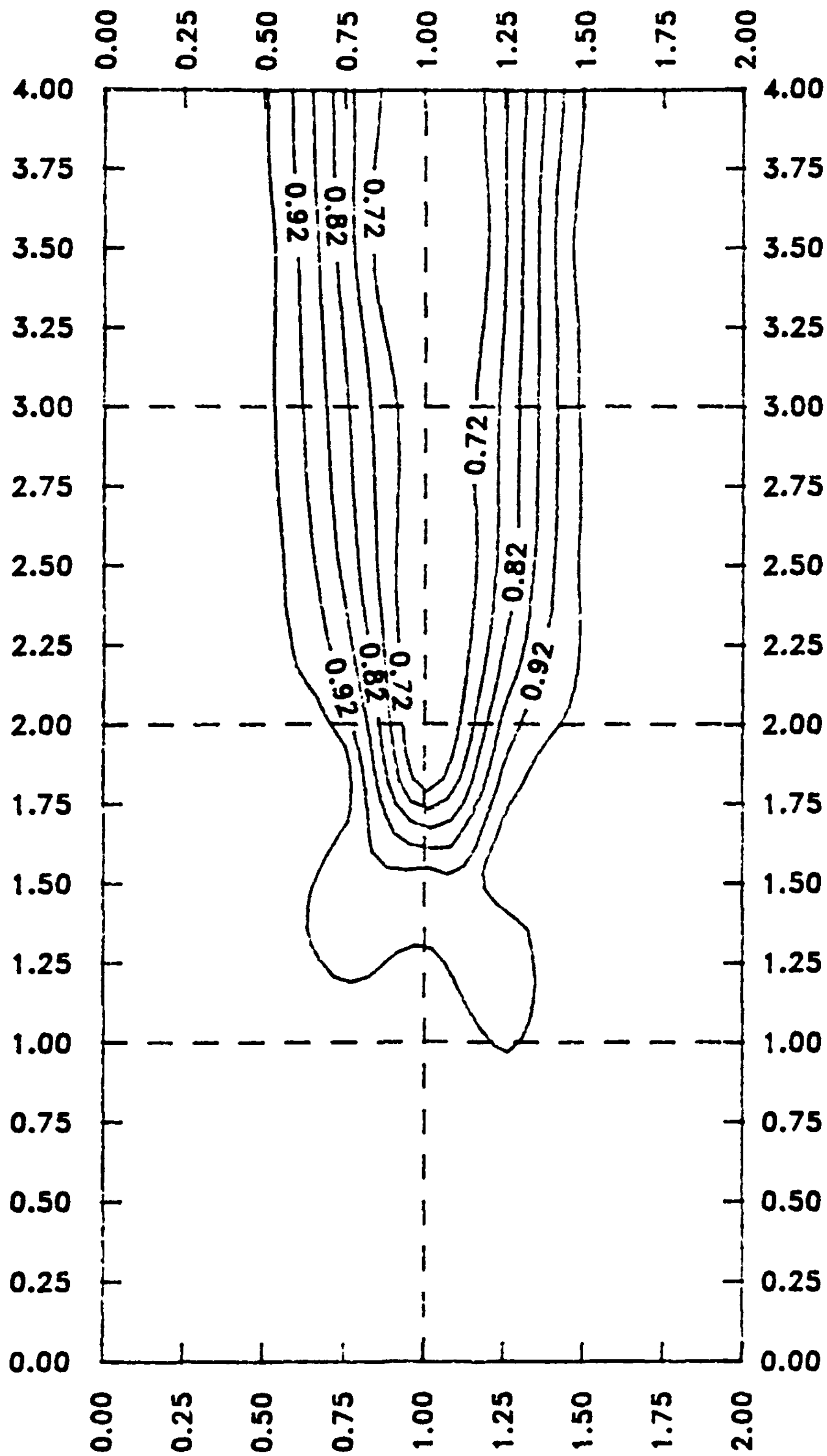

TRAVERSE PLANE SCALED IN INCHES
WINGTIP AT 1,1
VELOCITIES NON-DIMENSIONALIZED BY $u_{INFINITY}$

Venturi LE Wing L=1C

Wake Patterns

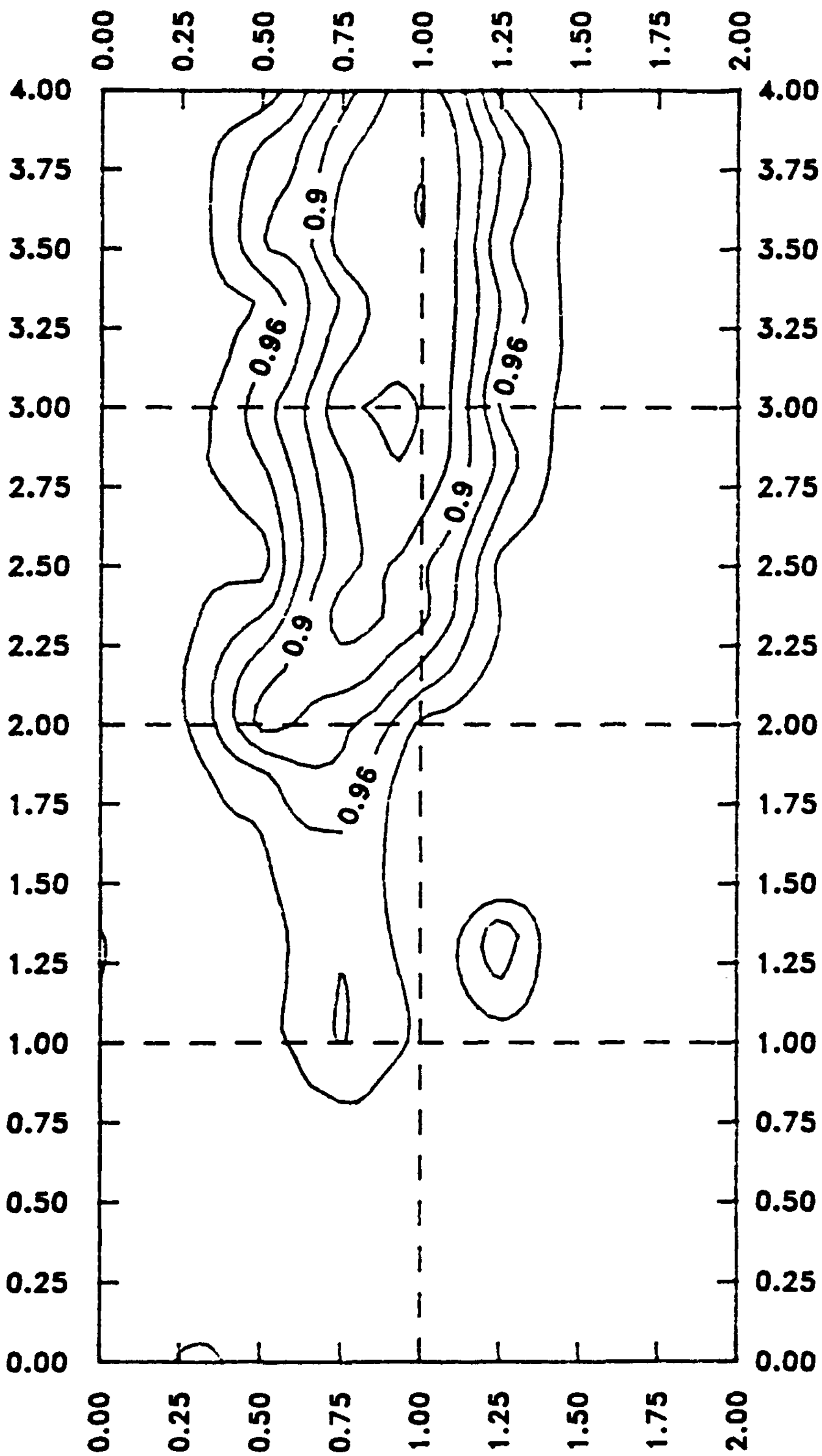

TRAVERSE PLANE SCALED IN INCHES
WINGTIP AT 1,1
VELOCITIES NON-DIMENSIONALIZED BY $u_{INFINITY}$

WRTE Wing L=1/4C

Wake Patterns

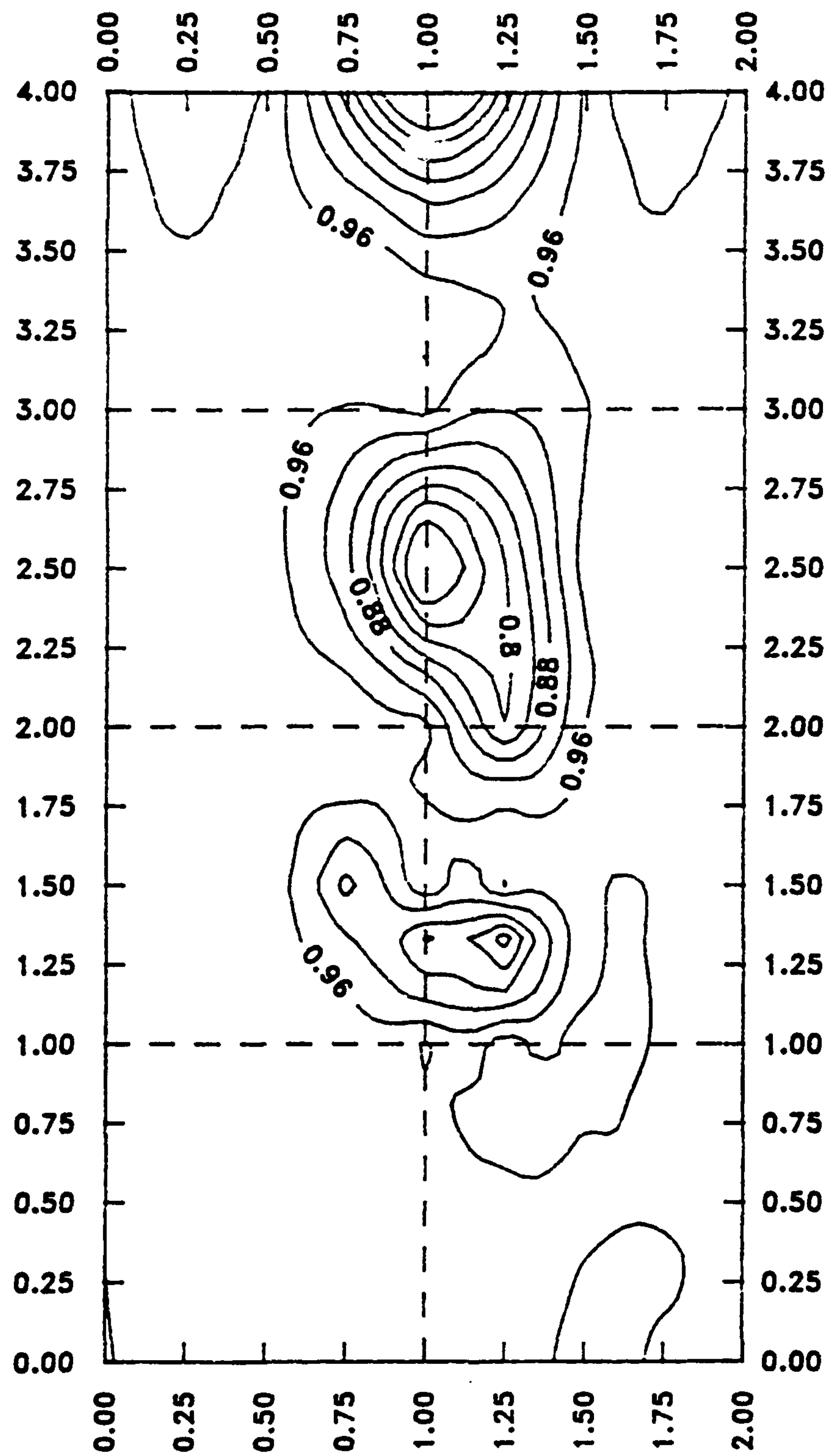

TRAVERSE PLANE SCALED IN INCHES
WINGTIP AT 1,1
VELOCITIES NON-DIMENSIONALIZED BY $u_{INFINITY}$

WRTE Wing L=1C

Wake Patterns

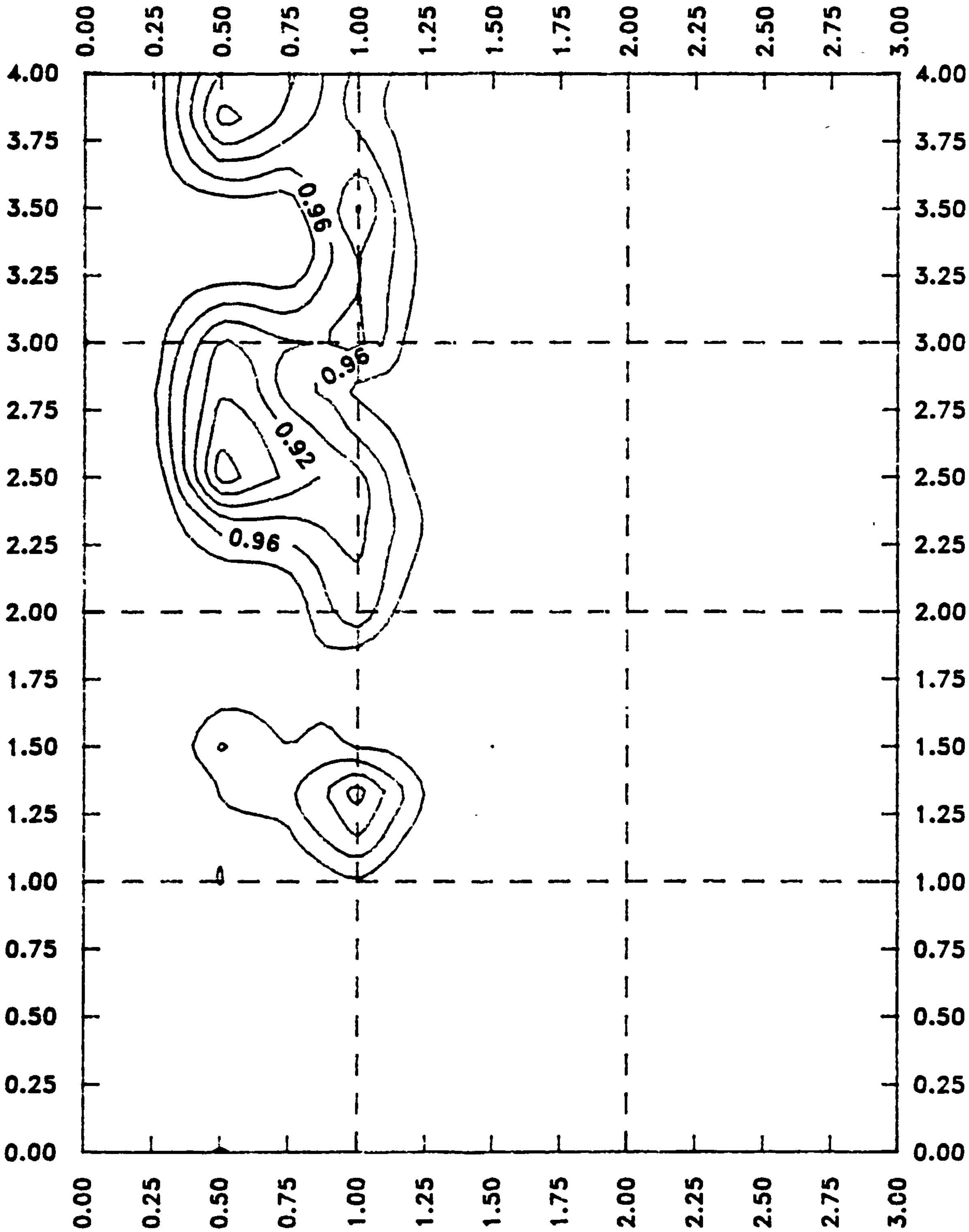

TRAVERSE PLANE SCALED IN INCHES
WINGTIP AT (1,1)
VELOCITIES NON-DIMENSIONALIZED BY $u_{INFINITY}$

Triangular TE Trip Wing L=1/4C

Wake Patterns

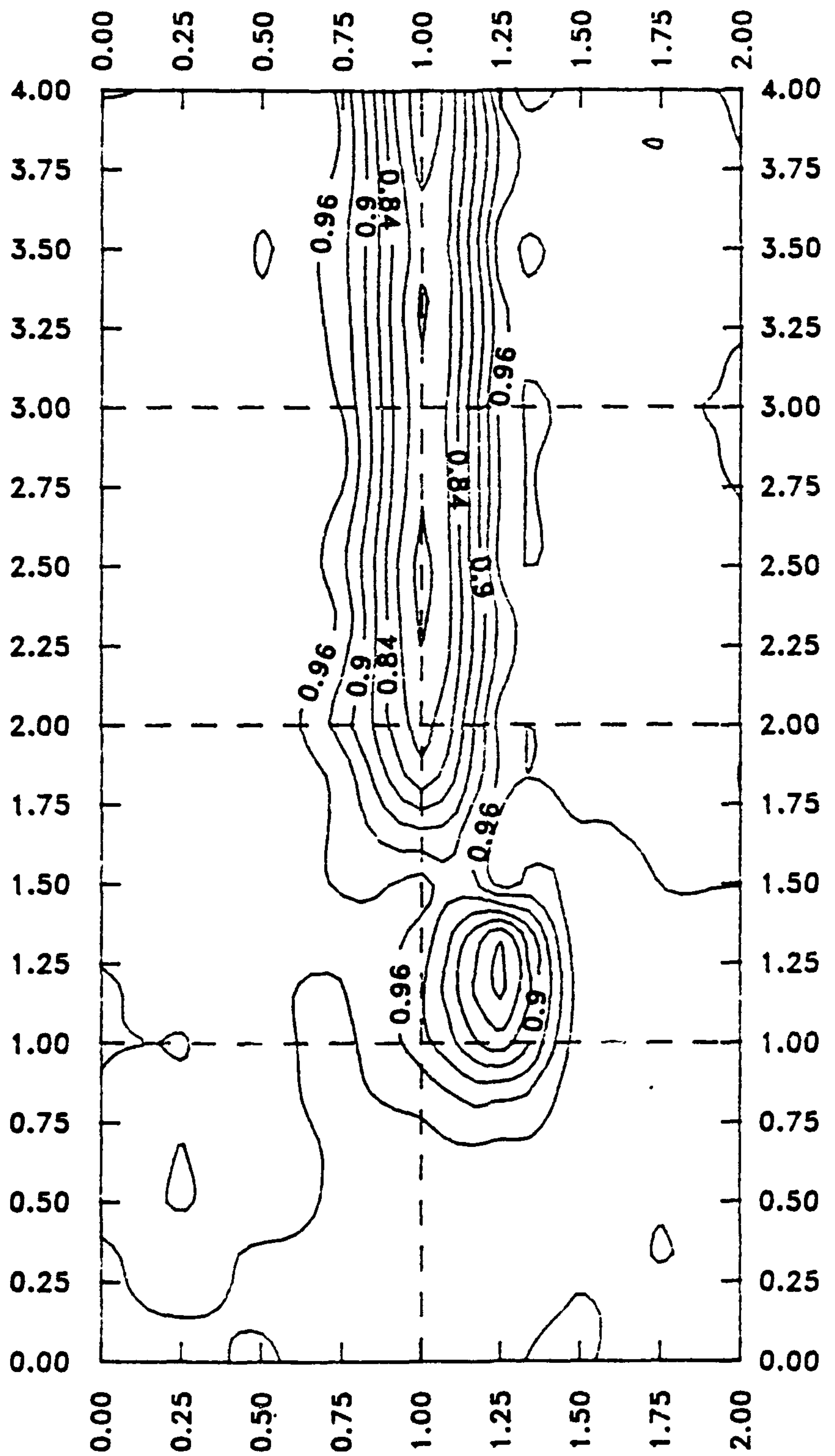

TRAVERSE PLANE SCALED IN INCHES
WINGTIP AT 1,1
VELOCITIES NON-DIMENSIONALIZED BY $u_{INFINITY}$

Triangular TE Trip Wing L=1C

Wake Patterns

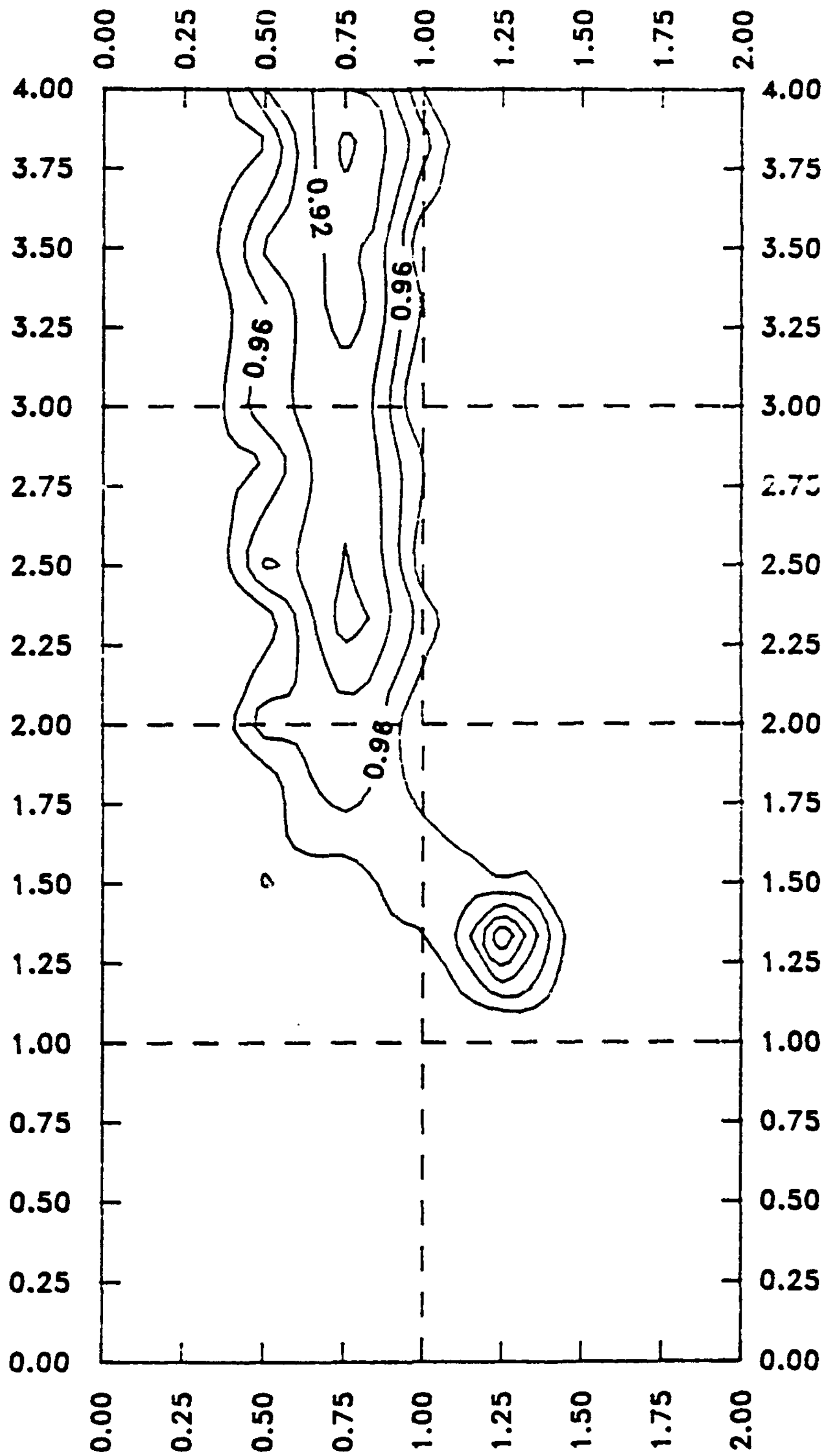

TRAVERSE PLANE SCALED IN INCHES
WINGTIP AT 1,1
VELOCITIES NON-DIMENSIONALIZED BY $u_{INFINITY}$

Triangular TE Trip Wing L=1.5C

Wake Patterns

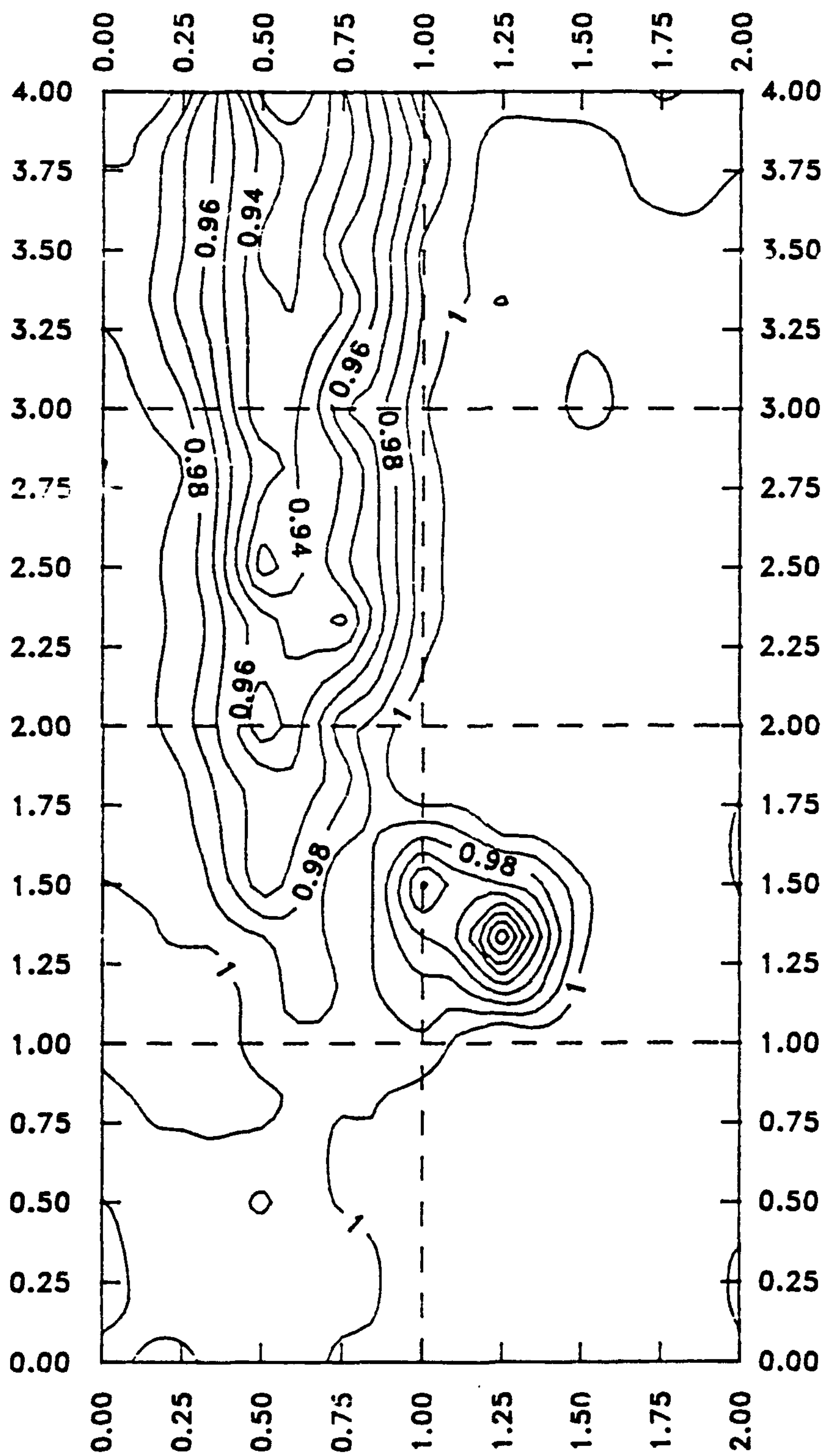

TRAVERSE PLANE SCALED IN INCHES
WINGTIP AT 1,1
VELOCITIES NON-DIMENSIONALIZED BY $u_{INFINITY}$

WRTE Trip Wing L=1/4C

Wake Patterns

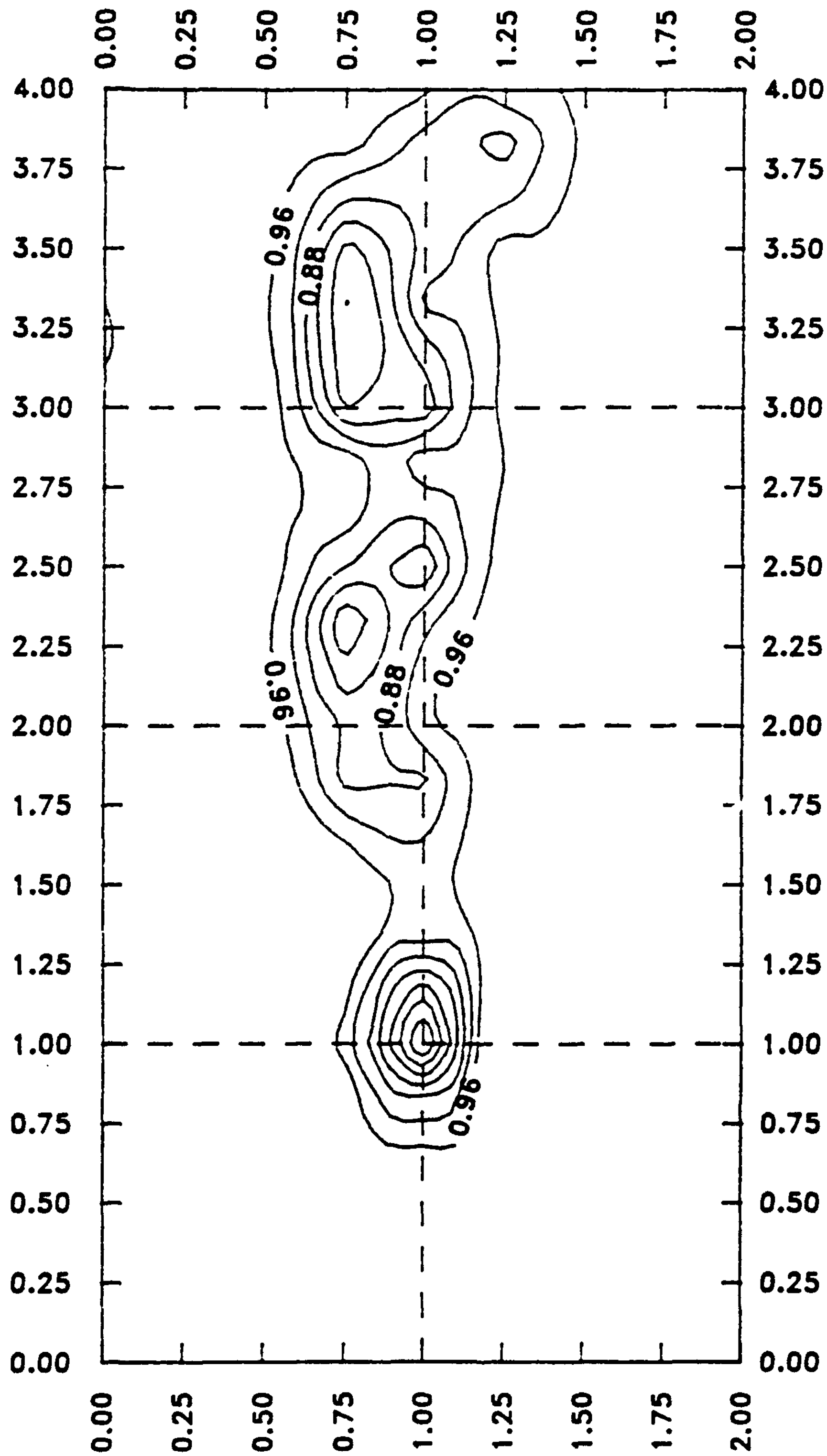

TRAVERSE PLANE SCALED IN INCHES
WINGTIP AT 1,1
VELOCITIES NON-DIMENSIONALIZED BY $u_{INFINITY}$

WRTE Trip Wing L=1C

Wake Patterns

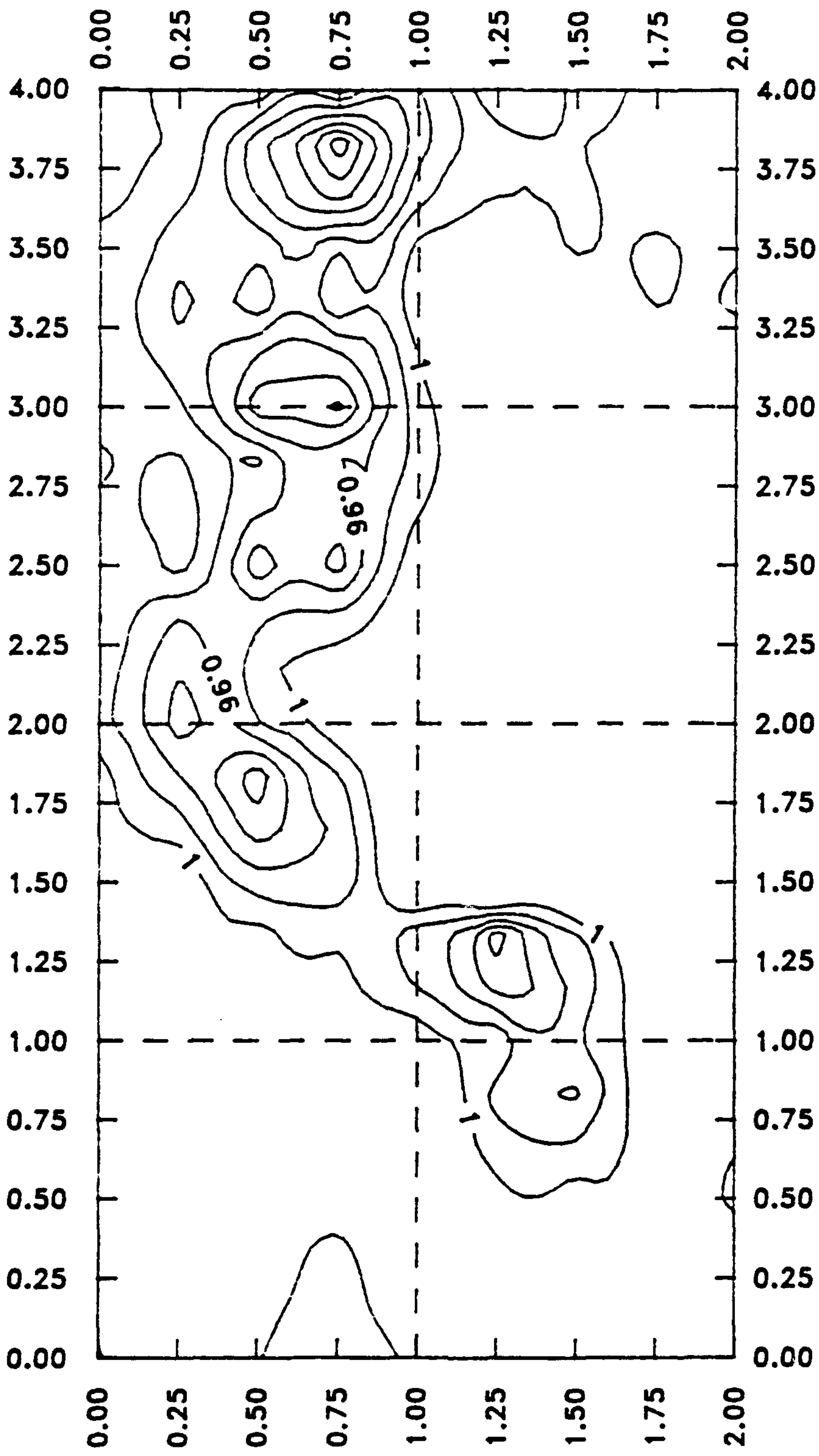

TRAVERSE PLANE SCALED IN INCHES
WINGTIP AT 1,1
VELOCITIES NON-DIMENSIONALIZED BY $u_{INFINITY}$

WRTE Trip Wing L=1.5C

Wake Patterns

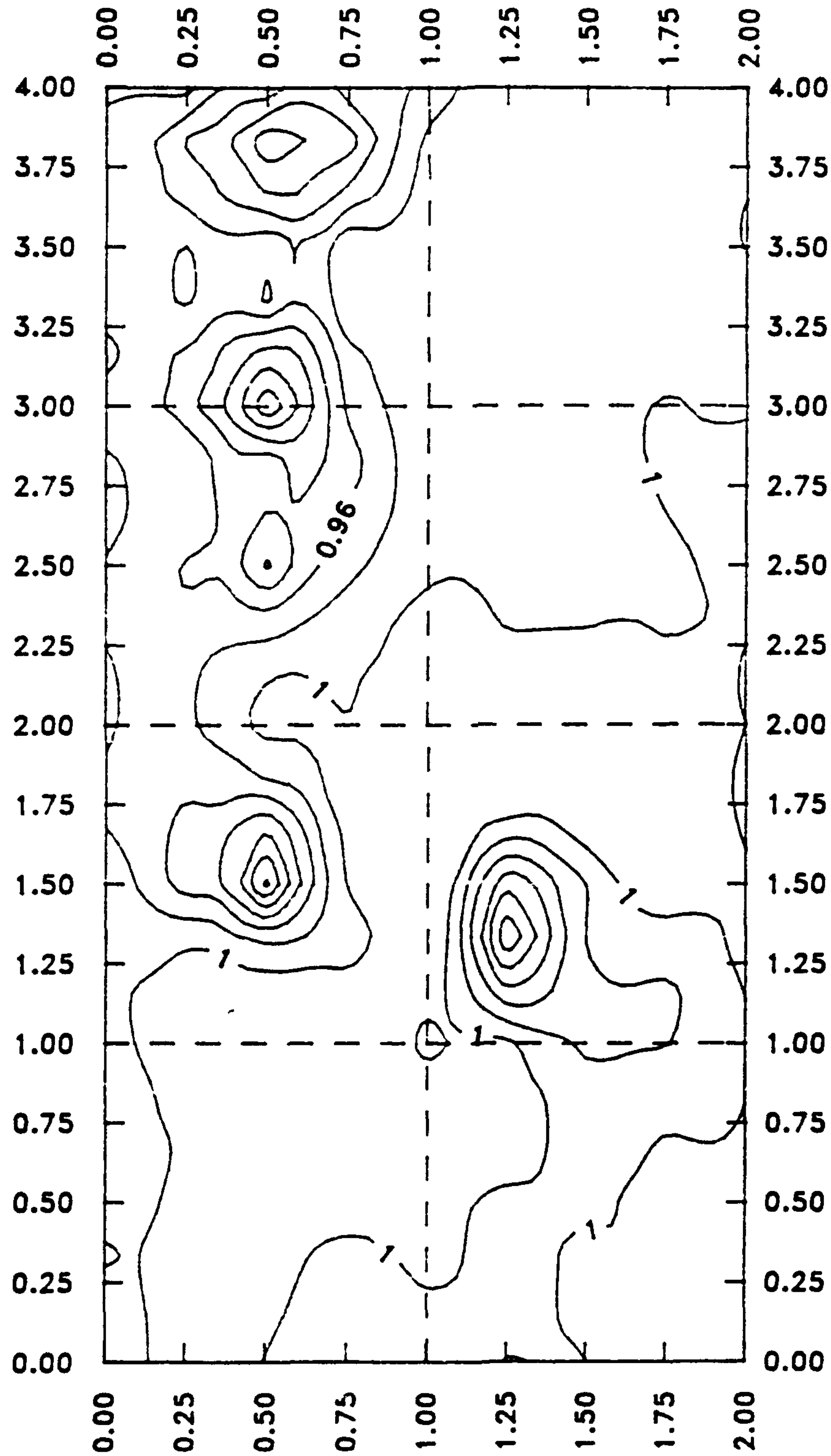

TRAVERSE PLANE SCALED IN INCHES
WINGTIP AT 1,1
VELOCITIES NON-DIMENSIONALIZED BY $u_{INFINITY}$

SRTE Wing L=1/4C

Wake Patterns

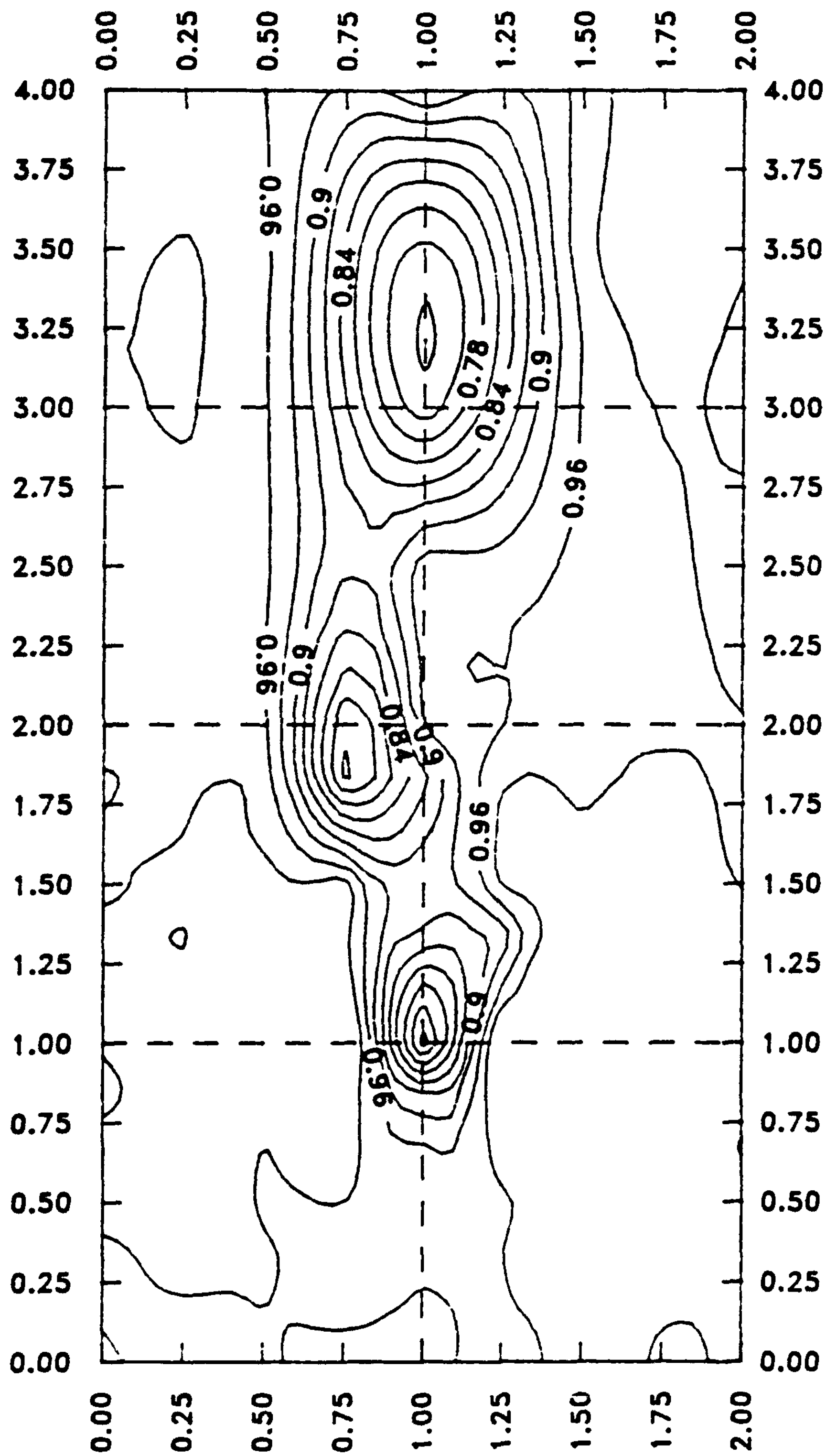

TRAVERSE PLANE SCALED IN INCHES
WINGTIP AT 1,1
VELOCITIES NON-DIMENSIONALIZED BY $u_{INFINITY}$

SRTE Wing L=1C

Wake Patterns

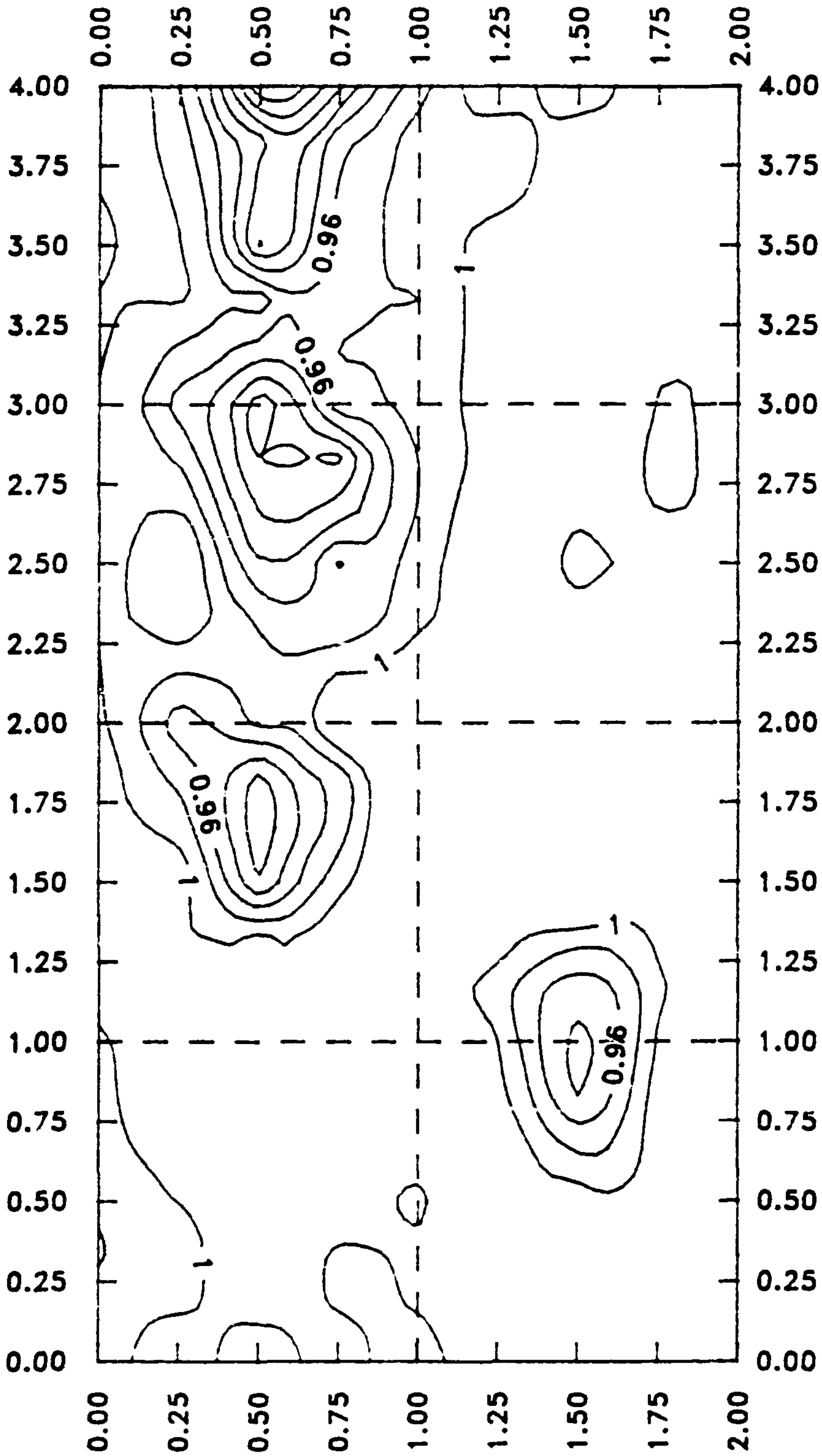

TRAVERSE PLANE SCALED IN INCHES
WINGTIP AT 1,1
VELOCITIES NON-DIMENSIONALIZED BY $u_{INFINITY}$

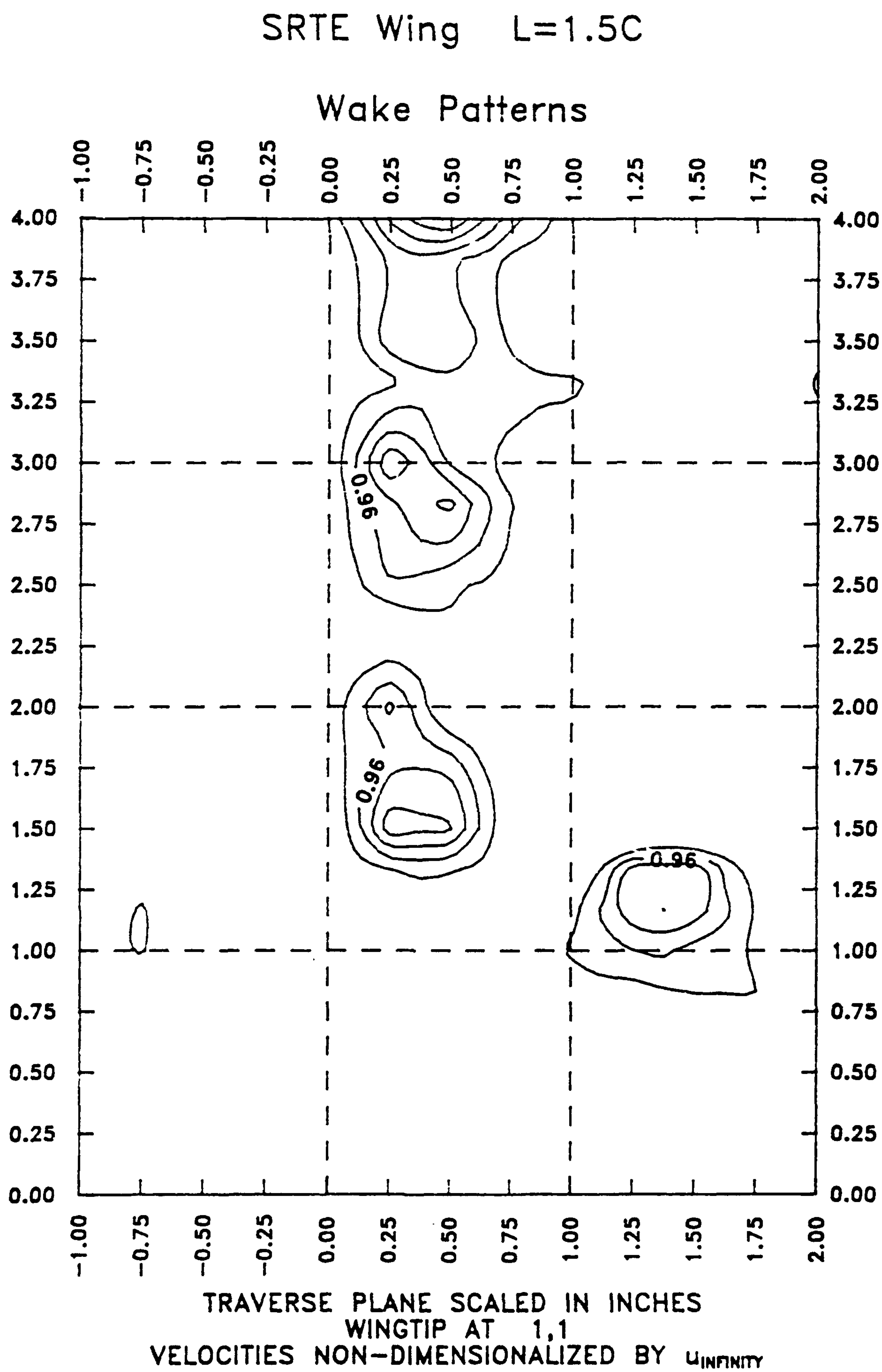

SRTE Wing L=1.5C
Wake Patterns
-1.00
-0.75
-0.50
-0.25
0.00
0.25
0.50
0.75
1.00
1.25
1.50
1.75
2.00
4.00
3.75
3.50
3.25
3.00
2.75
2.50
2.25
2.00
1.75
1.50
1.25
1.00
0.75
0.50
0.25
0.00
0.96
0.96
0.96
TRAVERSE PLANE SCALED IN INCHES
WINGTIP AT 1,1
VELOCITIES NON-DIMENSIONALIZED BY $u_{INFINITY}$

SRTE Trip Wing L=1/4C

Wake Patterns

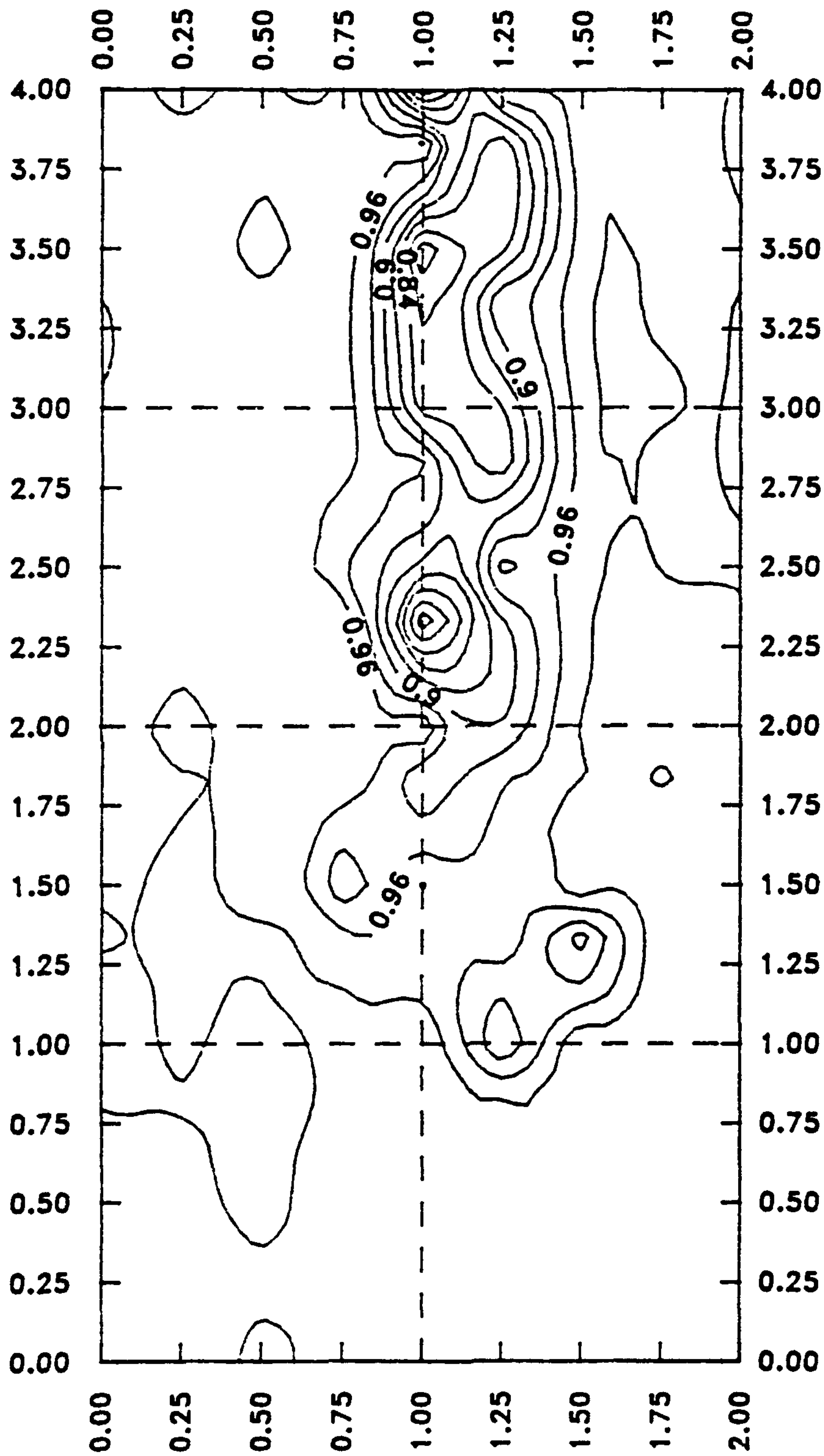

TRAVERSE PLANE SCALED IN INCHES
WINGTIP AT 1,1
VELOCITIES NON-DIMENSIONALIZED BY $u_{INFINITY}$

SRTE Trip Wing L=1C

Wake Patterns

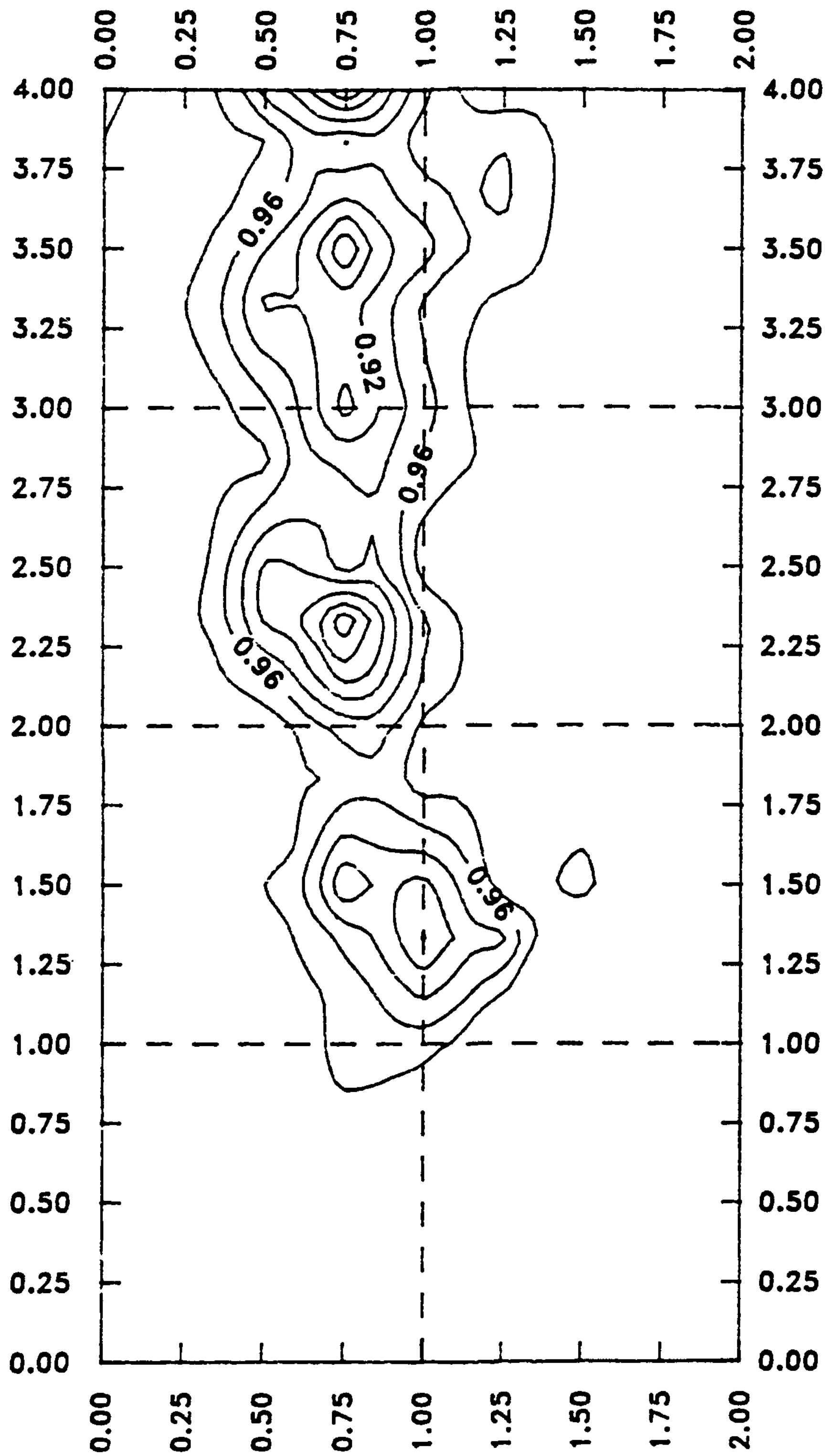

TRAVERSE PLANE SCALED IN INCHES
WINGTIP AT 1,1
VELOCITIES NON-DIMENSIONALIZED BY $u_{INFINITY}$

SRTE Trip Wing L=1.5C

Wake Patterns

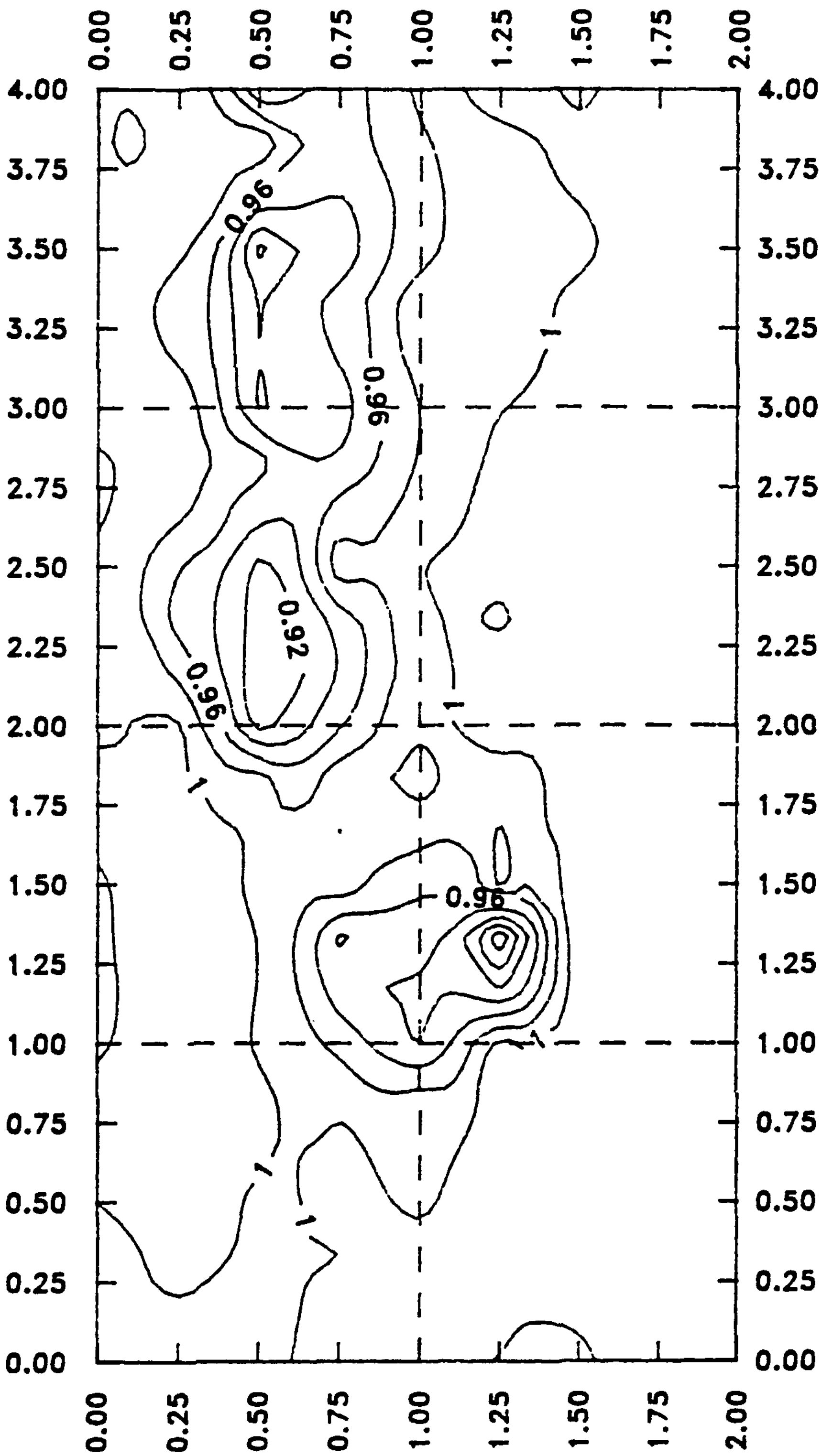

TRAVERSE PLANE SCALED IN INCHES
WINGTIP AT 1,1
VELOCITIES NON-DIMENSIONALIZED BY $u_{INFINITY}$

LE Groove Wing L=1/4C

Wake Patterns

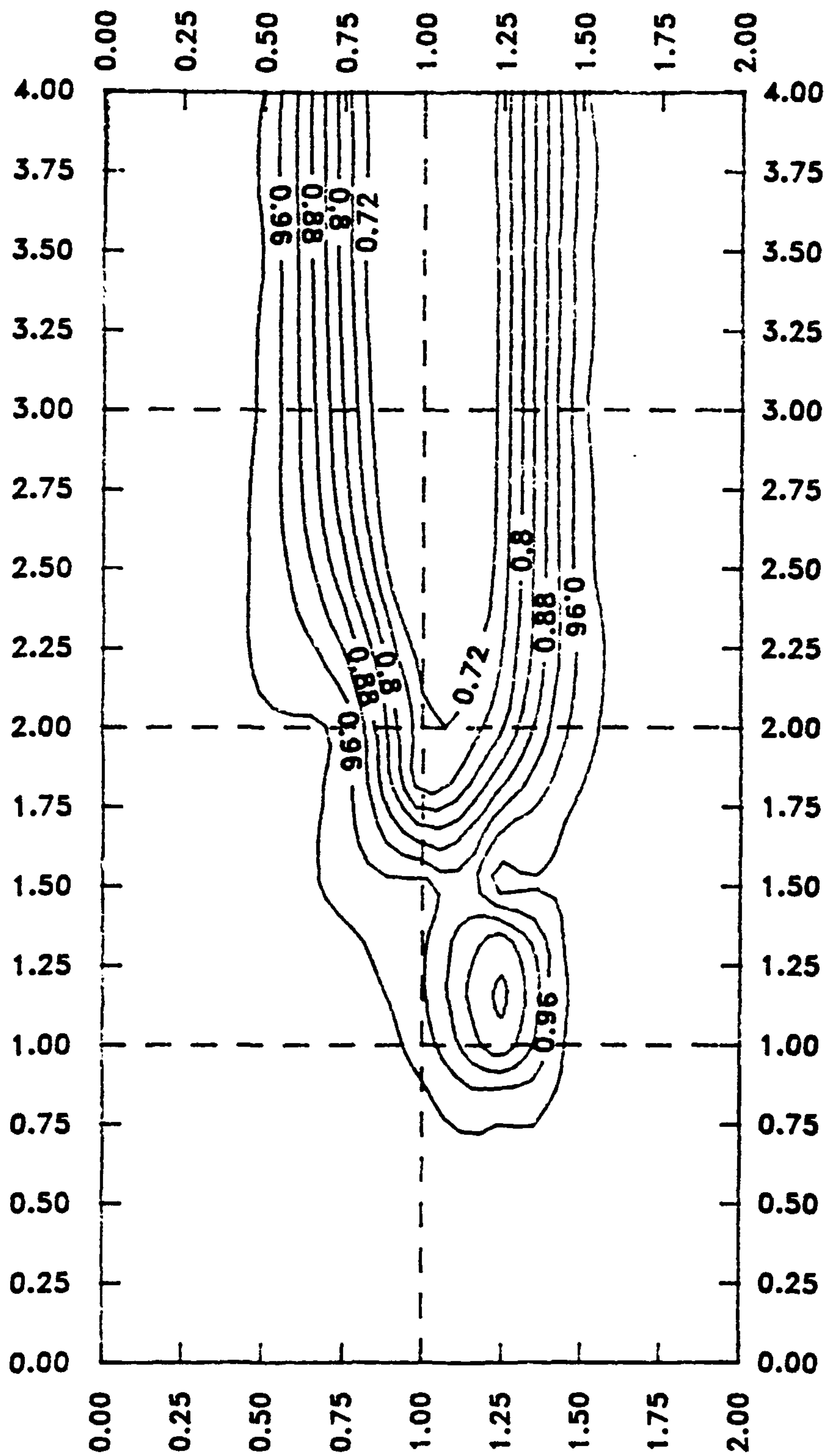

TRAVERSE PLANE SCALED IN INCHES
WINGTIP AT 1,1
VELOCITIES NON-DIMENSIONALIZED BY $u_{INFINITY}$

LE Groove Wing L=1C

Wake Patterns

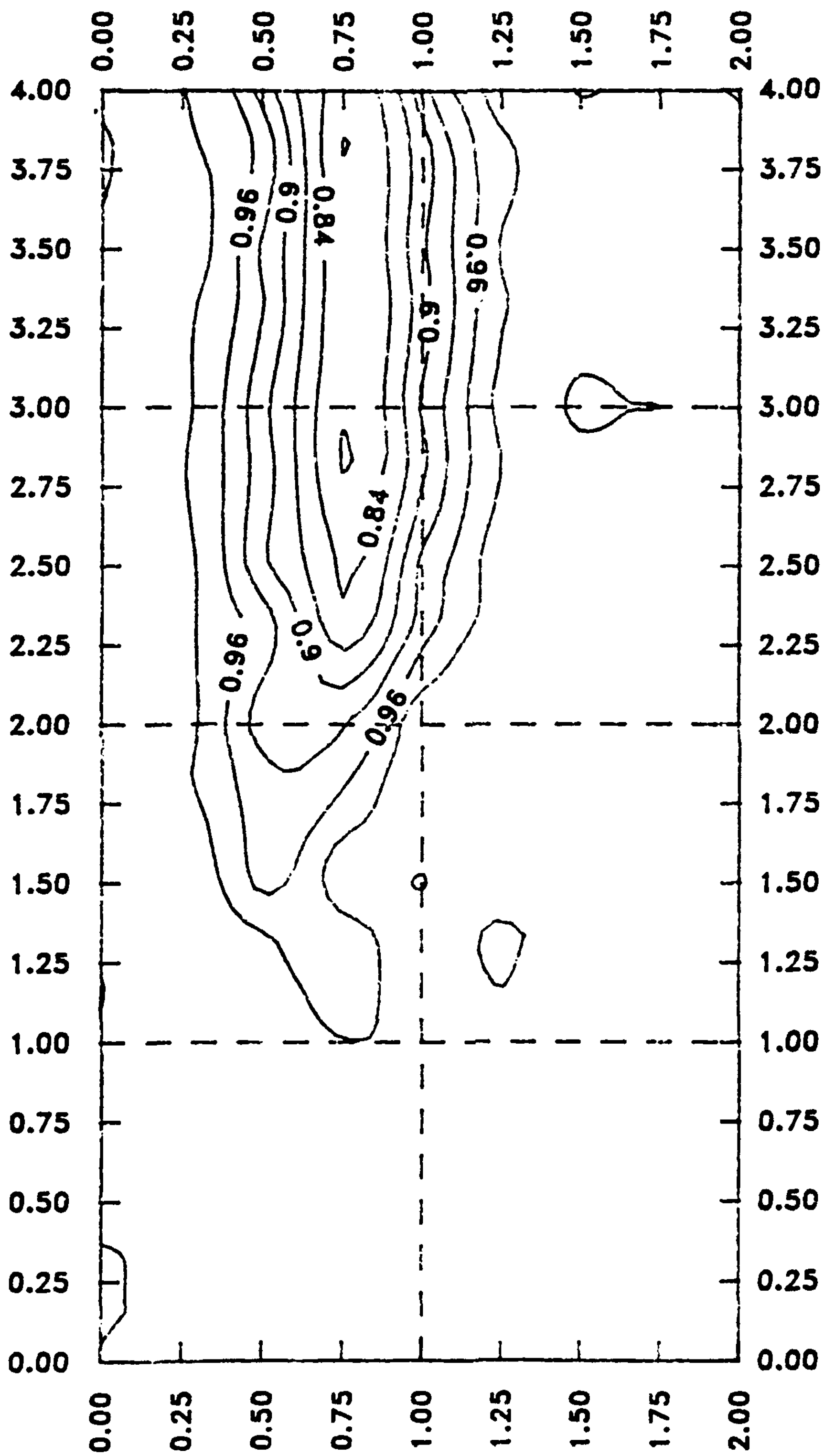

TRAVERSE PLANE SCALED IN INCHES
WINGTIP AT 1,1
VELOCITIES NON-DIMENSIONALIZED BY $u_{INFINITY}$

LE Groove Wing L=1.5C

Wake Patterns

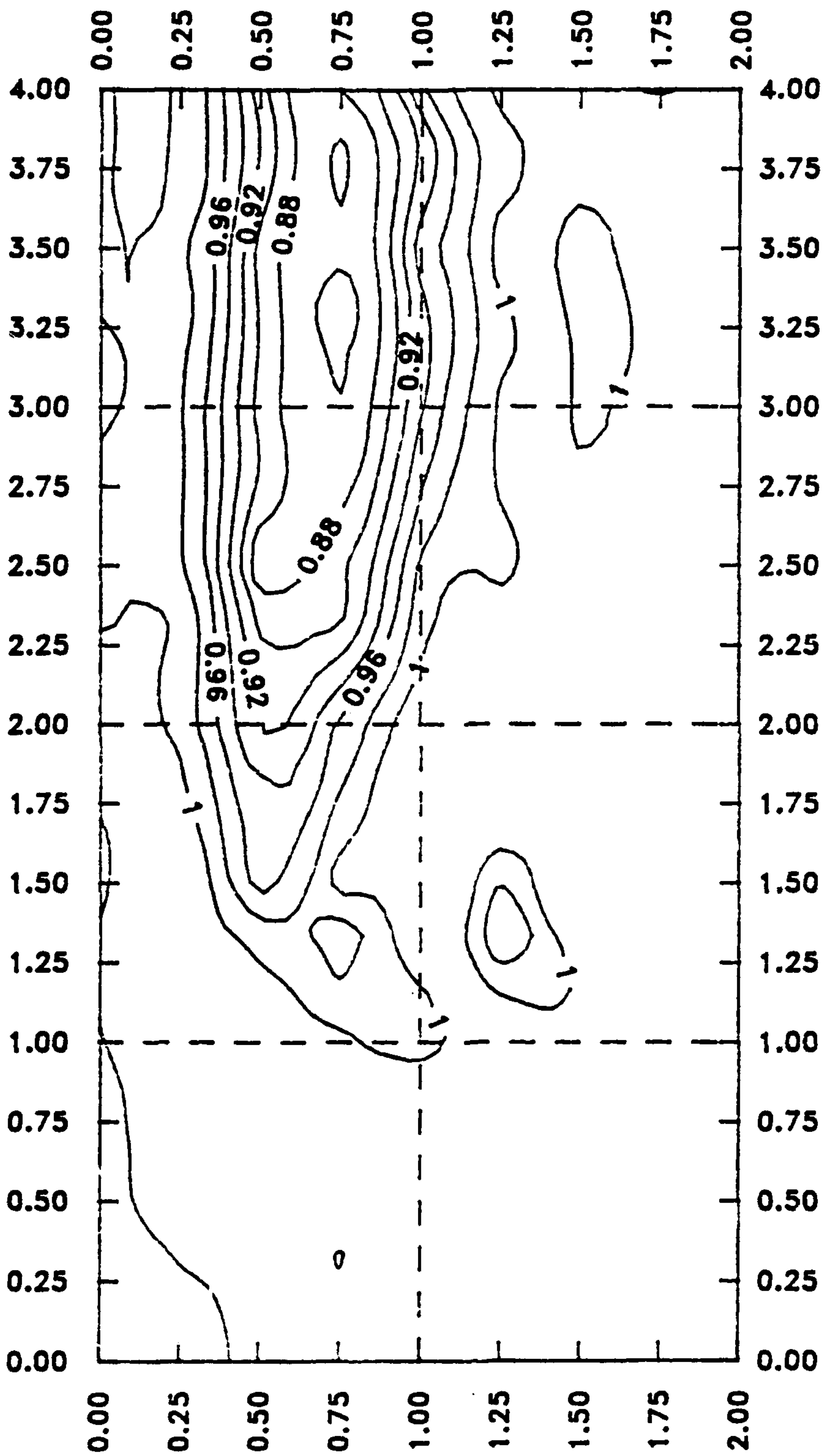

TRAVERSE PLANE SCALED IN INCHES
WINGTIP AT 1,1
VELOCITIES NON-DIMENSIONALIZED BY $u_{INFINITY}$

Middle Groove Wing L=1/4C

Wake Patterns

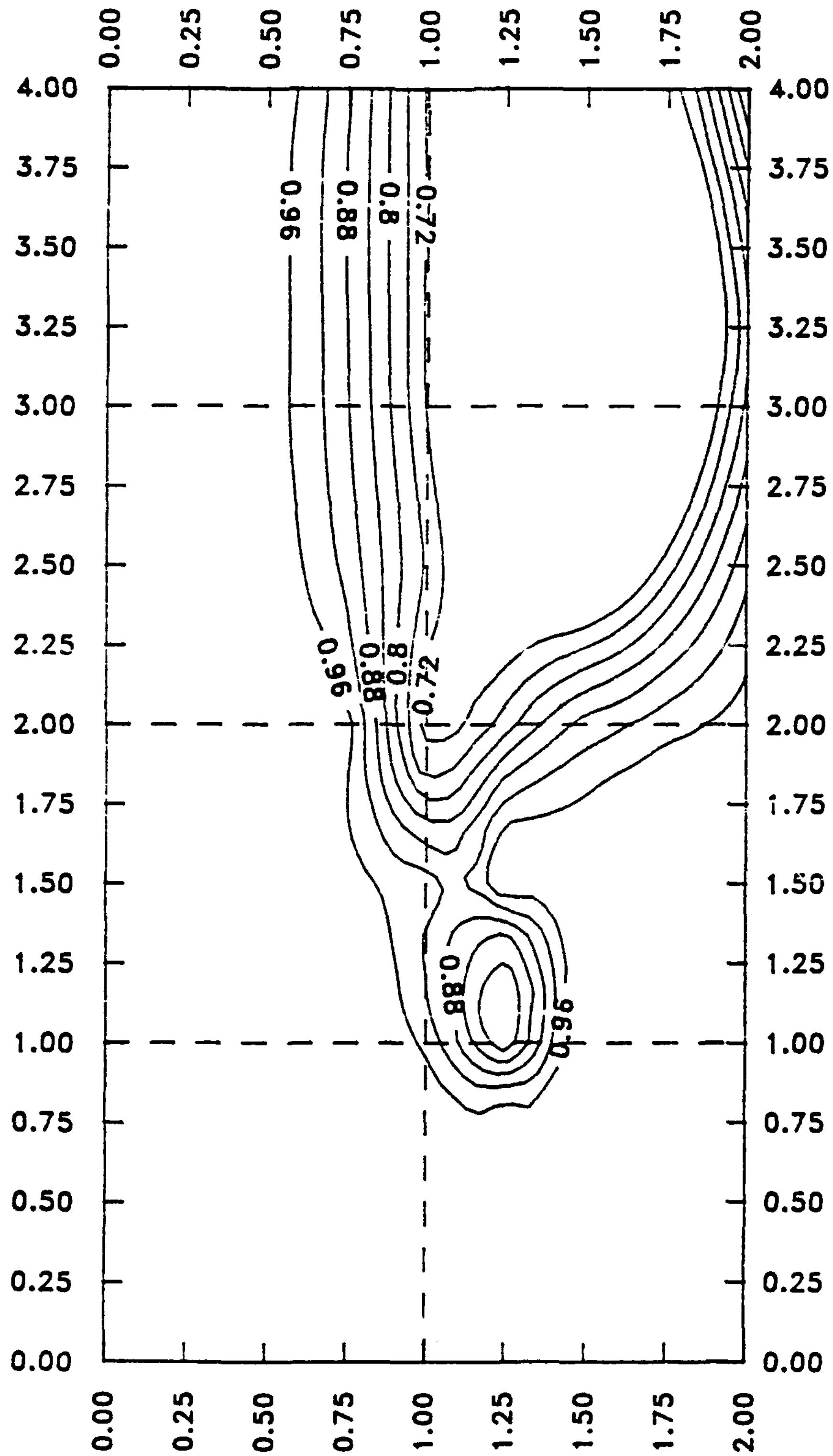

TRAVERSE PLANE SCALED IN INCHES
WINGTIP AT 1,1
VELOCITIES NON-DIMENSIONALIZED BY $u_{INFINITY}$

Middle Groove Wing L=1C

Wake Patterns

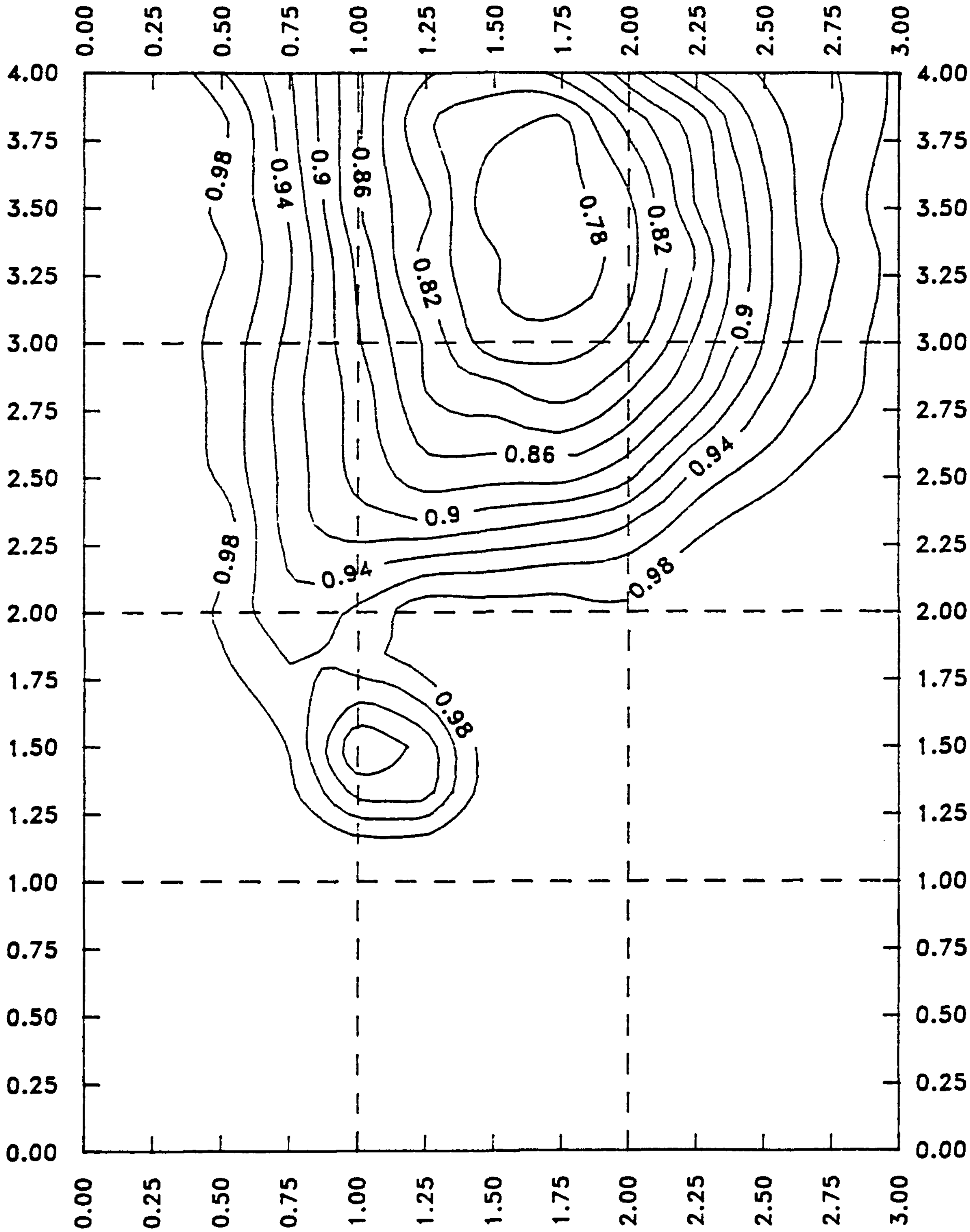

TRAVERSE PLANE SCALED IN INCHES
WINGTIP AT (1,1)
VELOCITIES NON-DIMENSIONALIZED BY $u_{INFINITY}$

Middle Groove Wing L=1.5C

Wake Patterns

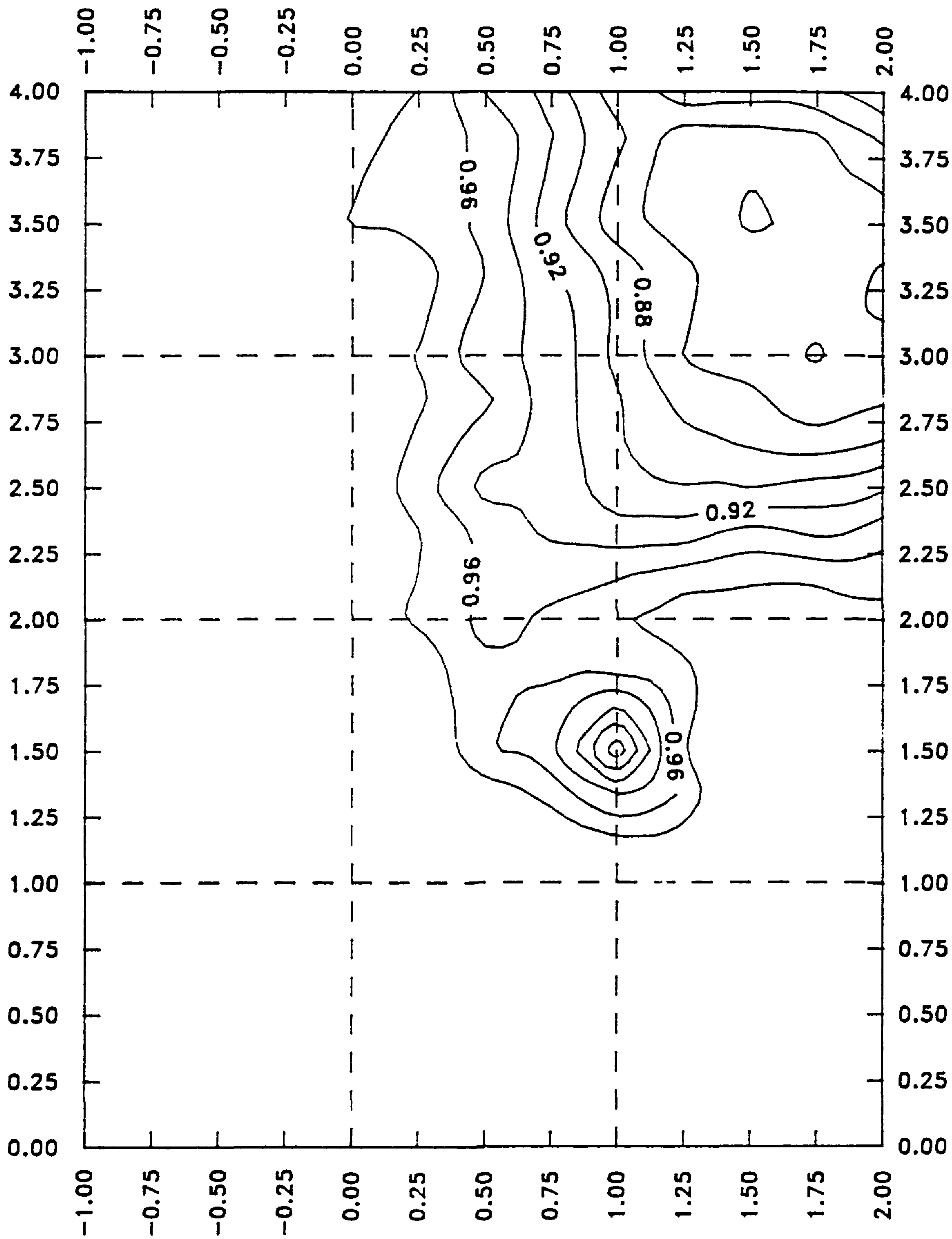

TRAVERSE PLANE SCALED IN INCHES
WINGTIP AT 1,1
VELOCITIES NON-DIMENSIONALIZED BY $u_{INFINITY}$

Appendix F

Calibration Data

Page ____

7/19/90

Spent time working on CNC with Bull and Dave Sheppard

THE SLOPE IS .9533939

THE Y INTERCEPT IS -9.594238E-04

THE X INTERCEPT IS 1.006325E-03

CALIBRATION OF MECHANICAL BALANCE ON SMALL WIND TUNNEL
DATE: 7/19/90 TYPE: drag CRAIG HUNTER

GRAMS	POUNDS	READING
0.000	0.000	0.000
50.100	0.110	0.105
70.100	0.155	0.150
90.100	0.199	0.195
110.100	0.243	0.235
130.100	0.287	0.282
150.100	0.331	0.320
170.100	0.375	0.360
190.100	0.419	0.400
210.100	0.463	0.445
230.100	0.507	0.485
250.100	0.551	0.525
270.100	0.595	0.560
290.100	0.640	0.600
270.100	0.595	0.563
250.100	0.551	0.520
230.100	0.507	0.485
210.100	0.463	0.445
190.100	0.419	0.400
170.100	0.375	0.355
150.100	0.331	0.315
130.100	0.287	0.275
110.100	0.243	0.230
90.100	0.199	0.185
70.100	0.155	0.140
50.100	0.110	0.100
0.000	0.000	-0.015

Page ___

CALIBRATION OF MECHANICAL BALANCE ON SMALL WIND TUNNEL

DATE: 7/19/90 TYPE: lift CRAIG HUNTER

GRAMS	POUNDS	READING
0.000	0.000	0.000
20.000	0.044	0.030
40.000	0.088	0.060
60.000	0.132	0.090
80.000	0.176	0.123
100.000	0.220	0.170
120.000	0.265	0.200
140.000	0.309	0.235
160.000	0.353	0.262
180.000	0.397	0.300
200.000	0.441	0.350
220.000	0.485	0.385
240.000	0.529	0.415
260.000	0.573	0.445
280.000	0.617	0.482
300.000	0.661	0.520
280.000	0.617	0.490
260.000	0.573	0.460
240.000	0.529	0.420
220.000	0.485	0.390
200.000	0.441	0.360
180.000	0.397	0.320
160.000	0.353	0.285
140.000	0.309	0.255
120.000	0.265	0.220
100.000	0.220	0.185
80.000	0.176	0.140
60.000	0.132	0.105
40.000	0.088	0.075
20.000	0.044	0.040
0.000	0.000	-1.000

THE SLOPE IS .794292

THE Y INTERCEPT IS -2.175258E-03

THE X INTERCEPT IS 2.738612E-03

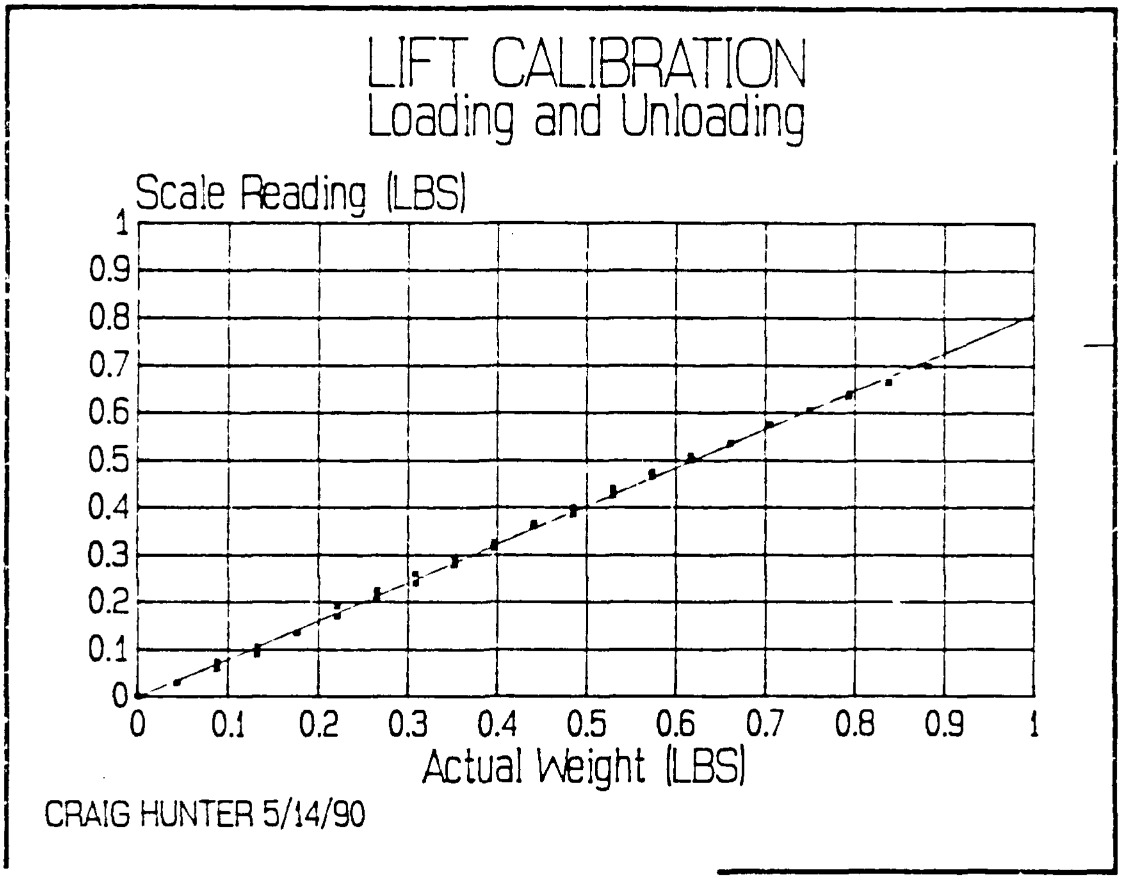

CALIBRATION OF MECHANICAL BALANCE ON SMALL WIND TUNNEL
DATE: 5/14/90 TYPE: LIFT CRAIG HUNTER

GRAMS	POUNDS	READING
0.000	0.000	0.000
20.000	0.044	0.030
40.000	0.088	0.060
~~0.090~~	~~0.090~~	~~0.090~~
60.000	0.132	0.090
80.000	0.176	0.135
100.000	0.220	0.170
120.000	0.265	0.210
140.000	0.309	0.240
160.000	0.353	0.280
180.000	0.397	0.315
200.000	0.441	0.360
220.000	0.485	0.385
240.000	0.529	0.425
260.000	0.573	0.465
280.000	0.617	0.500
300.000	0.661	0.535
320.000	0.705	0.575
340.000	0.750	0.605
360.000	0.794	0.635
380.000	0.838	0.665
400.000	0.882	0.700
380.000	0.838	0.665
360.000	0.794	0.640
340.000	0.750	0.605
320.000	0.705	0.575
300.000	0.661	0.535
280.000	0.617	0.510
260.000	0.573	0.475
240.000	0.529	0.440
220.000	0.485	0.400
200.000	0.441	0.365
180.000	0.397	0.325
160.000	0.353	0.295
140.000	0.309	0.260
120.000	0.265	0.225
100.000	0.220	0.190
80.000	0.176	0.135
60.000	0.132	0.105
40.000	0.088	0.075
20.000	0.044	[illegible]
0.000	[illegible]	[illegible]

```
THE SLOPE IS  .8093528

THE Y INTERCEPT IS -1.082829E-03

THE X INTERCEPT IS  1.337894E-03

A:\PROG>
```

```
CLS
INPUT "    ENTER THE CALIBRATION TYPE (LIFT/DRAG) ", A$
PRINT
PRINT
INPUT "          ENTER THE DATE  ", D$
KILL "DATAP.BAS"
KILL "DATAG.BAS"
OPEN "DATAP.BAS" FOR OUTPUT AS #1
OPEN "DATAG.BAS" FOR OUTPUT AS #2
LPRINT "   CALIBRATION OF MECHANICAL BALANCE ON SMALL WIND TUNNEL"
LPRINT "       DATE: "; D$, "     TYPE: "; A$, "   PASQUALE DELORE"
LPRINT : LPRINT : LPRINT
LPRINT "    GRAMS                       POUNDS                      READING"
LPRINT "__________________________________________________________"
LPRINT : LPRINT
WHILE G <> -1
PRINT
INPUT "         ENTER THE LOAD IN GRAMS   ", G
IF G = -1 THEN GOTO 10
INPUT "              ENTER THE SCALE READING IN POUNDS   ", S
P = G * (.0022046)
LPRINT USING "####.###                ####.###                 ##.###"; G
WRITE #1, P, S
WRITE #2, G, S
10      WEND
CLOSE #1
CLOSE #2
END
```

```
        CLS
        LOCATE 12, 15: INPUT "PLEASE ENTER THE NAME OF THE DATA FILE  ", DATA$
        LOCATE 15, 20: INPUT "PLEASE ENTER THE DATE  ", DAT$
        CLS
        OPEN DATA$ FOR OUTPUT AS #1
        APLAN = .09375
        VEL = 71.7
        RHO = .0023035
        DENOM = .5 * RHO * VEL ^ 2 * APLAN
        LPRINT : LPRINT : LPRINT
        LPRINT "          PASQUALE DELORE                                      ", DAT$
        LPRINT : LPRINT : LPRINT
        LPRINT "          ANGLE                  COF. DRAG                   COF.
        LPRINT "______________________________________________________________
        LPRINT : LPRINT
HOME:   INPUT "     ENTER THE ANGLE OF ATTACK IN DEGREES  ", ANGLE
        IF ANGLE < 0 THEN GOTO LAST
        PRINT
        INPUT "          ENTER THE LIFT FORCE IN POUNDS  ", LFR
        PRINT
        INPUT "               ENTER THE DRAG FORCE IN POUNDS  ", DFR
        PRINT : PRINT
        ALF = (LFR - .017438) / .791037
        ADF = (DFR - .0012966) / .936326
        CL = ALF / DENOM
        CD = ADF / DENOM
        LPRINT USING "     ####.###                  ####.###
        WRITE #1, ANGLE, CD, CL
        GOTO HOME
LAST:   CLOSE #1
        END
```

```
CLS
PRINT "PROGRAM FOR THE METHOD OF LEAST SQUARES": PRINT : PRINT
PRINT "DRAWS THE BEST STRAIGHT LINE THROUGH A SET OF POINTS": PRINT : :
INPUT "  ENTER THE NAME OF THE DATA FILE TO READ  ", A$
OPEN A$ FOR INPUT AS #1
PRINT : PRINT "INPUT THE NUMBER OF SETS OF POINTS": INPUT N: PRINT : P:
FOR I = 1 TO N
INPUT #1, X, Y
SUMXY = SUMXY + (X * Y)
SUMX = SUMX + X
SUMY = SUMY + Y
SUMX2 = SUMX2 + (X * X)
NEXT I
M = ((N * SUMXY) - (SUMX * SUMY)) / ((N * SUMX2) - (SUMX * SUMX))
B = ((SUMX2 * SUMY) - (SUMX * SUMXY)) / ((N * SUMX2) - (SUMX * SUMX))
XI = -B / M
CLS
PRINT "THE SLOPE IS "; M: PRINT
PRINT "THE Y INTERCEPT IS "; B: PRINT
PRINT "THE X INTERCEPT IS "; XI
CLOSE #1
END
```

CALIBRATION OF MECHANICAL BALANCE ON SMALL WIND TUNNEL

DATE: 11/04/89 TYPE: LIFT PASQUALE

GRAMS	POUNDS	READING
0.000	0.000	0.000
20.000	0.044	0.030
40.000	0.088	0.065
60.000	0.132	0.098
80.000	0.176	0.130
100.000	0.220	0.165
120.000	0.265	0.210
140.000	0.309	0.240
160.000	0.353	0.280
180.000	0.397	0.320
200.000	0.441	0.350
220.000	0.485	0.390
240.000	0.529	0.418
260.000	0.573	0.450
280.000	0.617	0.490
300.000	0.661	0.525
320.000	0.705	0.560
340.000	0.750	0.590
360.000	0.794	0.630
380.000	0.838	0.665
400.000	0.882	0.703
380.000	0.838	0.670
360.000	0.794	0.640
340.000	0.750	0.605
320.000	0.705	0.570
300.000	0.661	0.535
280.000	0.617	0.500
260.000	0.573	0.470
240.000	0.529	0.435
220.000	0.485	0.397
200.000	0.441	0.365
180.000	0.397	0.325
160.000	0.353	0.290
140.000	0.309	0.255
120.000	0.265	0.215
100.000	0.220	0.180
80.000	0.176	0.145
60.000	0.132	0.105
40.000	0.088	0.070
20.000	0.044	0.030
0.000	0.000	0.000

```
THE SLOPE IS  .8033251
THE Y INTERCEPT IS -1.392296E-03
THE X INTERCEPT IS  1.733166E-03
A:\PROG>
```

LIFT CALIBRATION
Loading and Unloading

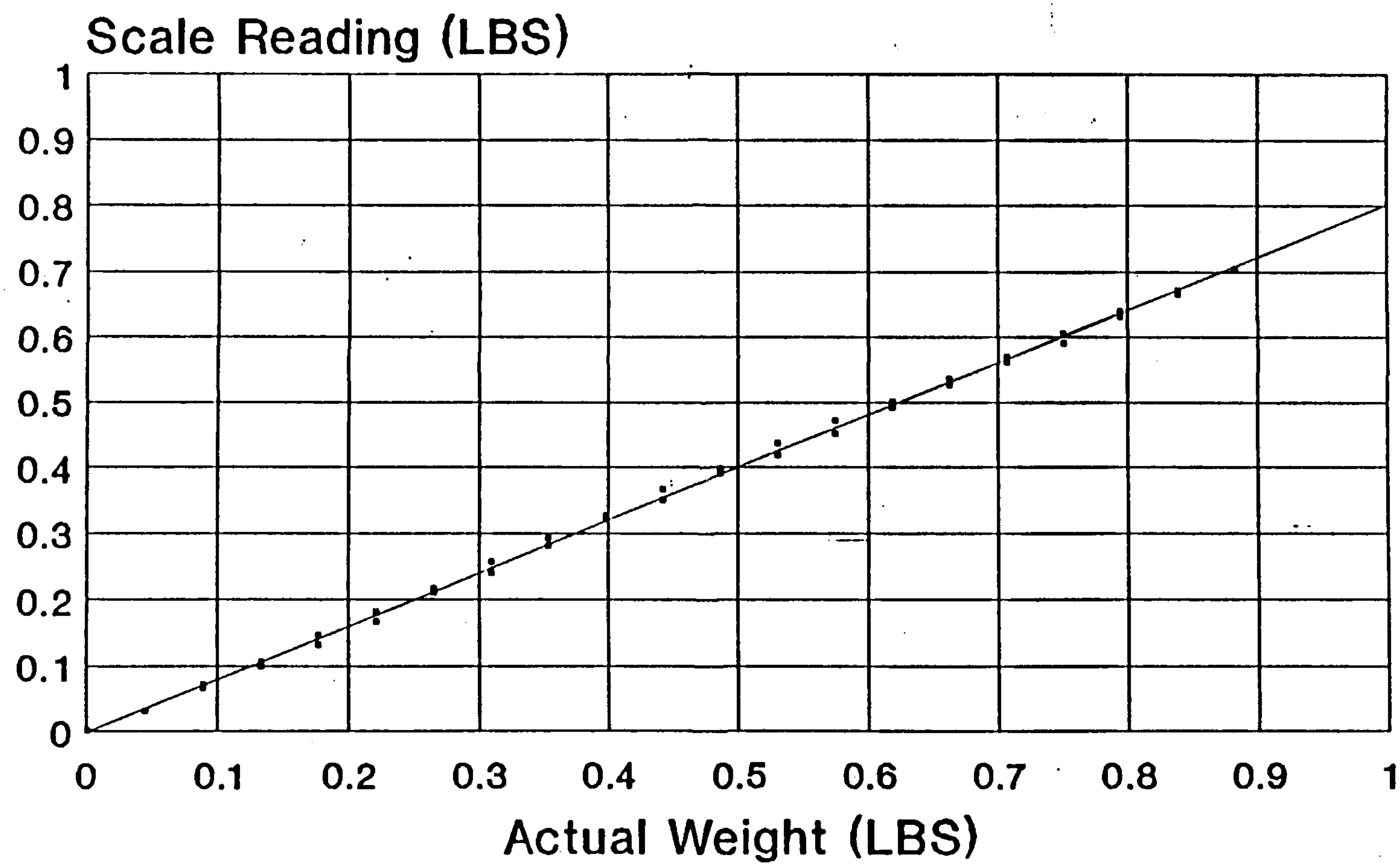

Pasquale Delore
11/04/89

CALIBRATION OF MECHANICAL BALANCE ON SMALL WIND TUNNEL
DATE: 11/04/89 TYPE: DRAG PASQUAL:

GRAMS	POUNDS	READING
0.000	0.000	0.000
20.000	0.044	0.045
40.000	0.088	0.090
60.000	0.132	0.135
80.000	0.176	0.180
100.000	0.220	0.225
120.000	0.265	0.270
140.000	0.309	0.310
160.000	0.353	0.355
180.000	0.397	0.400
200.000	0.441	0.448
220.000	0.485	0.483
240.000	0.529	0.523
260.000	0.573	0.570
280.000	0.617	0.617
300.000	0.661	0.656
320.000	0.705	0.705
~~0.745~~	~~0.882~~	~~0.745~~
340.000	0.750	0.745
360.000	0.794	0.787
380.000	0.838	0.827
400.000	0.882	0.865
380.000	0.838	0.830
360.000	0.794	0.790
340.000	0.750	0.747
320.000	0.705	0.705
300.000	0.661	0.663
280.000	0.617	0.623
260.000	0.573	0.575
240.000	0.529	0.530
220.000	0.485	0.485
200.000	0.441	0.445
180.000	0.397	0.405
160.000	0.353	0.360
140.000	0.309	0.315
120.000	0.265	0.273
100.000	0.220	0.224
80.000	0.176	0.180
60.000	0.132	0.137
40.000	0.088	0.093
20.000	0.044	0.045
0.000	0.000	0.000

```
THE SLOPE IS  .9874508
THE Y INTERCEPT IS  5.988509E-03
THE X INTERCEPT IS -6.064616E-03
A:\PROG>
```

DRAG CALIBRATION
Loading and Unloading

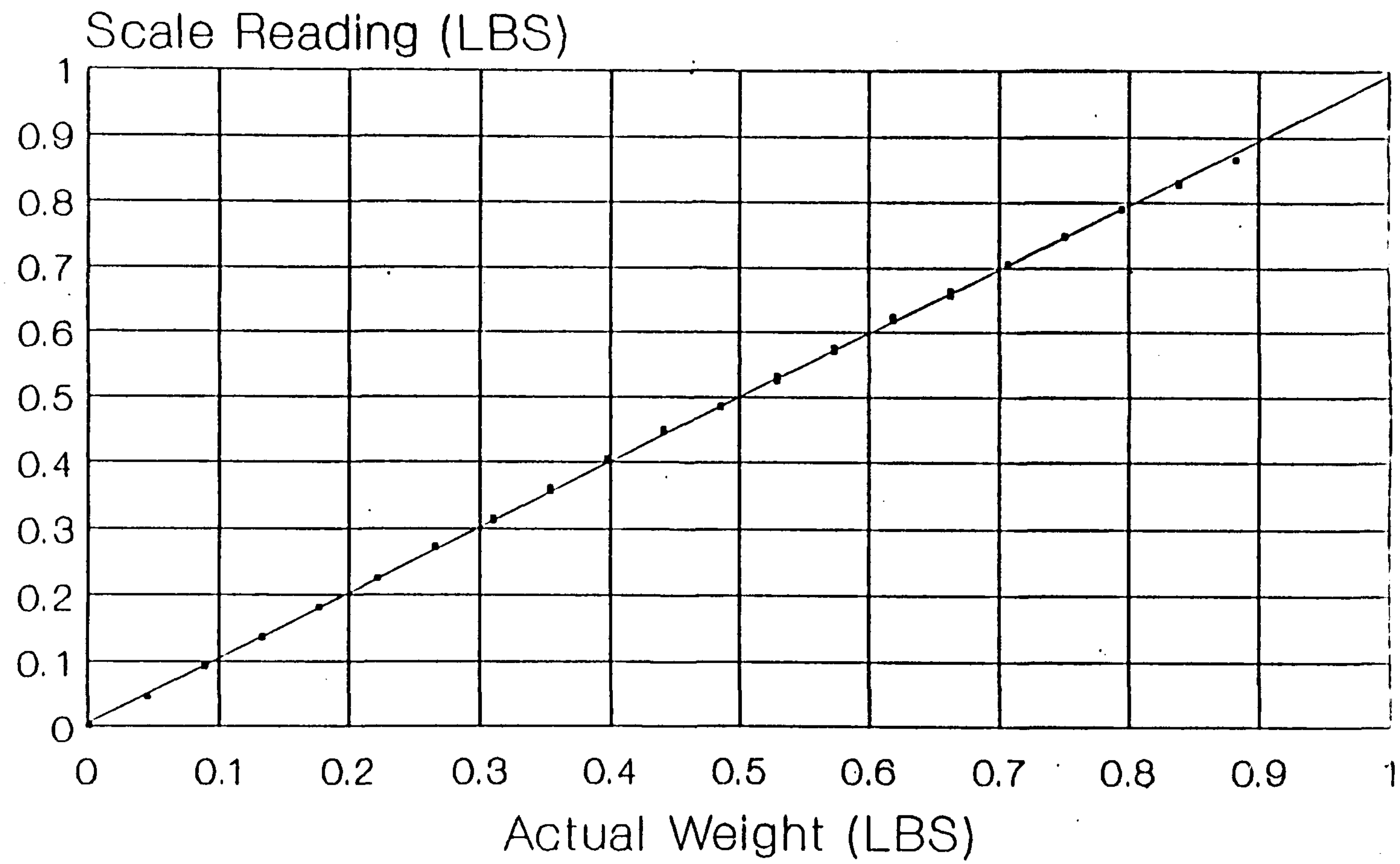

Pasquale Delore
11/04/89

Appendix G

Lift/Drag Data

Baseline Wing w/ LE Trip

Coefficient of Lift vs. Angle of Attack

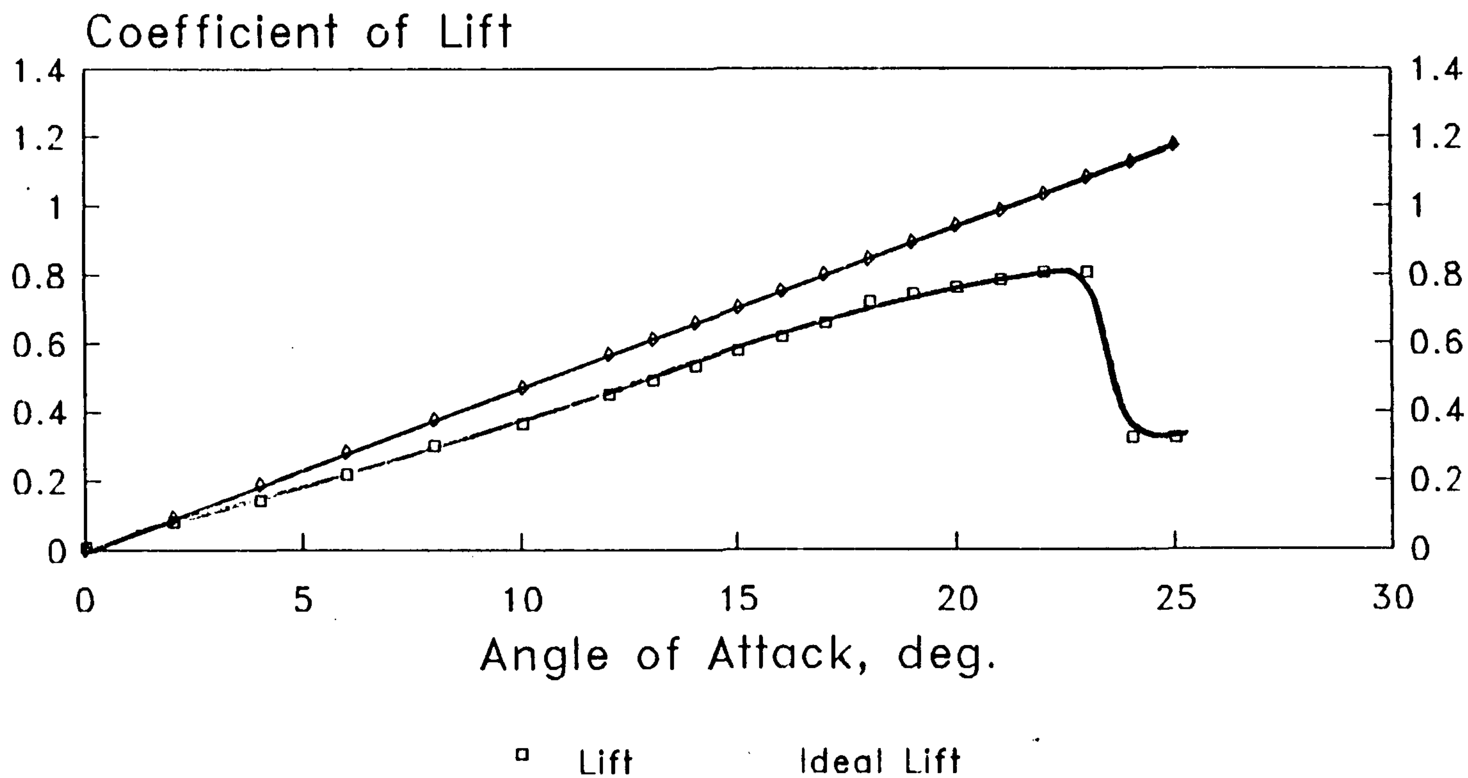

Craig Hunter 8/7/90

Baseline Wing w/ LE Trip

Coefficient of Drag vs. Angle of Attack

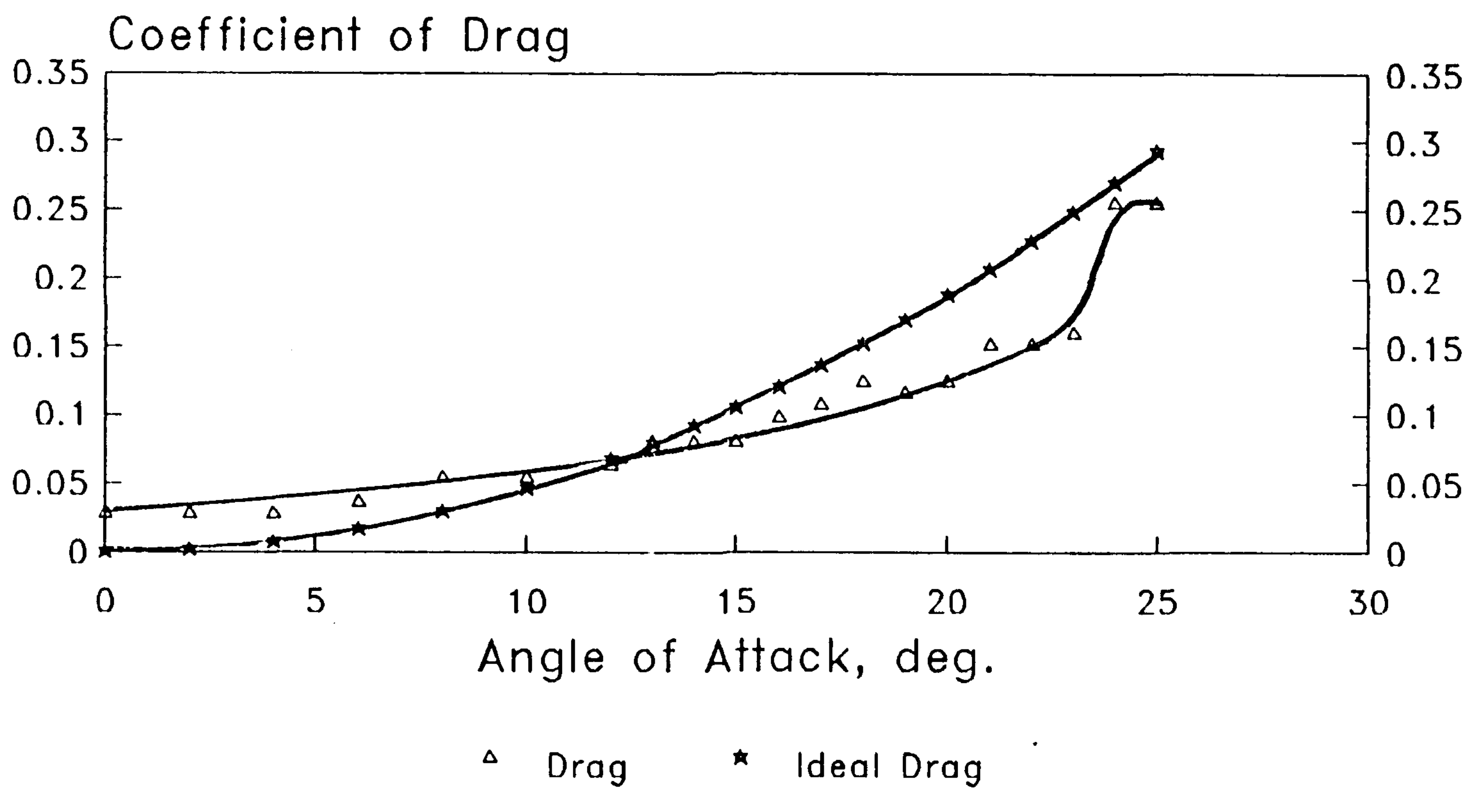

Craig Hunter 8/7/90

WRTE Wing
Coefficient of Lift
vs. Angle of Attack

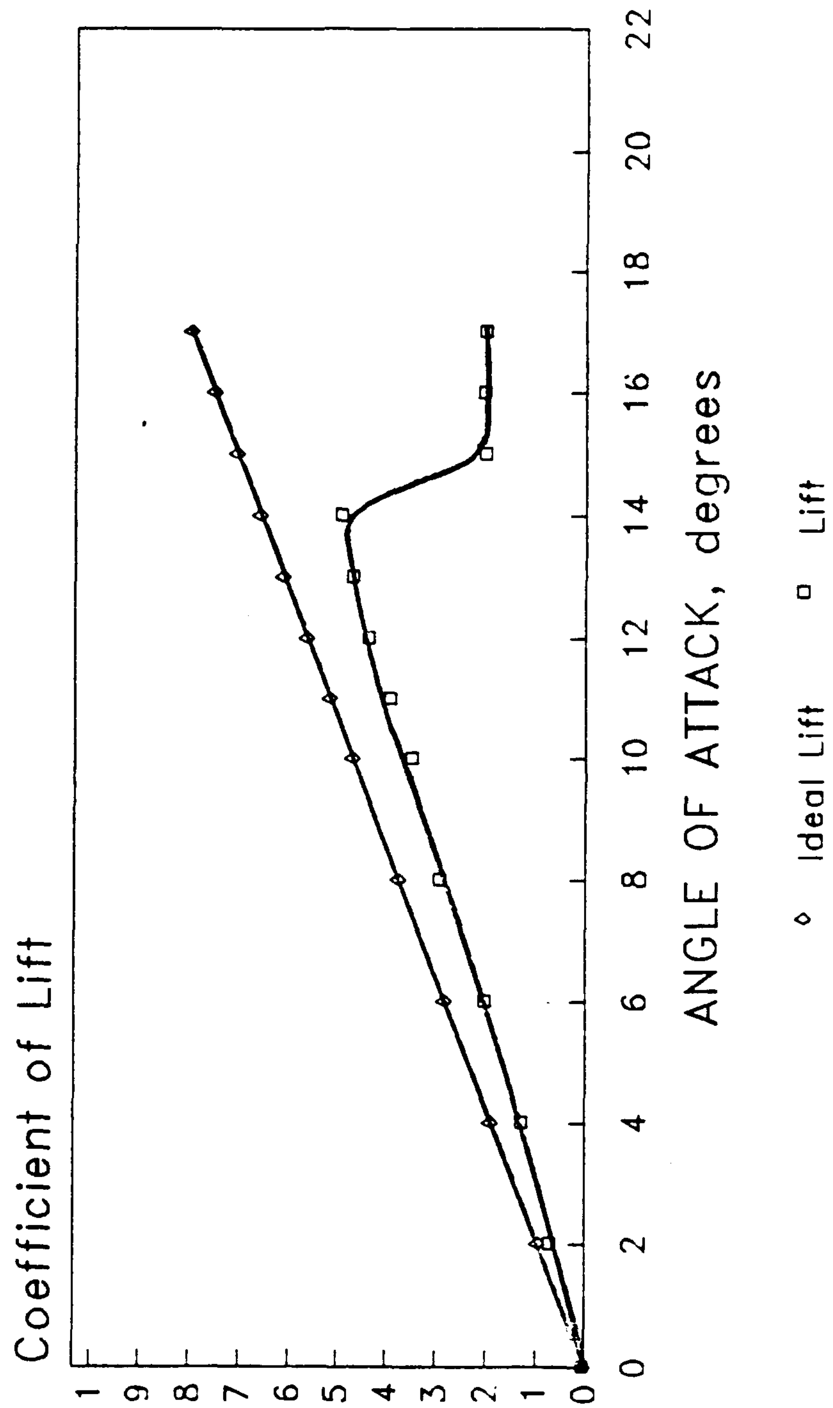

PASQUALE DELORE 03/22/90

WRTE Wing
Coefficient of Drag
vs. Angle of Attack

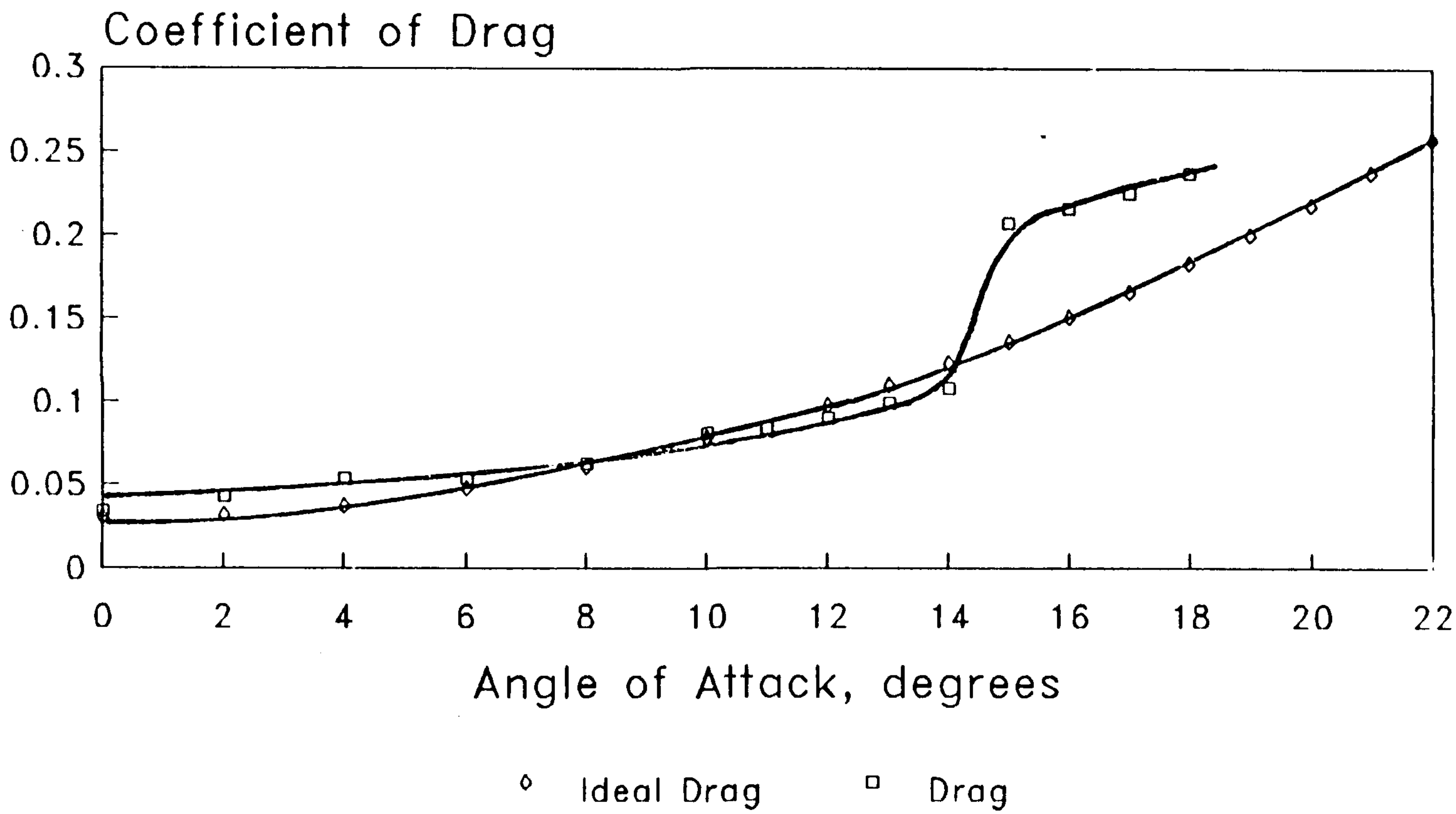

PASQUALE DELORE   03/22/90

WRTE Wing w/ LE Trip

Coefficient of Lift

vs. Angle of Attack

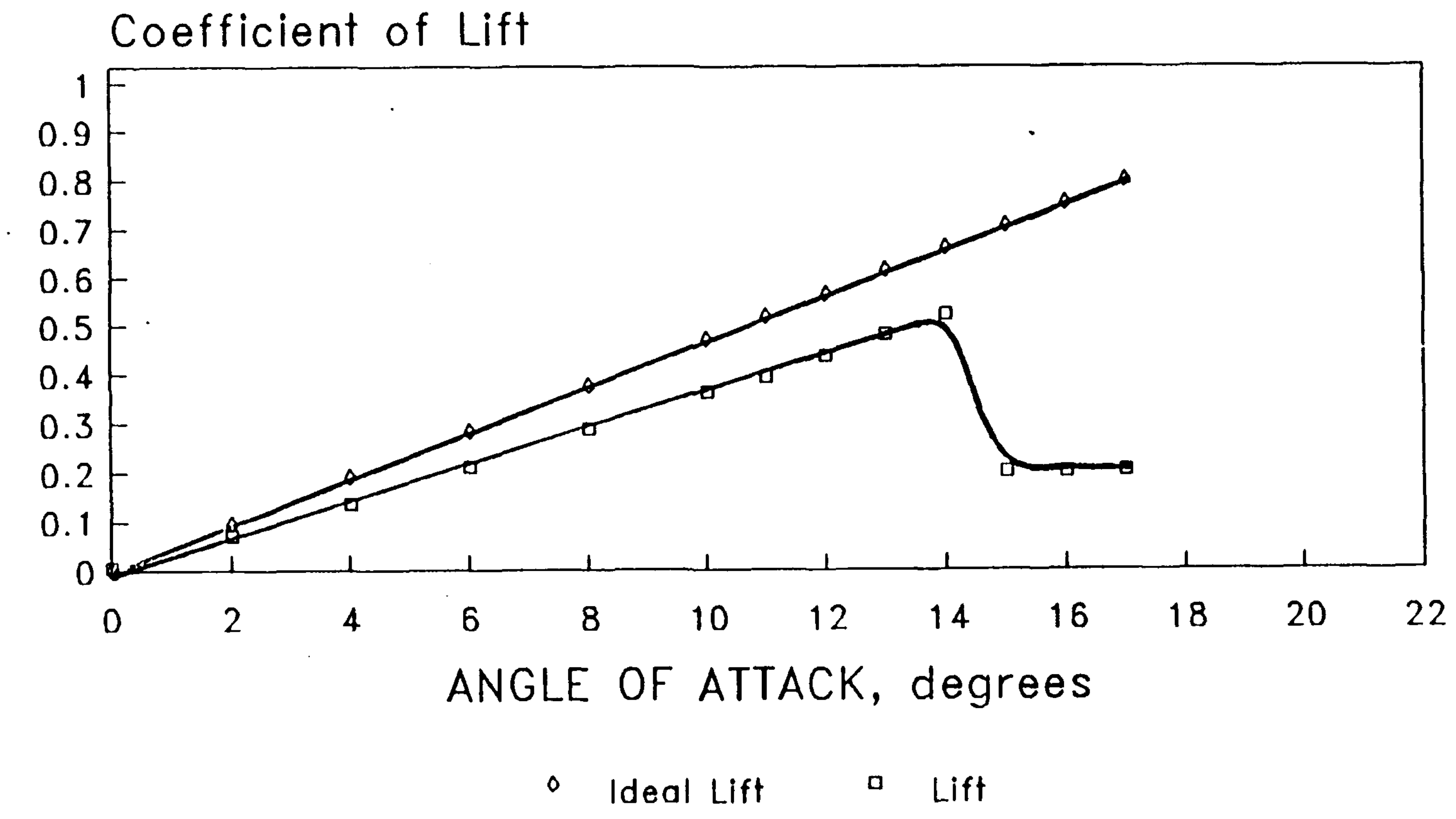

PASQUALE DELORE 03/22/90

WRTE Wing w/ LE Trip

Coefficient of Drag
vs. Angle of Attack

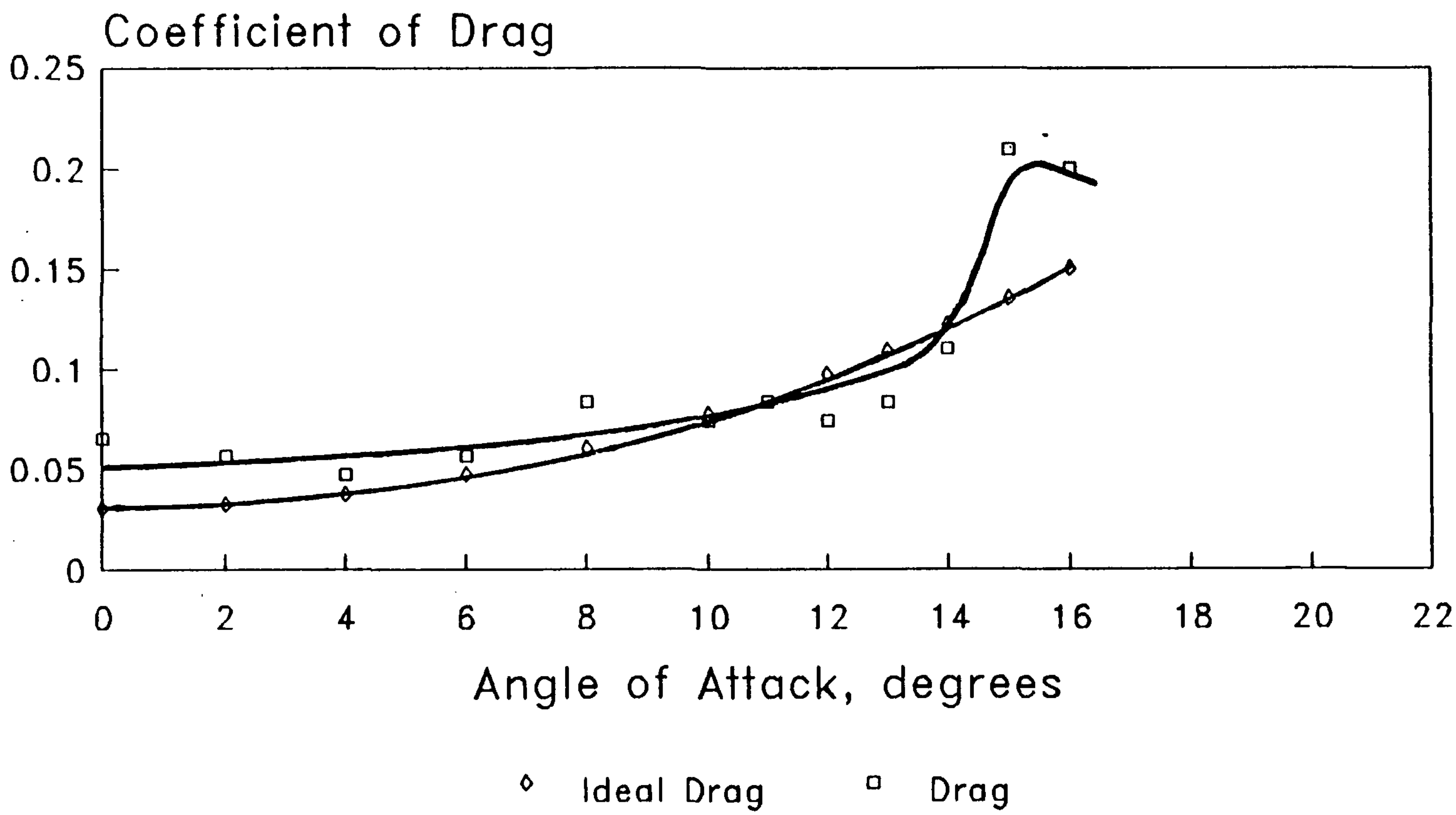

PASQUALE DELORE 03/22/90

Triangular TE Wing

Coefficient of Lift
vs. Angle of Attack

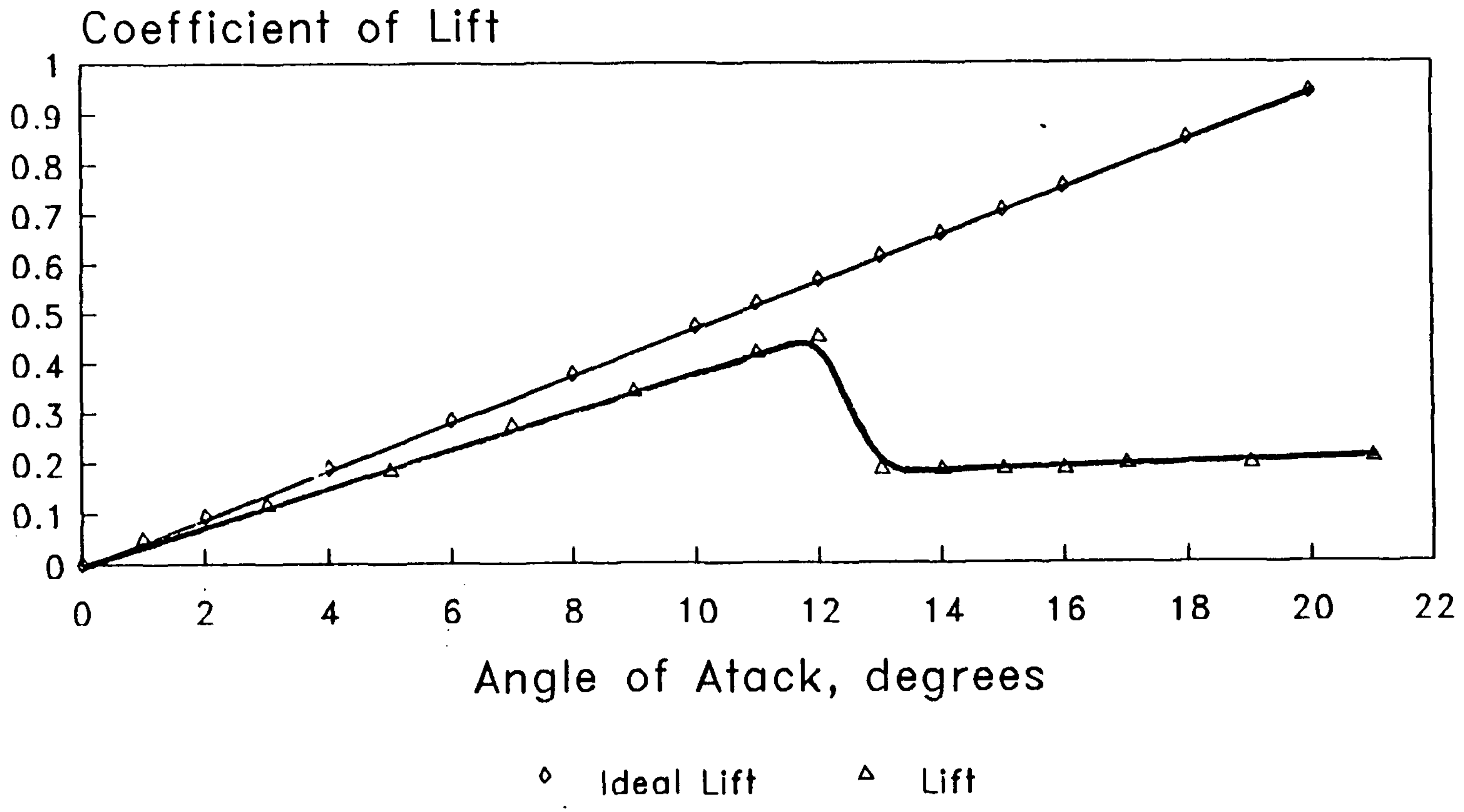

PASQUALE DELORE 01/26/90

Triangular TE Wing

Coefficient of Drag
vs. Angle of Attack

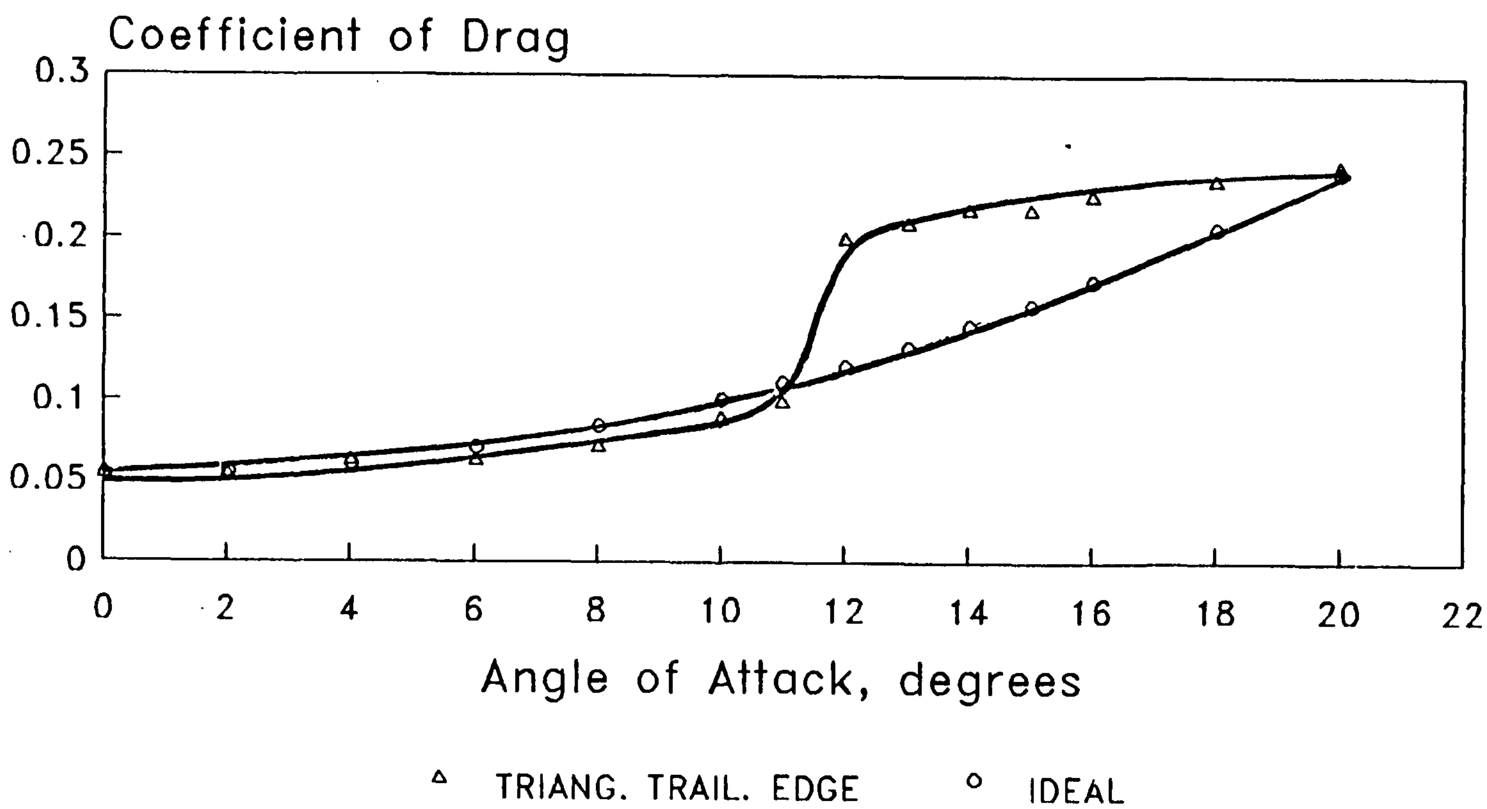

PASQUALE DELORE 01/26/90

Triangular TE Wing w/ LE Trip

Coefficient of Lift vs. Angle of Attack

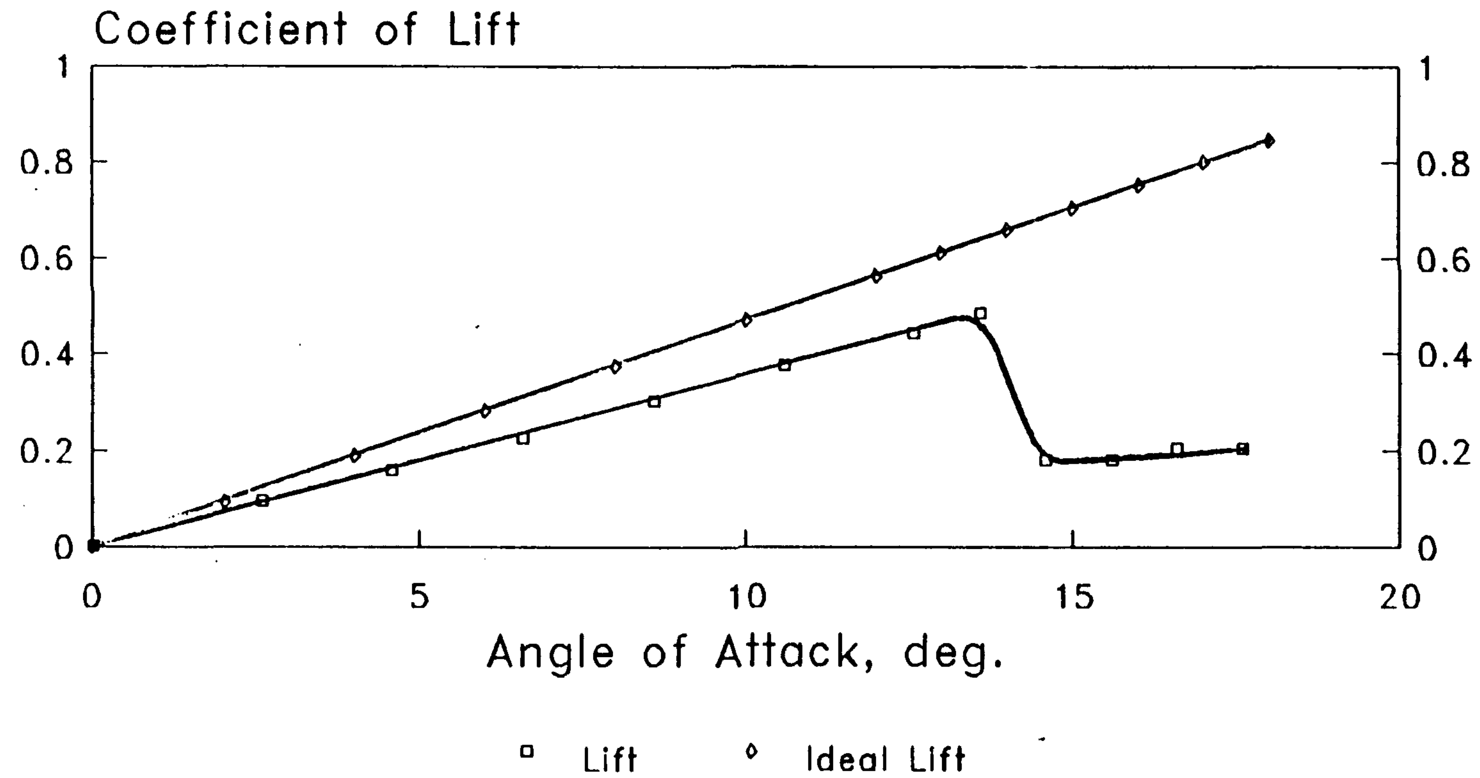

Craig Hunter 7/30/90

Triangular TE Wing w/ LE Trip

Coefficient of Drag vs. Angle of Attack

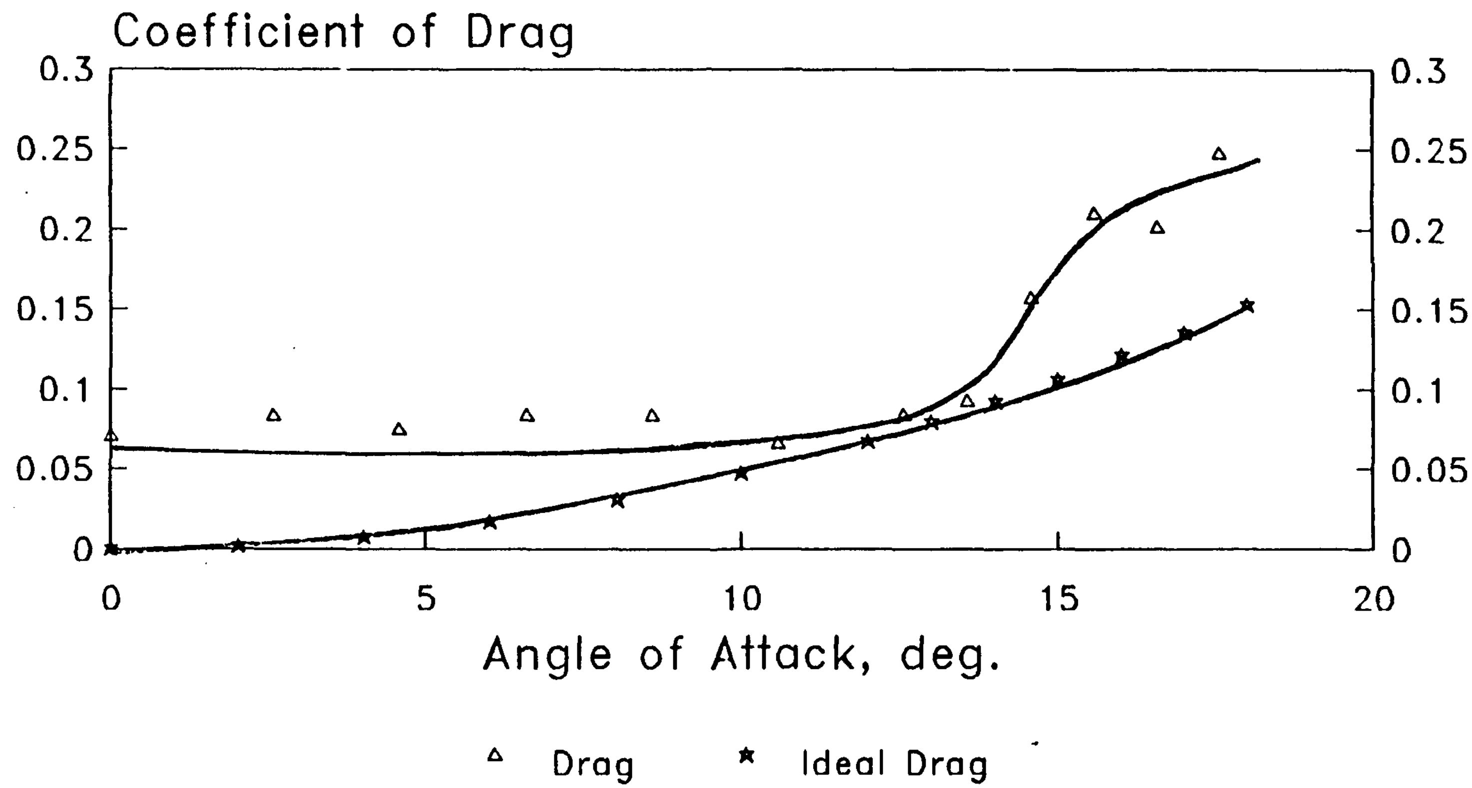

Craig Hunter 7/30/90

RIPPLED TRAILING EDGE WINGS
COMPARISON WITH BASELINE AND IDEAL

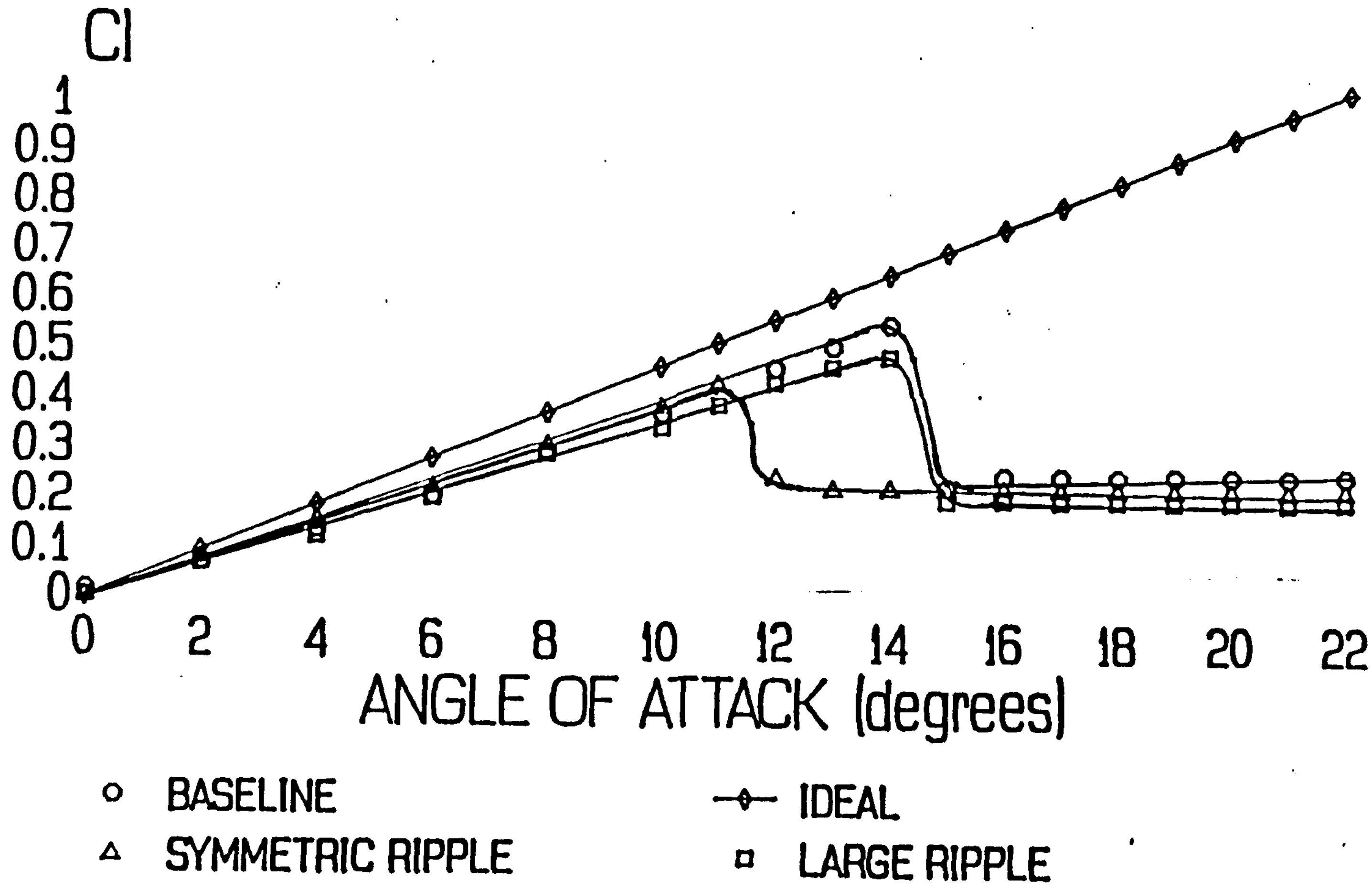

PASQUALE DELORE 03/22/90

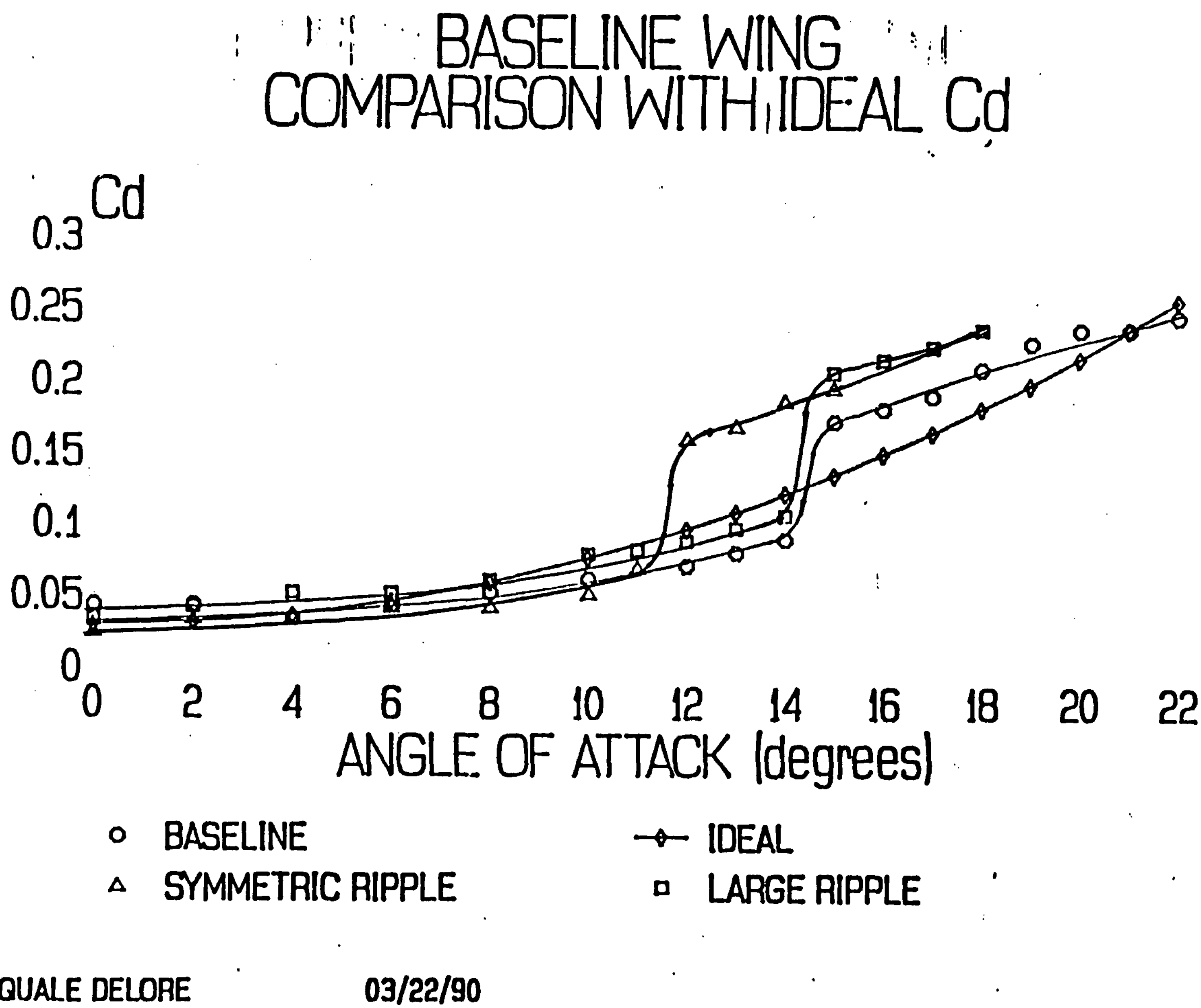
BASELINE WING
COMPARISON WITH IDEAL Cd
Cd
0.3
0.25
0.2
0.15
0.1
0.05
0
0
2
4
6
8
10
12
14
16
18
20
22
ANGLE OF ATTACK (degrees)
BASELINE
SYMMETRIC RIPPLE
IDEAL
LARGE RIPPLE
PASQUALE DELORE
03/22/90

SRTE Wing w/ LE Trip

Coefficient of Lift vs. Angle of Attack

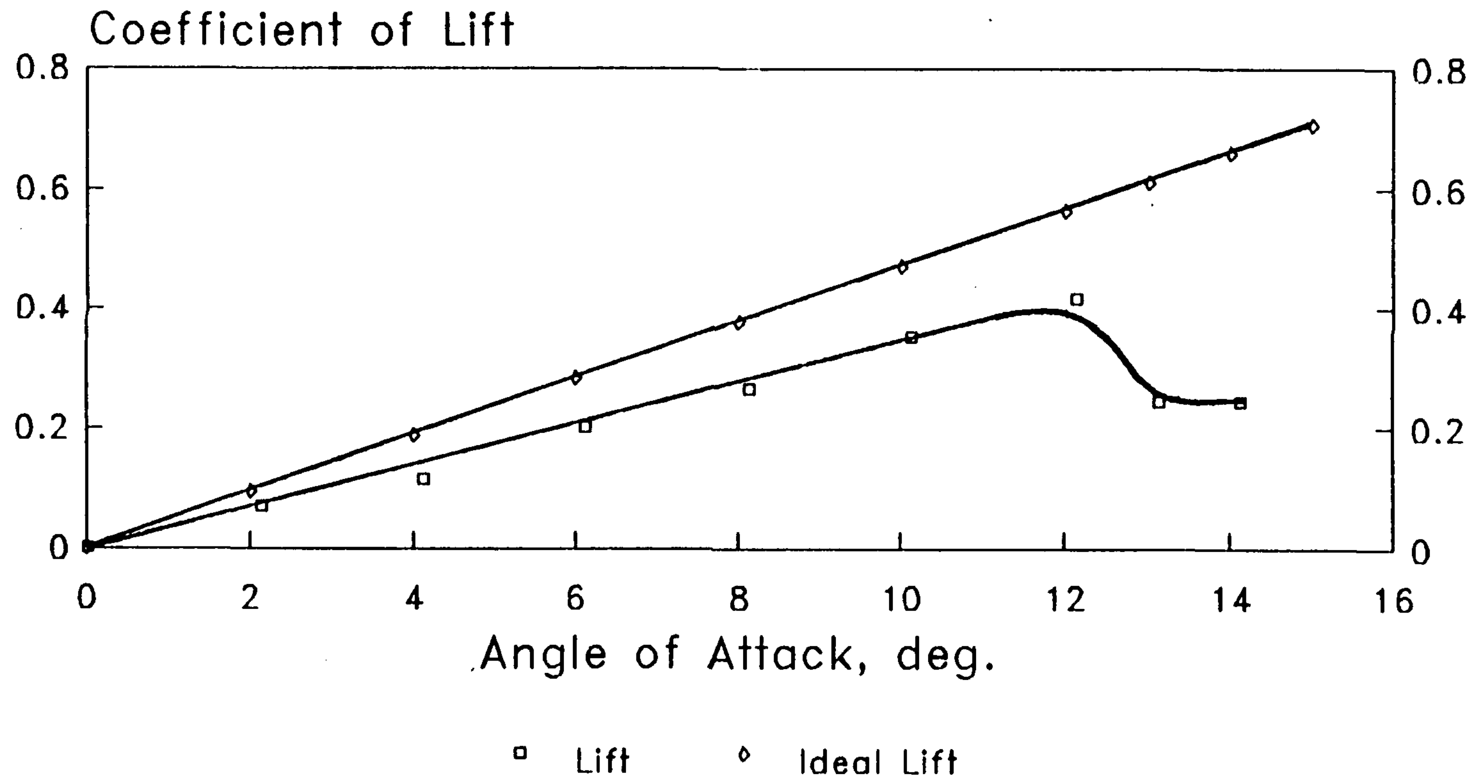

Craig Hunter 7/20/90

SRTE Wing w/ LE Trip

Coefficient of Drag vs. Angle of Attack

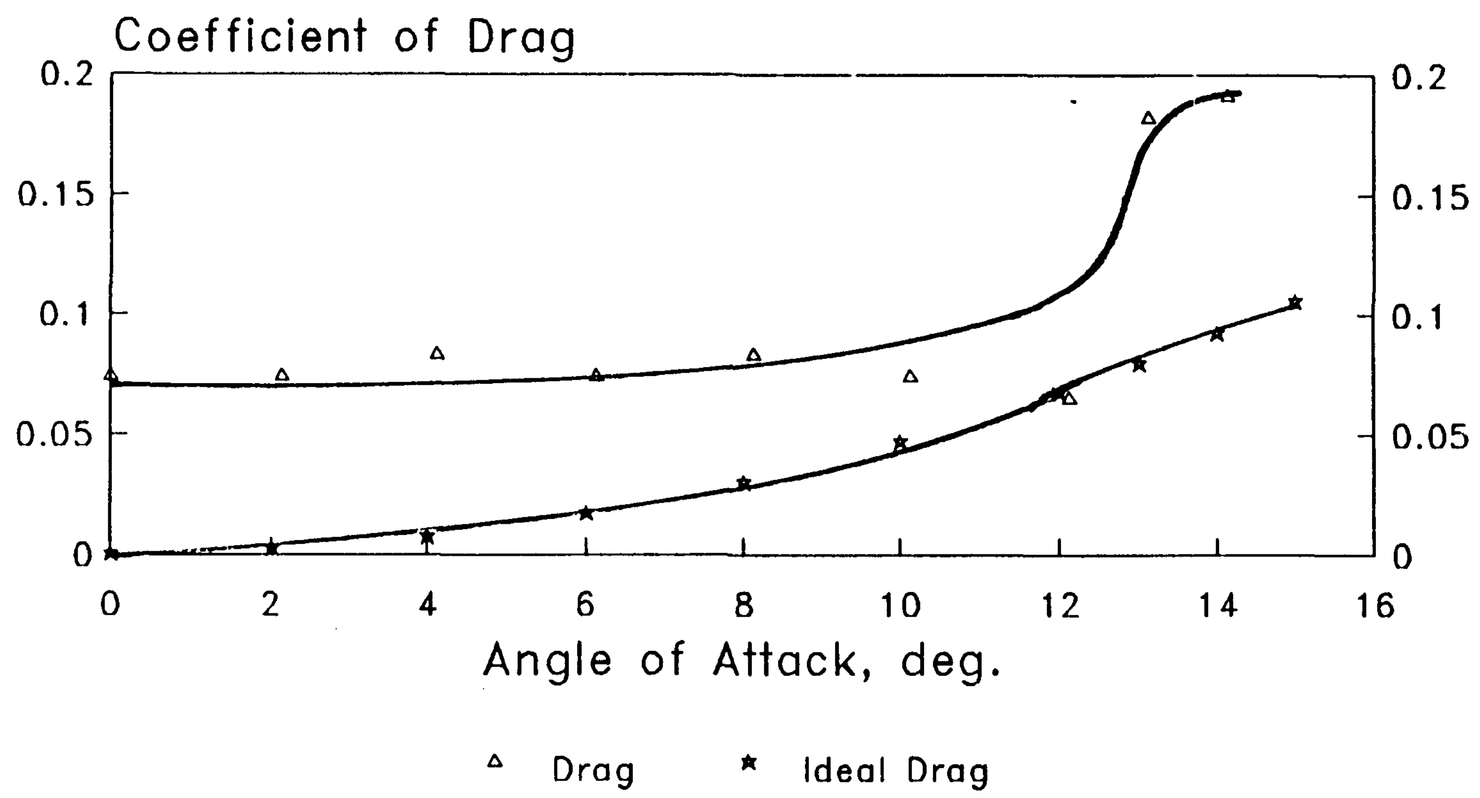

Craig Hunter 7/20/90

COEFFICIENTS OF LIFT VERSES ANGLE OF ATTACK

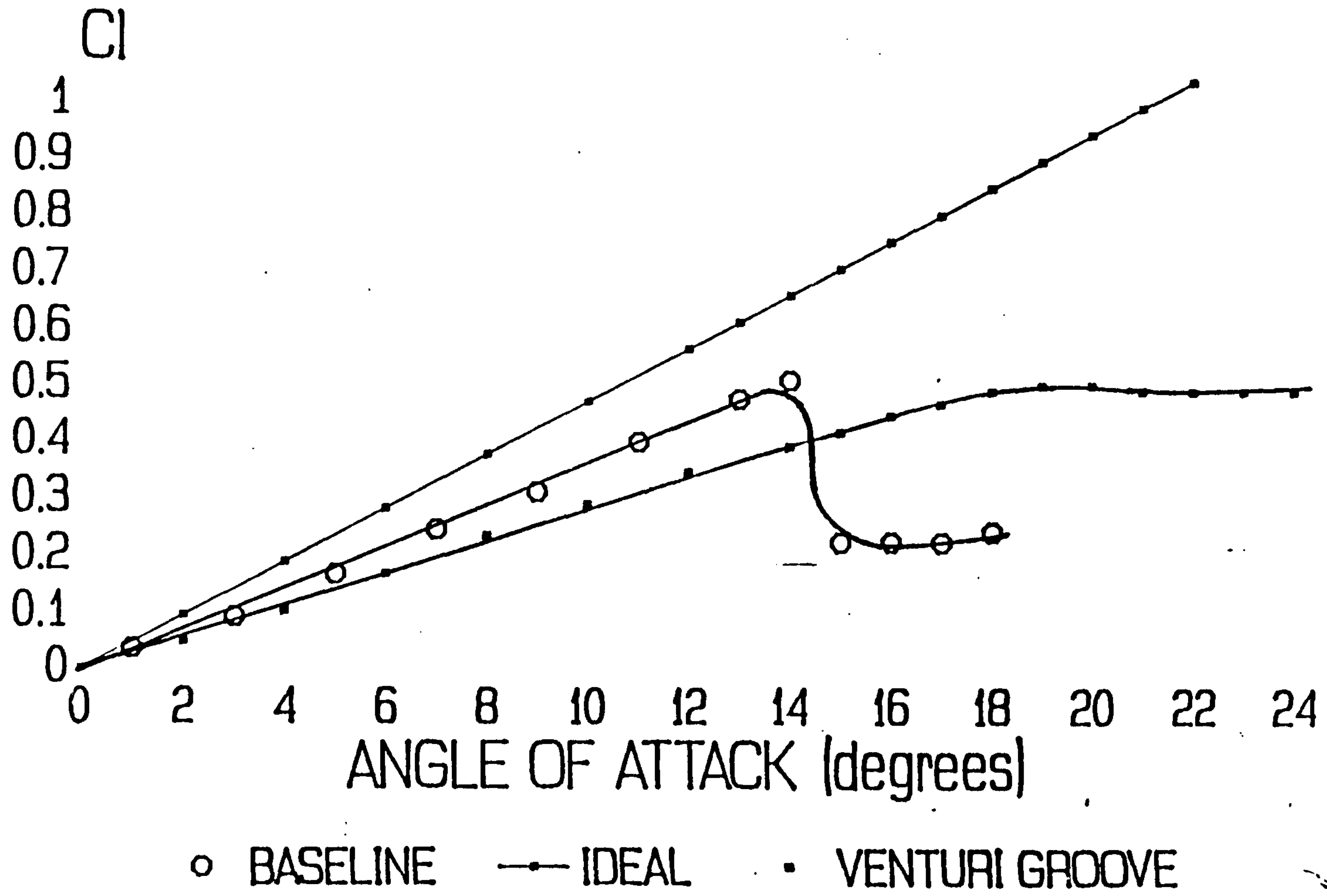

COEFFICIENTS OF DRAG VERSES ANGLE OF ATTACK

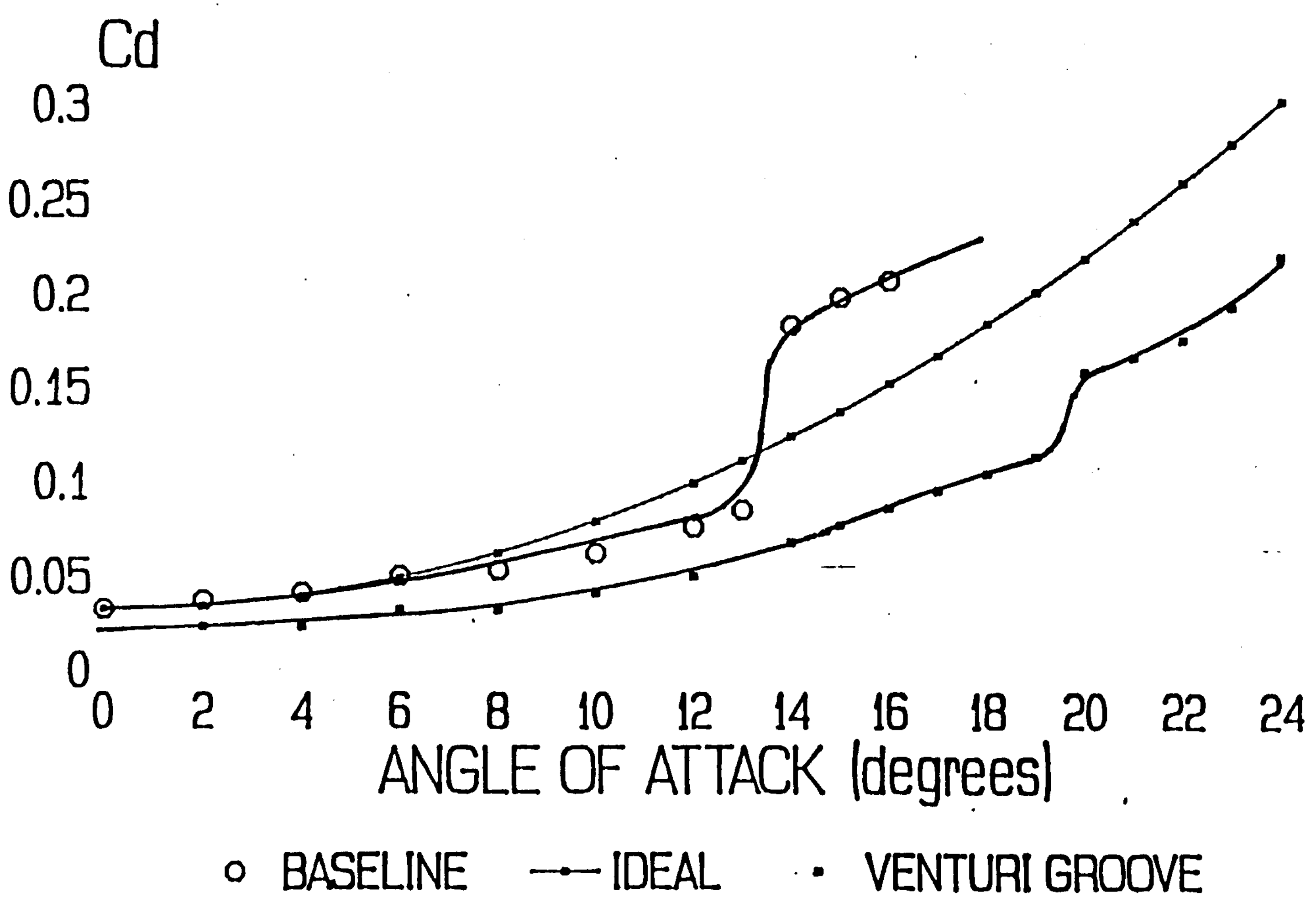

MIDDLE GROOVE WING COMPARISON WITH IDEAL Cl

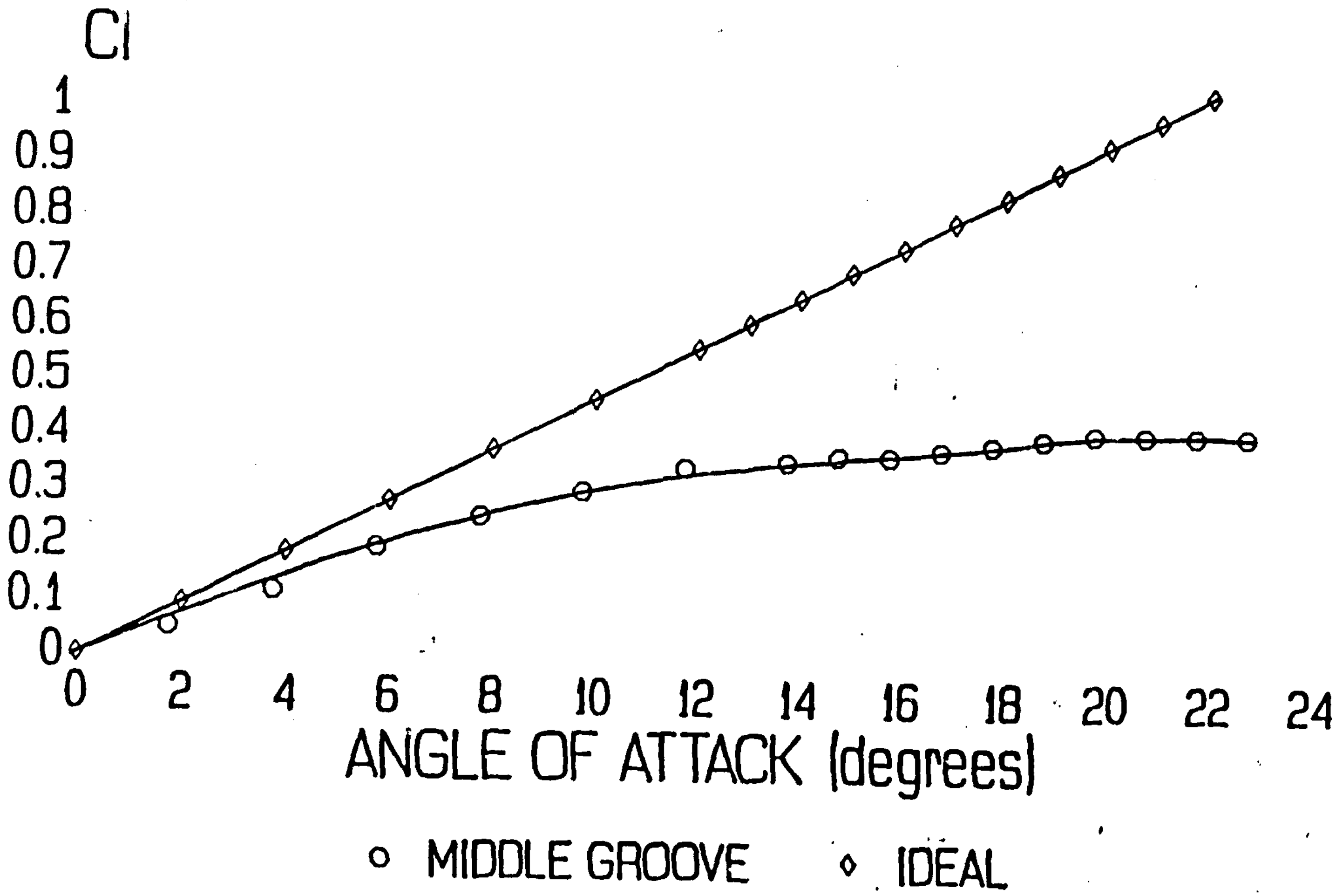

PASQUALE DELORE 11/24/89

MIDDLE GROOVE WING
COMPARISON WITH IDEAL Cd

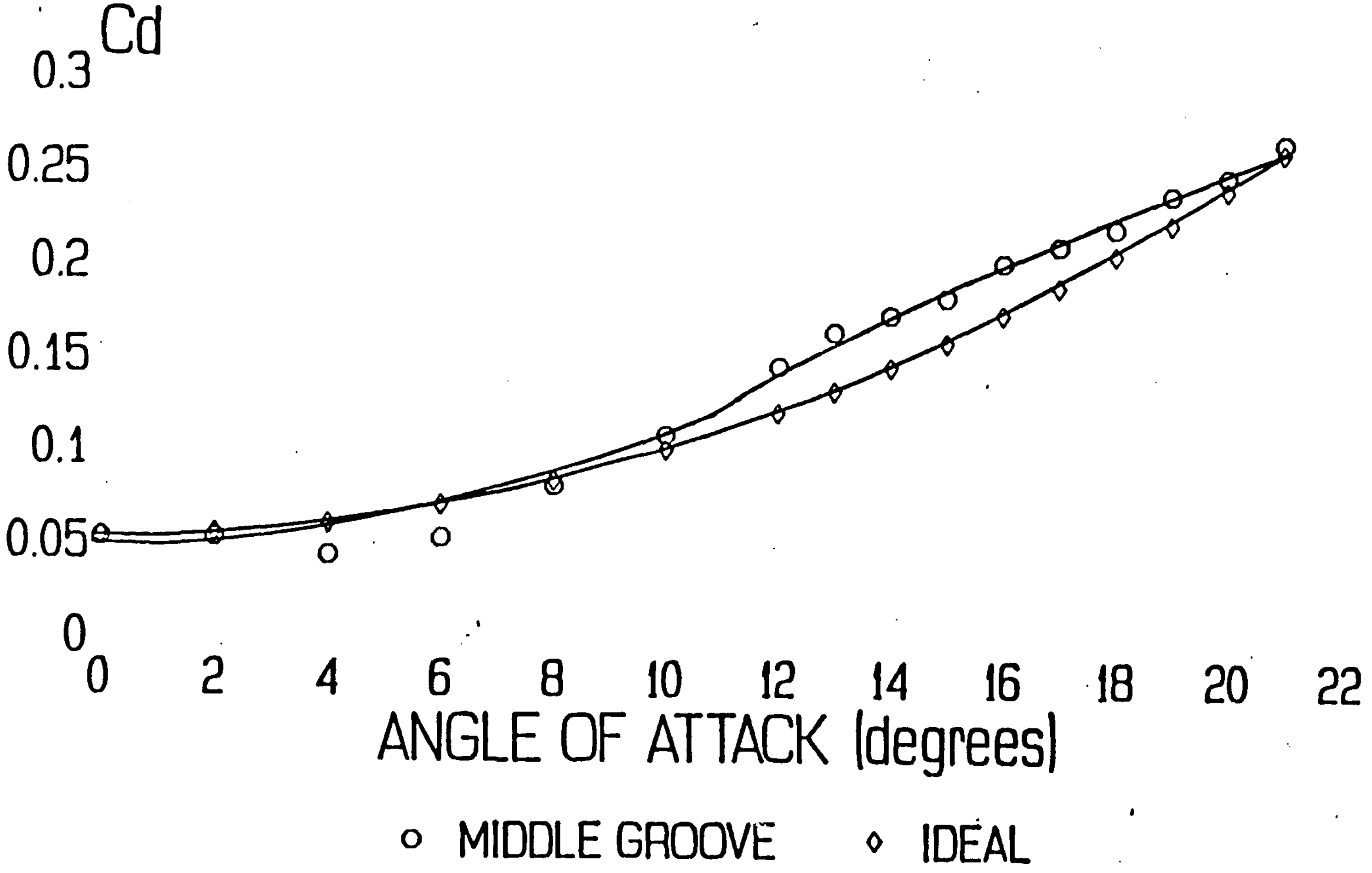

PASQUALE DELORE 11/24/89

LEADING EDGE GROOVE WING COMPARISON WITH IDEAL Cl

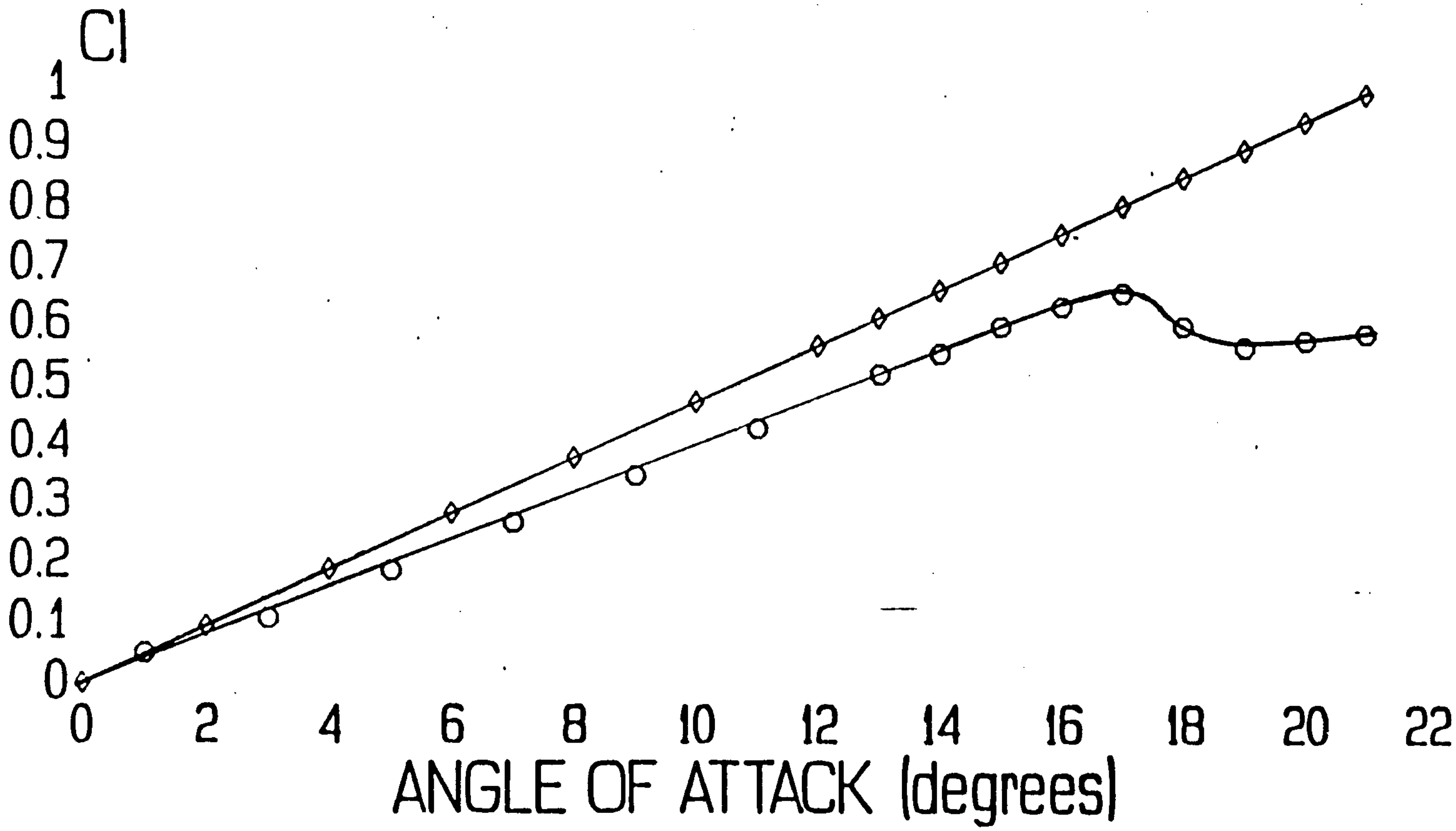

o LEADING EDGE GROOVE ◊ IDEAL

PASQUALE DELORE 11/24/89

LEADING EDGE GROOVE WING COMPARISON WITH IDEAL Cd

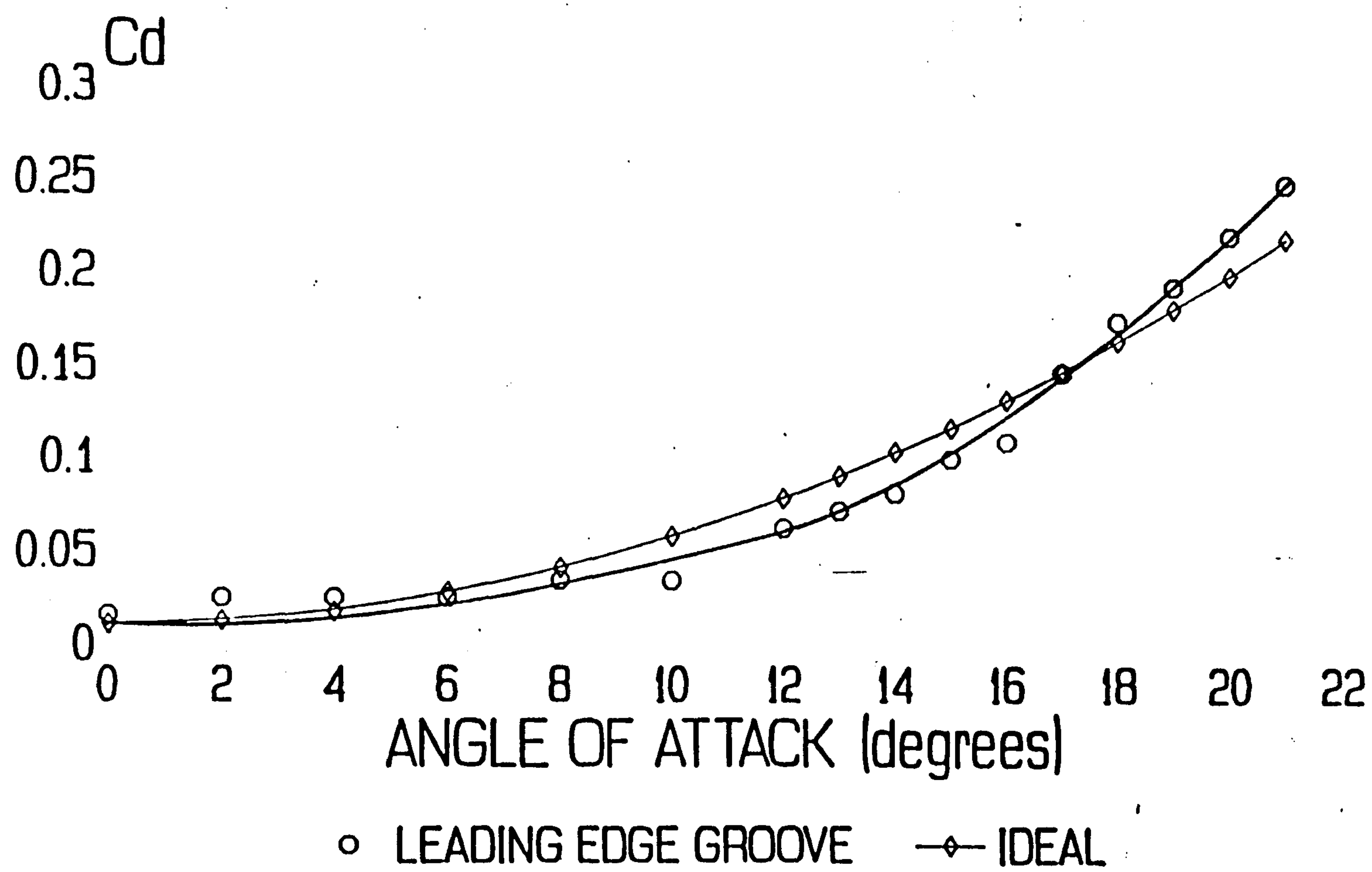

PASQUALE DELORE 11/24/89

Lift and Drag Polars
Triangular TE Wing w/ LE Trip

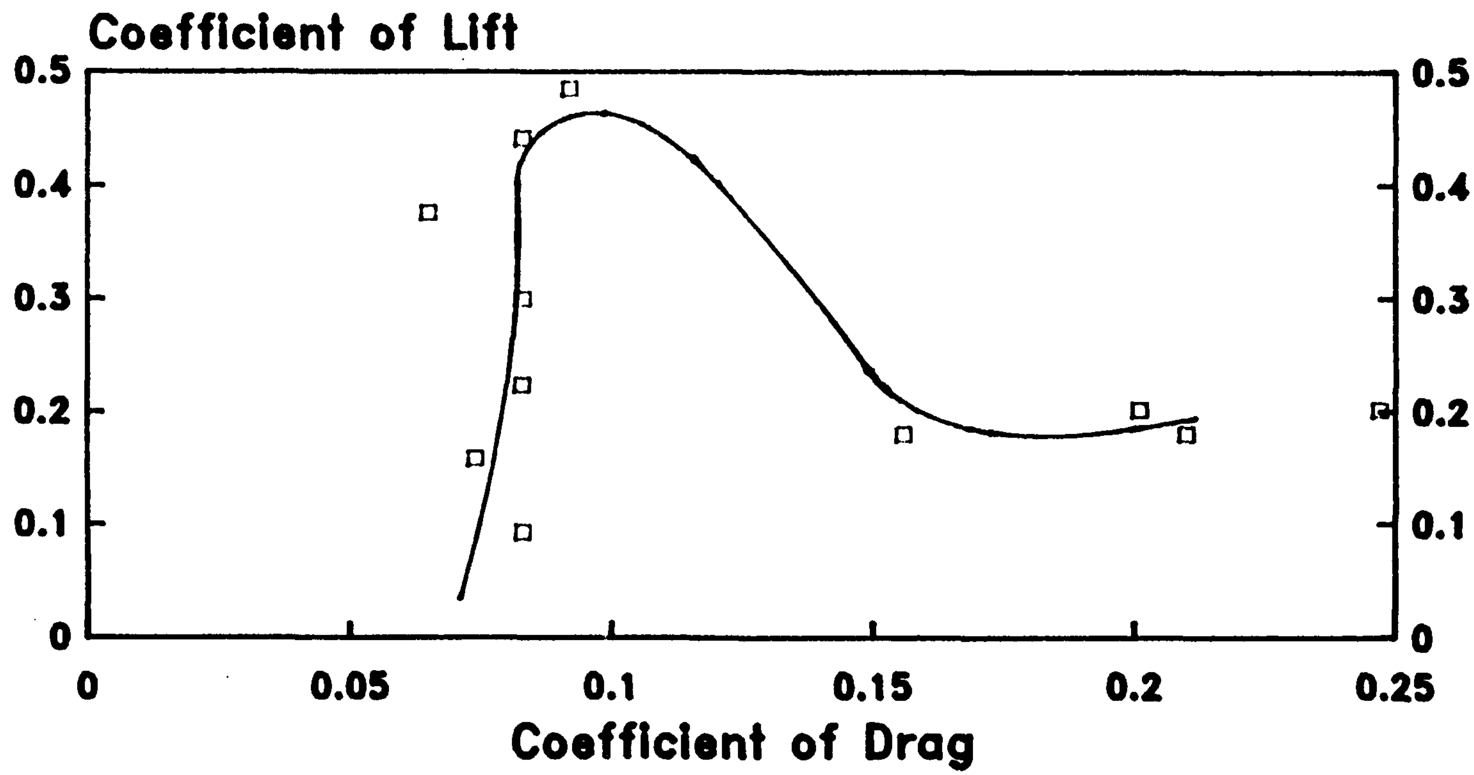

Craig Hunter 7/20/90 TEST#3

Lift and Drag Polars
Baseline Wing w/ LE Trip

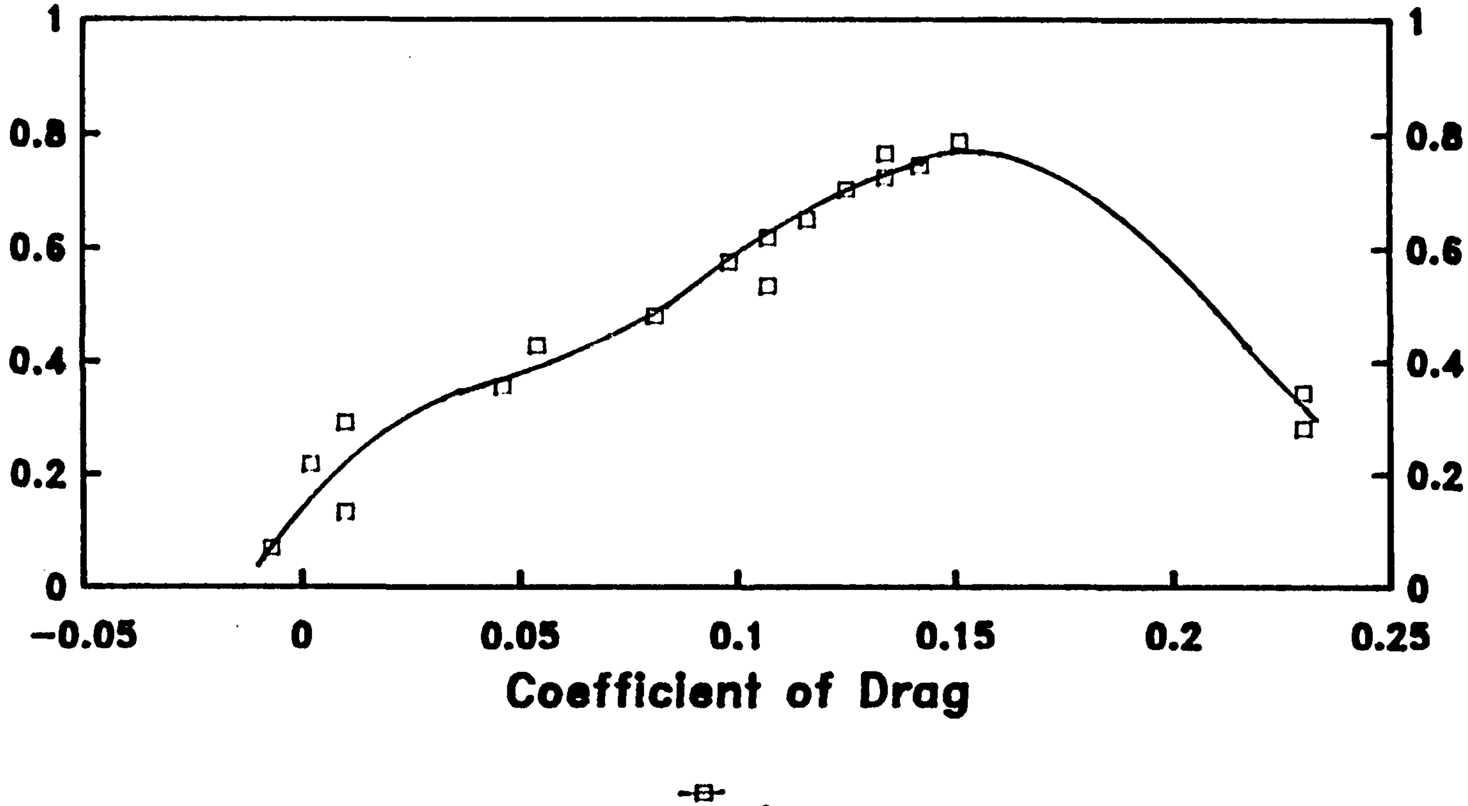

Craig Hunter 7/20/90 TEST#3

Lift and Drag Polars
SRTE Wing w/ LE Trip

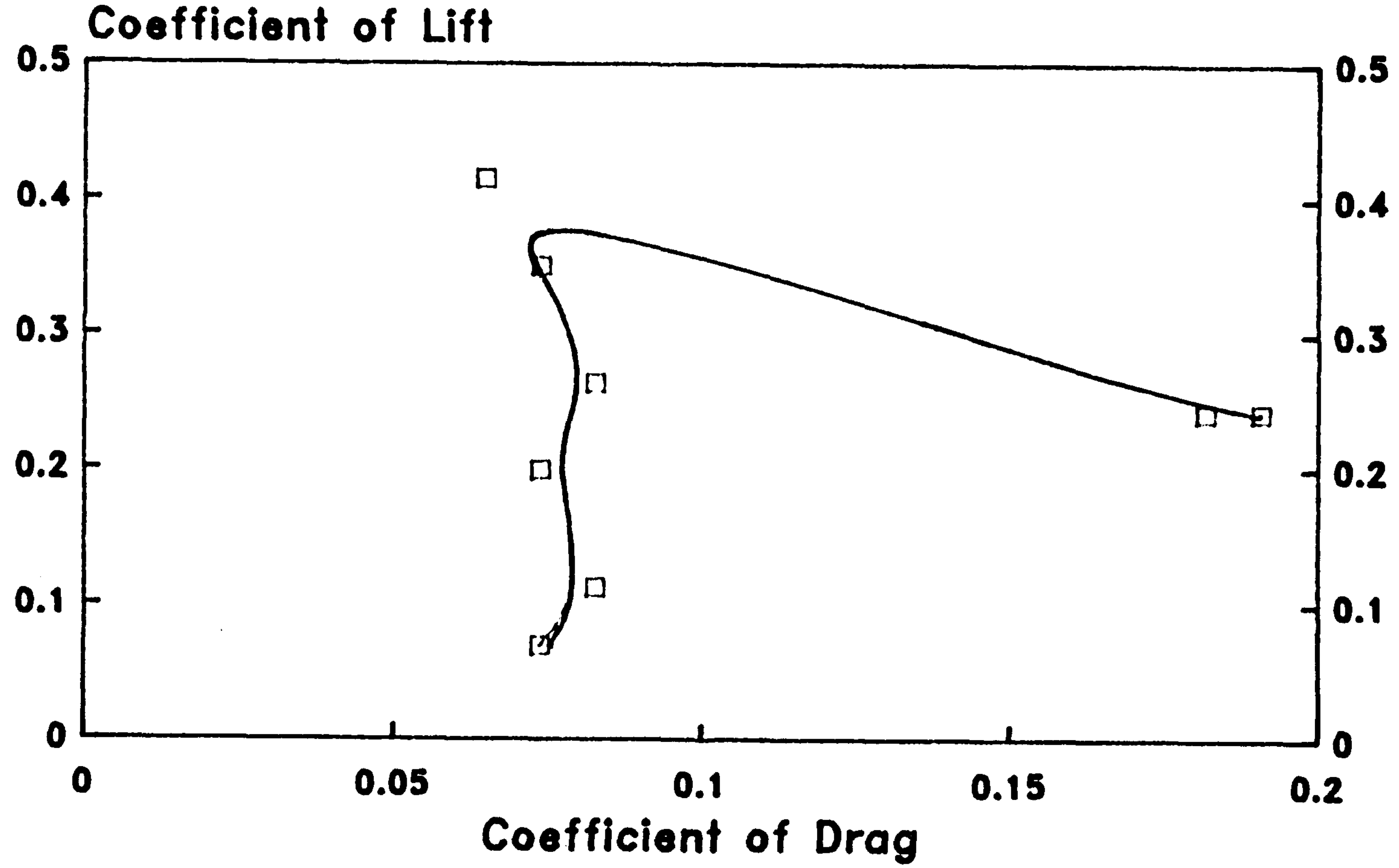

Craig Hunter 7/20/90

Appendix H

Control Volume Spreadsheet Data

CONTROL VOLUME ANALYSIS OF BASELINE WING
4 1/4 CHORD DATA

MAXIMUM THICKNESS = 0.7 INCHES
FREESTREAM VELOCITY = 73.23 FT/S
2/T = 2.857142

Y	V2	V2/V1	2/T(V2/V1(1-V2/V1))
5.00	74.746	1.0207	-0.06037
5.05	74.472	1.0170	-0.04927
5.10	73.982	1.0103	-0.02964
5.15	73.366	1.0019	-0.00531
5.20	72.588	0.9912	0.024828
5.25	71.991	0.9831	0.047522
5.30	71.516	0.9766	0.065308
5.35	71.102	0.9709	0.080613
5.40	71.038	0.9701	0.082963
5.45	71.070	0.9705	0.081788
5.50	71.389	0.9749	0.070022
5.55	71.865	0.9814	0.052264
5.60	72.588	0.9912	0.024828
5.65	73.025	0.9972	0.007975
5.70	73.490	1.0036	-0.01018
5.75	73.613	1.0052	-0.01502
5.80	74.136	1.0124	-0.03578
5.85	74.258	1.0140	-0.04067
5.90	74.35	1.0153	-0.04436
5.95	74.441	1.0165	-0.04802
6.00	74.502	1.0174	-0.05049
		TOTAL =	0.148961
		Cd =	0.044688

CONTROL VOLUME ANALYSIS OF BASELINE WING
2 1/2 CHORD DATA

MAXIMUM THICKNESS = 0.7 INCHES
FREESTREAM VELOCITY = 72.74 FT/S
2/T = 2.857142

Y	V2	V2/V1	2/T(V2/V1(1-V2/V1))
5.05	74.766	1.0279	-0.08179
5.10	74.501	1.0242	-0.07084
5.15	74.205	1.0201	-0.05870
5.20	73.67	1.0128	-0.03699
5.25	72.981	1.0033	-0.00949
5.30	72.011	0.9900	0.028347
5.35	70.904	0.9748	0.070295
5.40	70.251	0.9658	0.094419
5.45	69.622	0.9571	0.117221
5.50	69.937	0.9615	0.105855
5.55	70.563	0.9701	0.082950
5.60	71.460	0.9824	0.049392
5.65	72.559	0.9975	0.007091
5.70	73.162	1.0058	-0.01667
5.75	73.730	1.0136	-0.03941
5.80	73.879	1.0157	-0.04543
5.85	73.968	1.0169	-0.04904
		TOTAL =	0.147163
		Cd =	0.044149

CONTROL VOLUME ANALYSIS OF BASELINE WING
1 CHORD DATA

MAXIMUM THICKNESS = 0.7 INCHES
FREESTREAM VELOCITY = 70.4 FT/S
2/T = 2.857142

Y	V2	V2/V1	2/T(V2/V1(1-V2/V1))
5.20	73.937	1.0502	-0.15075
5.25	73.381	1.0423	-0.12610
5.30	71.972	1.0223	-0.06522
5.35	69.560	0.9881	0.033684
5.40	66.721	0.9477	0.141507
5.45	64.888	0.9217	0.206186
5.50	64.817	0.9207	0.208613
5.55	66.618	0.9463	0.145244
5.60	69.396	0.9857	0.040165
5.65	71.845	1.0205	-0.05984
5.70	72.945	1.0362	-0.10702
5.75	73.195	1.0397	-0.11793
		TOTAL =	0.148508
		Cd =	0.044552

CONTROL VOLUME ANALYSIS OF LEADING EDGE GROOVE WING
4 1/4 CHORD DATA 0.2" MAX. GROOVE DEPTH

MAXIMUM THICKNESS =	0.7	INCHES
FREESTREAM VELOCITY =	70.82	FT/S
2/T =	2.857142	

Y	V2	V2/V1	2/T(V2/V1(1-V2/V1))
4.75	74.277	1.0488	-0.14627
5.00	74.124	1.0467	-0.13951
5.05	74.124	1.0467	-0.13951
5.10	73.971	1.0445	-0.13277
5.15	73.509	1.0380	-0.11260
5.20	73.138	1.0327	-0.09657
5.25	72.577	1.0248	-0.07264
5.30	71.790	1.0137	-0.03966
5.35	71.123	1.0043	-0.01227
5.40	70.353	0.9934	0.018716
5.45	69.574	0.9824	0.049383
5.50	68.786	0.9713	0.079702
5.55	68.156	0.9624	0.103432
5.60	67.386	0.9515	0.131822
5.65	67.386	0.9515	0.131822
5.70	67.285	0.9501	0.135496
5.75	67.318	0.9506	0.134297
5.80	67.856	0.9581	0.114574
5.85	68.522	0.9676	0.089701
5.90	69.05	0.9750	0.069623
5.95	70.256	0.9920	0.022572
6.00	70.771	0.9993	0.001975
6.25	71.695	1.0124	-0.03573
6.50	73.293	1.0349	-0.10325
		TOTAL =	0.052277
		Cd =	0.015683

CONTROL VOLUME ANALYSIS OF LEADING EDGE GROOVE WING
2 1/2 CHORD DATA 0.2" MAX. GROOVE DEPTH

MAXIMUM THICKNESS = 0.7 INCHES
FREESTREAM VELOCITY = 69.63 FT/S
2/T = 2.857142

Y	V2	V2/V1	2/T(V2/V1(1-V2/V1))
5.00	73.787	1.0597	-0.18075
5.05	73.663	1.0579	-0.17507
5.10	73.355	1.0535	-0.16102
5.15	72.982	1.0481	-0.14416
5.20	72.514	1.0414	-0.12324
5.25	71.6	1.0283	-0.08312
5.30	70.643	1.0145	-0.04217
5.35	69.378	0.9964	0.010302
5.40	68.223	0.9798	0.056567
5.45	67.048	0.9629	0.102019
5.50	66.024	0.9482	0.140302
5.55	65.333	0.9383	0.165438
5.60	65.333	0.9383	0.165438
5.65	65.333	0.9383	0.165438
5.70	65.680	0.9433	0.152886
5.75	66.777	0.9590	0.112271
5.80	67.789	0.9736	0.073544
5.85	69.05	0.9917	0.023601
5.90	70.321	1.0099	-0.02863
5.95	71.314	1.0242	-0.07077
6.00	72.043	1.0347	-0.10244
		TOTAL =	0.056404
		Cd =	0.016921

CONTROL VOLUME ANALYSIS OF LEADING EDGE GROOVE WING
1 CHORD DATA 0.2" MAX. GROOVE DEPTH

MAXIMUM THICKNESS = 0.7 INCHES
FREESTREAM VELOCITY = 67 FT/S
2/T = 2.857142

Y	V2	V2/V1	2/T(V2/V1(1-V2/V1))
5.20	71.703	1.0702	-0.21463
5.25	70.56	1.0531	-0.15987
5.30	69.104	1.0314	-0.09254
5.35	67.114	1.0017	-0.00486
5.40	64.924	0.9690	0.085785
5.45	62.694	0.9357	0.171823
5.50	61.714	0.9211	0.207631
5.55	62.586	0.9341	0.175829
5.60	62.946	0.9395	0.162418
5.65	63.482	0.9475	0.142144
5.70	66.233	0.9886	0.032333
5.75	68.612	1.0241	-0.07039
5.80	70.368	1.0503	-0.15084
5.90	71.923	1.0735	-0.22536
		TOTAL =	0.059442
		Cd =	0.017832

CONTROL VOLUME ANALYSIS OF LARGE RIPPLED
4 1/4 CHORD DATA TRAILING EDGE WING

MAXIMUM THICKNESS = 0.7 INCHES
FREESTREAM VELOCITY = 73.32 FT/S
2/T = 2.857142

Y	V2	V2/V1	2/T(V2/V1(1-V2/V1))
5.00	73.795	1.0065	-0.01862
5.05	73.825	1.0069	-0.01981
5.10	73.674	1.0048	-0.01386
5.15	73.734	1.0056	-0.01622
5.20	73.643	1.0044	-0.01264
5.25	73.582	1.0036	-0.01024
5.30	73.339	1.0003	-0.00074
5.35	73.278	0.9994	0.001635
5.40	73.278	0.9994	0.001635
5.45	73.369	1.0007	-0.00191
5.50	73.278	0.9994	0.001635
5.55	73.156	0.9978	0.006376
5.60	72.880	0.9940	0.017043
5.65	72.818	0.9932	0.019428
5.70	72.788	0.9927	0.020580
5.75	72.695	0.9915	0.024147
5.80	72.665	0.9911	0.025296
5.85	72.603	0.9902	0.027666
5.90	72.665	0.9911	0.025296
5.95	72.726	0.9919	0.022959
6.00	72.88	0.9940	0.017043
6.25	73.247	0.9990	0.002841
		TOTAL =	0.119517
		Cd =	0.035855

CONTROL VOLUME ANALYSIS OF LARGE RIPPLED
2 1/2 CHORD DATA TRAILING EDGE WING

MAXIMUM THICKNESS = 0.7 INCHES
FREESTREAM VELOCITY = 72.75 FT/S
2/T = 2.857142

Y	V2	V2/V1	2/T(V2/V1(1-V2/V1))
5.50	73.497	1.0103	-0.02963
5.55	73.405	1.0090	-0.02595
5.60	73.344	1.0082	-0.02351
5.65	73.313	1.0077	-0.02228
5.70	73.160	1.0056	-0.01619
5.75	72.822	1.0010	-0.00283
5.80	72.172	0.9921	0.022519
5.85	71.517	0.9831	0.047603
5.90	71.045	0.9766	0.065391
5.95	71.076	0.9770	0.064230
6.00	71.202	0.9787	0.059501
6.25	72.761	1.0002	-0.00043
6.50	73.375	1.0086	-0.02475
		TOTAL =	0.113640
		Cd =	0.034092

CONTROL VOLUME ANALYSIS OF LARGE RIPPLED
1 CHORD DATA TRAILING EDGE WING

MAXIMUM THICKNESS = 0.7 INCHES
FREESTREAM VELOCITY = 70.95 FT/S
2/T = 2.857142

Y	V2	V2/V1	2/T(V2/V1(1-V2/V1))
5.65	72.665	1.0242	-0.07073
5.70	71.387	1.0062	-0.01770
5.75	69.020	0.9728	0.075606
5.80	67.341	0.9491	0.137941
5.90	69.603	0.9810	0.053213
6.00	71.481	1.0075	-0.02154
6.25	71.95	1.0141	-0.04083

TOTAL = 0.115942

Cd = 0.034782

CONTROL VOLUME ANALYSIS OF MIDDLE GROOVE WING
4 1/4 CHORD DATA 0.1" MAX. GROOVE DEPTH

MAXIMUM THICKNESS = 0.7 INCHES
FREESTREAM VELOCITY = 71.7 FT/S
2/T = 2.857142

Y	V2	V2/V1	2/T(V2/V1(1-V2/V1))
4.75	74.546	1.0397	-0.11791
5.00	74.546	1.0397	-0.11791
5.05	74.336	1.0368	-0.10890
5.10	74.036	1.0326	-0.09611
5.15	73.855	1.0301	-0.08845
5.20	73.432	1.0242	-0.07068
5.25	72.914	1.0169	-0.04919
5.30	72.515	1.0114	-0.03284
5.35	71.898	1.0028	-0.00791
5.40	71.276	0.9941	0.016795
5.45	70.332	0.9809	0.053472
5.50	69.855	0.9743	0.071628
5.55	69.214	0.9653	0.095628
5.60	68.956	0.9617	0.105159
5.65	68.697	0.9581	0.114653
5.70	68.632	0.9572	0.117024
5.75	68.729	0.9586	0.113484
5.80	69.053	0.9631	0.101585
5.85	69.535	0.9698	0.083667
5.90	70.173	0.9787	0.059552
5.95	70.648	0.9853	0.041305
6.00	71.276	0.9941	0.016795
6.25	73.158	1.0203	-0.05928
6.50	73.946	1.0313	-0.09230
		TOTAL =	0.149235
		Cd =	0.044770

CONTROL VOLUME ANALYSIS OF MIDDLE GROOVE WING
2 1/2 CHORD DATA 0.1" MAX. GROOVE DEPTH

MAXIMUM THICKNESS = 0.7 INCHES
FREESTREAM VELOCITY = 70.21 FT/S
2/T = 2.857142

Y	V2	V2/V1	2/T(V2/V1(1-V2/V1))
5.00	73.71	1.0499	-0.14953
5.05	73.501	1.0469	-0.14020
5.10	73.198	1.0426	-0.12676
5.15	73.046	1.0404	-0.12007
5.20	72.679	1.0352	-0.10400
5.25	72.156	1.0277	-0.08138
5.30	71.193	1.0140	-0.04056
5.35	70.375	1.0024	-0.00673
5.40	69.355	0.9878	0.034369
5.45	68.320	0.9731	0.074841
5.50	67.368	0.9595	0.110971
5.55	66.603	0.9486	0.139243
5.60	66.066	0.9410	0.158683
5.65	66.066	0.9410	0.158683
5.70	66.402	0.9458	0.146558
5.75	66.970	0.9539	0.125764
5.80	67.796	0.9656	0.094858
5.85	69.001	0.9828	0.048352
5.90	69.994	0.9969	0.008762
5.95	70.942	1.0104	-0.03009
6.00	71.536	1.0189	-0.05497
6.25	72.402	1.0312	-0.09198

TOTAL = 0.154766

Cd = 0.046430

CONTROL VOLUME ANALYSIS OF MIDDLE GROOVE WING
1 CHORD DATA 0.1" MAX. GROOVE DEPTH

MAXIMUM THICKNESS = 0.7 INCHES
FREESTREAM VELOCITY = 67.92 FT/S
2/T = 2.857142

Y	V2	V2/V1	2/T(V2/V1(1-V2/V1))
5.10	72.965	1.0743	-0.22798
5.20	72.566	1.0684	-0.20880
5.25	72.133	1.0620	-0.18821
5.30	71.259	1.0492	-0.14736
5.35	69.832	1.0282	-0.08269
5.40	67.883	0.9995	0.001555
5.45	65.876	0.9699	0.083395
5.50	63.208	0.9306	0.184464
5.55	61.522	0.9058	0.243787
5.60	60.937	0.8972	0.263547
5.65	61.157	0.9004	0.256166
5.70	63.101	0.9290	0.188334
5.75	65.433	0.9634	0.100788
5.80	68.212	1.0043	-0.01233
5.85	71.134	1.0473	-0.14159
5.90	71.541	1.0533	-0.16044
		TOTAL =	0.152588
		Cd =	0.045776

CONTROL VOLUME ANALYSIS OF TRIANGULAR
4 1/4 CHORD DATA TRAILING EDGE WING

MAXIMUM THICKNESS = 0.7 INCHES
FREESTREAM VELOCITY = 71.83 FT/S
2/T = 2.857142

Y	V2	V2/V1	2/T(V2/V1(1-V2/V1))
4.50	73.491	1.0231	-0.06759
4.75	73.491	1.0231	-0.06759
5.00	72.941	1.0155	-0.04487
5.05	72.695	1.0120	-0.03482
5.10	72.387	1.0078	-0.02232
5.15	72.046	1.0030	-0.00861
5.20	71.735	0.9987	0.003773
5.25	71.234	0.9917	0.023510
5.30	70.951	0.9878	0.034535
5.35	70.698	0.9842	0.044317
5.40	70.603	0.9829	0.047972
5.45	70.317	0.9789	0.058914
5.50	70.094	0.9758	0.067383
5.55	70.222	0.9776	0.062528
5.60	70.222	0.9776	0.062528
5.65	70.413	0.9803	0.055251
5.70	70.667	0.9838	0.045511
5.75	70.951	0.9878	0.034535
5.80	71.108	0.9899	0.028429
5.85	71.485	0.9952	0.013656
5.90	71.86	1.0004	-0.00119
5.95	72.139	1.0043	-0.01234
6.00	72.294	1.0065	-0.01857
6.25	73.156	1.0185	-0.05371
6.50	73.643	1.0252	-0.07393
		TOTAL =	0.177249
		Cd =	0.053174

CONTROL VOLUME ANALYSIS OF TRIANGULAR
2 1/2 CHORD DATA TRAILING EDGE WING

MAXIMUM THICKNESS = 0.7 INCHES
FREESTREAM VELOCITY = 71.04 FT/S
2/T = 2.857142

Y	V2	V2/V1	2/T(V2/V1(1-V2/V1))
4.75	73.197	1.0304	-0.08938
5.00	72.577	1.0216	-0.06315
5.05	72.077	1.0146	-0.04231
5.10	71.762	1.0102	-0.02933
5.15	71.447	1.0057	-0.01646
5.20	71.002	0.9995	0.001527
5.25	70.523	0.9927	0.020641
5.30	70.170	0.9878	0.034561
5.35	69.782	0.9823	0.049699
5.40	69.457	0.9777	0.062247
5.45	69.229	0.9745	0.070979
5.50	69.098	0.9727	0.075969
5.55	69.131	0.9731	0.074714
5.60	69.327	0.9759	0.067233
5.65	69.587	0.9795	0.057242
5.70	69.911	0.9841	0.044685
5.75	70.363	0.9905	0.026968
5.80	70.811	0.9968	0.009180
5.85	71.161	1.0017	-0.00487
5.90	71.478	1.0062	-0.01772
5.95	71.794	1.0106	-0.03064
6.00	72.108	1.0150	-0.04359
6.25	72.95	1.0269	-0.07888
		TOTAL =	0.179272
		Cd =	0.053781

CONTROL VOLUME ANALYSIS OF TRIANGULAR
1 CHORD DATA TRAILING EDGE WING

MAXIMUM THICKNESS = 0.7 INCHES
FREESTREAM VELOCITY = 69.76 FT/S
2/T = 2.857142

Y	V2	V2/V1	2/T(V2/V1(1-V2/V1))
5.00	72.497	1.0392	-0.11649
5.10	71.938	1.0312	-0.09198
5.20	71.092	1.0191	-0.05559
5.25	70.204	1.0064	-0.01830
5.30	69.273	0.9930	0.019806
5.35	68.460	0.9814	0.052251
5.40	67.670	0.9700	0.083035
5.45	67.004	0.9605	0.108417
5.50	66.904	0.9591	0.112183
5.55	67.071	0.9615	0.105887
5.60	67.570	0.9686	0.086879
5.65	68.427	0.9809	0.053552
5.70	69.240	0.9925	0.021138
5.75	70.141	1.0055	-0.01568
5.80	70.586	1.0118	-0.03423
5.90	71.155	1.0200	-0.05827
6.00	71.407	1.0236	-0.06904
		TOTAL =	0.183523
		Cd =	0.055057

CONTROL VOLUME ANALYSIS OF SYMMETRIC RIPPLED
4 1/4 CHORD DATA TRAILING EDGE WING

MAXIMUM THICKNESS = 0.7 INCHES
FREESTREAM VELOCITY = 71.59 FT/S
2/T = 2.857142

Y	V2	V2/V1	2/T(V2/V1(1-V2/V1))
5.45	69.375	0.9691	0.085665
5.50	69.702	0.9736	0.073362
5.55	70.189	0.9804	0.054819
5.60	70.640	0.9867	0.037411
5.65	71.025	0.9921	0.022371
5.70	71.344	0.9966	0.009784
5.75	71.598	1.0001	-0.00031
5.80	71.788	1.0028	-0.00792
5.85	71.946	1.0050	-0.01427
5.90	72.103	1.0072	-0.02062
5.95	72.26	1.0094	-0.02698
6.00	72.26	1.0094	-0.02698
6.25	72.73	1.0159	-0.04622
6.50	72.886	1.0181	-0.05265
		TOTAL =	0.087410
		Cd =	0.026223

CONTROL VOLUME ANALYSIS OF SYMMETRIC RIPPLED
2 1/2 CHORD DATA TRAILING EDGE WING

MAXIMUM THICKNESS = 0.7 INCHES
FREESTREAM VELOCITY = 72.14 FT/S
2/T = 2.857142

Y	V2	V2/V1	2/T(V2/V1(1-V2/V1))
5.65	71.025	0.9845	0.043477
5.70	71.344	0.9890	0.031178
5.75	71.598	0.9925	0.021304
5.80	71.788	0.9951	0.013873
5.85	71.946	0.9973	0.007662
5.90	72.103	0.9995	0.001464
5.95	72.26	1.0017	-0.00476
6.00	72.26	1.0017	-0.00476
6.25	72.73	1.0082	-0.02355
6.50	72.886	1.0103	-0.02985
		TOTAL =	0.085881
		Cd =	0.025764

CONTROL VOLUME ANALYSIS OF SYMMETRIC RIPPLED
1 CHORD DATA TRAILING EDGE WING

MAXIMUM THICKNESS = 0.7 INCHES
FREESTREAM VELOCITY = 66.25 FT/S
2/T = 2.857142

Y	V2	V2/V1	2/T(V2/V1(1-V2/V1))
5.20	68.499	1.0339	-0.10028
5.25	65.444	0.9878	0.034337
5.30	62.385	0.9417	0.156960
5.35	60.121	0.9075	0.239870
5.40	59.780	0.9023	0.251779
5.45	61.615	0.9300	0.185907
5.50	64.252	0.9698	0.083568
5.55	67.765	1.0229	-0.06683
5.60	69.028	1.0419	-0.12482
5.65	69.487	1.0489	-0.14642
5.70	70.462	1.0636	-0.19319
5.75	71.296	1.0762	-0.23419
		TOTAL =	0.086664
		Cd =	0.025999

CONTROL VOLUME ANALYSIS OF VENTURI LEADING EDGE WING
1/4 CHORD DATA

MAXIMUM THICKNESS = 0.7 INCHES
FREESTREAM VELOCITY = 68.348 FT/S
2/T = 2.857142

Y	V2	V2/V1	2/T(V2/V1(1-V2/V1))
3.00	71.995	1.0534	-0.16058
3.50	72.182	1.0561	-0.16926
4.00	71.776	1.0502	-0.15048
4.50	72.182	1.0561	-0.16926
5.00	70.609	1.0331	-0.09764
5.10	70.002	1.0242	-0.07081
5.15	69.325	1.0143	-0.04142
5.20	66.346	0.9707	0.081237
5.25	66.885	0.9786	0.059848
5.30	67.086	0.9815	0.051781
5.35	65.665	0.9607	0.107754
5.40	61.934	0.9062	0.242962
5.45	56.232	0.8227	0.416639
5.50	52.728	0.7715	0.503735
5.55	58.234	0.8520	0.360230
5.60	64.596	0.9451	0.148234
5.65	67.520	0.9879	0.034193
5.70	68.017	0.9952	0.013769
5.75	68.182	0.9976	0.006922
5.80	69.293	1.0138	-0.04004
5.85	69.616	1.0186	-0.05398
5.90	69.584	1.0181	-0.05260
6.00	69.809	1.0214	-0.06237
6.25	70.034	1.0247	-0.07221
6.50	71.4	1.0447	-0.13327
7.00	71.776	1.0502	-0.15048
7.50	72.026	1.0538	-0.16202
8.00	72.585	1.0620	-0.18809
8.50	72.182	1.0561	-0.16926

TOTAL = 0.083490

Cd = 0.025047

CONTROL VOLUME ANALYSIS OF VENTURI LEADING EDGE WING
1 CHORD DATA

MAXIMUM THICKNESS = 0.7 INCHES
FREESTREAM VELOCITY = 68.762 FT/S
2/T = 2.857142

Y	V2	V2/V1	2/T(V2/V1(1-V2/V1))
3.00	71.413	1.0386	-0.11439
3.50	71.977	1.0468	-0.13983
4.00	72.102	1.0486	-0.14552
4.50	72.877	1.0598	-0.18121
5.00	72.413	1.0531	-0.15975
5.10	71.413	1.0386	-0.11439
5.20	67.533	0.9821	0.050153
5.25	66.29	0.9640	0.099021
5.30	65.951	0.9591	0.112025
5.35	65.231	0.9486	0.139183
5.40	63.839	0.9284	0.189911
5.45	62.451	0.9082	0.238162
5.50	61.436	0.8935	0.271972
5.55	61.253	0.8908	0.277935
5.60	62.235	0.9051	0.245461
5.65	63.944	0.9299	0.186166
5.70	65.335	0.9502	0.135299
5.75	66.290	0.9640	0.099021
5.80	67.099	0.9758	0.067428
5.90	69.468	1.0103	-0.02963
6.00	71.13	1.0344	-0.10178
6.25	71.508	1.0399	-0.11865
6.50	72.196	1.0499	-0.14981
7.00	72.351	1.0522	-0.15691
7.50	72.258	1.0508	-0.15264
8.00	72.723	1.0576	-0.17406
8.50	72.164	1.0495	-0.14835
9.00	72.009	1.0472	-0.14128

TOTAL = 0.083467

Cd = 0.025040

May 18, 1990

CONTROL VOLUME ANALYSIS OF VENTURI LEADING EDGE WING
2-1/2 CHORD DATA

MAXIMUM THICKNESS =	0.7	INCHES
FREESTREAM VELOCITY =	69.24	FT/S
2/T =	2.857142857	

Y	V2	V2/V1	2/T(V2/V1(1-V2/V1))
2.50	72.430	1.0461	-0.13769169
2.75	71.994	1.0398	-0.11814976
3.00	72.025	1.0402	-0.11954200
3.25	72.087	1.0411	-0.12232815
3.50	72.337	1.0447	-0.13349500
3.75	72.554	1.0479	-0.14329497
4.00	72.616	1.0488	-0.14609990
4.25	72.863	1.0523	-0.15734135
4.50	73.264	1.0581	-0.17568225
4.75	73.570	1.0625	-0.18985178
5.00	72.956	1.0537	-0.16156582
5.05	72.956	1.0537	-0.16156582
5.10	72.399	1.0456	-0.13629224
5.15	71.461	1.0321	-0.09456793
5.20	70.510	1.0183	-0.05335875
5.25	69.546	1.0044	-0.01268585
5.30	68.470	0.9889	0.031407922
5.35	67.577	0.9760	0.066959075
5.40	66.470	0.9600	0.109738400
5.45	65.652	0.9482	0.140366354
5.50	65.136	0.9407	0.159293952
5.55	64.162	0.9267	0.194167342
5.60	63.987	0.9241	0.200330313
5.65	64.337	0.9292	0.187984606
5.70	64.666	0.9342	0.175560480
5.75	65.206	0.9417	0.156780008
5.80	66.062	0.9541	0.125104530
5.85	66.740	0.9633	0.099437310
5.90	67.411	0.9736	0.073489064
5.95	68.405	0.9879	0.034057834
6.00	69.384	1.0021	-0.00596073
6.25	72.150	1.0420	-0.12511653
6.50	72.833	1.0519	-0.15593427
6.75	73.110	1.0559	-0.16861736
7.00	72.833	1.0519	-0.15593427
7.25	72.554	1.0479	-0.14329497
7.50	72.554	1.0479	-0.14329497
7.75	72.863	1.0523	-0.15734135
8.00	72.863	1.0523	-0.15734135
		TOTAL =	0.083370714
		Cd =	0.025011214

CONTROL VOLUME ANALYSIS OF VENTURI LEADING EDGE WING
4-1/4 CHORD DATA

MAXIMUM THICKNESS =	0.7	INCHES
FREESTREAM VELOCITY =	70.203	FT/S
2/T =	2.857142857	

Y	V2	V2/V1	2/T(V2/V1(1-V2/V1))
2.50	72.892	1.0383	-0.11362954
2.75	72.582	1.0339	-0.10010228
3.00	72.551	1.0334	-0.09875568
3.25	72.644	1.0348	-0.10279882
3.50	72.830	1.0374	-0.11091518
3.75	73.015	1.0401	-0.11902769
4.00	73.170	1.0423	-0.12585521
4.25	73.262	1.0436	-0.12992085
4.50	73.477	1.0466	-0.13946033
4.75	73.783	1.0510	-0.15312988
5.00	73.783	1.0510	-0.15312988
5.05	73.508	1.0471	-0.14084021
5.10	73.108	1.0414	-0.12312086
5.15	72.737	1.0361	-0.10685198
5.20	72.208	1.0286	-0.08393059
5.25	71.580	1.0196	-0.05714079
5.30	70.757	1.0079	-0.02272478
5.35	69.955	0.9965	0.010057523
5.40	68.981	0.9826	0.048867633
5.45	68.324	0.9732	0.074425314
5.50	67.594	0.9628	0.102235762
5.55	66.823	0.9519	0.130937270
5.60	66.586	0.9485	0.139621419
5.65	66.246	0.9436	0.151965962
5.70	66.076	0.9412	0.158087971
5.75	66.348	0.9451	0.148276672
5.80	66.654	0.9494	0.137136426
5.85	67.159	0.9566	0.118513952
5.90	67.661	0.9638	0.099709048
5.95	68.324	0.9732	0.074425314
6.00	68.916	0.9817	0.051418478
6.25	71.706	1.0214	-0.06247914
6.50	72.83	1.0374	-0.11091518
6.75	72.984	1.0396	-0.11766553
7.00	72.83	1.0374	-0.11091518
7.25	72.706	1.0357	-0.10549981
7.50	72.644	1.0348	-0.10279882
7.75	72.768	1.0365	-0.10820527
8.00	72.799	1.0370	-0.10955966
8.25	72.675	1.0352	-0.10414876
8.50	72.582	1.0339	-0.10010228
8.75	72.364	1.0308	-0.09065629
9.00	72.364	1.0308	-0.09065629
		TOTAL =	0.083030881
		Cd =	0.024909264